Generalised Parton Distributions : from phenomenological approaches to Dyson-Schwinger equations

Cédric Mezrag

UNIVERSITÉ PARIS SUD

Comprendre le monde, construire l'avenir®

CEA - Saclay

Université Paris-Sud

Ecole Doctorale 517 Particules, Noyaux, Cosmos
Laboratoire Irfu/SPhN

Discipline : Physique

Thèse de doctorat

Soutenue le 16 juillet 2015 par

Cédric Mezrag

Generalised Parton Distributions: from phenomenological approaches to Dyson-Schwinger equations

Directeur de thèse :	Franck Sabatié	Ingénieur Chercheur (Irfu/SPhN)
Composition du jury :		
Président du jury :	Asmâa Abada	Professeur (Université Paris Sud)
Rapporteurs :	Jean-François Mathiot	Directeur de recherche (LPC Clermont)
	Barbara Pasquini	Associated professor (Universita di Pavia)
Examinateurs :	Hervé Moutarde	Ingénieur Chercheur (Irfu/SPhN)
	Craig Roberts	Senior Physicist and Group-Leader (ANL)
Invité :	José Rodrìguez-Quintero	Professeur (Universidad de Huelva)

«Pour un homme sans œillères, il n'est pas de plus beau spectacle
que celui de l'intelligence aux prises avec une réalité qui le dépasse».
A. Camus in *Le mythe de Sisyphe*.

Acknowledgements

My first acknowledgements go to my supervisors Hervé Moutarde and Franck Sabatié who made me discover hadron physics. Our discussions have sharpened my scientific mind and improved my methods. Moreover, Hervé has carefully followed the present work. He read the present manuscript, allowing me to improve it through his suggestions. I must add that I am indebted to Pp, also known as Jose Rodríguez-Quintero, for our discussions and all the answers he gave me on non-pertubative QCD. We have performed together a significant part of the calculations developed in this work. I would also like to thank him for his warm welcomes both in Huelva and in Punta Umbria.

I am also grateful to Craig Roberts, with whom I have a fruitful collaboration since our first meeting in Ubatuba. I thank him for his invitation at Argonne, where parts of this work has been finalised, and for the possibility he offered me to come to Argonne for a post-doc position. I am also indebted to Bernard Pire, who gave me advice and who has pushed my post-doc applications. In addition, together with Lech Szymanowski and Samuel Wallon, they allow me to better understand pertubative QCD, and therefore, I would like to thank them.

The present work, discussing GPDs from the theoretical side, has also benefited from the members of the CLAS group at SPhN. Therefore, I would like to thank Sébastien Procureur, Michel Garçon and Jacques Ball for their explanations on the experimental side of GPDs. I am also grateful to the post-docs and students of the CLAS group, Gabriel Charles, Maxime Defurne, Simons Bouteille, Maxence Vandenbroucke, Bryan Berthou and Adrien Besse, both for our interesting discussions and their friendships.

This work would not have been possible without the supports of the heads of SPhN. Therefore, I would like to thank Héloïse Goutte, Michel Garçon, Françoise Auger and Jacques Ball for having welcomed me at SPhN, and allowed me to work in good conditions. I am also grateful to the SPhN secretary staff, Daniel Coret and Isabelle Richard, who have always been very helpful. And so has been Gilles Tricoche, providing me with computer pieces of advice.

My gratitude extends to my *rapporteurs* Jean-François Mathiot and Barbara Pasquini for accepting to read my manuscript and providing me with instructive comments. I also thank my *examinateurs* Asmaa Abada and Craig Roberts.

On the personal side, I also have a special thank for all of my friends, especially my roommates Pierre Clavier, Pierre Ronceray, Nicolas Babinet and Lætitia Leduc, without whom, those 3 years would have been very different. I would also like to thank Florian Bellecourt and Angelo Petronio for having taught me how to play jazz during the last three years, and Eric Randrianarivelo for training me at the Dojo. I also have a thought to Thibaut Hiron and Jean Louet, the two other co-members of our *HLM jazz trio*.

Finally, I would like to express my gratitude to my family which supports me both in every day life and in hard times. Thanks to all of you.

Introduction

After the discovery at the Large Hadron Collider at CERN [1, 2] of the Brout-Englert-Higgs boson [3, 4], the successful so-called Standard Model (SM) of particle physics is complete. Yet, complete does not mean understood, and today particle physicists focus on two main tasks. The first one consists in looking for small deviations of experimental data from the SM predictions in order to extend it or to include it in a larger theory. The other one focuses on understanding the dynamics of the SM itself through phenomena which are still to be explained.

Among those phenomena, the ones related to the strong interaction and in particular *confinement* play a special role. Indeed, the fundamental degrees of freedom of the modern theory of the strong interaction *i.e.* Quantum Chromodynamics (QCD) are known and called quarks and gluons. However, they cannot be directly observed, and remain confined inside hadrons. Mass generation is also deeply related to QCD dynamics as the contribution of the breaking of the Electro-Weak (EW) symmetry contributes only to few percents of the total mass of hadrons. Consequently, most of the visible mass of the universe results from a mechanism which is not yet fully understood. Additionally, it is still not possible to predict the structure of hadrons in terms of quarks and gluons, based on QCD first principles only.

This is the apparent paradox of QCD: the fundamental theory is well established through a Lagrangian formulation, but the description of low-energy phenomena remains out of reach of traditional perturbative quantum field theory computations. If asymptotic freedom [5–7] ensures the validity of the perturbative expansion at high energy, Feynman diagram computations at a given order generate a diverging coupling constant in the infrared region. Therefore new ideas have emerged, like for instance the concept of *factorisation*, stating that if a hard scale is involved in a process, then it is possible to describe the considered process as a convolution of a partonic subprocess happening at the given hard scale and non-perturbative objects such as Parton Distributions Functions (PDFs), Generalised Parton Distributions (GPDs)... Those objects encode information on the internal structure of hadrons in terms of quarks and gluons and appear in different processes. For instance, PDFs, which have been introduced in the late 1960s, are a key element of data analyses at LHC.

Experimentally speaking, hadron physics is a very active field today as several facilities are ongoing all around the world. If Europe hosts most of the current installations (COSY, ELSA, MAMI, CERN...), Asia (Beijing Electron-Positron Collider, J-PARC) and USA (RHIC, JLab) take also a significant part of the experimental effort. The future is even more promising with starting projects like JLab 12 or FAIR, and data expected before 2020. On a longer time scale, an ambitious facility, the Electron Ion Collider (EIC), may be built in the 2020s in the USA.

If PDFs have been measured since the end of the 1960s, the experimental access to GPDs is more recent (2000s), and much more challenging, since the cross-section of processes giving

access to them is much smaller than those related to PDFs. Extracting the GPDs from data is also challenging on the theoretical side, since only a small part of the total phase-space is reachable with current facilities. This is about to change on short-term with JLab 12, which will greatly increase the kinematic coverage in the valence region, and is thought to be able to deliver data with only few percents statistical uncertainties. One can therefore expect that, with such a large kinematic coverage and high accuracy, JLab 12 data will challenge the current understanding of GPDs and more specifically the current models of GPDs. Until now, only phenomenological parameterisations have been compared to available data. They are successful enough to confirm the general framework and the GPD interpretation, but the agreement with some of the existing data already needs to be improved.

Moreover, contrary to PDFs which are hardly constrained by the factorisation framework, any GPD model has to fulfil a significant number of theoretical properties. The latter forbid the simpler Ansätze but are not constraining enough to select a given functional form. Thus, several modeling frameworks have been developed in the last decade, each one having its advantages and drawbacks. Until now, all of them have led to phenomenological models only. Several questions can consequently be raised. First of all, is it possible to improve the existing frameworks, and thus the phenomenological models? Can one work beyond phenomenological parameterisation in order to relate available structure data with QCD dynamical phenomena, like for instance the generation of mass? And of course, being given more and more constraining experimental data, can GPDs be modeled in agreement with them?

Existing phenomenological models can be modified in order to improve their agreement with available data. Nevertheless, they intrinsically preclude a full dynamical understanding of GPDs, *i.e.* how GPDs are generated from the fundamental degrees of freedom of the theory. This can only be achieved through models relying on non-perturbative methods. The approach retained here is based on Dyson-Schwinger equations which have achieved many successes recently due to new symmetry-preserving kernels.

GPDs, and more generally, the overall GPD framework, which is now well established, is introduced in chapter 1. Chapter 2 is devoted to the improvement of a phenomenological model of proton GPDs based on objects called Double Distributions (DDs). The latter are related to GPDs through the Radon transform. In the first part of chapter 3, the Dyson-Schwinger equations are introduced, and then used in the second part to compute a model of GPD for the pion. In chapter 4, an analysis of the gluon structure inside the model computed in chapter 3 is performed in order to improve it. Chapter 5 is an opening to lightcone models of GPDs, before the conclusion.

Contents

Chapter 1

Introduction to Generalised Parton Distributions

«L'expérience nous apprend que lorsqu'on entend sonner à la porte,
c'est qu'il n'y a jamais personne.»
Eugène Ionesco in *La cantatrice chauve*

1.1 From a point-like proton to Wigner Distributions

1.1.1 The parton model

Discovered in 1919 by E. Rutherford [8], the proton was first thought to be a point-like particle. One has to wait until 1933 to get the first experimental hint for the proton structure [9, 10], through the measurement of its magnetic moment. Due to the Dirac equation, the expected value of the magnetic moment of the proton seen as a point-like particle was:

$$\mu_p = \mu_N = \frac{e\hbar}{2M}, \tag{1.1}$$

were e is the proton charge, M the proton mass, and μ_N the so-called nuclear magneton. The results was about 2.5 times greater than expected, a first hint that the proton is not an elementary particle, but a composite one.

This was confirmed 23 years later by Hofstadter through elastic scattering of electrons on nucleons [11]. The amplitude $\mathcal{M}^{el}$ of the considered process shown on figure 1.1 can be written as:

$$\mathcal{M}^{el} = \frac{e^2}{q^2}\bar{u}(k')\gamma^\mu u(k) \left\langle p_2\right| J^{em}_\mu(0) \left|p_1\right\rangle, \tag{1.2}$$

where the momenta are defined on figure 1.1 and the matrix element $\left\langle p_2\right| J^{em}_\mu(0) \left|p_1\right\rangle$ is parameterised as:

$$\left\langle p_2\right| J^{em}_\mu(0) \left|p_1\right\rangle = \bar{u}(p_2)\left(\gamma_\mu F_1(q^2) + i\sigma^{\mu\nu}q_\nu\frac{F_2(q^2)}{2M}\right)u(p_1) \tag{1.3}$$

for a spin-1/2 target. $F_1(q^2)$ and $F_2(q^2)$ are called form factors and are normalised as:

$$F_1(0) = \mathcal{Q} \quad , \quad F_2(0) = \kappa \tag{1.4}$$

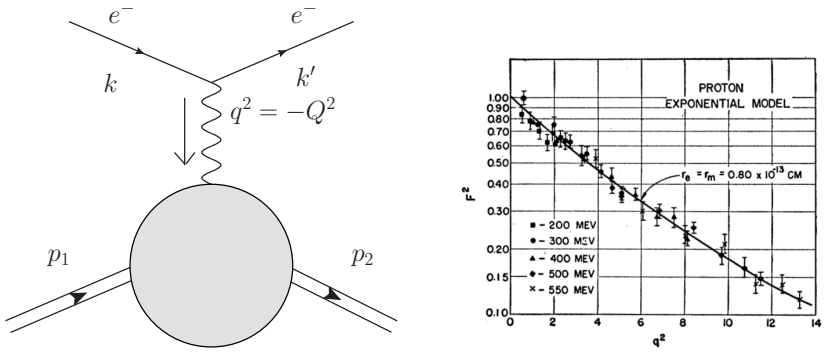

Figure 1.1: Left-hand side: elastic scattering of an electron on a proton target. Right-hand side: original measurement of the proton form factors by Hofstadter (figure from Ref. [12]).

with $\mathcal{Q}$ being the electric charge and κ the anomalous magnetic moment of the considered hadronic target. It is possible to show that in the case of a point-like target, those form factors do not depend on the photon virtuality Q^2. But this is not the case, as measured by Hofstadter (figure 1.1), definitely proving that the proton is an extended particle.

The following decade was very rich in terms of ideas of what the constituents of the proton (and other hadrons discovered in between) can be. In 1964, M. Gell-Mann [13] and G. Zweig [14, 15] introduced independently a new quantum number called flavour, in order to explain the diversity of hadrons using a $SU(3)$ symmetry. The particles carrying this quantum number were called quarks and thought to be mathematical representations rather than true particles. This status changed at the end of the 1960s with the first Deep Inelastic Scattering (DIS) experiment at SLAC [16, 17].

Indeed, the same year, Björken [18, 19] and Feynman [20] shed some light on the DIS measurements by suggesting that the proton was composed of point-like particles of spin 1/2. This so-called "parton model" was in good agreement with the SLAC results. Its main features are sketched below. Defining the photon virtuality as $Q^2 = -q^2$ and P the momentum of the considered hadron (see figure 1.2), it is possible to write the cross section in terms of the so-called leptonic $\ell^{\mu\nu}$ and hadronic $W_{\mu\nu}$ tensors:

$$\frac{\mathrm{d}^2\sigma}{\mathrm{d}^2\Omega \mathrm{d}E'} = \frac{\alpha^2}{Q^4}\frac{E'}{E}\ell_{\mu\nu}W^{\mu\nu}, \tag{1.5}$$

where $\alpha = \frac{e^2}{4\pi}$, Ω is the solid angle of the outgoing electrons, E' is the energy of the outgoing electron and E the energy of the incoming one. This is illustrated on figure 1.2. The leptonic tensor being described only with QED, it can be computed at tree level as:

$$\ell^{\mu\nu} = 2\left(k^\mu k'^\nu + k'^\mu k^\nu - \frac{Q^2}{2}g^{\mu\nu}\right). \tag{1.6}$$

where $g^{\mu\nu}$ is the metric tensor, k^μ and k'^μ are respectively the momenta of the incoming and outgoing electron. The hadronic tensor cannot be directly computed *a priori*. However, hermiticity and current conservation imply that:

$$\left\{ \begin{array}{rcl} W^{\mu\nu} & = & W^{\nu\mu} \\ q_\mu W^{\mu\nu} & = & 0 \end{array} \right. . \tag{1.7}$$

Thus, assuming the proton target is unpolarised, the hadronic tensor can be parameterised in terms of two structure function F_1 and F_2:

$$W^{\mu\nu}(q,P) = -\frac{F_1}{M}\left(g^{\mu\nu} - \frac{q^\mu q^\nu}{q^2}\right) + \frac{F_2}{M\ P\cdot q}\left(P^\mu - \frac{P\cdot q}{q^2}q^\mu\right)\left(P^\nu - \frac{P\cdot q}{q^2}q^\nu\right). \tag{1.8}$$

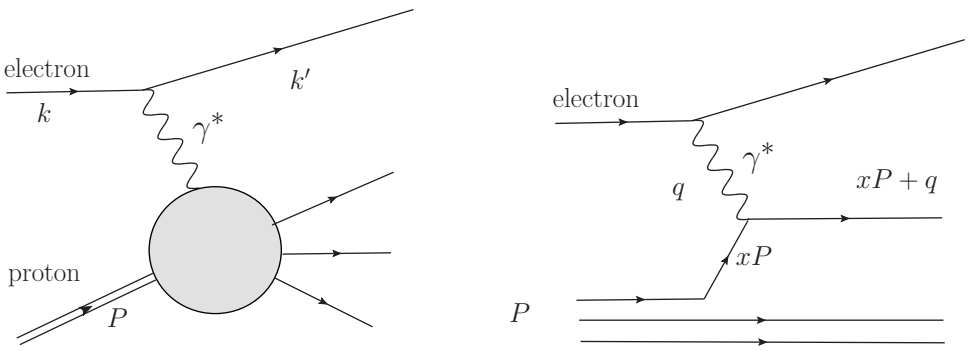

Figure 1.2: Left-hand side: Feynman Diagram of DIS. Right-hand side: interpretation within the parton model. Only the outgoing electron is detected in this process.

Within the parton model, the two functions F_1 and F_2 can actually be computed. To do so, it is necessary to introduce the so-called Bjorken variable x_B:

$$x_B = \frac{Q^2}{2P\cdot q}. \tag{1.9}$$

Denoting x the fraction of the proton momentum carried by the active quark (see figure 1.2), they are given as:

$$F_1 = \frac{1}{2}\delta(x - x_B), \tag{1.10}$$

$$F_2 = x\delta(x - x_B). \tag{1.11}$$

Introducing the probability density $q_i(x)$ to find a given charged parton of type i carrying the momentum fraction x, and averaging the structure functions, one gets:

$$F_1(x_B) = \sum_i \int \mathrm{d}x e_i^2 q_i(x)\frac{1}{2}\delta(x - x_B), \tag{1.12}$$

$$F_2(x_B) = \sum_i \int \mathrm{d}x e_i^2 q_i(x)\ x\ \delta(x - x_B). \tag{1.13}$$

The q_i are called Parton Distribution Functions (PDFs). Equations (1.12) and (1.13) have important consequences, as $F_1(x_B)$ and $F_2(x_B)$ are measurable. First, the fact that they do not depend on Q^2 is a direct consequence of the assumption that hadrons are composed of point-like particles. This is known as Björken scaling. In addition, the Dirac distribution allows one to access experimentally the probability density with respect to x_B of those point-like particles. Moreover, assuming they are spin-1/2 fermions implies the famous Callan-Gross relation [21]:

$$F_2(x_B) = 2x_B F_1(x_B). \tag{1.14}$$

The experimental agreement of both the Björken scaling[1] and the Callan-Gross relation strongly suggested in those days that the proton was composed of point-like particle of spin 1/2, forty years after the discovery of the proton itself by E. Rutherford.

1.1.2 QCD enters the game

The first DIS experiments were done in a feverish atmosphere around the internal structure of hadrons. After the quark model, it was suggested first that quarks do not obey neither to Bose nor to Fermi statistics [22], and then to add an additional quantum number to quarks called colour in order to explain the structure of the Δ^{++} in terms of fermionic quarks [23–25]. The authors also raised the possibility that quarks interact between themselves through eight gauge bosons. Indeed, despite the seminal paper by Yang and Mills in the 1950s [26], it was unclear in those days that strong interaction could be described using a quantum field theory. Light was shed on this in 1973 by Politzer [5] and by Gross and Wilczek [6, 7] who proved that non-abelian gauge theory are asymptotically free. Consequently, one can perform computations in a perturbative framework within a non-abelian gauge theory and thus, take into account the colour degrees of freedom: Quantum Chromodynamics (QCD) was born [27].

Within such a consistent framework for perturbative QCD, leading order (LO) and next-to-leading order (NLO) contributions to DIS were computed. The former give back the results of the parton model, especially equations (1.12) and (1.13). But computations at NLO break both the Björken scaling and the Callan-Gross relation. Predictions for the Q^2 dependence leads to the so-called DGLAP equations [28–30], allowing one to evolve the PDFs at any scale Q^2 from an original one Q_0^2. This scaling violation is illustrated on figure 1.3.

Yet until now, a key point was omitted, as one can wonder whether or not it is truly possible in QCD to split the DIS cross section between on one hand a short-range interaction between a charged parton and the incoming photon, and on the other hand a probability density containing all the infrared physics. In other words, whether or not it is possible to write the structure functions as:

$$F_1(x_B, Q^2) = \sum_i \int_0^1 \mathrm{d}x \; C_1^{(i)}(x, x_B, Q^2, \mu_R^2, \mu_F^2) \; q_i(x, \mu_R^2, \mu_F^2) + O(\frac{M^2}{Q^2}), \quad (1.15)$$

$$F_2(x_B, Q^2) = \sum_i \int_0^1 \mathrm{d}x \; C_2^{(i)}(x, x_B, Q^2, \mu_R^2, \mu_F^2) \; q_i(x, \mu_R^2, \mu_F^2) + O(\frac{M^2}{Q^2}), \quad (1.16)$$

where C_1 and C_2 are coefficient functions and do not depend of the considered hadron. M is the hadron mass, and μ_R and μ_F are the so-called renormalisation and factorisation scales. The coefficient functions depend on those two scales, which indicates that they have been "cured" from divergencies both in the IR and UV sectors. Still, as structure functions are measurable, the dependencies in μ_F and μ_R have to cancel out between the PDFs q_i and the coefficient functions $C_1^{(i)}$ and $C_2^{(i)}$. In the parton model, the fact that soft and hard part factorise comes from the assumption of incoherence between long- and short-distance effects. Proving that this is still true in QCD remains technical and a detailed proof is beyond the scope of this thesis. However, it is possible to give a taste of how things work. Full proofs can be found in original papers [32–35] or in textbooks [36, 37].

[1] The agreement of experimental data with the Björken scaling in the first DIS data is a coincidence. Indeed data were taken in a x_B-range were the scale dependence is small, and thus cannot be seen because of the precision of data at this time.

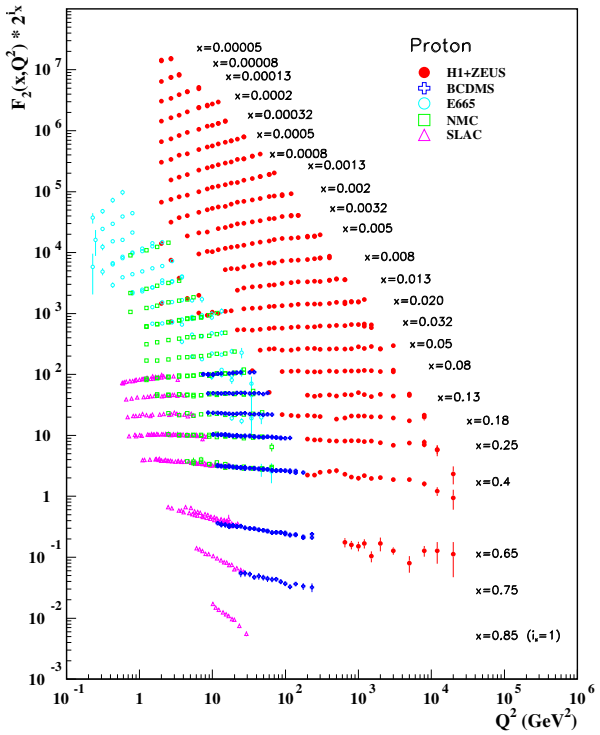

Figure 1.3: The structure function F_2 measured at different facilities as a function of Q^2, illustrating the Björken scaling violation. Figure taken from PDG [31].

Before starting, it must be noted that instead of dealing with the hadronic tensor $W^{\mu\nu}$, it is easier to focus on the Compton tensor $T^{\mu\nu}$ (figure 1.4) defined as:

$$T^{\mu\nu} = \frac{i}{2\pi}\int \mathrm{d}x^4 e^{iq\cdot x}\frac{1}{2}\sum_{\sigma}\langle p,\sigma|\,\mathrm{T}\left[J^{\mu}_{em}(x)J^{\nu}_{em}(0)\right]|p,\sigma\rangle\,. \tag{1.17}$$

where T denotes the time ordered products, σ the polarisation of the considered hadron and p its momentum. The Compton tensor is related to the hadronic tensor through the optical theorem:

$$W^{\mu\nu} = \frac{1}{M}\Im[T^{\mu\nu}], \tag{1.18}$$

where 1/M is merely a normalising factor[2], consistently with equation (1.8). One of the advantages of the Compton tensor is that there are no final-state interactions. Indeed, in figure 1.4 only one jet is allowed in the final state of the Compton tensor. On the opposite, in the case of the hadron tensor (see figure 1.2), multiple jets are allowed, generating soft interactions between them. When trying to factorise the Compton tensor, the first important point is to analyse the large Q^2 behaviour of the considered process and to show that there is a one-to-one correspondence with infrared (IR) divergences in massless perturbation theory (see *e.g.* [36] for an example on the Sudakov form factor). Then one needs to analyse those types of divergences and realises that they correspond to pinch singularities in momentum space. It is therefore possible to define Pinch Singularity Surfaces (PSS) for any considered graph. PSS can be identified through the Landau equations [39], and their contributions can be

[2]Normalisation conditions are taken from [38].

interpreted as relativistic on-shell particles in the Coleman-Norton picture [40]. This picture is often represented in terms of so-called reduced graphs. After that, power counting [35, 41] allows the identification of the leading contribution among the reduced graphs. The leading contribution for DIS is shown on figure 1.4, gluons being included in the Wilson lines [42]. The hard part H drawn on figure 1.4 includes all the high virtuality momenta contributions, *i.e.* $k^2 \approx Q^2$. Finally, a diagrammatic study of the possible values of x shows that the contributions for $x \notin [-1, 1]$ vanish, due to poles being in the same half-space of the complex plan. Negative x being interpreted as antiquarks, it is possible to restrict oneself to $x \in [0, 1]$, exactly as in the parton model.

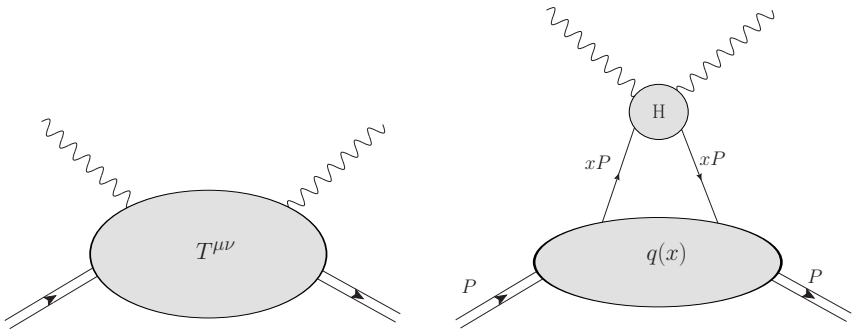

Figure 1.4: Compton Tensor. Left-hand side: Representation of the Compton tensor. Right-hand side: reduced graph of the leading PSS after including gluons in the Wilson line. H denotes the hard part where momenta have a virtuality of order Q^2, whereas $q(x)$ is the PDF.

Within this framework, PDFs can be defined as the Fourier transform of a non-local matrix element:

$$q(x) = \frac{1}{2}\int \frac{\mathrm{d}z^-}{2\pi} e^{ixP^+z^-} \left\langle P\right| \bar{\psi}^q\left(-\frac{z}{2}\right)\gamma^+\left[-\frac{z}{2};\frac{z}{2}\right]\psi^q\left(\frac{z}{2}\right)\left|P\right\rangle\Big|_{z^+=z_\perp=0}, \tag{1.19}$$

where $[z_1; z_2]$ is the Wilson line between the points z_1 and z_2 along the lightcone (LC). Lightcone (LC) variables are defined in appendix A. If DIS is the Golden channel to access PDFs, factorisation theorem allows one to describe different experimental processes. This universality property is a key point in modern hadron and particule physics, as PDFs may be measured in a given process, and used in other ones. They are key elements of physics at colliders, especially at the Large Hadron Collider (LHC). Indeed, computations are done in terms of quarks and gluons but collisions happened between protons. Being the probability density to find a given parton carrying a momentum fraction x inside a hadron, PDFs bridge this gap between fundamental degrees of freedom and observable ones. It should be noted however that within this formulation, there is no direct experimental access to PDFs anymore. Indeed, the structure functions F_1 and F_2 defined respectively in equations (1.15) and (1.16) give an experimental access only to convolutions of PDFs with hard scattering kernels. This is why PDF extractions techniques have been developed, see *e.g.* [43].

To conclude on DIS, one should add that PDFs give a one-dimensional information on the internal structure of the considered hadron. Yet, it is possible to generalise this concept to a multidimensional information and finally build an object which looks like probability densities in kinetic theory: the Wigner Distribution.

1.1.3 Wigner Distributions

Non-relativistic case

In 1932, E. Wigner [44] suggested a generalisation of the phase space distribution $f(r,p,t)$ in the framework of non-relativistic quantum mechanics. Denoting ψ the wave function of the considered particle, the Wigner Distribution is defined as:

$$W(\boldsymbol{r},\boldsymbol{p}) = \int \frac{\mathrm{d}^3\boldsymbol{R}}{(2\pi\hbar)^3} e^{-i\frac{\boldsymbol{p}\cdot\boldsymbol{R}}{\hbar}} \psi^*\left(\boldsymbol{r}-\frac{1}{2}\boldsymbol{R}\right)\psi\left(\boldsymbol{r}+\frac{1}{2}\boldsymbol{R}\right), \tag{1.20}$$

where bold letters correspond to 3-vectors. The Wigner distribution cannot be seen as a propability density as it contains information on interference, and thus is not positive definite. Yet, in the classical limit, the Wigner distribution becomes positive definite and reduces to the phase-space probability density. However, even in the quantum case, it is possible to compute the expectation value of an operator $\hat{O}(\hat{r},\hat{p})$ by convolution with the Wigner distribution [45] (see also Ref. [46]) using the Weyl association rule [47], *i.e.* associating with a function of $\boldsymbol{r}$ and $\boldsymbol{p}$ denoted $O_{\mathrm{Weyl}}(\boldsymbol{r},\boldsymbol{p})$:

$$\langle\hat{O}\rangle = \int \mathrm{d}^3\boldsymbol{p}\mathrm{d}^3\boldsymbol{r} W(r,p) O_{\mathrm{Weyl}}(\boldsymbol{r},\boldsymbol{p}). \tag{1.21}$$

It is also possible to get a probabilistic interpretation for projections of the Wigner distribution:

$$\int \mathrm{d}^3\boldsymbol{p} W((\boldsymbol{r},\boldsymbol{p}) = \rho(\boldsymbol{r}) \quad , \quad \int \mathrm{d}^3\boldsymbol{r} W((\boldsymbol{r},\boldsymbol{p}) = \rho(\boldsymbol{p}). \tag{1.22}$$

Relativistic case

It is possible to extend the notion of Wigner distribution within a a relativistic framework, *i.e.* using quantum field theory. Introducing gauge invariant quark fields Ψ:

$$\Psi(x) = \exp\left(-ig\int_0^\infty \mathrm{d}\lambda\ n\cdot A(\lambda n + x)\right)\psi(x), \tag{1.23}$$

where n is a constant four-vector, g the coupling constant and $\psi(x)$ a free quark field, the Wigner operator $\hat{W}_\Gamma$ is defined as [48, 49]:

$$\hat{W}_\Gamma(r,k^+,k_\perp) = \int \mathrm{d}z^-\ \mathrm{d}^2z_\perp\ e^{i(k^+z^- - k_\perp z_\perp)}\left[\bar{\Psi}(r-\frac{z}{2})\Gamma\Psi(r+\frac{z}{2})\right]_{z^+=0}, \tag{1.24}$$

where Γ stands for the relevant Dirac structure. $\hat{W}_\Gamma(r,k^+,k_\perp)$ is already considered at equal lightcone time $z^+=0$ *i.e.* integrated over k^-. The expectation value of this operator within a hadron gives the Wigner distribution of quarks inside this hadron:

$$\begin{aligned} W_\Gamma(r,k^+,\mathbf{k}_\perp) &= \frac{1}{2M}\int\frac{\mathrm{d}^3\boldsymbol{q}}{(2\pi)^3}\left\langle H;\ \frac{q}{2}\right|\hat{W}_\Gamma(r,k^+,\mathbf{k}_\perp)\left|H;\ -\frac{q}{2}\right\rangle \\ &= \frac{1}{2M}\int\frac{\mathrm{d}^3\boldsymbol{q}}{(2\pi)^3}e^{-i\boldsymbol{q}\cdot\boldsymbol{r}}\left\langle H;\ \frac{q}{2}\right|\hat{W}_\Gamma(0,k^+,\mathbf{k}_\perp)\left|H;\ -\frac{q}{2}\right\rangle, \end{aligned} \tag{1.25}$$

where M is the mass of the considered hadron. Integrating over $\mathbf{k}_\perp$ and $\boldsymbol{r}$ would get back the matrix element of equation (1.19) defining the PDFs.

If Wigner distributions have been originately introduced as six-dimensional objects, they do not correspond to any straightforward physical interpretation. Indeed, relativistic corrections (see *e.g.* Ref. [50]) preclude interpretations. A five-dimensional definition of the Wigner distributions has been given in Ref. [51], allowing a direct interpretation in the Infinite Momentum Frame (IMF). Five-dimensional Wigner Distributions are related to Generalised Transverse Momentum Distributions (GTMDs) through a Fourier transform on coordinate variables in the transverse plane.

Within the past decade, Wigner Distributions and GTMDs have been intensively studied in order to understand the orbital momenta of quarks and gluons inside hadrons (see *e.g.* [51–58]). Carrying information on both the momenta and the positions of partons, Wigner Distributions are indeed an appropriate object to study orbital momentum. Models of GTMDs based on lightcone constituent quark model, chiral quark soliton model or light-front wave functions have been developed [54, 57, 58], allowing one to visualise the distribution of transverse momentum.

It does remain unclear whether or not some observables could be directly sensitive to Wigner Distributions in hadron physics. However, today several processes allow to get an experimental access to projections of the Wigner Distributions. DIS is one of them but brings only a one-dimensional information on the hadron structure through PDFs. Nonetheless, it is nowadays possible to do better, for instance through exclusive processes.

1.2 Exclusive processes

1.2.1 Exclusive vs Inclusive

Contrary to inclusive processes like DIS, exclusive processes require to characterise every particles in the final state. They are therefore much harder to measure than inclusive ones. However they also contain much more information. Three different processes are considered here, with three particles in the final state. Deep Virtual Compton Scattering (DVCS) in which a lepton interacts with a hadron through the exchange of a virtual photon. A photon is detected in the final state together with the lepton and the hadron (figure 1.5). A crossed process can be identified in which a real photon interacts with the hadron, producing a virtual photon which decays into a lepton pair. This process is called Time-like Compton Scattering (TCS) and is illustrated on figure 1.5. A third process called Deep Virtual meson production (DVMP) contains three particles in the final state. This process is similar to DVCS except that in the final state, a meson is produced instead of a real photon.

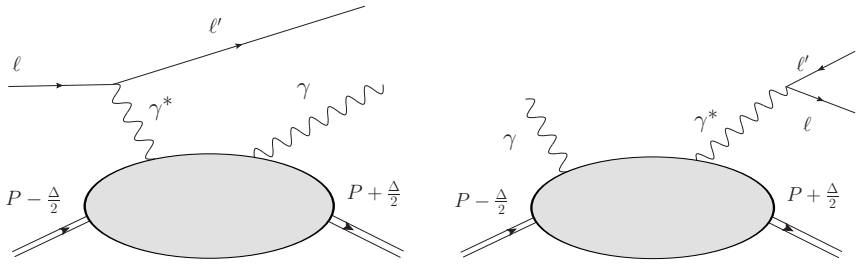

Figure 1.5: Example of exclusive processes. Left-hand side: DVCS. Right-hand side: TCS.

1.2.2 Factorisation and Generalised Parton Distributions

Just as in DIS, the question of the possibility to describe exclusive processes as convolutions of a hard part computed using QCD perturbative expansion, and a soft part encoding the non-perturbative information can be raised. In the case of DIS, the proof of this factorisation is already very technical. Dealing with exclusive processes, things do not simplify. Indeed, exclusive processes cannot be factorised at the level of the cross section, but at the level of the amplitude. It is then possible to apply the same machinery than for the DIS case, *i.e.* identify the PSS and select the relevant ones using power counting [59–61]. But other techniques have been developed in order to factorise the DVCS amplitude like for instance the one based on the Operator Product Expansion (OPE) done by the Leipzig group [62]. A third one consists in writing a general graph contribution to the process in the Schwinger α-representation and identifying within this framework the leading contributions in Q^2 [63–66].

All those methods show that it is indeed possible to factorise the DVCS (and also TCS and DVMP) amplitude into a hard part expandable within a perturbation theory framework and a soft part containing the non-perturbative information. Actually, the previous mentioned proofs of factorisation naturally lead to different objects encoding the non-perturbative behaviour. Dealing with PSS leads to the Generalised Parton Distributions (GPDs) (see for instance Ref. [60]) H^q and E^q which are defined in terms of matrix elements as:

$$\begin{aligned} F^q &= \frac{1}{2}\int \frac{\mathrm{d}z^-}{2\pi} e^{ixP^+z^-} \left\langle p_2\right| \bar{\psi}^q\left(-\frac{z}{2}\right)\gamma^+\psi^q\left(\frac{z}{2}\right)\left|p_1\right\rangle\Big|_{z^+=z_\perp=0} \\ &= \frac{1}{2P^+}\left[H^q(x,\xi,t)\bar{u}\left(p_2\right)\gamma^+u\left(p_1\right) + E^q(x,\xi,t)\bar{u}\left(p_2\right)\frac{i\sigma^{+\mu}\Delta_\mu}{2M}u\left(p_1\right)\right], \end{aligned} \tag{1.26}$$

where $P=\frac{p_1+p_2}{2}$ and $\Delta = p_2 - p_1$. x is the average fraction of the momentum of the active quark along the hadron direction, $\xi = -\frac{\Delta^+}{2P^+}$ is the boost along the same direction as shown on the left-hand side of figure 1.6. $t=\Delta^2$ is the Mandelstam variable, and q stands for the quark flavour. Two additional quark GPDs $\tilde{H}$ and $\tilde{E}$ can be introduced in the very same way:

$$\begin{aligned} \tilde{F}^q &= \frac{1}{2}\int \frac{\mathrm{d}z^-}{2\pi} e^{ixP^+z^-} \left\langle p_2\right| \bar{\psi}^q\left(-\frac{z}{2}\right)\gamma^+\gamma_5\psi^q\left(\frac{z}{2}\right)\left|p_1\right\rangle\Big|_{z^+=z_\perp=0} \\ &= \frac{1}{2P^+}\left[\tilde{H}^q(x,\xi,t)\bar{u}\left(p_2\right)\gamma^+\gamma_5u\left(p_1\right) + \tilde{E}^q(x,\xi,t)\bar{u}\left(p_2\right)\frac{\gamma_5\Delta^+}{2M}u\left(p_1\right)\right]. \end{aligned} \tag{1.27}$$

In addition to quark GPDs, gluon GPDs can be defined:

$$\begin{aligned} F^g &= \frac{1}{P^+}\int \frac{\mathrm{d}z^-}{2\pi} e^{ixP^+z^-} \left\langle p_2\right| G^{+\mu}\left(-\frac{z}{2}\right) {G_\mu}^+\left(\frac{z}{2}\right)\left|p_1\right\rangle\Big|_{z^+=z_\perp=0} \\ &= \frac{1}{2P^+}\left[H^g(x,\xi,t)\bar{u}\left(p_2\right)\gamma^+u\left(p_1\right) + E^g(x,\xi,t)\bar{u}\left(p_2\right)\frac{i\sigma^{+\mu}\Delta_\mu}{2M}u\left(p_1\right)\right], \end{aligned} \tag{1.28}$$

$$\begin{aligned} \tilde{F}^g &= \frac{1}{2}\int \frac{\mathrm{d}z^-}{2\pi} e^{ixP^+z^-} \left\langle p_2\right| G^{+\mu}\left(-\frac{z}{2}\right) \tilde{G}_\mu^+\left(\frac{z}{2}\right)\left|p_1\right\rangle\Big|_{z^+=z_\perp=0} \\ &= \frac{1}{2P^+}\left[\tilde{H}^g(x,\xi,t)\bar{u}\left(p_2\right)\gamma^+\gamma_5u\left(p_1\right) + \tilde{E}^g(x,\xi,t)\bar{u}\left(p_2\right)\frac{\gamma_5\Delta^+}{2M}u\left(p_1\right)\right], \end{aligned} \tag{1.29}$$

where $G^{\mu\nu}$ is the gluon field strength and $\tilde{G}^{\mu\nu} = \frac{1}{2}\epsilon_{\mu\nu\rho\sigma}G^{\rho\sigma}$. If gluon GPDs do not play any role in DVCS amplitude at LO, they do in DVMP. The latter also requires another

non-perturbative object, called Distribution Amplitude (DA), which describes the probability amplitude to create a meson, given the momentum fractions of the two quarks. This is illustrated on figure 1.6

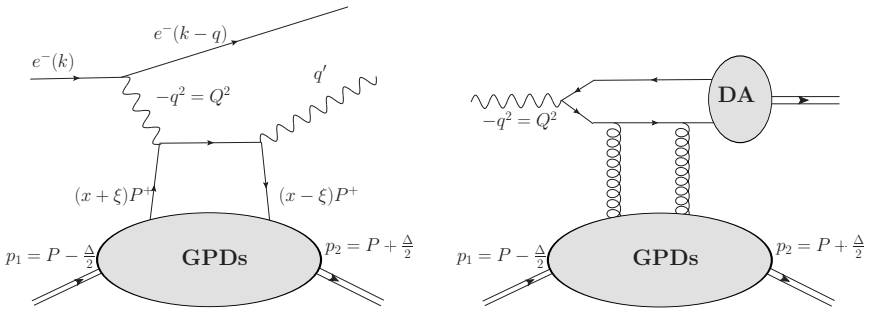

Figure 1.6: Left-hand side: One of the LO contribution of the quark GPDs to the DVCS amplitude. Right-hand side: One of the LO contribution of the gluon GPDs to the DVMP amplitude.

Equations (1.26), (1.27), (1.28) and (1.29) are relevant to define GPDs related to spin-1/2 hadrons. However, a significant part of the present work is devoted to the pion, whose relevant GPDs are defined as:

$$H_\pi^q(x,\xi,t) = \frac{1}{2}\int \frac{\mathrm{d}z^-}{2\pi} e^{ixP^+z^-} \langle p_2|\, \bar{\psi}^q\left(-\frac{z}{2}\right)\gamma^+\psi^q\left(\frac{z}{2}\right)|p_1\rangle\Big|_{z^+=z_\perp=0} \tag{1.30}$$

$$H_\pi^g(x,\xi,t) = \frac{1}{P^+}\int \frac{\mathrm{d}z^-}{2\pi} e^{ixP^+z^-} \langle p_2|\, G^{+\mu}\left(-\frac{z}{2}\right) G_\mu{}^+\left(\frac{z}{2}\right)|p_1\rangle\Big|_{z^+=z_\perp=0}. \tag{1.31}$$

The equivalents of $\tilde{H}^q$ and $\tilde{H}^g$ have to vanish due to discrete symmetries.

The Schwinger α-representation does not lead directly to GPDs, but rather to the so-called Double Distributions (DDs). Of course, as the same physics is described by those two non-perturbative objects there is a way to go from one to the other. The discussion on DDs and their relation to GPDs is left for chapter 2.

1.3 Generalised Parton Distributions: Properties

1.3.1 Support, continuity and interpretation

Just like in the case of PDFs, it is possible to perform an analysis of the analytic properties of the matrix elements defining the GPDs, and thus to deduce properties of GPDs themselves. In the lightcone gauge where $A^+ = 0$, the GPD H can be viewed as the projection of a off-shell parton-hadron scattering amplitude:

$$H(x,\xi,t) = \frac{1}{2}\int \mathrm{d}k^+\mathrm{d}^2k_\perp \delta\left(x - \frac{k^+}{P^+}\right)\int \mathrm{d}k^- \mathcal{A}(k) \tag{1.32}$$

with:

$$\mathcal{A}(k) = \int \mathrm{d}^4z e^{ik\cdot z}\left\langle P+\frac{\Delta}{2}\right|\mathrm{T}\left[\bar{\psi}\left(-\frac{z}{2}\right)\gamma^+\psi\left(\frac{z}{2}\right)\right]\left|P-\frac{\Delta}{2}\right\rangle, \tag{1.33}$$

T denoting time ordering. Following the arguments of Ref. [67], $\mathcal{A}$ depends on the following variables: t (fixed by the kinematics), $s = \left(P - \frac{\Delta}{2} - k_1\right)^2$, $u = \left(P + \frac{\Delta}{2} + k_1\right)^2$, $k_1^2 = (k - \frac{\Delta}{2})^2$

and $k_2^2 = (k + \frac{\Delta}{2})^2$. As done for instance in Ref. [67–69], we assume here that the analytic properties of the non-perturbative amplitude coincides with the ones given by a perturbative analysis through Feynman graphs. Therefore, cuts are expected in the s and u channel for non-negative $\Re(s)$ and $\Re(u)$, singularities for non-negative $\Re(k_1^2)$ and $\Re(k_2^2)$. Usually, those singularities are taken into account by adding a $-i\epsilon$ term, shifting them slightly below the real axis. In the case of equation (1.32), doing so regularise the integral over k^- and the amplitude $\mathcal{A}(k)$.

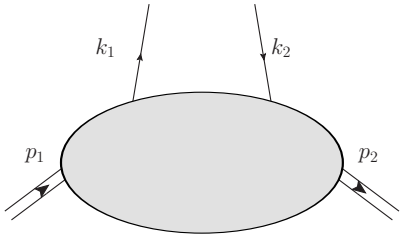

Figure 1.7: GPD as an off-shell scattering amplitude. As previously, $p_1 = P - \frac{\Delta}{2}$ and $p_2 = P + \frac{\Delta}{2}$.

In order to locate singularities of $\mathcal{A}(k)$ in the complex k^- plane, one can write k^- as:

$$s = \left(P - \frac{\Delta}{2} - k_1\right)^2 \quad \rightarrow \quad k^- = \frac{s + (k_\perp)^2}{2P^+(x-1)} + P^- \tag{1.34}$$

$$u = \left(P + \frac{\Delta}{2} + k_1\right)^2 \quad \rightarrow \quad k^- = \frac{u + (k_\perp)^2}{2P^+(x+1)} + P^- \tag{1.35}$$

$$k_1^2 = (k - \frac{\Delta}{2})^2 \quad \rightarrow \quad k^- = \frac{k_1^2 + \left(k_\perp - \frac{\Delta_\perp}{2}\right)^2}{2(x+\xi)P^+} + \frac{\Delta}{2}^- \tag{1.36}$$

$$k_2^2 = (k + \frac{\Delta}{2})^2 \quad \rightarrow \quad k^- = \frac{k_2^2 + \left(k_\perp + \frac{\Delta_\perp}{2}\right)^2}{2(x-\xi)P^+} - \frac{\Delta}{2}^- . \tag{1.37}$$

Due to the regularisation, poles and cuts of $\mathcal{A}(k)$ have now imaginary parts proportional to $-i\epsilon$. For instance, a pole originally located at $k_2^2 = q^2$ is now shifted at $q^2 - i\epsilon$. Fixing ξ such as $\xi \in [-1, 1]$, it is possible to locate the singularities in the complex plan with respect to the value of x. Indeed, the previous denominators change sign for $x = 1$, $x = -1$, $x = -\xi$ and $x = \xi$. Consequently, it appears that for $|x| > 1$, all the possible singularities are in the same half-part of the complex plane (below the real axis), and thus one can close the integration contour without including any singularities, as shown on figure 1.8. Therefore, providing that $\mathcal{A}$ vanishes sufficiently fast at infinity, the GPD is zero for $|x| > 1$. Then for all the different regions delimited by the change of signs in the denominators, looking carefully at the integration contour, it is possible to show that using or not using the time-ordered product leads to the same results [67].

Concerning the GPDs themselves (equation (1.26)) it is interesting to see what is going on when $\Delta = 0$, *i.e.* when the incoming and outgoing protons carry the same momenta:

$$H^q(x,0,0)\frac{\bar{u}(P)\gamma^+ u(P)}{2P^+} = \frac{1}{2}\int \frac{\mathrm{d}z^-}{2\pi} e^{ixP^+z^-} \left\langle P\right| \bar{\psi}^q\left(-\frac{z}{2}\right)\gamma^+\psi^q\left(\frac{z}{2}\right)\left|P\right\rangle\Big|_{z^+=z_\perp=0}. \tag{1.38}$$

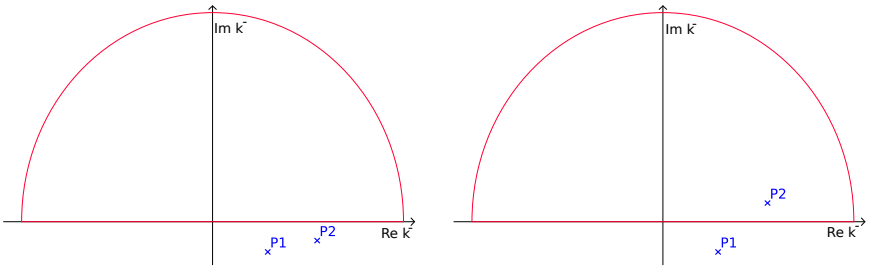

Figure 1.8: Momentum complexe plane integration. Left-hand side: $x > 1$; all poles and cuts are below the real axis, allowing integration around the upper half plan and leading to a vanishing GPD. Right-hand side: $-1 < x < 1$; poles and cuts are spread in the entire plane, leading to a non vanishing GPD.

As $\bar{u}(P)\gamma^+ u(P) = 2P^+$ in the infinit momentum frame, one realises that this matrix element is the one defining PDFs (equation (1.19)) and thus that:

$$H^q(x,0,0) = q(x) \quad \text{for } x \geq 0, \tag{1.39}$$
$$H^q(x,0,0) = -\bar{q}(-x) \quad \text{for } x \leq 0. \tag{1.40}$$

In addition to the PDFs, GPDs also contain the quark contribution to the form factors F_1 and F_2 defined in equation (1.3). For a spin-1/2 targets, integrating the GPDs H and E leads to:

$$\int_{-1}^{1} \mathrm{d}x\ H^q(x,\xi,t) = F_1^q(t) \quad , \quad \int_{-1}^{1} \mathrm{d}x\ E^q(x,\xi,t) = F_2^q(t). \tag{1.41}$$

Another interesting analytic property is the continuity at the point $x = \xi$. Continuity is required for the sake of factorisation. Indeed, if the GPDs were not continuous, logarithmic divergences would arise when computing observables (see section 1.4 for details). Therefore, consistency requires the GPDs to be continuous at $x = \xi$. The points $x = \pm\xi$ also play an important role in terms of the interpretation. Indeed, as shown on figure 1.9 for the quark GPD, one can see the virtual photon interacting with a quark ($\xi \leq x \leq 1$), with an anti-quark ($-1 \leq x \leq -\xi$) or with quark anti-quark pair ($-\xi \leq x \leq \xi$) [70–73].

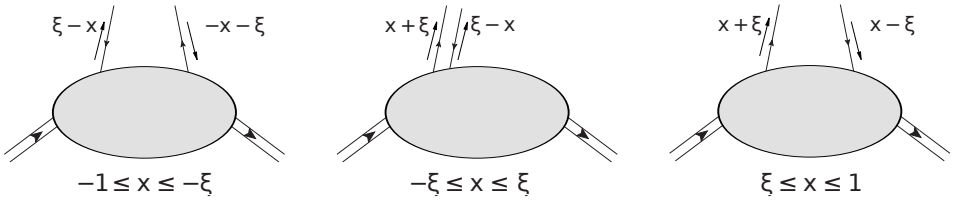

Figure 1.9: Different interpretations depending on the relative value of x and ξ respectively.

1.3.2 Mellin moments and symmetries

Discrete symmetries generate interesting GPD properties. In particular time reversal invariance constrains the GPDs to be even in ξ:

$$H^q(x,\xi,t) = H^q(x,-\xi,t) \quad , \quad E^q(x,\xi,t) = E^q(x,-\xi,t). \tag{1.42}$$

The same relations can be found for $\tilde{H}^q$, $\tilde{E}^q$, H^g, E^g, $\tilde{H}^g$ and $\tilde{E}^g$. This is expected as time reversal interchanges the initial and final states, *i.e.* interchanges the momenta in the definition of Δ and thus of $\xi = \frac{p_2^+ - p_1^+}{p_2^+ + p_1^+}$ leading to a additional minus sign. Details are given in appendix D. Another important point concerns the consequences of hermiticity. Taking the hermitian conjugate of the non-local matrix element (1.26) leads to:

$$[H(x,\xi,t)]^* = H(x,-\xi,t) \quad , \quad [E(x,\xi,t)]^* = E(x,-\xi,t), \tag{1.43}$$

which together with the time reversal results (1.42) force the GPDs to be real.

Beyond the form factors, it is also possible to relates higher Mellin moments $\mathcal{M}_m(\xi,t)$ defined as:

$$\mathcal{M}_m(\xi,t) = \int_{-1}^{1} \mathrm{d}x \; x^m H(x,\xi,t), \tag{1.44}$$

to local operators. Indeed, integrating the local matrix element of equation (1.26) in the lightcone gauge yields:

$$\begin{aligned}
& \int \mathrm{d}x \; x^m \frac{1}{2} \int \frac{\mathrm{d}z^-}{2\pi} e^{ixP^+z^-} \left\langle p_2 \right| \bar{\psi}^q \left(-\frac{z}{2}\right) \gamma^+ \psi^q \left(\frac{z}{2}\right) \left| p_1 \right\rangle \Big|_{z^+=z_\perp=0} \\
= \; & \frac{1}{2(iP^+)^m} \int \frac{\mathrm{d}z^-}{2\pi} \frac{\partial^m}{\partial z^{-m}} \left[\int \mathrm{d}x \; e^{ixP^+z^-} \right] \left\langle p_2 \right| \bar{\psi}^q \left(-\frac{z}{2}\right) \gamma^+ \psi^q \left(\frac{z}{2}\right) \left| p_1 \right\rangle \Big|_{z^+=z_\perp=0} \\
= \; & \frac{1}{2(iP^+)^{m+1}} \int \mathrm{d}z^- \frac{\partial^m}{\partial z^{-m}} \left[\delta\left(z^-\right) \right] \left\langle p_2 \right| \bar{\psi}^q \left(-\frac{z}{2}\right) \gamma^+ \psi^q \left(\frac{z}{2}\right) \left| p_1 \right\rangle \Big|_{z^+=z_\perp=0} \\
= \; & \frac{1}{2(P^+)^{m+1}} \left\langle p_2 \right| \bar{\psi}^q \left(0\right) \gamma^+ \left(i \overleftrightarrow{\partial^+}\right)^m \psi^q \left(0\right) \left| p_1 \right\rangle ,
\end{aligned} \tag{1.45}$$

where $\overleftrightarrow{\partial}^+ = \frac{\overrightarrow{\partial}^+ - \overleftarrow{\partial}^+}{2}$. In other gauges than the lightcone one, the gauge link generates a covariant derivative $\overleftrightarrow{D}$ instead of a partial one. Equation (1.45) also suggests to define a typical operator:

$$O^{\{\mu\mu_1 \ldots \mu_m\}} = \bar{\psi} \gamma^{\{\mu} i \overleftrightarrow{D}^{\mu_1} \ldots i \overleftrightarrow{D}^{\mu_m\}} \psi \tag{1.46}$$

with $\{...\}$ meaning that the operator is taken completely symmetrised and that the traces are removed. Defining the twist τ as the difference between the dimension d in mass units and the spin s:

$$\tau = d - s, \tag{1.47}$$

$O^{\{\mu\mu_1 \ldots \mu_m\}}$ is the twist-two operator of spin m. Within the Wilson OPE formalism [74] those local operators appear in the Taylor expansion of the non-local one along the lightcone [62, 75].

They can be parameterised as:

$$\begin{aligned}
\left\langle p_2 \right| O^{\{\mu\mu_1 \ldots \mu_m\}} \left| p_1 \right\rangle \; = \; & \bar{u}(p_2) \gamma^{\{\mu} u(p_1) \sum_{i=0}^{\left[\frac{m}{2}\right]} A^q_{m+1,2i}(t) \left(-\frac{\Delta}{2}^{\mu_1}\right) \ldots \left(-\frac{\Delta}{2}^{\mu_{2i}}\right) P^{\mu_{2i+1}} \ldots P^{\mu_m\}} \\
& + \bar{u}(p_2) \frac{\sigma^{\{\mu\alpha} \Delta_\alpha}{2M} u(p_1) \sum_{i=0}^{\left[\frac{m}{2}\right]} B^q_{m+1,2i}(t) \Delta^{\mu_1} \ldots \Delta^{\mu_{2i}} P^{\mu_{2i+1}} \ldots P^{\mu_m\}} \\
& - \mathrm{mod}(2,m) \bar{u}(p_2) \frac{\Delta^{\{\mu}}{2M} u(p_1) C^q_{m+1}(t) \left(-\frac{\Delta}{2}^{\mu_1}\right) \ldots \left(-\frac{\Delta}{2}^{\mu_m\}}\right),
\end{aligned} \tag{1.48}$$

where the even powers of ξ are selected by the time reversal invariance. $\mathrm{mod}(2,m)$ vanishes if m is even, and is 1 if m is odd, $[\cdot]$ is the floor function. As $\xi = -\frac{\Delta\cdot n}{2P\cdot n}$, it is straitforward to see that those local matrix elements are polynomials in ξ. Considering the Gordon identity relating the different Dirac structure among them, one gets:

$$\int \mathrm{d}x\ x^m H(x,\xi,t) = \sum_{j=0}^{\left[\frac{m}{2}\right]} \xi^{2j} A^q_{m+1,2i}(t) + \mathrm{mod}(m,2)\xi^{m+1} C^q_{m+1}(t), \tag{1.49}$$

$$\int \mathrm{d}x\ x^m E(x,\xi,t) = \sum_{j=0}^{\left[\frac{m}{2}\right]} \xi^{2j} B^q_{m+1,2i}(t) - \mathrm{mod}(m,2)\xi^{m+1} C^q_{m+1}(t). \tag{1.50}$$

This is the famous polynomiality property of the GPDs. The A^q, B^q and C^q are sometimes called generalised form factors. The polynomiality property comes from the decomposition of the local matrix elements (1.48) in terms of those generalised form factors. This decomposition encodes the Lorentz symmetry and so does the polynomiality property.

It is worth stressing that being given a full set of Mellin moments, it is possible to associate it to a unique function f providing that f is continuous on a segment. This is a consequence of the Stone-Weierstraß theorem. Thus it is possible to recover the original function from the Mellin moments.

1.3.3 Positivity

If polynomiality is a key property of GPDs coming from Lorentz invariance, the positivity property comes directly from wave function considerations and the Cauchy-Schwartz inequality. Indeed, considering the scalar case at $t = 0$, the GPD H can be described as:

$$H(x,\xi) = \sum_S \langle \Psi_{\mathrm{out}}(x,\xi,S) |\, \Psi_{\mathrm{in}}(x,\xi,S)\rangle, \tag{1.51}$$

where $\Psi_{\mathrm{in}}(x,\xi,S)$ is the probability amplitude that the considered hadron splits in a quark carrying a $x+\xi$ momentum fraction along the average direction P^+, and a spectator S. In the same way, $\Psi_{\mathrm{out}}(x,\xi,S)$ is the probability density that a quark with a momentum fraction $x-\xi$ recombines with the spectator S to give back the considered hadron. This decomposition of the GPDs in terms of wave functions has been derived in the lightcone quantisation framework [72] (see appendix E) and is detailed in chapter 5. From equation (1.51), applying the Cauchy-Schwarz inequality, one gets [76]:

$$\left|\sum_S \langle \Psi_{\mathrm{out}}(x,\xi,S) |\, \Psi_{\mathrm{in}}(x,\xi,S)\rangle\right|^2 \leq \sum_S \langle \Psi_{\mathrm{out}}(x,\xi,S) |\, \Psi_{\mathrm{out}}(x,\xi,S)\rangle \sum_{S'} \left\langle \Psi_{\mathrm{in}}(x,\xi,S') \right|\, \Psi_{\mathrm{in}}(x,\xi,S')\rangle. \tag{1.52}$$

Defining the variables x_1 and x_2 as:

$$x_1 = \frac{x-\xi}{1-\xi} = \frac{k_2^+}{p_2^+} \quad , \quad x_2 = \frac{x+\xi}{1+\xi} = \frac{k_1^+}{p_1^+}, \tag{1.53}$$

which are the momentum fractions of the quark interacting with respectively the outgoing and incoming hadrons, it is possible to identify the PDFs:

$$\sum_{S} \langle \Psi_{\text{out}}(x,\xi,S)| \, \Psi_{\text{out}}(x,\xi,S)\rangle \;=\; q(x_1), \tag{1.54}$$

$$\sum_{S'} \big\langle \Psi_{\text{in}}(x,\xi,S')\big| \, \Psi_{\text{in}}(x,\xi,S')\rangle \;=\; q(x_2). \tag{1.55}$$

This leads to the following inequality between GPDs and PDFs:

$$H^q(x,\xi) \leq \sqrt{q(x_1)q(x_2)}. \tag{1.56}$$

An equivalent inequality can be derived for gluon distributions:

$$H^g(x,\xi) \leq \sqrt{(1-\xi^2)x_1x_2g(x_1)g(x_2)}. \tag{1.57}$$

Those results are neither limited to the scalar case nor to the GPD H, and can be extended to other hadrons and other GPDs [72, 77, 78] or to the so-called impact parameter space GPDs [79].

Both polynomiality and positivity are fundamental properties of the Generalised Parton Distributions, and thus must be fulfilled in order to expect agreement on ξ-dependent observables. If different ways of modeling GPDs ensure automatically either polynomiality (see chapter 2) or positivity (see chapter 5), it remains hard to fulfil both at the same time [80, 81], despite attempts to create a framework ensuring both properties [82]. However it must be added that one type of Ansatz for the wave function allows to fulfil both [83, 84].

1.3.4 Evolution

Just like PDFs, GPDs depend on renormalisation and factorisation scales. The behaviour of GPDs with respect to the factorisation scale can be perturbatively computed at a given order. In this framework, quark and gluon GPDs *a priori* mix between each other. But it is possible to introduce linear combinations allowing one to deal with decoupled equations. Decoupled linear combinations are called non-singlet (NS), whereas coupled combinations are called singlet. One of the NS term can be defined as:

$$F^q_{NS}(x,\xi,t) = F^q(x,\xi,t) + F^q(-x,\xi,t), \tag{1.58}$$

which is also called the valence GPD due to its limit in the forward case. Such a combination has a fixed C-parity in the t-channel. In this case, $C=-1$, *i.e.* in the t-channel, exchanges have $C=-1$ parity. Evolving this combination, no $C=1$ exchanges can be added. Moreover, as gluons are their own anti-particles, gluon GPDs have a $C=1$ parity and thus they cannot be mixed with NS combinations. Due to the non-mixing with gluons, the NS GPDs obey an autonomous evolution equation:

$$\mu_F^2 \frac{\partial}{\partial \mu_F^2} F_{NS}(x,\xi,t) = \int \mathrm{d}y \frac{1}{|\xi|} K_{NS}\left(\frac{x}{\xi},\frac{y}{\xi}\right) F_{NS}(y,\xi,t), \tag{1.59}$$

where K_{NS} is called the NS evolution kernel.

Contrary to the NS case, the so-called singlet case defined as:

$$\sum_q \Big(F^q(x,\xi,t) - F^q(-x,\xi,t) \Big), \tag{1.60}$$

has a $C = 1$ parity in the t-channel, and thus gluon GPDs enter the computation of the singlet kernels through the exchange of two gluons in the t-channel producing a quark anti-quark pair. In order to deal with this mixing of quark and gluon contributions in the evolution kernel, it is convenient to introduce the vector $\boldsymbol{F}$:

$$\boldsymbol{F} = \begin{pmatrix} (2n_f)^{-1} \sum_q F^q(x,\xi,t) - F^q(-x,\xi,t) \\ F^g(x,\xi,t) \end{pmatrix}, \tag{1.61}$$

where n_f stand for the number of active flavour, and which fulfils a equation similar to equation (1.59) with a kernel $\boldsymbol{K}$:

$$\boldsymbol{K} = \begin{pmatrix} K^{qq}\left(\frac{x}{\xi},\frac{y}{\xi}\right) & K^{qg}\left(\frac{x}{\xi},\frac{y}{\xi}\right) \\ K^{gq}\left(\frac{x}{\xi},\frac{y}{\xi}\right) & K^{gg}\left(\frac{x}{\xi},\frac{y}{\xi}\right) \end{pmatrix}. \tag{1.62}$$

The evolution kernels K_{NS} and $\boldsymbol{K}$ can be computed perturbatively and are known at LO [62, 66, 85–92] and at NLO [93–97].

As it has been seen before in equations (1.39) and (1.40), GPDs reduce to PDFs in the forward limit (*i.e.* $\xi \to 0$). Consistently, the off-forward evolution kernels K_{NS} and $\boldsymbol{K}$ also reduce to the NS and singlet DGLAP kernels respectively. When $\xi \to 1$, the off-forward evolution kernels reduce to other well-known quantities. Indeed, one gets back the famous ERBL kernels [98–102] which describe the evolution of DAs. DAs will be introduced in further details in chapter 2.

Solving those equations is crucial for phenomenological applications. To proceed, one can either choose a numerical approach and use algorithms based for instance on Runge-Kutta methods, like the author of Ref. [103]. Or it is also possible to try through OPE to diagonalise those equations. This method is a classical way to evolve PDFs, as their Mellin moments $q_m(\mu_F)$ are directly related to local twist-two operators:

$$q_m(\mu_F) = \int \mathrm{d}x\; x^m q(x,\mu_F) = n_\mu n_{\mu_1} \cdots n_{\mu_m} \langle P| O^{\{\mu\mu_1\cdots\mu_m\}} |P\rangle . \tag{1.63}$$

Using the fact that the structure function $F_1(x,Q)$ defined at equation (1.15) is observable, and thus neither itself nor its Mellin moments depend on μ_F, one gets the following differential equation:

$$\mu_F \frac{\mathrm{d}}{\mathrm{d}\mu_F} \ln\left(q_m(\mu_F)\right) = -\gamma_m(\alpha_s(\mu_F^2)) \tag{1.64}$$

in the non-singlet case. α_s is the strong coupling constant and γ_m is the NS anomalous dimension. The singlet case is similar, and details can be found for instance in Ref. [37]. The operators $O^{\{\mu\mu_1\cdots\mu_m\}}$ do not mix with each other and support multiplicative renormalisation. Therefore, Mellin moments of PDFs evolve independently from each other within a multiplicative framework from the scale μ_F^0 to μ_F^1:

$$q_m(\mu_F^1) = q_m(\mu_F^0) \exp\left(-\frac{1}{2} \int_0^{2\ln\left(\frac{\mu_F^1}{\mu_F^0}\right)} \mathrm{d}t \gamma_m\left(\alpha_s\left[(\mu_F^0)^2 e^t\right]\right) \right). \tag{1.65}$$

The same approach can be used for GPDs, but using different local operators and thus different moments. Indeed, as soon as $\xi \neq 0$, GPD Mellin moments mix themselves through evolution equations. The same mixing problem has been stressed even for simpler objects like

DAs [98, 100–102]. But in this case, it has been proved that at LO, evolution equations can be diagonalised providing that one considers the so-called twist-two conformal operators:

$$\mathcal{O}_m^q = (\partial^+)^m \bar{\psi}^q \gamma^+ C_m^{3/2}\left(\frac{\overrightarrow{D}^+ - \overleftarrow{D}^+}{\overrightarrow{\partial}^+ + \overleftarrow{\partial}^+}\right)\psi^q, \tag{1.66}$$

where $C_m^{3/2}$ is the $\frac{3}{2}$-Gegenbauer polynomial of degree m. It should be noticed that the derivative at the denominators cancel with the one in front of the expression, leading to a well-defined expression. The importance of conformal moments here is not a coincidence. Indeed, the QCD Lagrangian fulfils conformal symmetry at a classical level. Consequently, the fact that the evolution equations are diagonalised on a basis of conformal operators testifies the presence of conformal symmetry. However, conformal symmetry is broken by quantisation. As quantum fluctuations introduce UV divergences, an intrinsic scale, the renormalisation scale and a renormalisation condition are needed to properly define the theory. The coupling constant varies with this scale, breaking the conformal symmetry. Thus, when taking into account quantum fluctuations, the multiplicative renormalisation of the conformal operators (1.66) have to break down at some point. This is the case at NLO, as they start mixing with each others.

Those arguments of conformal theory are detailed for instance in Ref. [69, 104] and can also be applied to GPDs. Indeed, defining GPDs conformal moments $\mathcal{C}_m^q(\xi,t)$ as:

$$\mathcal{C}_m^q(\xi,t) = \xi^m \int_{-1}^{1} \mathrm{d}x\; C_m^{3/2}\left(\frac{x}{\xi}\right) H^q(x\xi,t) \tag{1.67}$$

for quarks, and as:

$$\mathcal{C}_m^g(\xi,t) = \xi^{m-1} \int_{-1}^{1} \mathrm{d}x\; C_{m-1}^{5/2}\left(\frac{x}{\xi}\right) H^g(x\xi,t) \tag{1.68}$$

for gluons, they diagonalise the evolution equations of GPDs at LO.

1.3.5 Hadron 3D tomography

Just like PDFs, GPDs can be seen as projections of Wigner Distributions. Indeed, integrating equation (1.25) over $k_\perp$ leads to:

$$\begin{aligned}&\int \frac{\mathrm{d}^2\mathbf{k}_\perp}{(2\pi)^2} W_{\gamma^+}(\mathbf{r}, k^+, \mathbf{k}_\perp)\\ =\;& \frac{1}{2M}\int \frac{\mathrm{d}^3\mathbf{q}}{(2\pi)^3} e^{-i\mathbf{q}\cdot\mathbf{r}} \int \mathrm{d}z^- e^{ik^+z^-} \left\langle \frac{q}{2}\middle| \bar{\psi}\left(-\frac{z}{2}\right)\gamma^+\psi\left(\frac{z}{2}\right)\middle| -\frac{q}{2}\right\rangle\Big|_{z^+=\mathbf{z}_\perp=0},\end{aligned} \tag{1.69}$$

which is the Fourier transform of the GPDs (up to an overall factor) for $q = \Delta$. This suggests that GPDs are related to quark and gluon multidimensional probability densities. But as stressed already for Wigner Distributions, GPDs are not positive definite and thus the probabilistic interpretation is not straightforward. However, as it has been shown in Ref. [50], it is possible to get a true probabilistic interpretation at $\xi = 0$. More precisely, defining:

$$\rho^q(x,\mathbf{b}_\perp) = \int \frac{\mathrm{d}^2\Delta_\perp}{(2\pi)^2} e^{-i\mathbf{b}_\perp\Delta_\perp} H^q(x,0,-\Delta_\perp^2), \tag{1.70}$$

$\rho^q(x, \mathbf{b}_\perp)$ can be seen as the probability density to find a quark of flavour q carrying a given fraction x of the hadron momentum along the lightcone, and at a given position $\mathbf{b}_\perp$ in the transverse plane to this lightcone direction. An example of probability density is shown on figure 1.10.

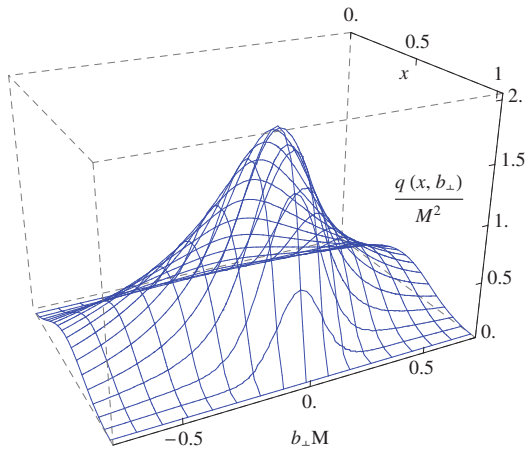

Figure 1.10: Transverse plane density of the pion GPD. 3D-plot of $\rho^q(x, \mathbf{b}_\perp)$ coming from Ref. [105].

1.4 GPD extraction

Focusing on the DVCS process, one can split the full Compton amplitude in eight contributions coming from the different quark and gluon GPDs. Those contributions are called Compton Form Factors (CFF) and are convolutions of the different GPDs with their respective hard parts. More explicitly, denoting $\mathcal{F}$ the CFF:

$$\mathcal{F}^{(i)}(\xi, t) = \int_{-1}^{1} \mathrm{d}x \; C^{(i)}(x, \xi) F^{(i)}(x, \xi, t), \tag{1.71}$$

where (i) denotes the different types of GPDs $F^{(i)}$ of quarks and gluons. $C^{(i)}$ stands for the hard part associated with the GPD $F^{(i)}$ and depending on the considered process. Dependencies in Q^2, renormalisation and factorisation scales of GPDs and hard parts are omitted here for brevity. Focusing on the GPD H, one can write its associated CFF $\mathcal{H}$ at LO as:

$$\mathcal{H}(\xi, t) = \int_{-1}^{1} \mathrm{d}x \; \left(\frac{1}{\xi - x - i\epsilon} - \frac{1}{\xi + x - i\epsilon} \right) H(x, \xi, t). \tag{1.72}$$

Due to the singularities at $x = \pm\xi$, the CFF $\mathcal{H}(\xi, t)$ is a complex number. It is possible to relate its real and imaginary parts to the GPD as:

$$\Re\left(\mathcal{H}(\xi, t)\right)|_{\mathrm{LO}} = \mathrm{p.v.} \int_{-1}^{1} \mathrm{d}x \left(\frac{1}{\xi - x} - \frac{1}{\xi + x} \right) H(x, \xi, t), \tag{1.73}$$

$$\Im\left(\mathcal{H}(\xi, t)\right)|_{\mathrm{LO}} = \pi \left(H(\xi, \xi, t) - H(-\xi, \xi, t) \right), \tag{1.74}$$

where p.v stand for the Cauchy principal value prescription. It should also be noticed that at LO, gluons do not play any role in the DVCS amplitude and therefore $C^g_{\mathrm{LO}} = \tilde{C}^g_{\mathrm{LO}} = 0$. Contrary to the DIS case where the PDFs are accessible directly at LO (see equations (1.12) and (1.13)), only the line $x = \xi$ of the entire GPDs phase space is directly accessible at LO through the imaginary part of the CFF $\mathcal{H}$. The real part is already a convolution.

Nonetheless, the extraction of the CFFs themselves is challenging. Considering the four GPDs previously introduced, one has *a priori* eight quantities to extract (real and imaginary parts). Yet, existing dispersion relations between real and imaginary parts of the CFFs reduce this number to four. Still, it remains a hard task as few data are actually available. Extraction techniques have been developed in order to fit CFFs to available data using least square minimisation. Two approaches can be highlighted: a local fit which considers CFFs as free parameters [106] and a global fit which parameterises the CFFs through a generic functional form of the GPD [107–109]. The former method has the advantage to be model-independent apart from the twist-two approximation, but is hardly suitable for extrapolation and hard to interpret. The latter can be extrapolated providing a suitable parameterisation, but carries an intrinsic model-dependence through the functional parameterisation. A third pioneering way is actually explored, which consists in extracting the CFFs using neural networks [110].

In addition to the difficulty of extracting CFFs, one should keep in mind that, just like in the case of DIS and PDFs, the interpretation of data in terms of GPDs becomes even harder at NLO. NLO corrections for DVCS are now well-known [111–117] and their effects are truly significant on CFFs [118]. One of the possible explanations is the role played by the gluon GPDs which do not appear at LO (see figure 1.11) and bring brand new contributions rather than a correction to the leading one. The importance of the gluon effects in the DVCS has motivated people to resum higher-order contributions. This has been done in the quark sector [119], and is still an ongoing work in the gluon sector. Resummation is also important due to the possible dependence of the CFF on the factorisation scale at NLO. The selection of the relevant factorisation scale and the understanding of such a dependence on CFF remain open questions.

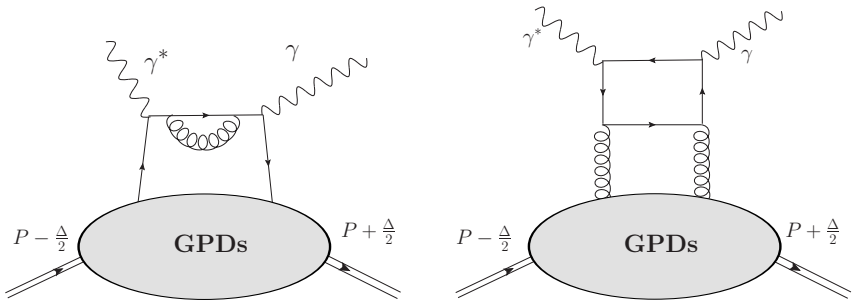

Figure 1.11: Example of possible NLO corrections. Left-hand side: quark GPD contribution. Right-hand side: gluon GPD contribution.

Data interpretation can also be challenged by the so-called target mass corrections. Indeed, the interpretation requires Q^2 to be large compared to any other energy scale of the process. Yet, as shown on figure 1.13, the current available DVCS data have been taken for values of $Q^2 \simeq 2$ GeV^2, except for H_1 and ZEUS data. Compared to the proton mass $M^2 \simeq 1$ GeV^2, the ratio between those two mass scales is not that small, generating correction depending on M^2/Q^2 (or t/Q^2). If this point was well-known for DIS [120, 121], those kind of corrections

have been computed only recently for exclusive processes [122, 123]. In the case of DVCS, the correction are significant, as shown in recent study [124] and illustrated on figure 1.12

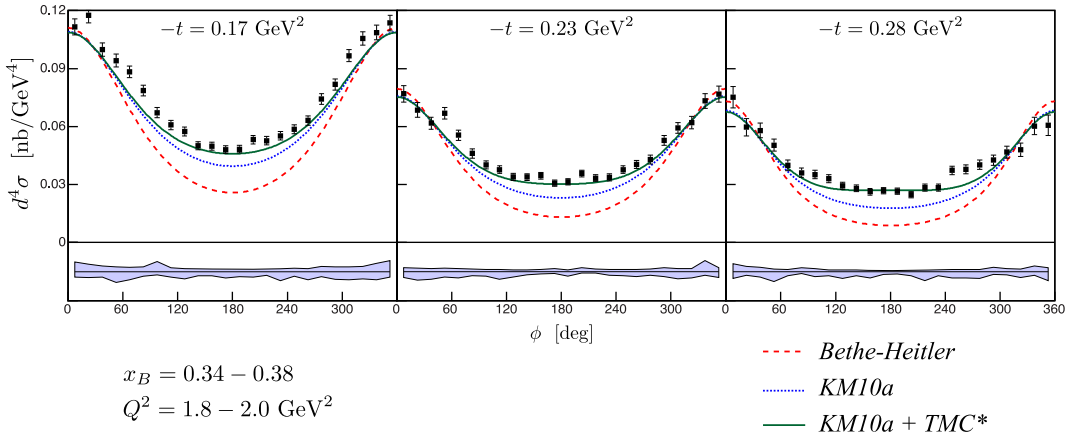

Figure 1.12: Effect of target mass corrections on DVCS unpolarised cross sections [124]. The model KM10a has been developed is the one of Ref. [108], and the target mass corrections derived in Ref. [122, 123] have been computed thanks to the KMS model of Ref. [125].

Several sets of data have been produced in the last 15 years both in fixed target and collider configurations. Collider results probe the small-x_B region as shown on figure 1.13, whereas fixed target experiments probe large to medium values of x_B. Among the latter, the HERMES collaboration has provided the community with asymmetries varying both the beam polarisation and the target polarisation. Within normalised notations [125], A_{BT} stands for the asymmetry measured with a beam polarisation B and a target polarisation T. The HERMES collaboration was able to measure all the independent DVCS observables, except cross-sections (see *e.g.* [126, 127] for a exhaustive description of the available data). DVCS cross-sections have been measured at Jefferson Laboratory (JLab), and published by the Hall-A [129] and CLAS [130] collaborations in addition to asymmetries measured by the CLAS collaboration [131]. Moreover, a recent reanalysis of the Hall-A data [124] suggests that target mass corrections are important when dealing with JLab kinematics.

Concerning future experiments, on a short time scale the upgrade of JLab from 6 GeV to 12 GeV energy beam should increase significantly both the kinematic range of available data and their precision, challenging our understanding of nucleon structure. On a longer time scale, an Electron-Ion Collider (EIC) should fill the gap between the current and future fixed target experiments, and the small-x data obtained by the ZEUS and H_1 collaborations.

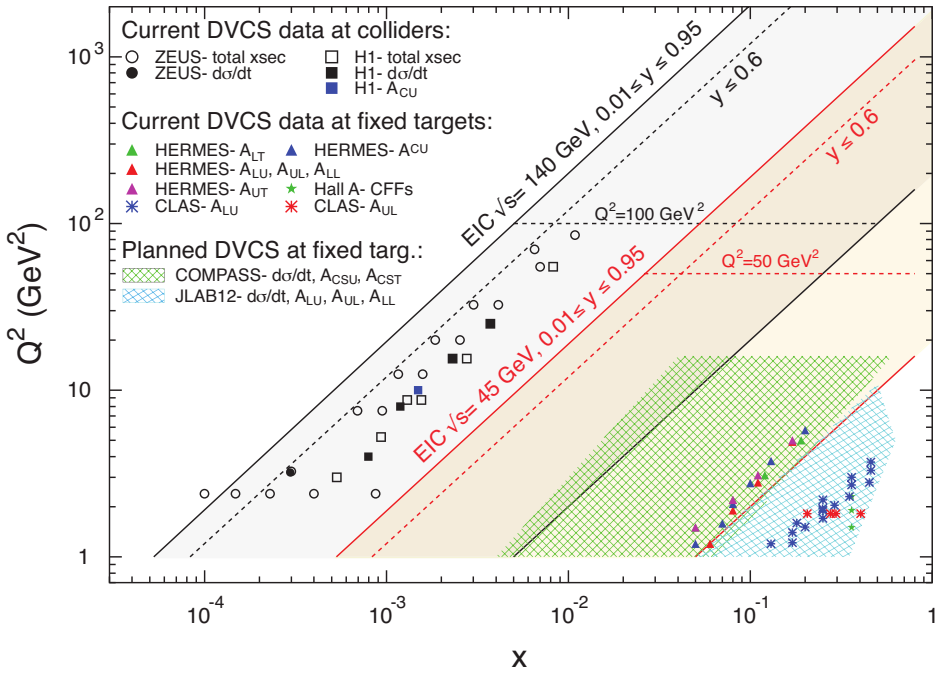

Figure 1.13: Existing DVCS measurement and planned experiements. Figure from EIC white paper [128].

Chapter 2

The Double Distributions Approach

«To succeed, planning alone is insufficient.
One must improvise as well.»
Isaac Asimov in *Fundation*.

2.1 Definitions and properties

As mentioned in section 1.2.2, when factorising exclusive processes, Generalised Parton Distributions are not the only way to parameterise the considered non-local matrix elements. The α parameterisation leads to another non-perturbative object called Double Distributions (DDs). Introduced at the same time as GPDs[1] [62, 65, 66, 132], they encode the information contained in a non-local matrix element as:

$$\begin{aligned}\left\langle P+\frac{\Delta}{2}\middle|\,\bar{q}\left(-\frac{z}{2}\right)\gamma_\mu q\left(\frac{z}{2}\right)\middle|P-\frac{\Delta}{2}\right\rangle\Big|_{z^2=0} &= 2P_\mu\int_\Omega \mathrm{d}\beta\mathrm{d}\alpha\, e^{-i\beta(P\cdot z)+i\alpha\frac{(\Delta\cdot z)}{2}}F^q(\beta,\alpha,t)\\ &\quad -\Delta_\mu\int_\Omega \mathrm{d}\beta\mathrm{d}\alpha\, e^{-i\beta(P\cdot z)+i\alpha\frac{(\Delta\cdot z)}{2}}G^q(\beta,\alpha,t)\\ &\quad +\text{ higher twist terms,}\end{aligned} \tag{2.1}$$

for a scalar hadron. $F^q(\beta,\alpha,t)$ and $G^q(\beta,\alpha,t)$ denote the two quark DDs. The analphabetic order of variables α and β follows the convention of Ref. [133]. Historically, the DD $G^q(\beta,\alpha,t)$ was first overlooked, then introduced under a specific form in Ref. [134] and generalised in Ref. [135]. Equivalent relations can be introduced for the different operators introduced in section 1.2.2, defining the corresponding DDs. In the case of a spin-1/2 hadron, the additional

[1] In Ref. [62], DDs are called "spectral functions".

Lorentz structure leads to an additional DD denoted $K^q(\beta,\alpha,t)$:

$$\begin{aligned}\left\langle P+\frac{\Delta}{2}\middle|\,\bar{q}\left(-\frac{z}{2}\right)\gamma_\mu q\left(\frac{z}{2}\right)\middle|P-\frac{\Delta}{2}\right\rangle\Big|_{z^2=0} &= \bar{u}\left(P+\frac{\Delta}{2}\right)\\ &\left[\gamma_\mu\int_\Omega \mathrm{d}\beta\mathrm{d}\alpha\, e^{-i\beta(P\cdot z)+i\alpha\frac{(\Delta\cdot z)}{2}}F^q(\beta,\alpha,t)\right.\\ &+\frac{i\sigma_{\mu\nu}\Delta^\nu}{2M}\int_\Omega \mathrm{d}\beta\mathrm{d}\alpha\, e^{-i\beta(P\cdot z)+i\alpha\frac{(\Delta\cdot z)}{2}}K^q(\beta,\alpha,t)\\ &\left.-\frac{\Delta_\mu}{2M}\int_\Omega \mathrm{d}\beta\mathrm{d}\alpha\, e^{-i\beta(P\cdot z)+i\alpha\frac{(\Delta\cdot z)}{2}}G^q(\beta,\alpha,t)\right]\\ &\times u\left(P-\frac{\Delta}{2}\right)+\text{ higher twist terms.}\end{aligned}\tag{2.2}$$

As shown on figure 2.1, both variable β and α have an interpretation in terms of parton and hadron momenta. In the forward case, *i.e.* $\Delta=0$, the variable β can be directly identified with the PDF momentum fraction x. On the other hand, when $P=0$ the diagram on figure 2.1 looks like the one of a DA, allowing one to relate α with a DA parameter.

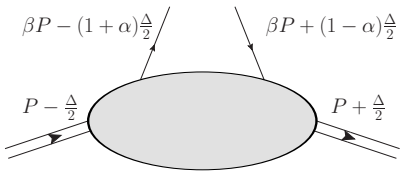

Figure 2.1: Momenta associated with hadrons and partons within a DD framework.

The α variable plays also an important role in terms of discrete symmetries. Indeed the analysis of time reversal invariance detailed in appendix D leads to definite parities in α for the DDs $F^q(\beta,\alpha,t)$, $K^q(\beta,\alpha,t)$ and $G^q(\beta,\alpha,t)$, as it was the case for the GPDs in terms of the variable ξ (equation (1.42). More precisely one gets:

$$\left\{\begin{array}{rcl}F^q(\beta,-\alpha,t) &=& F^q(\beta,\alpha,t)\\ K^q(\beta,-\alpha,t) &=& K^q(\beta,\alpha,t)\end{array}\right.,\qquad G^q(\beta,-\alpha,t)=-G^q(\beta,\alpha,t).\tag{2.3}$$

The Double Distributions depend on two adimensional variables juste like in the case of the GPDs and those variables live on a compact support Ω. The latter is defined by the following constraint:

$$\Omega=\{(\beta,\alpha),\ |\beta|+|\alpha|\leq 1\},\tag{2.4}$$

and is illustrated on figure 2.2. The proof of the DDs' support property is achieved using the α-representation of Feynman diagrams (see *e.g.* Ref. [66]).

Encoding the non-perturbative information contained in an exclusive process, DDs depend on a factorisation scale μ_R. Consequently, they obey evolution equations [62, 65, 66, 132] similar to equation (1.59). And once again, it is possible to define singlet and non-singlet sectors. In the present work, the choice has been done to evolve GPDs rather than DDs (the relation between the two is given in the next section).

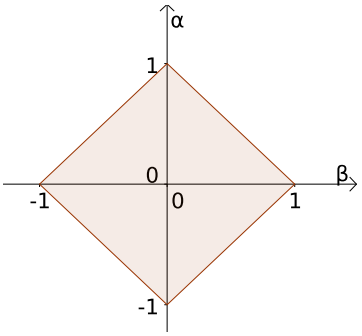

Figure 2.2: The rhombus defining the support of the Double Distributions in the (β, α) plane.

2.2 Recovering GPDs

2.2.1 Radon transform and operator product expansion

GPDs and DDs are Fourier transforms of the same operator. However, GPDs are single-dimensional Fourier transforms with respect to the variable z^- (1.26) assuming that $P \cdot z$ and $\Delta \cdot z$ are proportional to each other through the kinematics parameter ξ. Therefore, GPDs depend both on x, the conjugate variable of z^-, and ξ. On the other hand, DDs are two-dimensional Fourier transforms (equations (2.1) and (2.2)) of the considered light-front operator. Within the DD framework, $P \cdot z$ and $\Delta \cdot z$ are considered as independent and their Fourier conjugate variables are denoted β and α. Consequently the DDs do not depend on the kinematic parameter ξ. In the scalar case, the relation between GPDs and DDs comes from:

$$\begin{aligned}
H^q(x,\xi,t) &= \frac{1}{2}\int \frac{\mathrm{d}z^-}{2\pi} e^{ixP^+z^-} \left\langle p_2\right| \bar{\psi}^q\left(-\frac{z}{2}\right)\gamma^+\psi^q\left(\frac{z}{2}\right)\left|p_1\right\rangle\Big|_{z^+=z_\perp=0} \\
&= \frac{1}{2}\int \frac{\mathrm{d}z^-}{2\pi} e^{ixP^+z^-} 2P^+ \int_\Omega \mathrm{d}\beta\mathrm{d}\alpha\, e^{-i\beta(P^+z^-)+i\alpha\frac{(\Delta^+z^-)}{2}} \left(F^q(\beta,\alpha,t)+\xi G^q(\beta,\alpha,t)\right) \\
&= \int_\Omega \mathrm{d}\beta\mathrm{d}\alpha\, \left(F^q(\beta,\alpha,t)+\xi G^q(\beta,\alpha,t)\right) \int \frac{\mathrm{d}z^-}{2\pi}\, P^+ e^{iP^+z^-(x-\beta-\alpha\xi)} \\
&= \int_\Omega \mathrm{d}\beta\mathrm{d}\alpha\, \left(F^q(\beta,\alpha,t)+\xi G^q(\beta,\alpha,t)\right)\delta(x-\beta-\alpha\xi). \qquad (2.5)
\end{aligned}$$

The GPDs are therefore convolutions of the DDs with a Dirac δ. In a more geometrical point of view, the GPD $H^q(x,\xi,t)$ correspond of the DDs $F(\beta,\alpha,t)$ and $G(\beta,\alpha,t)$ integrated along a line of equation $x-\beta-\xi\alpha=0$ in the (β,α) plane. Mathematically, this kind of relation between two functions is known as the Radon Transform [136], and has revealed itself extremely convenient for tomography [137]. Considering a function f, its Radon transform $\mathcal{R}[f]$ is given by:

$$\mathcal{R}[f](s,\phi) = \int \mathrm{d}u\,\mathrm{d}v\, f(u,v)\delta(u\cos(\phi)+v\sin(\phi)-s). \qquad (2.6)$$

In the language of GPDs, $x=\frac{s}{\cos(\phi)}$ and $\xi=\tan(\phi)$. Mathematically, the Radon transform can be inverted, and thus it would be in principle possible to get back the Double Distributions from the GPDs. However, numerically inverting the Radon transform reveals itself technical in the case of GPDs. Consequently, the discussion on inversion of the equation (2.5) is left for

chapter 5. In the case of a spin-1/2 hadron, one has to use the Gordon identity:

$$\bar{u}(p_2)\gamma^\mu u(p_1) = \frac{1}{2M}\bar{u}(p_2)(2P^\mu + i\sigma^{\mu\nu}\Delta_\nu)u(p_1), \tag{2.7}$$

in order to reduce the number of tensorial structures from three to two. The most common choice is to include the $\bar{u}(p_2)u(p_1)$ into the two others, leading to:

$$H^q(x,\xi,t) = \int_\Omega \mathrm{d}\beta\mathrm{d}\alpha\ \left(F^q(\beta,\alpha,t) + \xi G^q(\beta,\alpha,t)\right)\delta(x-\beta-\alpha\xi), \tag{2.8}$$

$$E^q(x,\xi,t) = \int_\Omega \mathrm{d}\beta\mathrm{d}\alpha\ \left(K^q(\beta,\alpha,t) - \xi G^q(\beta,\alpha,t)\right)\delta(x-\beta-\alpha\xi). \tag{2.9}$$

One of the main advantages of DDs, is that they make the polynomiality property of the GPDs manifest. Indeed, computing the GPD Mellin moment:

$$\begin{aligned}\mathcal{M}_m(\xi,t) &= \int \mathrm{d}x\, x^m H(x,\xi,t)\\ &= \int \mathrm{d}x\, x^m \int_\Omega \mathrm{d}\beta\mathrm{d}\alpha\ \left(F^q(\beta,\alpha,t) + \xi G^q(\beta,\alpha,t)\right)\delta(x-\beta-\alpha\xi)\\ &= \int_\Omega \mathrm{d}\beta\mathrm{d}\alpha\,(\beta+\xi\alpha)^m\left(F^q(\beta,\alpha,t) + \xi G^q(\beta,\alpha,t)\right),\end{aligned} \tag{2.10}$$

one gets back a polynomial in ξ of degree at most $m+1$. The parity in ξ is controlled by the parity in α of the DDs $F(\beta,\alpha,t)$ and $G(\beta,\alpha,t)$. Consequently, any DD model fulfilling the parity property in α automatically generate a GPD fulfilling the polynomiality property and being even in ξ. This partly explains why DDs have been broadly used in order to model GPDs.

It is possible to go further by expanding equation (2.10):

$$\mathcal{M}_m(\xi,t) = \sum_{j=0}^{m}\binom{m}{j}\xi^j\int_\Omega \mathrm{d}\beta\mathrm{d}\alpha\,\alpha^j\beta^{m-j}\left(F^q(\beta,\alpha,t) + \xi G^q(\beta,\alpha,t)\right). \tag{2.11}$$

Comparing equation (2.11) with equation (1.49), it is possible to directly relate the generalised form factors with the bi-dimensional Mellin moments of the DDs. An equivalent relation holds for the GPD $E^q(x,\xi,t)$. However, those relations work in one direction only, *i.e.* being given the Mellin moments of the DDs, one can get back the generalised form factors, as it will be explained below.

2.2.2 The Double Distributions ambiguity

Coming back to equation (1.49) one can rewrite the $A^q_{m+1,2j}(t)$ as:

$$A^q_{m+1,2j}(t) = \frac{m!}{(2j)!(m-2j+1)!}\Big((m-2j+1)F^q_{m,2j} + (2j)G^q_{m,2j-1}\Big) \tag{2.12}$$

providing that $2j \neq 0$ and $2j \neq m+1$, else the generalised for factor depend only on one DD. Consequently, any but two generalised form factor are defined through both $F^q_{m,2j}$ and $G^q_{m,2j-1}$

which denote the Mellin moments of the Double Distributions $F^q(\beta,\alpha,t)$ and $G^q(\beta,\alpha,t)$ respectively:

$$F^q_{m,j}(t) = \int_{-1}^{1} \mathrm{d}\beta \int_{-1+|\beta|}^{1-|\beta|} \mathrm{d}\alpha\ \beta^{m-j}\alpha^j\ F^q(\beta,\alpha,t), \tag{2.13}$$

$$G^q_{m,j}(t) = \int_{-1}^{1} \mathrm{d}\beta \int_{-1+|\beta|}^{1-|\beta|} \mathrm{d}\alpha\ \beta^{m-j}\alpha^j\ G^q(\beta,\alpha,t). \tag{2.14}$$

It is therefore possible to define the following transformation:

$$F^q_{m,2j} \to F^q_{m,2j} + (2j)\sigma_{m,j}, \qquad G^q_{m,2j-1} \to G^q_{m,2j-1} - (m-2j+1)\sigma_{m,j}. \tag{2.15}$$

Consequently, the separation of $A^q_{m+1,2j}(t)$ in terms of Mellin moments of DDs is ambiguous. There are two exceptions:

- if $j = 0$, then the generalised form factor is completely defined through the Mellin moments of F:
$$A^q_{m+1,0}(t) = F^q_{m,0}(t), \tag{2.16}$$
- if $2j = m+1$, then the generalised form factor is called $C^q_{m+1}(t)$ and is related to the Mellin moments of G through:
$$C^q_{m+1}(t) = G^q_{m,m+1}(t). \tag{2.17}$$

The effects of this ambiguity on the Mellin moment of the DDs have also been studied directly on the DDs themself in Ref. [135] using the assumption that DDs vanish on the edges of the rhombus. The result have been generalised in Ref. [138] to the case of non-vanishing DDs at the boundaries of their support. As it will be shown below, for instance in equation (2.45), DDs vanishing on the boundaries of the rhombus are of phenomenological relevance. Therefore, only this case will be presented here. Contracting equation (2.1) with z^μ and then integrating it by parts, one gets:

$$\left\langle P+\frac{\Delta}{2}\middle|\,\bar{q}\left(-\frac{z}{2}\right) z\cdot\gamma q\left(\frac{z}{2}\right)\middle|P-\frac{\Delta}{2}\right\rangle\Big|_{z^2=0} = -2i\int_\Omega \mathrm{d}\beta\mathrm{d}\alpha\, e^{-i\beta(Pz)+i\alpha\frac{(\Delta z)}{2}} N^q(\beta,\alpha,t) \tag{2.18}$$

with

$$N^q(\beta,\alpha,t) = \frac{\partial F^q}{\partial\beta}(\beta,\alpha,t) + \frac{\partial G^q}{\partial\alpha}(\beta,\alpha,t). \tag{2.19}$$

It is here possible to make an analogy with electromagnetism. Denoting $G^q(\beta,\alpha,t) = A_\beta$, $F^q(\beta,\alpha,t) = -A_\alpha$ and $N^q(\beta,\alpha,t) = B_z$, one can write equation (2.19) as:

$$\boldsymbol{B} = \overrightarrow{\mathrm{rot}}\boldsymbol{A}. \tag{2.20}$$

Following this analogy, it is possible to add a gradient such that $\boldsymbol{B}$ remains unchanged. In other words, the following transformation:

$$F^q(\beta,\alpha,t) \to F^q(\beta,\alpha,t) + \frac{\partial\sigma^q}{\partial\alpha}(\beta,\alpha,t), \tag{2.21}$$

$$G^q(\beta,\alpha,t) \to G^q(\beta,\alpha,t) - \frac{\partial\sigma^q}{\partial\beta}(\beta,\alpha,t), \tag{2.22}$$

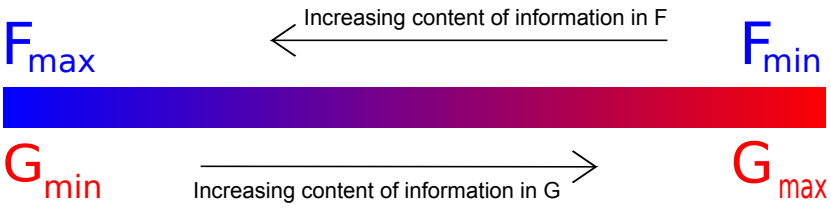

Figure 2.3: Representation of the DD ambiguity in terms of information exchange.

leaves the effective DD $N^q(\beta,\alpha,t)$ unchanged, providing that:

$$\sigma^q(\beta,-\alpha,t) = -\sigma^q(\beta,\alpha,t). \tag{2.23}$$

Consequently, the DDs $F^q(\beta,\alpha,t)$ and $G^q(\beta,\alpha,t)$ are not uniquely defined from the considered matrix element of equation (2.1). Note that due to the analogy with electromagnetism, the transformation of equations (2.21) and (2.22) is called "Double Distributions gauge transformation" (see *e.g.* Ref. [135] or Ref. [69]). In order to avoid confusion with the QCD gauge, the terminology chosen here is "choice of DD scheme" rather than "fixation of DD gauge".

The D-Term

Looking at equations (2.21) and (2.22), the DD ambiguity can also be seen as a choice to include the information content of the matrix element of equation (2.1) preferentially either into the DD $F^q(\beta,\alpha,t)$ or into the DD $G^q(\beta,\alpha,t)$. But, as highlighted in equations (2.16) and (2.17), it is not possible to absorb one completely into the other. For instance, it is possible to reduce the β dependence of the DD $G^q(\beta,\alpha,t)$ to Dirac δ. To do so, it is necessary to introduce the C-odd and C-even decomposition of the GPDs:

$$H^{q(+)}(x,\xi,t) = H^q(x,\xi,t) - H^q(-x,\xi,t), \tag{2.24}$$
$$H^{q(-)}(x,\xi,t) = H^q(x,\xi,t) + H^q(-x,\xi,t), \tag{2.25}$$

and their DD counterpart:

$$F^{q(\pm)}(\beta,\alpha,t) = F^q(\beta,\alpha,t) \mp F^q(-\beta,\alpha,t), \tag{2.26}$$
$$G^{q(\pm)}(\beta,\alpha,t) = G^q(\beta,\alpha,t) \mp G^q(-\beta,\alpha,t). \tag{2.27}$$

Then, it is possible to define a new scheme using the following transformation:

$$\sigma_D^{q(\mp)}(\beta,\alpha) = -\frac{1}{2}\left[\int_{-1+|\alpha|}^{\beta} d\beta' G^{q(\pm)}(\beta',\alpha) - \int_{\beta}^{1-|\alpha|} d\beta' G^{q(\pm)}(\beta',\alpha) - \frac{1\pm 1}{2}\,\mathrm{sgn}(\beta) D^q(\alpha)\right], \tag{2.28}$$

where:

$$D(\alpha) = \int_{|\alpha|-1}^{1-|\alpha|} \mathrm{d}\eta\, G^q(\eta,\alpha,t), \tag{2.29}$$

is the so-called Polyakov-Weiss D-term introduced in Ref. [134]. Within this scheme, the DDs reduce to:

$$F^q(\beta,\alpha,t) \to F^q_{\mathrm{DD+D}}(\beta,\alpha,t), \tag{2.30}$$
$$G^q(\beta,\alpha,t) \to D(\alpha,t)\delta(\beta). \tag{2.31}$$

In the following, this DD scheme will be denoted DD+D (Double Distribution plus D-term). The D-term is here the smallest piece of $G^q(\beta,\alpha,t)$ that cannot be absorbed into $F^q(\beta,\alpha,t)$ *i.e.* on the left side of figure 2.3. Indeed, injecting equation (2.31) in (2.11) one gets the D-term contributions to the GPD Mellin moments as:

$$\xi^{m+1}\int_{-1}^{1}\mathrm{d}\alpha D(\alpha,t)\alpha^m = \xi^{m+1}C^q_{m+1}(t), \tag{2.32}$$

which is consistent with the Mellin moment analysis developed before.

Forward case

One could also like to work on the opposite side of figure 2.3, *i.e.* in the scheme where most of the information is contained in the DD $G^q(\beta,\alpha,t)$. In this case, it is easier to get some physics intuition of what is going on. As when $\xi\to 0$ $G^q(\beta,\alpha,t)$ does not contribute to the GPD, $F^q(\beta,\alpha,t)$ contains the forward information (even for non-vanishing t). Consequently one gets:

$$F^q(\beta,\alpha,t) \;\to\; q(\beta,t)\delta(\alpha), \tag{2.33}$$
$$G^q(\beta,\alpha,t) \;\to\; G^q_{\mathrm{Max}}(\beta,\alpha,t), \tag{2.34}$$

and thus the PDF is given at vanishing t by:

$$q(\beta) = \int_{-1+|\beta|}^{1-|\beta|}\mathrm{d}\alpha\; F^q(\beta,\alpha,0). \tag{2.35}$$

One Component DD

In the two precedent examples of DD schemes, the strategy consisting in maximising the information content of one of the DDs never allows one to get rid entirely of the other DD. Therefore the two previous schemes are called two Component DD schemes (2CDD). However, as shown in Ref. [139], it is possible to merge the two DDs generating a One Component DD scheme (1CDD). This could be seen as a balance of information between the $F^q(\beta,\alpha,t)$ and the $G^q(\beta,\alpha,t)$, *i.e.* being somewhere in the middle of figure 2.3. Within this scheme, the non-trivial β and α dependence of the DDs $F^q(\beta,\alpha,t)$ and $G^q(\beta,\alpha,t)$ is contained in a third function $f^q(\beta,\alpha,t)$:

$$F^q_{\mathrm{1CDD}}(\beta,\alpha) = \beta f^q(\beta,\alpha), \tag{2.36}$$
$$G^q_{\mathrm{1CDD}}(\beta,\alpha) = \alpha f^q(\beta,\alpha). \tag{2.37}$$

This DD scheme is less known than the 2CDD but is equivalent as it can be obtained from the 2CDD representation by a gauge transform (see Ref. [138]). Within the 1CDD scheme, equation (2.1) can thus be written:

$$\left\langle P+\frac{\Delta}{2}\middle|\,\bar q\left(-\frac{z}{2}\right)\gamma_\mu q\left(\frac{z}{2}\right)\middle|P-\frac{\Delta}{2}\right\rangle_{z^2=0} = \int_\Omega \mathrm{d}\beta\mathrm{d}\alpha\, e^{-i\beta(Pz)+i\alpha\frac{(\Delta z)}{2}}\Big(2P_\mu\beta-\Delta_\mu\alpha\Big)f^q(\beta,\alpha,t) + \text{higher twist terms.} \tag{2.38}$$

The relation between the GPD $H(x,\xi,t)$ and the DDs becomes in the 1CDD scheme:

$$H(x,\xi,t) = x\int_\Omega \mathrm{d}\beta\mathrm{d}\alpha f^q(\beta,\alpha,t)\delta(x-\beta-\alpha\xi). \tag{2.39}$$

2.2.3 Extension to GDA

Looking at equations (2.8) and (2.9) one can realise that the right-hand side is not vanishing for (x, ξ) beyond the support of the GPDs, *i.e.* for $|\xi| \geq 1$ and $|x| \geq 1$. More precisely, it allows the ERBL region to increase up to $|\xi| \to \infty$ as illustrated on figure 2.4. In order to understand this support extension, it is necessary to introduce new non-perturbative objects called Distributions Amplitudes (DAs) and Generalised Distributions Amplitudes (GDAs). In the following, only the pion case will be discussed.

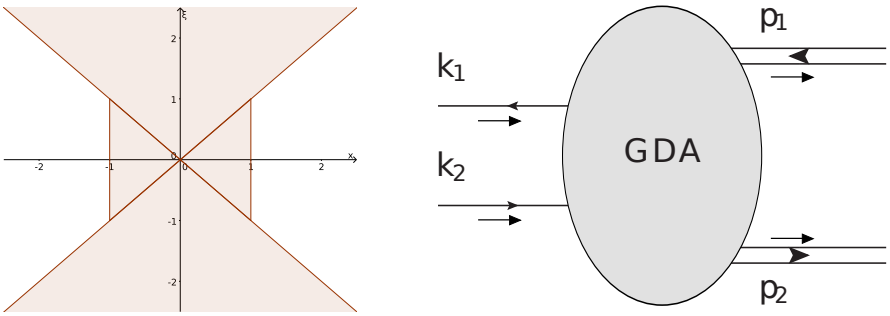

Figure 2.4: Left-hand side: total support allowed by the right-hand side of equations (2.8) and (2.9). Right-hand side: momentum flow of a GDA.

The pion DA $\varphi_\pi(u)$ is the probability amplitude to find inside the pion a quark with a momentum fraction u along the lightcone and an antiquark with a momentum fraction $1-u$. Formally, it is defined through the following matrix elements:

$$f_\pi \varphi_\pi(u) = \int \frac{\mathrm{d}z^-}{2\pi} e^{i(2u-1)P^+ \frac{z^-}{2}} \langle \pi, P | \, \bar{\psi}(-\frac{z}{2}) \gamma \cdot n \gamma_5 \psi(\frac{z}{2}) \, |0\rangle \Big|_{z^+=z_\perp=0}, \tag{2.40}$$

where f_π is the so-called pion decay constant. The notion of DA has been extended in Ref. [62, 140, 141] to the case of two pions, defining the so-called GDAs. In terms of matrix element, they are defined as:

$$\begin{aligned} \Phi_\pi^q(u,\zeta,s) &= \int \frac{\mathrm{d}z^-}{2\pi} e^{i(2u-1)(p_1+p_2)^+ \frac{z^-}{2}} \\ &\quad \langle \pi_1(p_1)\pi_2(p_2) | \, \bar{\psi}^q \left(-\frac{z}{2}\right) \gamma^+ \psi^q \left(\frac{z}{2}\right) |0\rangle \Big|_{z^+=z_\perp=0}, \end{aligned} \tag{2.41}$$

$$\begin{aligned} \Phi_\pi^g(u,\zeta,s) &= \frac{1}{(p_1+p_2)^+} \int \frac{\mathrm{d}z^-}{2\pi} e^{i(2u-1)(p_1+p_2)^+ \frac{z^-}{2}} \\ &\quad \langle \pi_1(p_1)\pi_2(p_2) | \, G^{+\mu} \left(-\frac{z}{2}\right) G_\mu{}^+ \left(\frac{z}{2}\right) |0\rangle \Big|_{z^+=z_\perp=0}, \end{aligned} \tag{2.42}$$

for the quark and gluon matrix element. GDA depends on the plus-momentum fraction u of the considered parton with respect to $p_1 + p_2$ and on $\zeta = \frac{p_1^+}{(p_1+p_2)^+}$, which describes the splitting of the plus-momentum between the two pions. s is here the Mandelstam variable associated with the Feynman graph of figure 2.4. Comparison of equations (2.41) and (2.42) with (1.30) and (1.31) shows that GPD and GDA come from the same operator, taken between different incoming and outgoing states. In fact, as suggested on figure 2.4 GPD and GDA are

related between each other through the crossing symmetry. It is then possible to identify the correspondence between GPD variables and GDA ones:

$$1-2\zeta \leftrightarrow \frac{1}{\xi}, \qquad 1-2u \leftrightarrow \frac{x}{\xi}. \tag{2.43}$$

As $0 \leq \zeta \leq 1$, one can directly deduce from equation (2.43) that the GDA corresponds to the $|\xi| \geq 1$ region of figure 2.4. In addition as $0 \leq u \leq 1$, the support of the GDA can indeed be seen as an extension of the ERBL region. This leads to an expression of the GDA in terms of DDs:

$$-\frac{1}{2}\Phi\left(u,\zeta,s\right) = (1-2\zeta)\int_{\Omega} \mathrm{d}\beta\mathrm{d}\alpha\delta\left(1-2u-\beta(1-2\zeta)-\alpha\right)\left(F^q(\beta,\alpha,t)+\frac{G^q(\beta,\alpha,t)}{1-2\zeta}\right). \tag{2.44}$$

2.3 Modeling GPDs from Double Distributions

Double Distributions have been broadly used in order to model GPDs. This enthusiasm is partially explained by the fact that, as it has been shown in equation (2.10), DD-based models automatically fulfil the polynomiality property. As it will be shown below, it is also possible to build phenomenological models very easily. Among all the developed model, two have been widely used so far, the VGG (Vanderhaeghen, Guichon and Guidal) [133, 142–145] and the GK (Goloskokov and Kroll) [146–148] models.

2.3.1 RDDA and GK model

Both the VGG and the GK models are build on the same fundamental ingredient, the so-called Radyushkin Double Distribution Ansatz (RDDA). In Ref. [149], it was suggested to model the DD $F^q(\beta,\alpha,t)$ in the DD+D scheme as:

$$F^q(\beta,\alpha,t) = \pi_N(\beta,\alpha)q(\beta,t), \tag{2.45}$$

where $\pi_N(\beta,\alpha)$ is the so-called profiled function depending on a single parameter N. It is defined as:

$$\pi_N(\beta,\alpha) = \frac{\Gamma\left(N+\frac{3}{2}\right)}{\sqrt{\pi}\Gamma(N+1)}\frac{[(1-|\beta|)^2-\alpha^2]^N}{(1-|\beta|)^{2N+1}}, \tag{2.46}$$

Γ being the Euler gamma function. The coefficient $\Gamma(N+3/2)/(\sqrt{\pi}\Gamma(N+1))$ guarantees the normalisation of the profile function:

$$\int_{-1+|\beta|}^{+1-|\beta|} \mathrm{d}\alpha\, \pi_N(\beta,\alpha) = 1\ . \tag{2.47}$$

It also ensures that in the forward limit, the DD $F^q(\beta,\alpha,t)$ produces the PDF as expected (2.35). However, if the RDDA provides a simple and efficient way to model the DD $F^q(\beta,\alpha,t)$, it does not say anything on the D-term, and thus the VGG and GK models differ on their treatment of the latter. It should also be noticed here that the parameter N controls the ξ-dependence of the GPD. An interesting case is the limit of infinite N as:

$$\lim_{N\to\infty} \pi_N(\beta,\alpha) = \delta(\alpha), \tag{2.48}$$

leading to a ξ-independent contribution of the DD $F^q(\beta,\alpha,t)$.

Focusing on the GK model, it is necessary to introduce a new decomposition in terms of valence and sea PDFs and DDs. In the case of the PDF whose support is extended to $[-1,1]$, following Ref. [150]:

$$q_{\rm val}(\beta) = \theta(\beta) q_{\rm val\,|[0,1]}(\beta), \tag{2.49}$$
$$q_{\rm sea}(\beta) = {\rm sgn}(\beta) q_{\rm sea\,|[0,1]}(|\beta|), \tag{2.50}$$

where $q_{|[0,1]}$ denotes the restriction of the PDF q to the interval $[0,1]$. The valence and sea contributions $F^q_{\rm val}$ and $F^q_{\rm sea}$ to the DD F^q are:

$$F^q_{\rm val}(\beta,\alpha) = \Big(F^q(\beta,\alpha) + F^q(-\beta,\alpha)\Big)\theta(\beta), \tag{2.51}$$
$$F^q_{\rm sea}(\beta,\alpha) = F^q(\beta,\alpha)\theta(\beta) - F^q(-\beta,\alpha)\theta(-\beta). \tag{2.52}$$

Within this decomposition, the RDDA introduced in equation (2.45) writes:

$$F^q_{\rm val}(\beta,\alpha) = \pi_{N_{\rm val}}(\beta,\alpha) q_{\rm val}(\beta), \tag{2.53}$$
$$F^q_{\rm sea}(\beta,\alpha) = \pi_{N_{\rm sea}}(\beta,\alpha) q_{\rm sea}(\beta), \tag{2.54}$$

where $N_{\rm val}$ and $N_{\rm sea}$ are two independent parameters.

In the following, only the treatment of the valence part of the GPD $H(x,\xi,t)$ is explicitely given. The reason for that comes from the fact that, in the end, models are compared to JLab data which are taken in the large-x_B region (*i.e.* are dominated by the valence contribution) and are mainly sensitive to the CFFs $\Re\mathcal{H}$ and $\Im\mathcal{H}$. The GK model assumes a vanishing D-term, and this specific representation will be simply referred to as "DD". The valence contibution to the GPD $H(x,\xi,t)$ is given by:

$$H^q_{\rm val}(x,\xi,t,\mu^2) = \int_\Omega {\rm d}\beta {\rm d}\alpha\, \pi_N(\beta,\alpha)\theta(\beta) q_{\rm val}(\beta,t,\mu^2)\delta(x-\beta-\alpha\xi), \tag{2.55}$$

with the t-dependent PDF $q_{\rm val}(\beta,t,\mu^2)$ parameterised as:

$$q_{\rm val}(\beta,t,\mu^2) = \beta^{-\alpha' t}\beta^{-\delta}(1-\beta)^{2n+1}\sum_{j=0}^{2} c_j \beta^{\frac{j}{2}}. \tag{2.56}$$

Within this specific choice of the PDF parameterisation, it is possible to compute analytically the GPD $H^q_{\rm val}$. However, in the following, computations are done numerically, analytic formulations allowing a useful cross-check of the results. Concerning the coefficients, of the parameterisation (2.56), n is fixed to 1. Then δ and the c_j have been determined in a fit to the CTEQ6m PDFs [151]. The mass-scale coefficient α' has been tuned in order to approximate the small t-dependence of the quark contribution F_1^q to the proton form factor F_1. All the values of these coefficients are recalled in Tab. 2.1 for both u and d quarks.

Contrary to what has been done in Ref. [125, 146–148] where the profile function parameter N is fixed to 1, in the following it is allowed to take real values between 1 and $+\infty$. Such a

change of N does not modify the description of the form factor F_1:

$$\begin{aligned} F_1^q(t) &= \int_{-1}^{+1} \mathrm{d}x \int_\Omega \mathrm{d}\beta \mathrm{d}\alpha\, \pi_N(\beta,\alpha)\theta(\beta) q_{\mathrm{val}}(\beta,t,\mu^2)\delta(x-\beta-\alpha\xi) \\ &= \int_0^{+1} \mathrm{d}\beta q_{\mathrm{val}}(\beta,t,\mu^2) \int_{-1+\beta}^{+1-\beta} \mathrm{d}\alpha\, \pi_N(\beta,\alpha) \\ &= \int_0^{+1} \mathrm{d}\beta q_{\mathrm{val}}(\beta,t,\mu^2), \end{aligned} \tag{2.57}$$

since the profile function is normalised (2.47).

	u_{val}	d_{val}
δ	0.48	0.48
c_0	1.52 + 0.248 L	0.76 + 0.248 L
c_1	2.88 - 0.940 L	3.11 - 1.36 L
c_2	-0.095 L	-3.99 + 1.15 L
$\alpha'(\mathrm{GeV}^{-2})$	0.9	0.9
n	1.	1.

Table 2.1: parameterization of the valence quark PDFs in (2.56) with $L = \log(Q^2/Q_0^2)$ and $Q_0^2 = 4$ GeV^2.

Using the notations x_1 and x_2 introduced in equation (1.53), equation (2.55) can be further simplified:

$$\begin{aligned} H^q_{\mathrm{val}}(x,\xi,t,\mu^2) &= \frac{1}{\xi}\theta(x>\xi)\int_{x_1}^{x_2} \mathrm{d}\beta\, \pi_N\left(\beta, \frac{x-\beta}{\xi}\right) q_{\mathrm{val}}(\beta,t,\mu^2) \\ &\quad + \frac{1}{\xi}\theta(x<\xi)\int_0^{x_2} \mathrm{d}\beta\, \pi_N\left(\beta, \frac{x-\beta}{\xi}\right) q_{\mathrm{val}}(\beta,t,\mu^2). \end{aligned} \tag{2.58}$$

As in the end of this chapter, GPDs will be compared to DVCS data, ξ is supposed to be positive, consistently with DVCS kinematics. The dependence of the PDF on the factorization scale μ^2 is approximated through the L-dependence of the PDF coefficients exhibited in Tab. 2.1. In the GK model, this is the only dependence of the GPDs on the factorization scale. The factorization scale is chosen to be equal to the photon virtuality : $\mu^2 = Q^2$.

An equivalent parameterisation has been developed for the GPD $E(x,\xi,t)$. Within the GK model, the valence part of this GPD also relies on a forward-like function e^q_{val} and the usual RDDA *i.e.* :

$$E^q_{\mathrm{val}}(x,\xi,t) = \int_\Omega \mathrm{d}\beta \mathrm{d}\alpha\, \delta(x-\beta-\alpha\xi)\pi_N(\beta,\alpha)\theta(\beta) e^q_{\mathrm{val}}(\beta,t), \tag{2.59}$$

with:

$$e^q_{\mathrm{val}}(\beta,t) = \beta^{-\alpha' t}\frac{\kappa_q}{B(1-\mu_{\mathrm{val}}, 1+\nu_{\mathrm{val}})}\beta^{-\mu_{\mathrm{val}}}(1-\beta)^{\nu_{\mathrm{val}}}, \tag{2.60}$$

where B is the Euler Beta function. The values of the coefficients of (2.60) are given in Tab. 2.2.

	u	d
κ	1.67	-2.03
ν_{val}	4	5.6
μ_{val}	0.48	0.48
$\alpha'(\text{GeV}^{-2})$	0.9	0.9

Table 2.2: Parameters of forward-like GPD $E(x,0,0)$ in (2.60).

Parameters of the GK model have been tuned in order to fit the DVMP data, *i.e.* in the kinematic region of small to intermediate x_B. There, sea quark and gluon contributions are dominant. Nonetheless, this model has been confronted to DVCS data, especially those taken at JLab in the valence region [125]. If the model gets a reasonable agreement without tuning any parameters, this agreement could be improved by for instance taking into account the 2 components of the DD formalism, or in working in the 1CDD scheme.

2.3.2 Modeling Double Distributions in the 1CDD scheme

If both the GK and VGG models use the DD+D scheme to model the DD $F^q(\beta,\alpha,t)$, it is partially because in this scheme, the RDDA leads to a more divergent Ansatz:

$$f^q(\beta,\alpha) = \frac{q(\beta)}{\beta}\pi_N(\beta,\alpha). \tag{2.61}$$

As the valence PDF typically behave as $q_{\text{val}}(\beta) \propto \beta^{-0.5}$, the present singularity is here *a priori* non-integrable. It should be noticed at this point that applying the RDDA in one scheme does *not* produce the same model than doing it in another scheme. In other words, the transformation defined in equations (2.21) and (2.22) does not preserve the RDDA. Consequently, when using RDDA, the choice of scheme becomes a model assumption.

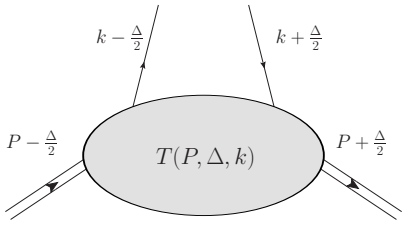

Figure 2.5: Amplitude Diagram used to compute the GPD $H(x,\xi,t)$ in Ref. [152].

A way to regularise equation (2.61) was introduced by Radyushkin in Ref. [152] in the case of a scalar target, and applied to experimental data in Ref. [153]. The regularisation framework comes from the insights of a simple quark-hadron subtracted scattering amplitude $T(P,\Delta,k)$ modeled as:

$$T(P,\Delta,k) = T_0(t) + \int_0^{+\infty} \mathrm{d}\sigma\, \rho(\sigma) \left[\frac{1}{\sigma - (P-k)^2} - \frac{1}{\sigma}\right], \tag{2.62}$$

where the T dependent term $T_0(t)$ is unknown and ρ is a spectral function responsible for the Regge-behaviour of the PDFs. In addition to this scattering amplitude, the quark propagator

denominators are modified as:

$$\frac{1}{(m^2-k_i^2)} \to \frac{1}{(m^2-k_i^2)^N} \quad \text{for } i=1,2, \tag{2.63}$$

in order to take into account non-perturbative effects. Writing $H(x,\xi,t)$ as:

$$H^q_{\text{val}}(x,\xi,t) = \frac{1}{\pi^2}\frac{(N!)^2}{(2N)!}\int \frac{k\cdot n}{P\cdot n}\frac{\mathrm{d}^4k\delta\left(x-\frac{k\cdot n}{P\cdot n}\right)}{(m_1^2-(k-\frac{\Delta}{2}))^N(m_2^2-(k-\frac{\Delta}{2}))^N}T(P,\Delta,k), \tag{2.64}$$

it is possible to perform the computations using the α-parameterisation in order to get[2]:

$$\frac{H^q_{\text{val}}(x,\xi,t)}{x} = \int_0^1 \mathrm{d}\beta \int_{-1+\beta}^{+1-\beta} \mathrm{d}\alpha\, \frac{q_{\text{val}}(\beta,t)}{\beta}\pi_N(\beta,\alpha)\left[\delta(x-\beta-\alpha\xi) - \frac{1}{(1-\beta)^2}\delta\left(x-\frac{\alpha\xi}{1-\beta}\right)\right], \tag{2.65}$$

trading the spectral function ρ for the forward limit $q_{\text{val}}(x)$.

The next step is to perform a change of variables in the second term of equation (2.65) in order to get rid of the fraction in the Dirac δ *i.e.* taking $\alpha' = \frac{\alpha}{1-\beta}$. Stressing that $\pi_N\Big(\beta,\alpha(1-\beta)\Big) = \pi_N(0,\alpha)/(1-\beta)$, such a change of variables yields:

$$\frac{H^q_{\text{val}}(x,\xi,t)}{x} = \int_0^1 \mathrm{d}\beta \int_{-1+\beta}^{+1-\beta} \mathrm{d}\alpha\, \delta(x-\beta-\alpha\xi)\left[\frac{q_{\text{val}}(\beta,t)}{\beta}\pi_N(\beta,\alpha) - \delta(\beta)\pi_N(0,\alpha)\int_0^1 \mathrm{d}\gamma \frac{q_{\text{val}}(\gamma,t)}{\gamma(1-\gamma)^2}\right] \tag{2.66}$$

Under this form, the 1CDD structure of the Radyushkin model becomes plain, with:

$$f^q_{\text{val}}(\beta,\alpha,t) = \frac{q_{\text{val}}(\beta,t)}{\beta}\pi_N(\beta,\alpha) - \delta(\beta)\pi_N(0,\alpha)\int_0^1 \mathrm{d}\gamma \frac{q_{\text{val}}(\gamma,t)}{\gamma(1-\gamma)^2}. \tag{2.67}$$

Equation (2.67) explicitely shows that the singular behaviour of the forward function $q_{\text{val}}(\beta)/\beta$ is regularized by a "D-term-like" function coming from the $\frac{1}{\sigma}$ regulator of the scattering amplitude $T(P,\Delta,k)$ (2.62).

Finally, the subtraction constant T_0 generates an additional term denoted D_0^q:

$$D_0^q\left(\frac{x}{\xi},t\right) = \frac{T_0^q(t)}{2N2^{2N}}\frac{x}{\xi}\left(1-\frac{x^2}{\xi^2}\right)^N \theta(|x|<\xi). \tag{2.68}$$

This term can be recast in the 1CDD framework by introducing:

$$f_0^q(\beta,\alpha,t) = \int_\Omega \mathrm{d}\beta\mathrm{d}\alpha\, \delta(x-\beta-\alpha\xi)\delta(\beta)\frac{D_0^q(\alpha,t)}{\alpha}. \tag{2.69}$$

2.3.3 Comparison of a simple model with experimental data

Within the previous framework of regularisation, it is now possible to build models using the RDDA in the 1CDD scheme following equation (2.61). Thus, the idea is to modify the GK model in the valence sector to implement RDDA in the 1CDD scheme instead of the DD scheme, and look at the phenomenological consequences. This is done when comparing the

[2]There is a typing mistake in equation (36) of Ref. [152] modifying the expression of the regularisation term. The expression given here is the correct one. See also Ref. [154] for further details.

prediction of the model with observables coming from the measurements and analyses of the Hall A collaboration [129] and the CLAS collaboration [131]. As the GPD $E^q_{\rm val}(x,\xi,t)$ has a small effect on those observables compared to $H^q_{\rm val}(x,\xi,t)$, it will be neglected in this section, leading to a "scalar-like" description of the proton. The effects of the GPD $E^q_{\rm val}(x,\xi,t)$ are studied in section 2.4. The first step is to come back to equation (2.65) and integrate it over α to get:

$$\begin{aligned} H^q_{\rm val}(|x|<\xi,\xi,t,\mu^2) &= \frac{x}{\xi}\int_0^{x_2} \mathrm{d}\beta\, \frac{q_{\rm val}(\beta,t,\mu^2)}{\beta}\left[\pi_N\left(\beta,\frac{x-\beta}{\xi}\right)-\pi_N\left(\beta,\frac{x}{\xi}(1-\beta)\right)\right] \\ &\quad +\frac{x}{\xi}\int_0^{x_2} \mathrm{d}\beta\, \frac{q_{\rm val}(\beta,t,\mu^2)}{\beta}\pi_N\left(\beta,\frac{x}{\xi}(1-\beta)\right)\left[1-\frac{1}{1-\beta}\right] \\ &\quad -\frac{x}{\xi}\int_{x_2}^1 \mathrm{d}\beta\, \frac{q_{\rm val}(\beta,t,\mu^2)}{\beta(1-\beta)}\pi_N\left(\beta,\frac{x}{\xi}(1-\beta)\right) \qquad (2.70) \\ H^q_{\rm val}(x>\xi,\xi,t,\mu^2) &= \frac{x}{\xi}\int_{x_1}^{x_2} \mathrm{d}\beta\, \frac{q_{\rm val}(\beta,t,\mu^2)}{\beta}\pi_N\left(\beta,\frac{x-\beta}{\xi}\right). \qquad (2.71) \end{aligned}$$

At this point, one should note that applying the RDDA in the 1CDD scheme does not impact the form factor since:

$$\begin{aligned} F^q_1(t) &= \int_{-1}^{+1}\mathrm{d}x\, x\int_\Omega \mathrm{d}\beta\mathrm{d}\alpha\, \pi_N(\beta,\alpha)\theta(\beta)\frac{q_{\rm val}(\beta,t,\mu^2)}{\beta} \\ &\quad \times\left[\delta(x-\beta-\alpha\xi)-\frac{1}{(1-\beta)^2}\delta\left(x-\frac{\alpha\xi}{1-\beta}\right)\right] \\ &= \int_0^{+1}\mathrm{d}\beta q_{\rm val}(\beta,t,\mu^2)\int_{-1+\beta}^{+1-\beta}\mathrm{d}\alpha\,\pi_N(\beta,\alpha) \\ &\quad +\xi\int_0^{+1}\mathrm{d}\beta\,\frac{q_{\rm val}(\beta,t,\mu^2)}{\beta}\left[1-\frac{1}{(1-\beta)^3}\right]\int_{-1+\beta}^{+1-\beta}\mathrm{d}\alpha\,\alpha\pi_N(\beta,\alpha) \\ &= \int_0^{+1}\mathrm{d}\beta\, q_{\rm val}(\beta,t,\mu^2). \qquad (2.72) \end{aligned}$$

This is due to the normalisation of the profile function (2.47) and its parity with respect to α (2.46).

Using the parameterisation of the GK model for the t-dependent PDF $q_{\rm val}(\beta,t,\mu^2)$ (2.56), it is possible to compute the CFF associated with the GPD $H(x,\xi,t)$ at LO (1.73) and (1.74), as shown on figure 2.6. The GK model fixes all the parameters but one, N appearing the profile function. An interesting point here is to compare the sensitivity of the 1CDD and DD scheme to this parameter. To do so, an additional parameterisation has been plotted on figure 2.6 called "Forward Parton Density" (FDP) and being nothing else than the GK model taken for $N\to\infty$, which generates a GPD independent of ξ according to equation (2.48). It appears that the original GK model is hardly sensitive to this parameter as it converges very quickly to its infinity limit. This have been already noticed some time ago [133]. On the other hand, the 1CDD approach developed here shows a significant sensitivity with respect to N, allowing one to expect significant variations on observables at low values of N. Nevertheless, at high values of N, the 1CDD scheme should give back the results of the GK model. Therefore, it makes sens to fit this parameter on the current available data.

The Hall A collaboration [129] has released beam helicity-dependent $\Delta\sigma$ and independent $\Sigma\sigma$ cross section in the valence region. Tuning N in order to get a good agreement with

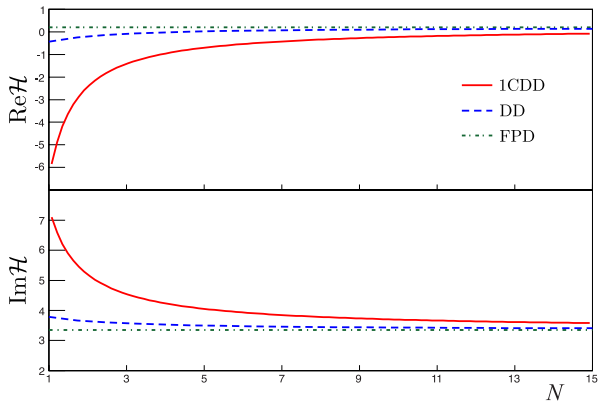

Figure 2.6: Real and imaginary parts of the CFF $\mathcal{H}$ as a function of the parameter N of the profile function π_N. Kinematics parameters are taken as following: $x_B = 0.36$, $Q^2 = 2.3$ GeV^2 and $t =$ -0.23 GeV^2 for the 1CDD (solid red line), DD (dashed blue line) and FPD (dash-dotted green line) parameterisations.

Parameterization	χ^2/d.o.f
1CCD ($N \simeq 1.86$)	4.0
DD	5.9
FPD	7.2

Table 2.3: χ^2 per degrees of freedom for the comparison of the different parameterizations with the subset of Hall A beam helicity-dependent and independent cross sections such that $|t|/Q^2 < 0.1$. No fit was made for the DD or FPD cases, while the parameter N of the profile function was extracted from data in the 1CDD case.

experimental data leads to the χ^2 shown in table 2.3. The comparison with cross-sections are shown on figure 2.7. To remain consistent in our leading-twist approach, only kimematics such that $\frac{|t|}{Q^2} \leq 0.1$ are taken into account. It should be noticed that the 1CDD model does not describe the helicity-dependent cross-section as well as the original GK model. But it does significantly better on the spin-independent cross section, especially for ϕ around 0° and 180°, where the DVCS contribution is supposed to be significant.

2.3.4 Considerations on the D-term

Until now, the term $T_0(t)$ of the scattering amplitude (2.62) has not been taken into account. Nonetheless, it generates a contribution $D_0\left(\frac{x}{\xi}, t\right)$ which looks like a D-term (2.68), (2.69). And indeed, due to its definition (2.29), the full D-term denoted $D^q(\alpha, t)$ depends on two contributions:

$$D^q_{\text{val}}(\alpha, t) = D^q_{\text{1CDD}}(\alpha, t) + D^q_0(\alpha, t), \tag{2.73}$$

where

$$D^q_{\text{1CDD}}(\alpha, t) = \alpha \int_{-1+|\alpha|}^{+1-|\alpha|} \mathrm{d}\beta \, f^q_{\text{val}}(\beta, \alpha, t). \tag{2.74}$$

A priori, a contribution of the $D_0(\alpha, t)$ term can improve the comparison of the present model with the helicity independent data for the bin at $t = -0.17\text{GeV}^2$. Yet, T_0 remains unknown.

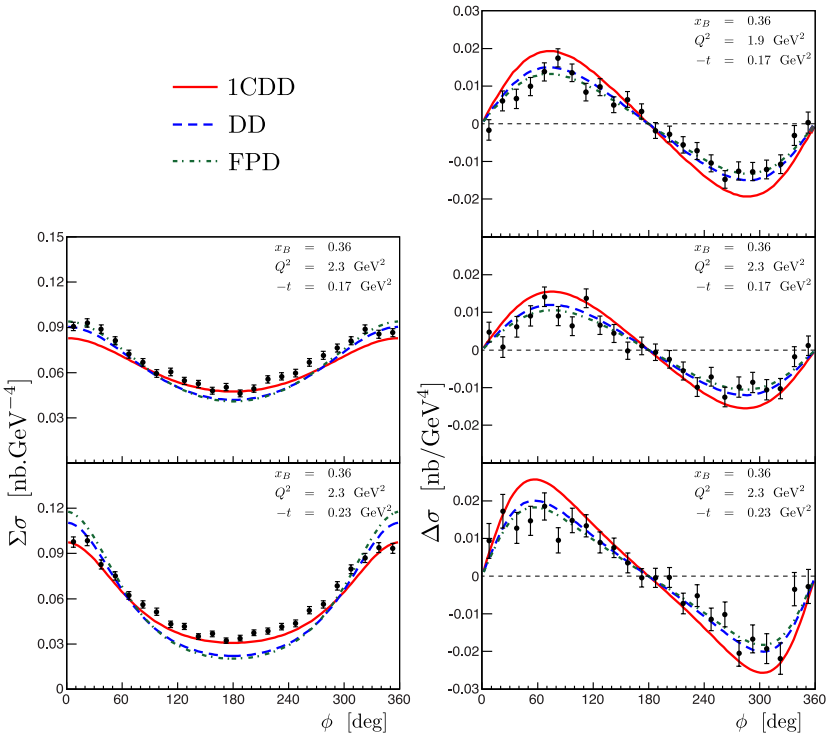

Figure 2.7: Comparison to Hall A data : results at $x_B = 0.36$, $Q^2 = 2.3$ GeV^2 (four lower plots) and $Q^2 = 1.9$ GeV^2 (upper plot), $t = -0.23$ GeV^2 (two lower plot) and $t = -0.17$ GeV^2 (three upper plots). The full red line corresponds to the 1CDD model, the dashed blue line to the classical DD Ansatz and the dash-dotted green line to the unskewed FPD limit. All of them are based on the GK model.

Consequently, T_0 is fitted on the data and then, the resulting D-term is compared to those computed in the literature. The D-term has indeed been studied, especially through the so-called flavour singlet combination $D(\alpha, t)$ such that:

$$D(\alpha, t) = \sum_{q=u,d,s} D^q(\alpha, t). \tag{2.75}$$

It is then usually projected on the $C_n^{3/2}$ Gegenbauer polynomials basis:

$$D(\alpha, t) = (1-\alpha^2) \sum_{\substack{n=0 \\ n \text{ odd}}}^{\infty} d_n(t, \mu^2) C_n^{3/2}(\alpha). \tag{2.76}$$

Consequently it is possible to compare conformal moments of the considered model with those computed through the Chiral Quark Soliton Model (χQSM). Comparison is shown in table 2.4, and details can be found in Ref. [133, 153].

It is also worth highlighting that the coefficient d_1 has attracted attention due to its relation with the quark contribution $T^q_{\mu\nu}$ to the symmetric energy momentum tensor defined in the Breit frame [155]:

$$d_1^q(t = 0 \text{ GeV}^2) = -\frac{M}{2} \int d^3\boldsymbol{r}\, T^q_{ij}(\boldsymbol{r}) \left(r^i r^j - \frac{1}{3}\delta^{ij} r^2 \right), \tag{2.77}$$

Coefficients	χQSM	Fit	
	$t = 0$ GeV^2	$t = -0.17$ GeV^2	$t = -0.23$ GeV^2
d_1^{u+d}	- 3.12	0.39	- 1.83
d_3^{u+d}	- 0.71	- 0.65	0.018
d_5^{u+d}	- 0.20	0.12	0.14

Table 2.4: . Comparison of the coefficients of the D-term expansion (2.76) evaluated from the Chiral Quark Soliton Model and extracted from Hall A data with the Ansatz (2.73). The factorisation scale is $\mu_R = 2.3$ GeV^2.

where i, j are spatial indices.

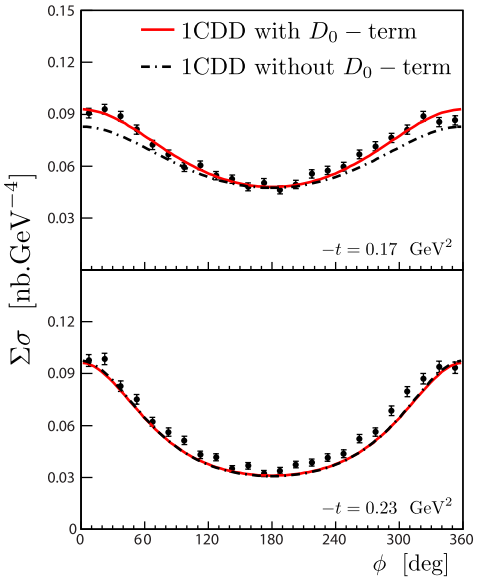

Figure 2.8: Impact of the additional $D_0(t)$ term on the considered helicity-independent Hall A cross section.

The effects of the additional $D_0(t)$ term are shown on figure 2.8. Improvement is significant on the $t = -0.17$ GeV^2 kinematics. The CLAS collaboration has produced beam spin asymmetries in the same kinematic range than the Hall A collaboration [131]. It is therefore natural to compare the 1CDD model considered here and tuned on Hall A data to the GK model. Yet, as $D_0(t)$ as been added to the 1CDD model, the same type of additional D-term (2.68) has also been added to the GK model, leading to a full DD+D scheme. Both of them are in agreement with CLAS data, even if the DD+D model seems to provide a better description of the asymmetry. That can be easily explained as the observable here are defined as:

$$A_{\mathrm{LU}}(\phi) = \frac{\Delta\sigma}{\Sigma\sigma}. \tag{2.78}$$

As shown on figure 2.7, the 1CDD scheme brings a significant improvement on the helicity independant cross-section for ϕ around 0° and 180°. It is precisely where the helicity-dependent

cross-section vanishes. Thus any improvement brought by the 1CDD model is then hidden on asymmetries.

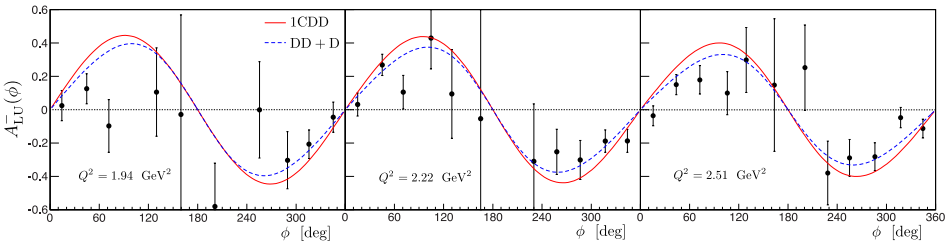

Figure 2.9: Comparison of 1CDD (full red line) and DD+D (dashed blue line) models with CLAS data at $t \simeq -0.17$ GeV^2 and such that $\frac{|t|}{Q^2} \leq 0.1$. From left to right: $x_B = 0.3205$, $t = -0.1705$ GeV^2 and $Q^2 = 1.9424$ GeV^2; $x_B = 0.3215$, $t = -0.1719$ GeV^2 and $Q^2 = 2.217$ GeV^2; $x_B = 0.3215$, $t = -0.1743$ GeV^2 and $Q^2 = 2.5078$ GeV^2.

2.4 The proton in 1CDD

In the previous section, the GPD $E(x, \xi, t)$ was not taken into account due to its small impact on observables. However, in the continuity of his work on regularisation of GPDs in the 1CDD case for scalar hadrons [152], Radyushkin also regularised GPDs in the 1CDD scheme in the case of spin-1/2 hadrons [156]. This framework is used here to build a complete model of the nucleon GPD.

2.4.1 1CDD scheme in the case of a spin-1/2 hadron

Equations (2.8) and (2.9) relate the three DDs needed for the proton to the two GPDs $H(x, \xi, t)$ and $E(x, \xi, t)$. Those equations show that if the DD $G^q(\beta, \alpha, t)$ is required to get $H(x, \xi, t)$ or $E(x, \xi, t)$ independently, the sum of the two GPDs is clearly independent of the DD $G^q(\beta, \alpha, t)$, and is given by the sum of the two DDs $F^q(\beta, \alpha, t)$ and $K^q(\beta, \alpha, t)$. Just as in the scalar case (see equations (2.21) and (2.22)), it is possible to find a transformation which leaves invariant the description of the matrix element (2.2). It is given by Ref. [138][3]:

$$F^q(\beta, \alpha) \rightarrow F^q(\beta, \alpha) + \frac{\partial \sigma^q}{\partial \alpha}(\beta, \alpha), \tag{2.79}$$

$$K^q(\beta, \alpha) \rightarrow K^q(\beta, \alpha) - \frac{\partial \sigma^q}{\partial \alpha}(\beta, \alpha), \tag{2.80}$$

$$G^q(\beta, \alpha) \rightarrow G^q(\beta, \alpha) - \frac{\partial \sigma^q}{\partial \beta}(\beta, \alpha). \tag{2.81}$$

At this point, it appears that the sum $F^q(\beta, \alpha, t) + K^q(\beta, \alpha, t)$ is left unchanged by such a transformation. As this sum plays a specific role in the scheme transformation, it is worth writing the matrix element (2.2) in term of it. To do so, one has to inject the Gordon identity

[3] See Ref. [138] for a detailed treatment of the boundary conditions on DDs.

(2.7) into the definition of the DDs to get:

$$\begin{aligned}
&\left\langle P+\frac{\Delta}{2}\middle|\,\bar{q}\left(-\frac{z}{2}\right)\gamma_\mu q\left(\frac{z}{2}\right)\middle|P-\frac{\Delta}{2}\right\rangle\Big|_{z^2=0}\\
=\;&\bar{u}\left(P+\frac{\Delta}{2}\right)\left[\gamma_\mu\int_\Omega \mathrm{d}\beta\mathrm{d}\alpha\, e^{-i\beta(P\cdot z)+i\alpha\frac{(\Delta\cdot z)}{2}}\Big(F^q(\beta,\alpha,t)+K^q(\beta,\alpha,t)\Big)\right.\\
&-\frac{P_\mu}{M}\int_\Omega \mathrm{d}\beta\mathrm{d}\alpha\, e^{-i\beta(P\cdot z)+i\alpha\frac{(\Delta\cdot z)}{2}}K^q(\beta,\alpha,t)\\
&\left.-\frac{\Delta_\mu}{2M}\int_\Omega \mathrm{d}\beta\mathrm{d}\alpha\, e^{-i\beta(P\cdot z)+i\alpha\frac{(\Delta\cdot z)}{2}}G^q(\beta,\alpha,t)\right]u\left(P-\frac{\Delta}{2}\right)+\text{ higher twist terms.}
\end{aligned}\tag{2.82}$$

Within this formulation, the DDs $K^q(\beta,\alpha,t)$ and $G^q(\beta,\alpha,t)$ play the same roles than the DDs $F^q(\beta,\alpha,t)$ and $G^q(\beta,\alpha,t)$ in the scalar case (2.1) whereas the sum $F^q(\beta,\alpha,t)+K^q(\beta,\alpha,t)$ is an invariant of this transformation. Thus, it is possible to apply all the previous machinery developed in the scalar case and rewrite $K^q(\beta,\alpha,t)$ and $G^q(\beta,\alpha,t)$ in the 1CDD scheme. Consequently, following Ref. [156], one can define the DD[4] $a(\beta,\alpha,t)$ and $b(\beta,\alpha,t)$, such that:

$$\begin{aligned}
\left\langle P+\frac{\Delta}{2}\middle|\,\bar{q}\left(-\frac{z}{2}\right)\gamma_\mu q\left(\frac{z}{2}\right)\middle|P-\frac{\Delta}{2}\right\rangle\Big|_{z^2=0} \;=\;&\bar{u}\left(p_2\right)\left[\gamma_\mu\int_\Omega \mathrm{d}\beta\mathrm{d}\alpha\, e^{-i\beta(Pz)+i\alpha\frac{(\Delta z)}{2}}a^q(\beta,\alpha,t)\right.\\
&+\int_\Omega \mathrm{d}\beta\mathrm{d}\alpha\, e^{-i\beta(Pz)+i\alpha\frac{(\Delta z)}{2}}\\
&\left.\left(\beta\frac{P_\mu}{M}+\alpha\frac{\Delta_\mu}{2M}\right)b^q(\beta,\alpha,t)\right]u\left(p_1\right)\\
&+\text{ higher twist terms.}
\end{aligned}\tag{2.83}$$

with $b^q(\beta,\alpha,t)$ being the equivalent function of $f^q(\beta,\alpha,t)$ in equations (2.36) and (2.37). The DDs $a^q(\beta,\alpha,t)$ and $b^q(\beta,\alpha,t)$ are related to the GPDs through:

$$H^q(x,\xi,t)+E^q(x,\xi,t) = \int_\Omega \mathrm{d}\beta\mathrm{d}\alpha\, a^q(\beta,\alpha,t)\delta(x-\beta-\alpha\xi),\tag{2.84}$$

$$-E^q(x,\xi,t) = x\int_\Omega \mathrm{d}\beta\mathrm{d}\alpha\, b^q(\beta,\alpha,t)\delta(x-\beta-\alpha\xi).\tag{2.85}$$

2.4.2 The D-term as a regulator

Equations (2.84) and (2.85) suggest to use the following Ansätze for $a(\beta,\alpha,t)$ and $b(\beta,\alpha,t)$:

$$a(\beta,\alpha,t) = \big(q(\beta,t)+e(\beta,t)\big)\pi_{N_{H+E}}(\beta,\alpha),\tag{2.86}$$

$$b(\beta,\alpha,t) = -\frac{e(\beta,t)}{\beta}\pi_{N_E}(\beta,\alpha),\tag{2.87}$$

where $e(\beta,t)$ is the "forward-like" limit of the GPD $E(x,\xi,t)$ as defined in equation (2.60). As previously, RDDA generates in the 1CDD scheme a non-integrable singularity and have

[4] $b(\beta,\alpha,t)$ is not a proper DD, but plays the same role than f in equations 2.36 and 2.37. Thus, the true DDs are $\beta b(\beta,\alpha,t)$ and $\alpha b(\beta,\alpha,t)$. Still, we stick to the name DD as a misuse of language.

to be regularised. A possible way to do so is to use the D-term regularisation introduced in Ref. [156]. Writing a generic GPD $F(x,\xi,t)$ in the 1CDD scheme as:

$$F(x,\xi,t) = x\int_\Omega \mathrm{d}\beta\mathrm{d}\alpha\,\delta(x-\beta-\alpha\xi)f(\beta,\alpha,t). \tag{2.88}$$

it is possible to split the associated DD $f(\beta,\alpha,t)$ into a "plus"-component and a D-term:

$$f(\beta,\alpha) = [f]_+(\beta,\alpha) + \delta(\beta)\frac{D(\alpha)}{\alpha}, \tag{2.89}$$

$D(\alpha)$ being defined in equation (2.74). This decomposition of the DD produces two GPDs:

$$\begin{aligned} F(x,\xi) &= [F]_+(x,\xi) + F_D(x,\xi), & (2.90)\\ [F]_+(x,\xi) &= x\int_\Omega \mathrm{d}\beta\mathrm{d}\alpha\,\Big(\delta(x-\beta-\alpha\xi)-\delta(x-\alpha\xi)\Big)f(\beta,\alpha), & (2.91)\\ F_D(x,\xi) &= x\int_{-1}^{+1}\mathrm{d}\alpha\,\frac{D(\alpha)}{\alpha}\delta(x-\alpha\xi). & (2.92)\end{aligned}$$

The next step is to apply the RDDA to the DD as previously. Denoting by ϕ the "forward-like" limit of the GPD $F(x,\xi,t)$ such that $\phi(\beta)\propto 1/\beta^a$ with $0<a<1$, one gets:

$$f(\beta,\alpha) = \pi_N(\beta,\alpha)\frac{\phi(\beta)}{\beta}. \tag{2.93}$$

It is then possible to write equation (2.93) in the same way than equation (2.70):

$$\begin{aligned}[F]_+(x,\xi) &= \frac{x}{\xi}\int_0^{x_2}\mathrm{d}\beta\left[\pi_N\left(\beta,\frac{x-\beta}{\xi}\right)-\pi_N\left(\beta,\frac{x}{\xi}\right)\right]\frac{\phi(\beta)}{\beta}\\ &\quad -\int_{x_2}^{1-\frac{|x|}{\xi}}\mathrm{d}\beta\,\pi_N\left(\beta,\frac{x}{\xi}\right)\frac{\phi(\beta)}{\beta}, \end{aligned}\tag{2.94}$$

and:

$$\pi_N\left(\beta,\frac{x-\beta}{\xi}\right)-\pi_N\left(\beta,\frac{x}{\xi}\right) = -\frac{N}{4^N x}\left(1-\frac{x^2}{\xi^2}\right)^{N-1}\frac{\Gamma(2+2N)}{\Gamma(1+N)^2}\beta+\mathcal{O}(\beta^2). \tag{2.95}$$

Therefore, as $\phi(\beta,t)$ has an integrable singularity when $\beta\to 0$, the integral defined in equation (2.91) converges.

Applying such a prescription to the DD $b(\beta,\alpha,t)$, it is possible to get a well-defined model for the GPDs $H^q_{\mathrm{val}}(x,\xi,t)$ and $E^q_{\mathrm{val}}(x,\xi,t)$. Indeed two contributions can be highlighted here, one coming from the DD modeling of the sum $H^q_{\mathrm{val}}(x,\xi,t)+E^q_{\mathrm{val}}(x,\xi,t)$ and denoted $H^q_{\mathrm{val\ DD}}$ (resp. $E^q_{\mathrm{val\ DD}}$). It is directly given through:

$$\begin{aligned} H^q_{\mathrm{val\ DD}}(x,\xi,t)+E^q_{\mathrm{val\ DD}}(x,\xi,t) &= \int_\Omega \mathrm{d}\beta\mathrm{d}\alpha\,\delta(x-\beta-\alpha\xi)\theta(\beta)\\ &\qquad \pi_{N_{H+E}}(\beta,\alpha)\Big(q_{\mathrm{val}}(\beta,t)+e_{\mathrm{val}}(\beta,t)\Big), & (2.96)\\ [E^q_{\mathrm{val}}]_+(x,\xi,t) &= x\int_\Omega \mathrm{d}\beta\mathrm{d}\alpha\,\frac{e^q_{\mathrm{val}}(\beta,t)}{\beta}\\ &\qquad \pi_{N_E}(\beta,\alpha)\Big(\delta(x-\beta-\alpha\xi)-\delta(x-\alpha\xi)\Big). & (2.97)\end{aligned}$$

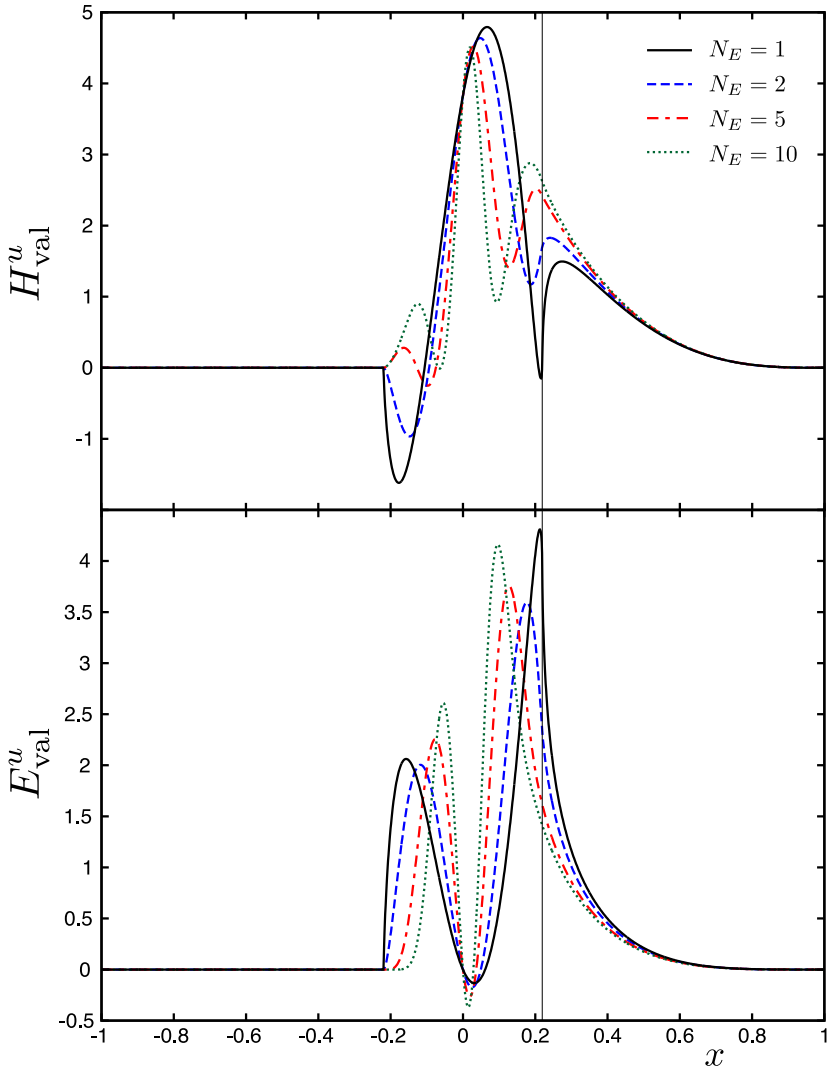

Figure 2.10: Valence contributions to the GPDs H^u in Eq. (2.98) (upper plot) and E^u in Eq. (2.99) (lower plot) vs x for different values of N_E in the nucleon model for $x_B = 0.36$, $t = -0.23$ GeV^2 and $Q^2 = 2.3$ GeV^2. The vertical black line signals $x = \xi$. In these plots the D-term (2.100) is arbitrarily set to 0.

The full GPD $E^q_{\rm val}(x,\xi,t)$ is obtained after addition of the D-term D. Indeed, the D-term has been subtracted to ensure the convergence in the 1CDD formalism (2.91). This leads to:

$$H^q_{\rm val}(x,\xi,t) = H^q_{\rm val\ DD}(x,\xi,t) + E^q_{\rm val\ DD}(x,\xi,t) - [E^q_{\rm val}]_+(x,\xi,t) + D^q\left(\frac{x}{\xi},t\right), \quad (2.98)$$

$$E^q_{\rm val}(x,\xi,t) = [E^q_{\rm val}]_+(x,\xi,t) - D^q\left(\frac{x}{\xi},t\right), \quad (2.99)$$

with a D-term chosen as:

$$D^q(\alpha,t) = C(t)\alpha(1-\alpha^2). \quad (2.100)$$

The resulting GPDs are plotted on figure 2.10. As seen previously, the DD models built in

the DD+D scheme are hardly sensitive to the profile function parameter N. Therefore it is expected that this model is more sensitive to N_E, which is the parameter of the profile function in the 1CDD scheme, rather than N_{H+E}. Consequently, figure 2.10 shows the evolution of the GPDs $H^q_{\text{val}}(x,\xi,t)$ and $E^q_{\text{val}}(x,\xi,t)$ given in equations (2.98) and (2.99) for $N_{H+E}=1$ and N_E between 1 and 10.

2.4.3 Comparison to experimental data

At this stage, it appears judicious to provide a reminder of the different model acronyms used through this chapter:

DD+D GK model supplemented by a D-term as in (2.100) obtained from a fit of the data.

spin-0 1CDD Adaptation of the 1CDD formalism in the spinless case to the GPD H as discussed in sections 2.3.2 and 2.3.4.

spin-1/2 1CDD Combination of 1CDD and DD formalisms as detailed in section 2.4.2.

Looking at the CFF $\mathcal{H}$ shown on figure 2.11, it appears that the 1CDD model in the spin-1/2 case is less flexible than the scalar one.

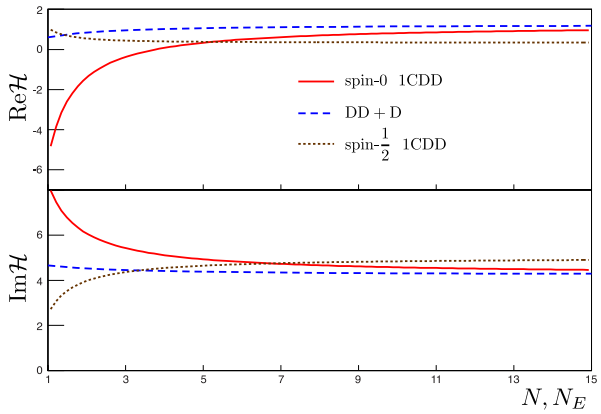

Figure 2.11: Comparison of flavour and charge singlet CFFs $\mathcal{H}$ and $\mathcal{E}$ when evolving N_E (spin-1/2 model discussed in this section) and N (spin-0 and GK models discussed in previous sections) for $x_B = 0.36$, $t = -0.23$ GeV^2 and $Q^2 = 2.3$ GeV^2. The full red line corresponds to the spin-0 1CDD parameterisation, the dashed blue line to the DD+D parameterisation, the dotted brown line to the spin-1/2 1CDD GPD H.

When comparing the model with the same data as previously on figures 2.12 and 2.13, it appears that the spin-1/2 1CDD model is hardly distinguishable from the DD+D one. This situation, at first quite surprising, can be explained by the lack of sensitivity of the data to the GPD $E(x,\xi,t)$. As the model for the GPD $E(x,\xi,t)$ has been deeply modified here from the original GK model, the situation would be probably different by adding data more sensitive to $E(x,\xi,t)$. Unfortunately, no such DVCS measurement is currently available in the valence region.

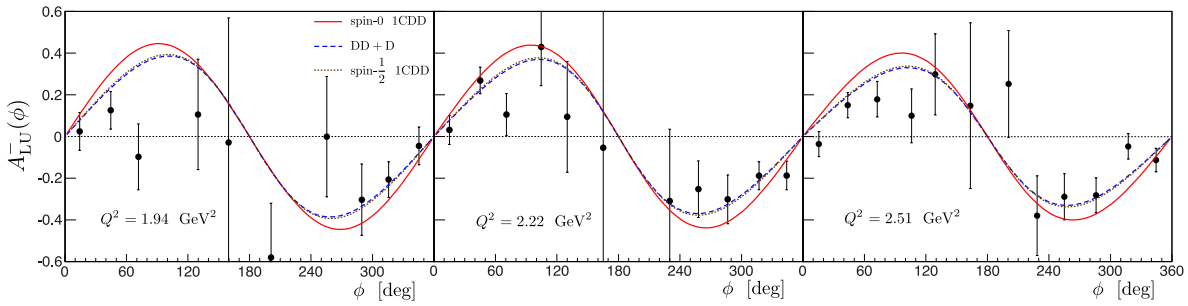

Figure 2.12: Comparison of 1CDD (full red line) and DD+D (dashed blue line) models with CLAS data at $t \simeq -0.17$ GeV^2 and such that $\frac{|t|}{Q^2} \leq 0.1$. From left to right: $x_B = 0.3205$, $t = -0.1705$ GeV^2 and $Q^2 = 1.9424$ GeV^2; $x_B = 0.3215$, $t = -0.1719$ GeV^2 and $Q^2 = 2.217$ GeV^2; $x_B = 0.3215$, $t = -0.1743$ GeV^2 and $Q^2 = 2.5078$ GeV^2. The full red line corresponds to the spin-0 1CDD parameterisation, the dashed blue line to the DD+D parameterisation, and the dotted brown line to the spin-1/2 1CDD parameterisation.

2.4.4 Beyond this approach

Within this approach of phenomenological parameterisation, it is possible to describe GPDs through DDs. Yet, DD models are most of the time implemented thanks to the RDDA, which is a simple way to ensure the forward limit. Playing on the DD scheme for implementing the RDDA adds an additional "degree of freedom", leading to different models with the same Ansatz. The models developed here in the 1CDD scheme suggest that it could be a way to model the GPD $H(x, \xi, t)$ and $E(x, \xi, t)$ consistently together.

Apart from DDs, other phenomenological approaches have been developed. For instance, the authors of Ref. [108, 157] have developed a method consisting in parameterising the Mellin moments of the GPDs and then rebuild it through the inverse Mellin-Barnes transform. Another method called "dual parameterisation" [155, 158, 159] consists in writing the GPDs as an infinite series of t-channel exchanges. It has been shown recently that those two approaches are in fact the same [160]. Both have been compared successfully to experimental data as well (see *e.g.* Ref. [127]).

All those phenomenological parameterisations played a key role in the establishment of the overall GPD framework. However, to deeply relate the hadron structure with QCD dynamics, one needs to turn to *ab-initio* computations. This is the topic of the next chapter, focusing on Dyson-Schwinger equations.

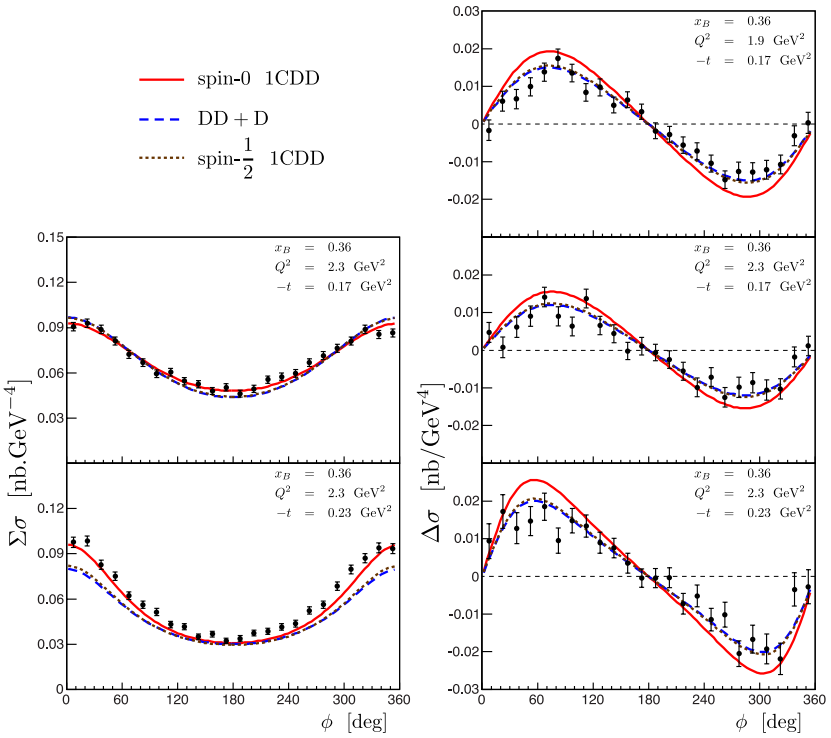

Figure 2.13: Comparison to JLab Hall A helicity-dependent and independent cross sections such that $\frac{|t|}{Q^2} \leq 0.1$. The full red line corresponds to the spin-0 1CDD parameterisation, the dashed blue line to the DD+D parameterisation, and the dotted brown line to the spin-1/2 1CDD parameterisation.

Chapter 3

The Dyson-Schwinger Approach

«Wozu jetzt noch so klug sein wollen,
wenn wir endlich ein klein wenig weniger dumm sein können?»
Bertolt Brecht in *Leben des Galilei.*

3.1 The Dyson-Schwinger equations

The Dyson-Schwinger equations (DSEs) [161–163] have been introduced at the very beginning of quantum field theory and have become classics, which can be found in textbooks like for instance in Ref. [164, 165]. In a nutshell, from the partition function of a quantum field theory, one can derive an infinite number of coupled equations relating the Green functions of the theory among themselves in a fully renormalised framework [166].

Just like lattice computations, Dyson-Schwinger equations are solved in Euclidean space. Therefore the question of how one should translate the results from Euclidean space to Minkowskian space must be raised. In the following, unless stated otherwise, Euclidean time will be used for computations, *i.e.* Schwinger functions are considered instead of Green functions. Then assuming that the measure fulfils the good properties, it is possible to get Wightman and Green functions by analytic continuation [167–169]. Therefore, comparison with experimental data will be done in Minkowskian space after continuation of the Schwinger functions. More details can be found in appendix B.

3.1.1 Gap equation

One of the most studied equations of the DSEs is the so called "gap" equation, which allows the computation of the quark propagator. As shown on figure 3.1 the gap equation bounds the fully dressed quark propagator with the fully dressed gluon propagator and the fully dressed quark-gluon vertex. More formally the quark propagator S writes:

$$S_q^{-1}(p) = Z_2(i\gamma\cdot p + m_q^0) + Z_1 \int_\Lambda \frac{\mathrm{d}^4k}{(2\pi)^4} g^2 D_{\mu\nu}(p-k)\gamma^\mu \frac{\lambda^a}{2} S(k) \frac{\lambda_a}{2} \Gamma_q^\nu(k,p), \qquad (3.1)$$

where q denotes the quark flavour, $D_{\mu\nu}$ is the gluon propagator, Γ_q^ν is the quark-gluon vertex, λ^a are the Gell-Mann matrices. The subscript Λ indicates that the integral is regularised, generally using the Pauli-Villard approach (like for instance in Ref. [170]). m_q^0 is the bare

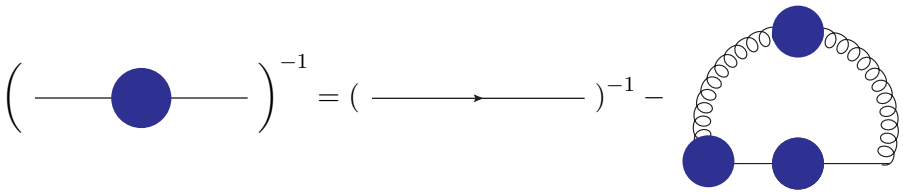

Figure 3.1: Graphical representation of the gap equation. Blue disks on Schwinger functions correspond to fully non-perturbative ones.

current quark mass. Z_2 and Z_1 are respectively the quark wave function and the quark-gluon vertex renormalisation constants. Indeed defining[1]:

$$\psi_0^{q_1} = \sqrt{Z_q}\psi^{q_1}, \quad A_0^\mu = \sqrt{Z_A}A^\mu, \quad g_0 = Z_g\ g, \tag{3.2}$$

one has:

$$Z_2 = Z_q \quad Z_1 = Z_g Z_q \sqrt{Z_A}. \tag{3.3}$$

They both depend on the renormalisation scale μ_R and on the regulator Λ. Therefore, a renormalisation condition is mandatory to fully define the gap equation:

$$S^{-1}(p)\Big|_{p^2=\mu_R^2} = i\gamma\cdot p + m_q(\mu_R), \tag{3.4}$$

where $m_q(\mu_R)$ is the renormalised current quark mass defined as:

$$m_q(\mu_R) = Z_m^{-1} Z_2 m_q^0, \tag{3.5}$$

with Z_m being the renormalisation constant associated with the Lagrangian mass term. It is also assumed that the renormalisation of the quark propagator is multiplicative. Then, the solution of the gap equation can be written as:

$$S_q(p) = -i\gamma\cdot p\sigma_{Vq}(p^2,\mu_R^2) + \sigma_{Sq}(p^2,\mu_R^2) = (i\gamma\cdot pA_q(p^2,\mu_R^2) + B_q(p^2,\mu_R^2))^{-1}, \tag{3.6}$$

but in order to solve it, one needs expressions of the two-point function $D_{\mu\nu}$ and of the three-point function Γ_q^ν. The reader should note that when properly renormalised, the quark propagator $S^q(p)$ does not depend on the regulator Λ but on the renormalisation scale μ_R. It is indeed the case in practice for large enough values of Λ [171]. The so-called dressed quark mass M_q is defined as:

$$M_q(p^2) = \frac{B_q(p^2,\mu_R^2)}{A_q(p^2,\mu_R^2)}, \tag{3.7}$$

and is independent of the renormalisation scale due to multiplicative renormalisation. Using the renormalisation conditions of equation (3.4) one can relate $M_q(p^2)$ with $m_q(\mu_R^2)$ through:

$$m_q(\mu_R) = M_q(\mu_R^2). \tag{3.8}$$

[1] Ghost and gauge parameter renormalisation constants not being used in the following, there are not defined here.

Coming back to equation (3.1), both of the gluon propagator and the quark gluon vertex satisfy Dyson-Schwinger equations which involve higher n-point functions. Consequently, in order to make actual computations, one need to define a truncation scheme. The best known is the weak-coupling expansion, which gives back usual perturbation theory. Due to asymptotic freedom, this scheme is one of the major successes of particle physics. However, it is not possible to obtain non-perturbative information within this approximation framework, *i.e.* it precludes an accurate description of low energy phenomena. Relevant non-perturbative schemes are detailed below (section 3.1.3). They allow the computation of the dressed quark mass M_q. As shown on figure 3.2, at low energy, the dressed quark mass increases even in the chiral limit. Mass is generated from nothing through a dynamical non-perturbative mechanism thought to be chiral symmetry breaking.

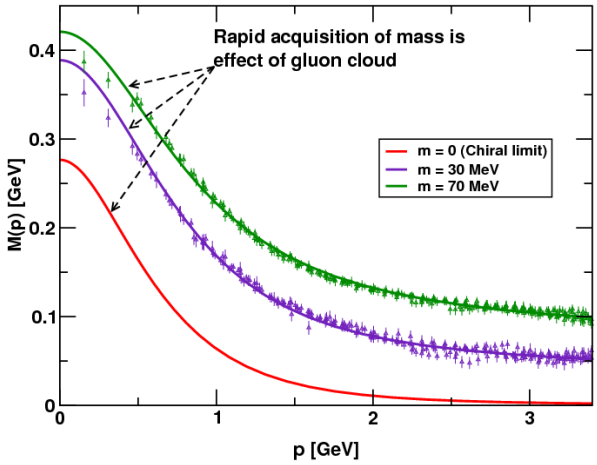

Figure 3.2: Computations of the dressed quark mass M_q with respect to the quark momentum p within the Dyson-Schwinger equation framework compared to lattice-QCD results. The colours correspond to different bare quark masses. At low p, QCD dynamics generates a significant mass term, even in the chiral limit. Dyson-Schwinger results come from Ref. [172, 173] whereas lattice data are taken from Ref. [174]. This figure comes from Ref. [175].

3.1.2 Pion Bethe-Salpeter equation

Just like Schwinger functions, bound state amplitudes can also be formulated in terms of self-consistent integral equations. It as been formulated at the beginning of the 1950's independently by several groups [162, 163, 176–178]. In the pion case and in coordinate space, one can write the Bethe-Salpeter wave function as:

$$\chi_{ij;q_1q_2}(x_1,x_2) = \langle 0|\,\mathrm{T}\left[\psi_i^{q_1}(x_1)\bar{\psi}_j^{q_2}(x_2)\right]|\pi,K\rangle\,, \tag{3.9}$$

where q_2 and q_1 stand for flavour indices, while i and j are Dirac indices. Due to translational invariance, $\chi_{ij;q_1q_2}(x_1,x_2)$ only depends on x_2-x_1. Thus in momentum space, the Bethe-Salpeter amplitude reads:

$$\chi_{ij;q_1q_2}(k,K) = \delta(K-k_1-k_2)\int \mathrm{d}^4x e^{+ik\cdot x}\,\langle 0|\,\mathrm{T}\left[\psi_i^{q_1}(\eta x)\bar{\psi}_j^{q_2}(-(1-\eta)x)\right]|\pi,K\rangle\,, \tag{3.10}$$

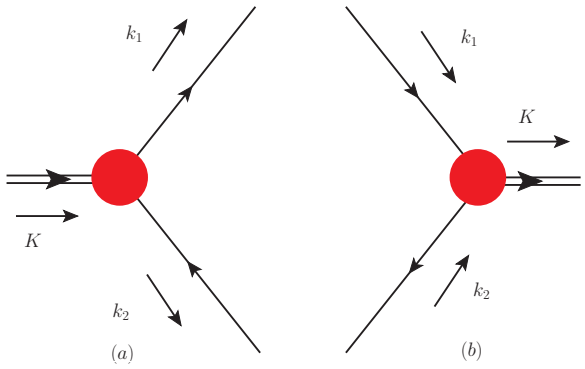

Figure 3.3: Momenta configurations for the Bethe-Salpeter amplitude defined in equation ((3.10)) (a) and its conjugate (b) defined in (3.12).

with:

$$\begin{array}{rclcrcl} X &=& \eta x_1 + (1-\eta)x_2 \ , & & K &=& k_1 + k_2 \ , \\ x &=& x_1 - x_2 \ , & & k &=& (1-\eta)k_1 - \eta k_2 \ , \end{array} \tag{3.11}$$

k_1 and k_2 being defined for the Bethe-Salpeter wave function on figure 3.3 and $\eta \in [0,1]$. Integration over X leads to the momentum conservation Dirac δ. One can also define the conjugate of the Bethe-Salpeter wave function:

$$\bar{\chi}_{ji,q_1q_2}(k,K) = \delta(K-k_1-k_2)\int \mathrm{d}^4x e^{+ik\cdot x}\,\langle \pi,K|\,\mathrm{T}\left[\psi_j^{q_2}(-(1-\eta)x)\bar{\psi}_i^{q_1}(\eta x)\right]|0\rangle\,, \tag{3.12}$$

and also the Bethe-Salpeter amplitudes:

$$\begin{array}{rcl} \Gamma_\pi(k,K) &=& S^{-1}(-k_2)\ \chi(k,K)\ S^{-1}(k_1) \\ \bar{\Gamma}_\pi(k,K) &=& S^{-1}(-k_2)\ \bar{\chi}(k,K)\ S^{-1}(k_1) \end{array} . \tag{3.13}$$

Due to discrete symmetries, Γ_π and $\bar{\Gamma}_\pi$ are related to each other through:

$$\bar{\Gamma}_\pi(k,K) = C^\dagger \Gamma_\pi^T(-k,-K)C, \tag{3.14}$$

where ^{T} denotes transposition and $C = i\gamma^2\gamma^4$ is the charge conjugation operator in the Dirac space (see appendix C). As shown in Ref. [179], the Bethe-Salpeter amplitude can be expanded in a Dirac basis such that:

$$\Gamma_\pi(k,K) = \gamma_5[iE(k,K) + \gamma\cdot K\ F(k,K) + k\cdot K\ k\cdot\gamma G(k,K) + \sigma_{\mu\nu}k^\mu K^\nu H(k,K)], \tag{3.15}$$

in order to deal with four scalar form factors. The Bethe-Salpeter amplitude is the solution of the so-called homogeneous Bethe-Salpeter equation:

$$\Gamma_{\pi;ij}(p,P) = \int \frac{\mathrm{d}^4k}{(2\pi)^4}\,[S(k_{\bar{\eta}})\Gamma_\pi(k,P)S(k_\eta)]_{ab}\,K_{ij}^{ab}(k,p,P), \tag{3.16}$$

where:

$$\begin{array}{rcl} k_\eta &=& \ \ k_1 = k + \eta P, \\ k_{\bar{\eta}} &=& -k_2 = k - (1-\eta)P, \end{array} \tag{3.17}$$

η is defined in equations (3.11), and is an arbitrary choice of definition of the relative momentum between the 2 quarks. Therefore, no observables should depend on η. Here $K(k,p,P)$ is

the amputated quark-antiquark scattering kernel as shown on figure 3.4. At this point, the expression of such a scattering kernel remains a major difficulty. Indeed, it involves all the 2-particle irreducible diagrams in the s-channel (see *e.g.* Ref. [37]), and it is hardly possible to construct a kernel satisfying all the required symmetry properties. For instance, in modeling such a kernel, one should be very careful to fulfil properties like the Ward-Takahashi Identities (WTI) and to make the model consistent with the gap equation (3.1).

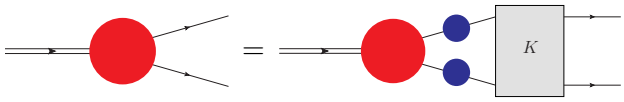

Figure 3.4: Graphical represenation of the homogeneous Bethe-Salpeter equation. Red disks represent objects fulfilling an homogeneous Dyson-Schwinger equation.

The question of the normalisation of the Bethe-Salpeter wave function must also be mentioned. Indeed, being an eigenvalue equation, the Bethe-Salpeter equation does not fix the normalisation of the Bethe-Salpeter amplitude and therefore, a normalisation condition must be chosen. The usual quantum mechanic condition $\int \mathrm{d}x|\psi(x)|^2 = 1$ cannot be applied here for the Bethe-Salpeter wave function. Indeed it is not a "true" wave function in the sense that its norm cannot be seen as a probability density. Only projections of the Bethe-Salpeter wave function on the instant front or on the light front (see chapter 5 and appendix E) can be seen as "true" wave functions. Therefore, it is legitimate to wonder how to normalise the Bethe-Salpeter wave function. A normalisation condition have been elegantly derived by Lurié *et al.* [180] (for previous derivations, see references therein) without using any conserved quantities. In a covariant form this normalisation condition gives [181]:

$$\begin{aligned} 2P^\mu \quad = \quad & \mathrm{Tr}_{\mathrm{CDF}}\left[\int \frac{d^4k}{2\pi^4}\bar{\Gamma}_\pi\left(k,P\right)\frac{\partial S(k_\eta)}{\partial P_\mu}\Gamma_\pi\left(k,P\right)S(k_{\bar{\eta}})\right] \\ & +\mathrm{Tr}_{\mathrm{CDF}}\left[\int \frac{d^4k}{2\pi^4}\bar{\Gamma}_\pi\left(k,P\right)S(k_\eta)\Gamma_\pi\left(k,P\right)\frac{\partial S(k_{\bar{\eta}})}{\partial P_\mu}\right] \\ & +\mathrm{Tr}_{\mathrm{CDF}}\left[\int \frac{d^4k}{2\pi^4}\frac{d^4q}{2\pi^4}\bar{\chi}_\pi(q,P)\frac{\partial K(q,k,P)}{\partial P^\mu}\chi_\pi(k,P)\right], \end{aligned} \tag{3.18}$$

where $K(q,k,P)$ is the Bethe-Salpeter kernel of equation (3.16) (see also figure 3.4) and $\mathrm{Tr}_{\mathrm{CDF}}$ stands for the trace on colour, Dirac and flavour indices.

3.1.3 Existing truncation schemes

As stressed above, if equations (3.1) and (3.16) can be derived from path integrals, solving them requires to know higher n-point functions which themselves obey their own Dyson-Schwinger equations. In order to say something non-perturbative on the propagator and the Bethe-Salpeter amplitude, one need to use a symmetry-preserving truncation scheme which is also non-perturbatively applicable (contrarily to the weak coupling approximation).

Such truncation schemes have been introduced in the 1990s [182, 183] and recently refined [184]. They have achieved many successes, among them (non exhaustively) the computation of the quark running masses compared to lattice data (figure 3.2), the ab-initio computations

of mesons masses (*e.g.* Ref. [185]) and form factors (*e.g.* Ref. [186]). One of the key points of those schemes is their fulfilment of WTI and the Axial-Vector WTI (AVWTI). The latter relate the axial-vector vertex $\Gamma^i_{5\mu}(p,P)$ to the axial vertex $\Gamma^i_5(p,P)$ where i is an isospin index, through:

$$P^\mu \Gamma^i_{5\mu}(p,P) = \frac{\tau^i}{2}\left(S^{-1}(k_\eta) i\gamma_5 + i\gamma_5 S^{-1}(k_{\bar{\eta}})\right) - i\left[m_{q_1}(\mu_R) + m_{q_2}(\mu_R)\right]\Gamma^i_5(p,P), \tag{3.19}$$

where the $m_q(\mu_R)$ are the renormalised current quark masses of flavour q defined in equation (3.5), and the τ^i are the Pauli matrices. $\Gamma^i_{5\mu}$ and Γ^i_5 are defined as:

$$S(-p_2)\Gamma^i_{5\mu}(p,P)S(p_1) = \mathrm{FT}\left[\langle 0|\,\mathrm{T}\left[J^i_{5\mu}(x)\psi(y)\bar{\psi}(z)\,|0\rangle\right]\right], \tag{3.20}$$

$$S(-p_2)\Gamma^i_{5}(p,P)S(p_1) = \mathrm{FT}\left[\langle 0|\,\mathrm{T}\left[J^i_{5}(x)\psi(y)\bar{\psi}(z)\right]|0\rangle\right], \tag{3.21}$$

where FT stands for the Fourier Transform, $J^i_{5\mu}(x) = \bar{\psi}(x)\gamma_\mu\gamma_5\tau^i\psi(x)$ and $J^i_5(x) = \bar{\psi}(x)\gamma_5\tau^i\psi(x)$. Partially Conserved Axial Current (PCAC) relations relate the axial vector current to the effective pion fields $\pi^i(x)$ through the approximate relation [187, 188]:

$$m_\pi^2 f_\pi \pi^i(x) = \partial^\mu J^i_{5\mu}(x), \tag{3.22}$$

m_π being the pion mass and f_π the pion decay constant. Consequently, when $P^2 + m_\pi^2 = 0$, $\Gamma^i_{5\mu}$ and Γ^i_5 are dominated by contributions from an on-shell pion, *i.e.* from the pion Bethe-Salpeter amplitude. Those contributions appear as poles at $P^2 + m_\pi^2 = 0$ in $\Gamma^i_{5\mu}$ and Γ^i_5 [189]. Therefore, to get access to the pion Bethe-Salpeter amplitude, one can compute $\Gamma^i_{5\mu}$ and Γ^i_5 and then extract Γ_π from them.

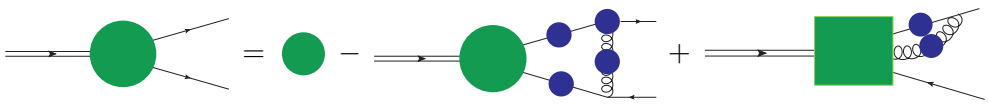

Figure 3.5: Graphical representation of the inhomogeneous Bethe-Salpeter equation for the axial-vector vertex. The large green circles correspond to $\Gamma_{5\mu}$, the green colour encoding the fact that this objetc obey to an inhomogeneous Bethe-Salpeter equation. The small green cirle is the inhomogene term $\gamma^\mu\gamma_5$, and the green square $\Lambda_{5\mu\nu}$. This graphical representation also work for the axial vertex.

The Axial-Vector vertex fulfils an inhomogeneous equation (omitting the isospin indices for brevity):

$$\begin{aligned}\Gamma_{5\mu}(p,P) &= Z_2\gamma_\mu\gamma_5 \\ &\quad - Z_1\, g^2 \int \frac{\mathrm{d}^4k}{(2\pi)^4} D_{\alpha\beta}(p-k)\frac{\lambda^a}{2}\gamma^\alpha S(-k_{\bar{\eta}})\Gamma_{5\mu}(k,P)S(k_\eta)\frac{\lambda_a}{2}\Gamma^\beta(q_{\bar{\eta}},k_{\bar{\eta}}) \\ &\quad + Z_1\, g^2 \int \frac{\mathrm{d}^4k}{(2\pi)^4} D_{\alpha\beta}(p-k)\frac{\lambda^a}{2}\gamma^\alpha S(k_\eta)\frac{\lambda_a}{2}\Lambda_{5\mu\beta}(k,q,P).\end{aligned} \tag{3.23}$$

As it can be seen on figure 3.5, $\Lambda_{5\mu\nu}$ is a four-point function involving the bound state itself. This equation can be established using the functional integral framework and a Cornvall-Jackiw-Tomboulis-like effective action [190]. The proof is sketched in Ref. [191] and more

formal details can be found in Ref. [182]. In the same way, the pseudo-scalar vertex $\Gamma_5(k,P)$ and its four-point counterpart $\Lambda_{5\beta}(q,k,P)$ satisfy a similar Bethe-Salpeter equation:

$$\begin{aligned}\Gamma_5(p,P) &= Z_2\gamma_5 \\ &\quad -Z_1\, g^2 \int \frac{\mathrm{d}^4k}{(2\pi)^4} D_{\alpha\beta}(p-k)\frac{\lambda^a}{2}\gamma^\alpha S(-k_{\bar\eta})\Gamma_5(k,P)S(k_\eta)\frac{\lambda_a}{2}\Gamma^\beta(q_{\bar\eta},k_{\bar\eta}) \\ &\quad +Z_1\, g^2 \int \frac{\mathrm{d}^4k}{(2\pi)^4} D_{\alpha\beta}(p-k)\frac{\lambda^a}{2}\gamma^\alpha S(k_\eta)\frac{\lambda_a}{2}\Lambda_{5\beta}(k,q,P). \end{aligned} \tag{3.24}$$

It has been shown [184] that the AVWTI (3.19) implies the following relation for the four-point functions $\Lambda_{5\mu\beta}$ and $\Lambda_{5\mu}$:

$$P^\mu\Lambda_{5\mu\beta}(k,q,P) = \Gamma_\beta(k_\eta,q_\eta)i\gamma_5 + i\gamma_5\Gamma_\beta(k_{\bar\eta},q_{\bar\eta}) - i\left[m_{q_1}(\mu_R)+m_{q_2}(\mu_R)\right]\Lambda_{5\beta}(k,p,P), \tag{3.25}$$

with $\Gamma_\beta(q,k)$ being the quark-gluon vertex. Then assuming that the quark-gluon vertex $\Gamma^\mu(k,P)$ satisfies a WTI-like relation:

$$iP_\mu\Gamma^\mu(k,P) = \mathcal{N}(P^2)\left[S^{-1}(k_\eta) - S^{-1}(k_{\bar\eta})\right], \tag{3.26}$$

where $\mathcal{N}$ is flavour-independent, it is possible to close the system and solve the equations by directly relating $\Lambda_{5\mu}(q,k,P)$ to the form factors entering the expansion of $\Gamma_5(k,P)$ in a Dirac basis. The true quark-gluon vertex does not satisfy a WTI-like relation. Instead it fulfils the Slavnov-Taylor identity. This should be considered as part of the approximations in the truncation scheme [184, 192].

Rainbow Ladder truncation scheme

At this stage, the remaining missing piece is the gap equation kernel (3.1). Two main approximations can be made in order to evaluate this kernel [193]. The first one, called the "*Rainbow Ladder*" (RL) approximation, assumes that the "gap" kernel has the form:

$$Z_1 g^2 D_{\mu\nu}(p-k)\Gamma^\nu_a(k,p) = (p-k)^2\mathcal{G}\left((p-k)^2\right)D^{\text{free}}_{\mu\nu}(p-k)\gamma^\nu, \tag{3.27}$$

where $D^{\text{free}}_{\mu\nu}(p-k)$ is the free gluon propagator in the Landau gauge, and $\mathcal{G}(s)$ models the non-perturbative behaviour of the propagator at small s, and sticks to the perturbative one at large s, *i.e.* $s \geq 2$ GeV^2. Of course, several models for the gluon propagator in the infrared have been suggested. They are summarised in Ref. [194], where the authors also suggest a new expression:

$$\left\{\begin{array}{rcl} \mathcal{G}(s) &=& \frac{8\pi^2}{\omega^4}De^{-\frac{s}{\omega^2}} + \frac{8\pi^2\gamma_m K(s)}{\ln\left[e^2-1+\left(1+\frac{s}{\Lambda_{\text{QCD}}}\right)^2\right]} \\ K(s) &=& \frac{1-e^{-\frac{s}{4m_{IR}^2}}}{s} \end{array}\right. \tag{3.28}$$

where $\gamma_m = \frac{12}{33-2N_f}$ (N_f being the number of involved flavours), $m_{IR} = 0.5$ GeV (this value is chosen to ensure the perturbative behaviour for $s \geq 2$ GeV^2 [181]). The results are not very sensitive to the two remaining parameters D and ω, provided that $\omega \in [0.4, 0.6]$ GeV and $D\omega$ remains constant [194]. The RL approximation also assumes that the quark-gluon vertex is bare:

$$\lambda^a\Gamma^\mu(k,P) = \gamma^\mu\lambda^a. \tag{3.29}$$

Injected in equation (3.25), this expression of the quark-gluon vertex is compatible with $\Lambda_{5\mu\beta} = \Lambda_{5\mu} = 0$, which is the solution mostly chosen in this case.

Another possible truncation scheme is the so-called "*Dynamical-Chiral-Symmetry-Breaking improved kernel*" (DCSB). Within this scheme, the kernel of gap equation is expressed as:

$$Z_1 g^2 D_{\mu\nu}(p-k)\Gamma^\nu_a(k,p) = \mathcal{G}\left((p-k)^2\right) D^{\text{free}}_{\mu\nu}(p-k) Z_2 \tilde{\Gamma}^\nu(k,p), \tag{3.30}$$

where the gluon propagator model $\mathcal{G}$ has already been described in equation (3.28). The difference here between the RL and the DCSB approximations is mainly contained inside the effective quark-gluon vertex $\tilde{\Gamma}^\nu$. Indeed, in the DCSB case, the vertex Ansatz is non-point-like and is built in order to fulfil equation (3.26). Therefore, it induces through equation (3.25) non-zero $\Lambda_{5\mu\nu}$ and $\Lambda_{5\nu}$ contributions. The choice of the vertex Ansatz is crucial in order to accurately describe observables. One possible choice is to combine the so-called Ball-Chiu vertex [195], with an additional component generating the contribution of the anomalous chromomagnetic moment (ACM)[193]:

$$\tilde{\Gamma}^\nu(k,p) = \Gamma^\nu_{\text{BC}}(k,p) + \Gamma^\nu_{\text{ACM}}(k,p). \tag{3.31}$$

Details on those Ansätze are given in Ref. [193].

Finally, one should keep in mind that the Landau gauge plays an important role here. Indeed, considering the covariant gauge parameter κ, $\kappa = 0$ is a fixed point of the renormalisation group, *i.e.* κ remains equal to 0 at any order of perturbation theory. It allows one to model the quark-gluon vertex without adding an explicit dependence on the gauge parameter.

3.1.4 Numerical solutions and analytic parameterisations

Using the pion decomposition in equation (3.15), it is then possible to numerically solve equations (3.1) and (3.16) through (3.23) using discretisation schemes, and thus to get grids of numerical estimates for A, B, E_π, F_π and G_π (within the presented scheme, H_π does not contribute significantly and consequently is usually neglected [196]). Yet, those kinds of grids may be inadequate to further computations of non-perturbative functions. Therefore, parameterisations have been developed in order to interpolate inside these grids.

In the case of the propagator, a typical parameterisation involves complex conjugate poles [197]:

$$S(k) = \sum_j^N \left[\frac{z_j}{i\gamma\cdot k + m_j} + \frac{z_j^*}{i\gamma\cdot k + m_j^*} \right], \tag{3.32}$$

where the m_j and the z_j are fitted to the numerical results. One of the advantages of this parameterisation is that dealing with space-like momenta, it cannot produce on-shell quarks. It provides good fits for $N \geq 2$.

The pion components in a Dirac basis are parameterised using the so-called Nakanishi integral representation. It has been shown in Ref. [198], that the solutions of the Bethe-Salpeter equation in Minkowskian space could be written as:

$$\chi(k,P) = \mathcal{Y}_{lm}(\mathbf{p}) \int_{-1}^{1} \mathrm{d}z \int_0^\infty \mathrm{d}\gamma \frac{\varphi_l^{[n]}(z,\gamma)}{\left(\gamma + \tilde{m}^2 - \frac{1}{4}M^2 - k^2 - P\cdot k z - i\epsilon\right)^{n+2}}, \tag{3.33}$$

where $\tilde{m}$ is the constituent mass, M the bound state mass, and n is a dummy parameter providing that:

$$\lim_{\gamma\to\infty} \frac{\varphi_l^{[n]}(z,\gamma)}{\gamma^n} = 0. \tag{3.34}$$

It should be stressed here that $\varphi(z,\gamma)$ may contain various structures like Dirac δ, cuts, etc. Still, this formula is used in modern computations of Bethe-Salpeter amplitudes (see *e.g.* Ref. [196, 199]), and is a generalisation of a work done by Wick on S-waves only [200] for particles of any orbital momentum l. $\mathcal{Y}_{lm}$ is the so-called solid harmonic:

$$\mathcal{Y}_{lm}(\mathbf{p}) = |\mathbf{p}|^l \; Y_{lm}(\theta,\phi), \tag{3.35}$$

with Y_{lm} being the spherical harmonic. Such a parameterisation has been used for instance in Ref. [196] to compute the pion DA from the numerical solutions of the Dyson-Schwinger equations. Introducing a generic notation $\mathcal{F}_\pi$ to denote E_π, F_π and G_π, $\mathcal{F}_\pi$ is split into two parts corresponding to the dominant contribution, respectively in the IR and the UV regions:

$$\mathcal{F}_\pi(k,P) = \mathcal{F}_{IR}(k,P) + \mathcal{F}_{UV}(k,P). \tag{3.36}$$

Then, $\mathcal{F}_{IR}(k,P)$ and $\mathcal{F}_{UV}(k,P)$ are parameterised independently using a functional form *à la* Nakanishi (equation (3.33)). Details and values of the parameters can be found in Ref. [196].

3.1.5 An algebraic model

Based on the Nakanishi representation, it is possible to provide an algebraic and insightful model for both the quark propagator and the Bethe-Salpeter amplitude [196]. The idea is to keep only the diagonal term of the Bethe-Salpeter amplitude (3.15) in the Nakanishi representation (3.33), assuming that it is dominant. Concerning the quark propagators, the algebraic model use one of the building blocks of the parameterisation (3.32):

$$\begin{aligned}
S(p) &= \big[-i\gamma\cdot p + M\big]\Delta_M(p^2), && (3.37)\\
\Delta_M(s) &= \frac{1}{s+M^2}, && (3.38)\\
\Gamma_\pi(k,P) &= i\gamma_5 \frac{M}{f_\pi} M^{2\nu} \int_{-1}^{+1} \mathrm{d}z\, \rho_\nu(z)\; \big[\Delta_M(k_{+z}^2)\big]^\nu, && (3.39)\\
\rho_\nu(z) &= R_\nu (1-z^2)^\nu, && (3.40)\\
k_{+z} &= k - \left(\frac{1-z}{2} - \eta\right) P, && (3.41)
\end{aligned}$$

with the parameter ν controlling the width of the vertex. Focusing on the pion DA $\varphi_\pi(x)$ defined in equation (2.40), one can compute it by projecting the Bethe-Salpeter wave function on the lightcone:

$$f_\pi \varphi_\pi(u) = \mathrm{Tr}\left[Z_2 \int \frac{\mathrm{d}^4k}{(2\pi)^4}\; \delta(k_\eta\cdot n - uP\cdot n)\; \gamma\cdot n\; \gamma_5\; \chi_\pi(k,P)\right], \tag{3.42}$$

k_η being defined in equation (3.17). Using the parameterisation provided above (equations (3.37) to (3.41)), the authors of Ref. [196] have computed the Mellin moments $\mathcal{M}_m^{\mathrm{DA}}$ of the

DA $\phi_\pi(u)$ through usual Feynman parameterisation. After normalising those Mellin moments, they get:

$$\mathcal{M}_m^{\mathrm{DA}} = \frac{\Gamma(1+m+\nu)}{\Gamma(2+m+2\nu)} \frac{\Gamma(2+2\nu)}{\Gamma(1+\nu)}, \tag{3.43}$$

which correspond to a DA such that:

$$\varphi_\pi(u) = \frac{\Gamma(2\nu+2)}{\Gamma(\nu+1)^2} u^\nu (1-u)^\nu. \tag{3.44}$$

Two interesting points should be stressed. There are only two dimensional parameters here, f_π and M. Being a probability amplitude, the DA is dimensionless and thus can only depend on ratios of M and f_π. However, in the previous result, it does not. In addition, for $\nu = 1$, one finds the so-called asymptotic DA:

$$\varphi_\pi^{\mathrm{Asymp.}}(x) = 6x(1-x). \tag{3.45}$$

3.2 Mellin moments of the pion GPD

3.2.1 Isospin properties

The successes of the DSE-BSE in the case of the pion DA encourage us to turn to more complicated objects like GPDs. As we have seen previously in equation (1.30), the pion being a spinless hadron, one has to deal with only one GPD[2] that we will denote $H_\pi^q(x,\xi,t)$. Yet, it will be useful to introduce another basis, not built on eigenvalues of the charge operator, but on eigenvalues of the isospin operator, *i.e.* :

$$\begin{aligned} \delta^{ab} H^{I=0}(x,\xi,t) &= \frac{1}{2}\int \frac{\mathrm{d}z^-}{2\pi} e^{ixP^+z^-} \\ &\times \left\langle \pi^b, P+\frac{\Delta}{2}\middle| \bar\psi\left(-\frac{z}{2}\right) \mathcal{I}\left[-\frac{z}{2};\frac{z}{2}\right] \gamma^+ \psi\left(\frac{z}{2}\right) \middle| \pi^a, P-\frac{\Delta}{2}\right\rangle_{z^+=0,z_\perp=0}, \end{aligned} \tag{3.46}$$

$$\begin{aligned} i\epsilon^{abc} H^{I=1}(x,\xi,t) &= \frac{1}{2}\int \frac{\mathrm{d}z^-}{2\pi} e^{ixP^+z^-} \\ &\times \left\langle \pi^b, P+\frac{\Delta}{2}\middle| \bar\psi\left(-\frac{z}{2}\right) \tau^c\gamma^+ \left[-\frac{z}{2};\frac{z}{2}\right] \psi\left(\frac{z}{2}\right) \middle| \pi^a, P-\frac{\Delta}{2}\right\rangle_{z^+=0,z_\perp=0}, \end{aligned} \tag{3.47}$$

where ϵ^{abc} is the fully anti-symmetric tensor. $H^{I=0}(x,\xi,t)$ is called the isoscalar GPD, and $H^{I=1}(x,\xi,t)$ the isovector one. ψ denotes the quark flavour doublet u and d. The $\left|\pi^i\right\rangle$ stand for a cartesian basis of the adjoint representation of the Lie algebra $\mathfrak{su}(2)$, on which eigenstates of the charge operator can be expanded:

$$\left|\pi^\pm\right\rangle = \frac{1}{\sqrt{2}}\left(\left|\pi^1\right\rangle \pm i\left|\pi^2\right\rangle\right), \tag{3.48}$$

$$\left|\pi^0\right\rangle = \left|\pi^3\right\rangle. \tag{3.49}$$

[2]Due to the available experimental data, the helicity flip GPD H_π^T is not considered in this study, even if the computation would be rather similar.

From the previous definitions, one can deduce the relations between the "isospin" GPDs and the "quark" GPDs:

$$\begin{aligned} H^{I=0}(x,\xi,t) &= H^u_{\pi^\pm}(x,\xi,t) + H^d_{\pi^\pm}(x,\xi,t) && (3.50)\\ &= H^u_{\pi^0}(x,\xi,t) + H^d_{\pi^0}(x,\xi,t), && (3.51)\\ H^{I=1}(x,\xi,t) &= H^u_{\pi^+}(x,\xi,t) - H^d_{\pi^+}(x,\xi,t) && (3.52)\\ &= -\big(H^u_{\pi^-}(x,\xi,t) - H^d_{\pi^-}(x,\xi,t)\big), && (3.53)\\ 0 &= H^u_{\pi^0}(x,\xi,t) - H^d_{\pi^0}(x,\xi,t). && (3.54) \end{aligned}$$

One can deduce from (3.50), (3.52) and (3.53) that:

$$\begin{aligned} H^u_{\pi^+}(x,\xi,t) &= H^d_{\pi^-}(x,\xi,t), && (3.55)\\ H^d_{\pi^+}(x,\xi,t) &= H^u_{\pi^-}(x,\xi,t), && (3.56) \end{aligned}$$

and adding (3.51) and (3.54):

$$H^u_{\pi^0}(x,\xi,t) = H^d_{\pi^0}(x,\xi,t) = \frac{1}{2}\big(H^u_{\pi^+}(x,\xi,t) + H^d_{\pi^+}(x,\xi,t)\big). \quad (3.57)$$

The charge symmetry also strengthens the constraints on quark GPDs:

$$\begin{aligned} H^u_{\pi^+}(x,\xi,t) &= -H^u_{\pi^-}(-x,\xi,t), && (3.58)\\ H^d_{\pi^+}(x,\xi,t) &= -H^d_{\pi^-}(-x,\xi,t), && (3.59)\\ H^u_{\pi^0}(x,\xi,t) &= -H^u_{\pi^0}(-x,\xi,t). && (3.60) \end{aligned}$$

which yields:

$$H^u_{\pi^+}(x,\xi,t) = -H^d_{\pi^+}(-x,\xi,t). \quad (3.61)$$

In terms of the GPDs corresponding to the π^+ state, we get:

$$\begin{aligned} H^{I=0} &= H^u(x,\xi,t) - H^u(-x,\xi,t), && (3.62)\\ H^{I=1} &= H^u(x,\xi,t) + H^u(-x,\xi,t). && (3.63) \end{aligned}$$

which makes $H^{I=0}$ (resp. $H^{I=1}$) an odd (resp. even) function of x:

$$H^I(-x,\xi,t) = (-1)^{1-I} H^I(x,\xi,t) \quad \text{for } I = 0, 1. \quad (3.64)$$

The parity of the isospin GPDs has a important role on the D-term. Indeed, as we have previously seen, when computing the Mellin moments of the GPD, the D-Term contribution corresponds to the highest degree in ξ in odd moments. Therefore, the D-term is entirely carried by $H^{I=0}(x,\xi,t)$.

3.2.2 The triangle diagram approximation

Computing the pion GPD requires several assumptions. Restricting the study to the description of a pion composed of two dressed valence quarks, a covariant way to compute the GPD is to deal with a triangle Feynman diagram (see figure 3.6). Within this assumption, one will get the so-called valence GPD. But in order to get it, one needs three main ingredients: an effective propagator, an effective $q\bar{q}\pi$ vertex, and a non-local operator to put between

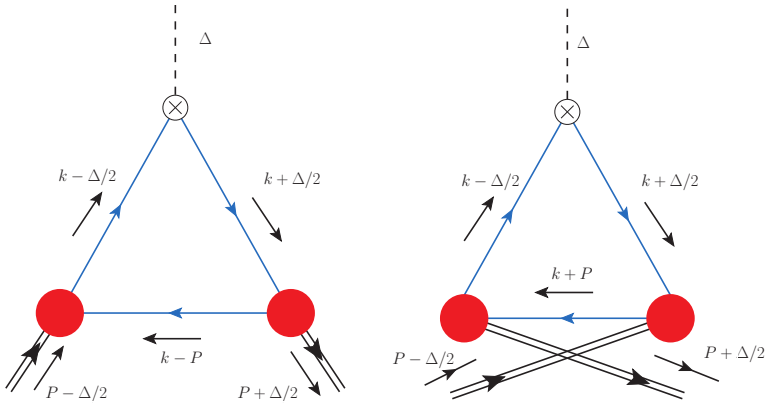

Figure 3.6: Triangle diagram approximation. *Left*: case of the quark GPD. *Right*: case of the anti-quark GPD. Computations of the Mellin moments requires to integrate on the four dimensions of space, and thus the lightcone direction is not emphasised like in figure 1.6.

dressed quark states. Several attempts have been made in the past to compute pion GPDs. Some techniques use for instance effective Lagrangians [134, 201], defining effective couplings between hadrons and partons. Other approaches have been developed, based on the Nambu-Jona-Lasinio model like for instance in Ref. [202, 203]. Those approaches are based on triangle diagrams computations.

The next step in GPD modeling was to use the Bethe-Salpeter framework. This has been done in several studies [204–208], usually with simple Bethe-Salpeter vertices and using the triangle diagrams approach. In Ref. [204, 208] and Ref. [206] the $q\bar{q}\pi$ coupling has the form $i\gamma^5 g$ with constant g. However, this point-like vertex introduces divergences when computing triangle diagrams and must be regularized using in the first case a Pauli-Villars approach, and in the second case, a sharp cut-off on the square of relative 4-momenta.

Difficulties have also been stressed. Van Dyck [207] highlighted the support problem that one can meet in Bethe-Salpeter constituent quark models in the instant front. Discontinuities are reported in Ref. [202, 203, 205] for models which fulfil the support properties: one at the boundary $x = 1$ and another at $x = \xi$.

Other techniques have been used in order to compute GPDs. For instance in Ref. [208], the authors model the pion GPD within three different approaches: a covariant one, a second one based on Vector Meson Models and a third one using Hamiltonien Lightcone dynamics. All those approaches seem complementary with each others. One should also keep in mind that the helicity flip GPD H_T has also been modeled, for instance in Ref. [209].

In the continuation of those works, the pion GPD is studied here using the Bethe-Salpeter approach developed in the previous section within the triangle diagram framework. Still, two main differences can be outlined: the complexity of the Bethe-Salpeter vertex (equation (3.39)), and the idea of modeling the Mellin moments $\mathcal{M}_m(\xi, t)$ of the GPD defined in equation (1.44) rather than the GPD itself. The latter point has several advantages. One can show that they are proportional to a *local* matrix element:

$$\mathcal{M}_m(\xi,t) = \frac{1}{2(P\cdot n)^{m+1}} \left\langle \pi, P + \frac{\Delta}{2} \middle| \bar{q}(0)\gamma^+ (i\overleftrightarrow{D}\cdot n)^m q(0) \middle| \pi, P - \frac{\Delta}{2} \right\rangle, \tag{3.65}$$

which allows one to get a local object at the top corner of the triangle diagram. Here $\overleftrightarrow{D} =$

$\frac{1}{2}\left(\overrightarrow{D}-\overleftarrow{D}\right)$, where D is the covariant derivative:

$$D\cdot n = n\cdot\partial - ig\ n\cdot A. \tag{3.66}$$

Consequently, GPDs are often computed in the light-cone gauge where $A^+=0$ in order to kill the Wilson line. However, the choice of gauge must be consistent with the one used to solve the Dyson-Schwinger equations. In this case, it is the Landau gauge. Consequently, one has:

$$(\overleftrightarrow{D}\cdot n)^m = \frac{1}{2^m}\sum_{j=0}^{m}\binom{m}{j}(\overrightarrow{\partial}\cdot n - n\cdot\overleftarrow{\partial})^j(2ig\ n\cdot A)^{m-j}, \tag{3.67}$$

which means that gluon field enters the game inside the twist-two operator. It is assumed here that gluon field contributions do not modify significantly the results. Thus the Mellin moments are restricted to the case $j=m$.

The normalisation of the overall triangle diagram strongly depends of the twist-two operators. Mandelstam [210] has introduced a normalisation condition of the Bethe-Salpeter amplitude based on charge conservation in the ladder approximation. It relies on the computation of a form factor at vanishing momentum transfer within the triangle diagram approximation. The value of the form factor is then fixed to 1. In terms of Mellin moments of the pion GPD, it is nothing else than fixing $\mathcal{M}_0(0,0)$ to 1. Using the Ward-Takahashi identity:

$$i\Delta^\mu\Gamma_\mu(k+\frac{\Delta}{2},k-\frac{\Delta}{2}) \ = \ S^{-1}(k+\frac{\Delta}{2}) - S^{-1}(k-\frac{\Delta}{2}), \tag{3.68}$$

Mandelstam's condition was shown [180, 211] to be equivalent to the canonical normalisation of the Bethe-Salpeter amplitude given in equation (3.18).

3.2.3 Computing Mellin Moments

Following the Mandelstam approach, the $m=0$ local twist-two operator is assimilated to the quark-photon vertex Γ_μ, ensuring charge conservation. Higher-m operators are built on the first one, by adding the action of the $(i\overleftrightarrow{D}\cdot n)^m$ on the incoming and outgoing quarks. Applied to the quark fields, these operators give: $(k\cdot n)^m$. Consequently, one arrives to the following formula:

$$\begin{aligned}
2(P\cdot n)^{m+1}\mathcal{M}_m(\xi,t) \ = \ & \mathrm{Tr}_{\mathrm{CFD}}\left[\int\frac{\mathrm{d}^4k}{(2\pi)^4}(k\cdot n)^m\,\tau_- i\bar{\Gamma}_\pi\left((1-\eta)\left(k+\frac{\Delta}{2}\right)+\eta(k-P),P+\frac{\Delta}{2}\right)\right. \\
& S(k+\frac{\Delta}{2})\ i\ n\cdot\Gamma(k+\frac{\Delta}{2},k-\frac{\Delta}{2})\ S(k-\frac{\Delta}{2}) \\
& \left.\tau_+ i\Gamma_\pi\left(\eta(k-P)+(1-\eta)\left(k-\frac{\Delta}{2}\right),P-\frac{\Delta}{2}\right)S(k-P)\right],
\end{aligned} \tag{3.69}$$

S and Γ_π have been defined in equations (3.37) and (3.39) respectively. $n\cdot\Gamma$ is the dressed quark-photon vertex Γ^μ projected onto the light-cone. $k\cdot n$ comes from the $(\overleftrightarrow{D}\cdot n)^m$ applied to quark and antiquark fields. $\tau^\pm$ are linear combination of Pauli matrices:

$$\tau^\pm = \tau^1 \pm i\tau^2. \tag{3.70}$$

The equivalence between the Mandelstam normalisation condition and the canonical normalisation of the Bethe-Salpeter amplitude relies on the WTI. It is therefore necessary to

choose an Ansatz for Γ_μ consistent with the quark propagator Ansatz given in equation (3.37). In the present case, the quark propagators yield:

$$S^{-1}(k+\frac{\Delta}{2}) - S^{-1}(k-\frac{\Delta}{2}) = i\Delta\cdot\gamma. \tag{3.71}$$

Therefore, $\Gamma^\mu = \gamma^\mu$ is sufficient to secure the normalisation. In addition, in the following, the value of η is fixed to 0, which has no consequence as the result is independent of η.

Taking the trace of equation (3.69) on flavor and color indices generates an overall multiplicative factor. The Dirac structure of equation (3.69) is more complicated:

$$\begin{aligned} &\mathrm{Tr}\left(i\gamma_5\left[-i\left(k-\frac{\Delta}{2}\right)\cdot\gamma+M\right]\gamma^\mu\left[-i\left(k+\frac{\Delta}{2}\right)\cdot\gamma+M\right]i\gamma_5\big[-i(k-P)\cdot\gamma+M\big]\right) \\ =\;& 4i\left[k^\mu\left(k^2-2k\cdot P+M^2+\left(\frac{\Delta}{2}\right)^2\right)+P^\mu\left(k^2-\left(\frac{\Delta}{2}\right)^2+M^2\right)-\frac{\Delta}{2}^\mu 2k\cdot\frac{\Delta}{2}\right]. \end{aligned} \tag{3.72}$$

Based on the approach of Ref. [204], A, B and C are introduced as the denominators of the propagators:

$$A = \left(k-\frac{\Delta}{2}\right)^2+M^2, \tag{3.73}$$

$$B = \left(k+\frac{\Delta}{2}\right)^2+M^2, \tag{3.74}$$

$$C = (k-P)^2+M^2. \tag{3.75}$$

Thus, equation (3.72) becomes:

$$\mathrm{Tr}[\ldots] = 4i\left[k^\mu\left(C+\left(\frac{\Delta}{2}\right)^2-P^2\right)+\frac{P^\mu}{2}\left(A+B-4\left(\frac{\Delta}{2}\right)^2\right)-\frac{\Delta^\mu}{2}\left(\frac{B-A}{2}\right)\right]. \tag{3.76}$$

This shows that four different integrals will arise from this computation: three with simplifications due to A, B or C and one with no denominator simplifications.

With the help of Feynman parameters $x, y, u, v, w \in [0,1]$ (while $z, z' \in [-1,+1]$ originate from the Ansatz (3.39) for the Bethe-Salpeter vertex), one can express the denominator of

(3.69) as:

$$\begin{aligned}
&\left\{x\left(\left[k-\frac{\Delta}{2}-\frac{1-z}{2}\left(P-\frac{\Delta}{2}\right)\right]^2+M^2\right)+y\left(\left[-k-\frac{\Delta}{2}+\frac{1-z'}{2}\left(P+\frac{\Delta}{2}\right)\right]^2+M^2\right)\right.\\
&\left.+u\big((k-P)^2+M^2\big)+v\left[\left(k-\frac{\Delta}{2}\right)^2+M^2\right]+w\left[\left(k+\frac{\Delta}{2}\right)^2+M^2\right]\right\}^{2\nu+3}\\
=\;&\left\{\left[k-P\left(\frac{1-z'}{2}y+x\frac{1-z}{2}+u\right)-\frac{\Delta}{2}\left(-y\frac{1+z'}{2}+x\frac{1+z}{2}+v-w\right)\right]^2\right.\\
&-P^2\left(\frac{1-z'}{2}y+x\frac{1-z}{2}+u\right)^2-\left(\frac{\Delta}{2}\right)^2\left(-y\frac{1+z'}{2}+x\frac{1+z}{2}+v-w\right)^2\\
&+P^2\left(\left(\frac{1-z'}{2}\right)^2y+x\left(\frac{1-z}{2}\right)^2+u\right)\\
&\left.+\left(\frac{\Delta}{2}\right)^2\left(y\left(\frac{1+z'}{2}\right)^2+x\left(\frac{1+z}{2}\right)^2+v+w\right)+M^2\right\}^{2\nu+3}.
\end{aligned}\tag{3.77}$$

Introducing:

$$f=f(x,y,v,w,z,z')=\frac{1}{2}\left(-\frac{1+z'}{2}y+\frac{1+z}{2}x+v-w\right),\tag{3.78}$$

$$g=g(x,y,u,z,z')=\left(\frac{1-z'}{2}\right)y+x\frac{1-z}{2}+u,\tag{3.79}$$

$$\begin{aligned}
M'(t,P^2,x,y,u,v,w,z,z')^2=\;&M^2+\frac{t}{4}\left(-4f^2+y\left(\frac{1+z'}{2}\right)^2+x\left(\frac{1+z}{2}\right)^2+v+w\right)\\
&+P^2\left(-g^2+\left(\frac{1-z'}{2}\right)^2y+\left(\frac{1-z}{2}\right)^2x+u\right)
\end{aligned}\tag{3.80}$$

and performing the change of variables $k'=k-f\Delta-gP$, one can compute the loop integral. The unsimplified part of the numerator (3.76) associated to equation (3.77) becomes (omitting $'$):

$$T_0=4ix^{\nu-1}y^{\nu-1}\frac{\Gamma(2\nu+3)}{\Gamma(\nu)^2}\left[(k^\mu+f\Delta^\mu+gP^\mu)\left(\left(\frac{\Delta}{2}\right)^2-P^2\right)-2P^\mu\left(\frac{\Delta}{2}\right)^2\right],\tag{3.81}$$

whereas the three other terms read:

$$T_A=4ix^{\nu-1}y^{\nu-1}\frac{\Gamma(2\nu+2)}{\Gamma(\nu)^2}\frac{1}{2}\left(P^\mu+\frac{\Delta}{2}^\mu\right)\delta(v),\tag{3.82}$$

$$T_B=4ix^{\nu-1}y^{\nu-1}\frac{\Gamma(2\nu+2)}{\Gamma(\nu)^2}\frac{1}{2}\left(P^\mu-\frac{\Delta}{2}^\mu\right)\delta(w),\tag{3.83}$$

$$T_C=4ix^{\nu-1}y^{\nu-1}\frac{\Gamma(2\nu+2)}{\Gamma(\nu)^2}\left(k^\mu+f\Delta^\mu+gP^\mu\right)\delta(u).\tag{3.84}$$

Keeping in mind that $n^2 = 0$, one can compute the integration over k:

$$\begin{aligned}\mathcal{M}_m(\xi,t) &= \frac{M^2}{2\pi^2 f_\pi^2}\int_0^1 \mathrm{d}x\,\mathrm{d}y\,\mathrm{d}u\,\mathrm{d}v\,\mathrm{d}w\int_{-1}^{+1}\mathrm{d}z\,\mathrm{d}z'\,\delta(x+y+u+v+w-1)x^{\nu-1}y^{\nu-1}\rho(z)\rho(z') \\ &\frac{M^{4\nu}}{2}\left[\frac{\Gamma(2\nu+1)}{\Gamma(\nu)^2}\left(\left(f\Delta\cdot n+gP\cdot n\left(\left(\frac{\Delta}{2}\right)^2-P^2\right)-2P\cdot n\left(\frac{\Delta}{2}\right)^2\right)\frac{1}{(M')^{2\nu+1}}\right.\right. \\ &+\frac{\Gamma(2\nu)}{\Gamma(\nu)^2}\frac{1}{2}\left(P\cdot n+\frac{\Delta}{2}\cdot n\right)\delta(v)\frac{1}{(M')^{2\nu}}+\frac{\Gamma(2\nu)}{\Gamma(\nu)^2}\frac{1}{2}\left(P\cdot n-\frac{\Delta}{2}\cdot n\right)\delta(w)\frac{1}{(M')^{2\nu}} \\ &\left.\left.+\frac{\Gamma(2\nu)}{\Gamma(\nu)^2}\left(f\Delta\cdot n+gP\cdot n\right)\delta(u)\frac{1}{(M')^{2\nu}}\right]\frac{(f\Delta\cdot n+gP\cdot n)^m}{2(P\cdot n)^{m+1}}. \qquad (3.85)\end{aligned}$$

The computation of the crossed diagram can be performed along the same lines. It is easy to see, since $\xi = -\frac{\Delta\cdot n}{2P\cdot n}$, that equation (3.85) provides a polynomial with the expected degree in ξ. One can also use the properties of the functions f and g in order to show that the computed Mellin moments are even in ξ, and that the isoscalar and isovector GPDs are respectively odd and even in x. Those properties are showed in section 3.3.3.

3.2.4 Comparison with experimental data

Unfortunately, no data on pion GPDs are currently available at non-zero skewness, even if some work has been done considering virtual pion targets [212]. Still, some measurements of the form factor and of the valence PDF are available. Therefore, the present model can be compared with experimental data.

Remembering that the form factor is directly given by the Mellin moment of order 0 of the GPD:

$$F_\pi(t) = \int_{-1}^{+1}\mathrm{d}x\,H(x,\xi,t), \qquad (3.86)$$

the model can be easily compared to experimental data (figure 3.7). However one has to deal with two parameters, coming from the fact that the propagators (3.37) and the Bethe-Salpeter amplitudes (3.39) are building blocks of the numerical solutions (equations (3.32), (3.33) and (3.36)). One parameter is ν, which controls the shape of the vertex and which here is fixed to 1. The other one is M which can be seen as the effective quark mass, and which controls the t-behaviour as equation (3.85) depends only on $\theta = \frac{t}{M^2}$. The available experimental data of Ref. [213, 214] would allow one to fit precisely the parameter M. Yet, this is beyond the scope of this study. It is more insightful to see how strongly the variations of M modify the form factor. Therefore, figure 3.7 shows that for $M \approx 0.35$ GeV, which is a typical constituent quark mass, the data are well described. The sensitivity with respect to M is highlighted by plotting two additional curves: one for $M = 0.25$ GeV and one for $M = 0.45$ GeV. It should be stressed here that the form factor is giving a mass scale to the algebraic model.

Another important experimental point is the charge radius of the pion. The NA7 collaboration gives in Ref. [213] its experimental result:

$$\left\langle r_\pi^2\right\rangle^{\exp} = -6\frac{dF_\pi}{dt}\bigg|_{t=0} = 0.439 \pm 0.008\ \mathrm{fm}^2. \qquad (3.87)$$

Our model would reach agreement with the NA7 Collaboration value for $M = 339 \pm 3$ MeV, which is close to our choice of $M = 350$ MeV.

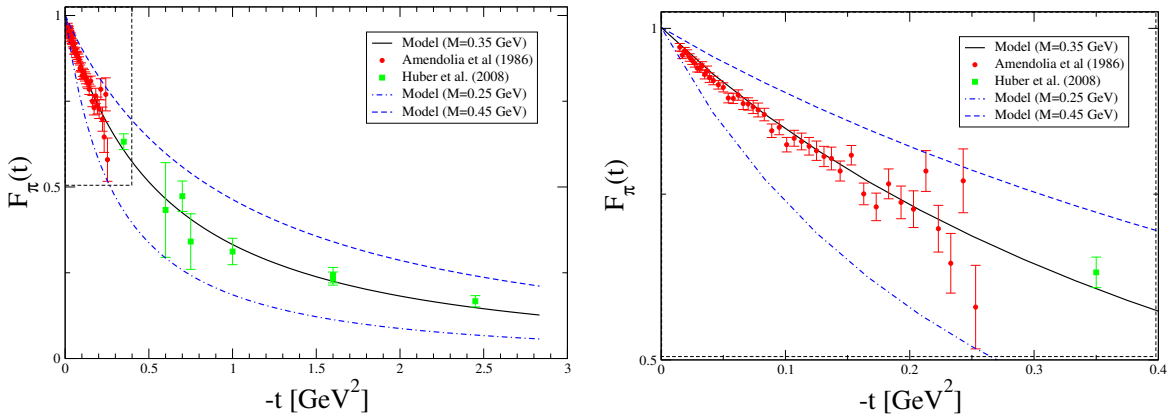

Figure 3.7: The pion form factor F_π computed at $M = 0.35$ GeV(solid black line), 0.25 GeV(dot-dashed blue line) and 0.45 GeV(dashed blue line), with $\nu = 1$ for the three cases. Experimental data are taken from Ref. [213, 214]. The rightmost plot corresponds to a zoom of the dashed square in the leftmost plot allowing to emphasise the constraint provided by the large number of data points in the low-momentum region.

The pion valence PDF have also been measured, and analysed using a resummation procedure [215]. Then a phenomenological parameterisation described in Ref. [215] has been fitted on the resulting data. The Mellin moments can consequently be computed and compared to those of equation (3.85). However, the PDF depends also on both renormalisation and factorisation scales, both of them taken to the same value here. In the case of the numerical solution of the Dyson-Schwinger equations, such scales are explicit (see *e.g.* equation (3.6)), but in the algebraic approach detailed above, nothing fixes the scales explicitly. As the PDF is defined for $\theta = 0$, it does not depend on the mass scale M fitted on the form factor. Therefore, the dependence in the factorisation scale is hidden in ν, providing that the parameterisation is flexible enough. Consequently, one has to evolve the moments of the Ref. [215] parameterisation to another scale to see if it can at some points agree with the present model. As shown on figure 3.8, this is the case at a very low scale. The form factor data and the PDF data are

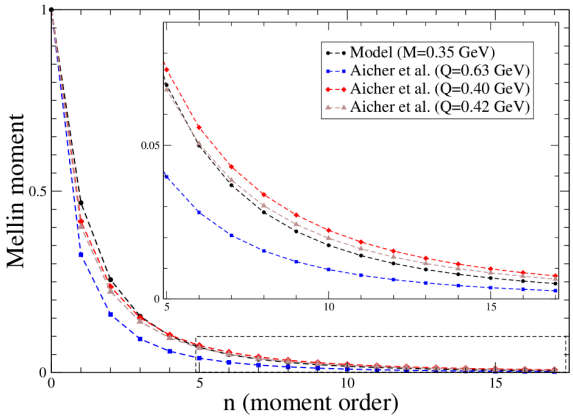

Figure 3.8: Mellin moments from our model and obtained with the parameterisation of Aicher *et al.* [215] run with DGLAP equation down to $Q = 0.40$ GeV and 0.42 GeV.

in good agreement with the algebraic model.

3.3 From Mellin moments to Double Distributions

The success of the comparison of the Mellin moments with available experimental data is a strong encouragement to try to compute the GPD itself. Solution of the inverse Mellin problems are indeed known and the inverse Mellin transform well defined mathematically. However, in the case of GPDs, inverting the Mellin transform remains a hard task, which has been done only for analytic expressions much simpler than equation (3.85) [157]. Other approaches are considered here.

3.3.1 Polynomial reconstruction and numerical instability

Projection

In order to recover the GPD from its Mellin moments, one can try to rewrite it using a polynomial basis:

$$H(x,\xi,t) = (1-x^2)^{\alpha-\frac{1}{2}} \sum_{n=0}^{N(\alpha)} d_n^{(\alpha)}(\xi,t) C_n^{(\alpha)}(x), \tag{3.88}$$

where the $C_n^{(\alpha)}(x)$ are the Gegenbauer polynomials which can be explicitely computed using the Rodrigues formula:

$$C_n^{(\alpha)}(x) = \frac{(-2)^n}{n!} \frac{\Gamma(n+\alpha)\Gamma(n+2\alpha)}{\Gamma(\alpha)\Gamma(2n+2\alpha)} (1-x^2)^{-\alpha+1/2} \frac{d^n}{dx^n} \left[(1-x^2)^{n+\alpha-1/2} \right]. \tag{3.89}$$

It is possible to relate the coefficients $d_n^{(\alpha)}(\xi,t)$ to the Mellin moments $\mathcal{M}_m(\xi,t)$:

$$\begin{pmatrix} \mathcal{M}_1(\xi,t) \\ \mathcal{M}_2(\xi,t) \\ . \\ . \\ . \\ \mathcal{M}_N(\xi,t) \end{pmatrix} = \begin{pmatrix} g_{11} & 0 & 0 & . & . & . & 0 \\ g_{21} & g_{22} & 0 & . & . & . & 0 \\ . & & & & & & \\ . & & & & & & \\ . & & & & & & \\ g_{N1} & . & . & . & & & g_{NN} \end{pmatrix} \begin{pmatrix} d_1^{\alpha}(\xi,t) \\ d_2^{\alpha}(\xi,t) \\ . \\ . \\ . \\ d_N^{\alpha}(\xi,t) \end{pmatrix} \tag{3.90}$$

with:

$$g_{i,j}(\alpha) = \frac{\sqrt{\pi}}{4^{(i-j)}} \frac{\Gamma(j-1+\alpha)\Gamma(j+\alpha-\frac{1}{2})\Gamma(2i-1)}{\Gamma(\alpha)\Gamma(2j-1)\Gamma(i-j+1)\Gamma(i+j+\alpha-1)}. \tag{3.91}$$

The linear relation of equation (3.90) can be inverted in order to recover the coefficients $d_n^{(\alpha)}(\xi,t)$ from the computed Mellin moments $\mathcal{M}_m(\xi,t)$.

Numerical reconstruction and instabilities

Therefore, it is possible to reconstruct numerically the GPD, as shown on figure 3.9 for $\xi = 0.5$. The reconstruction described here will be focused on the so-called 3/2-Gegenbauer polynomials. This choice seems natural as those polynomials diagonalise the evolution equations of quark GPDs at LO. The convergence seems to be quite fast on the definition domain (*i.e.*

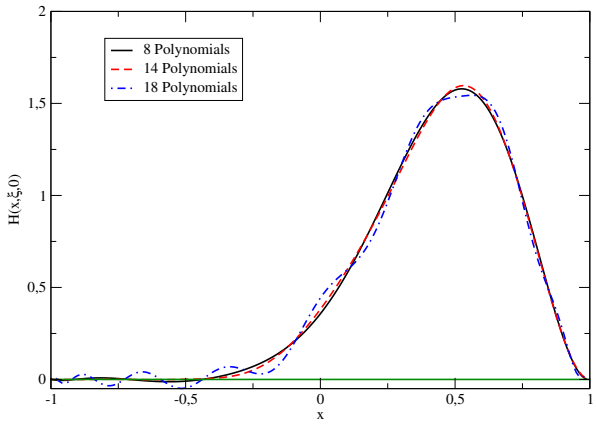

Figure 3.9: Reconstruction of the GPD for $\nu = 1$, $t = 0$ and $\xi = 0.5$ using different numbers of polynomials. For 18 polynomials, numerical instabilities are clearly visible.

for $x \in [-0.5, 1]$), since using 8 or 14 polynomials does not seem to make a significant difference. It is slower for $x \in [-1, -0.5]$, where the GPD is supposed to vanish. In this area, the truncation automatically generates noise. Another interesting point is the effects of numerical precision and generated instabilities. Indeed, due to the very large numbers entering in the inverse of the matrix in equation (3.90), the Mellin moments have to be computed with a tremendous precision when m increases. The required precision is of the same order of magnitude than the smaller $g_{i,j}(\alpha)$ of the matrix (3.90). Considering $g_{N,N}(\alpha)$ this precision must be of order $\simeq 10^{-4}$ when considering 8 polynomials, $\simeq 10^{-10}$ for 18 polynomials and $\simeq 10^{-29}$ for 50 polynomials. One can easily be convinced that integrating numerically a multidimensional integral like the one of equation (3.85) with a high accuracy is time-consuming.

Evolution of the PDF

Using the reconstruction method developed below, it is possible to compare the PDF parameterisation of Ref. [215] with our model, using the DGLAP equations at LO. This is shown on figure 3.10.

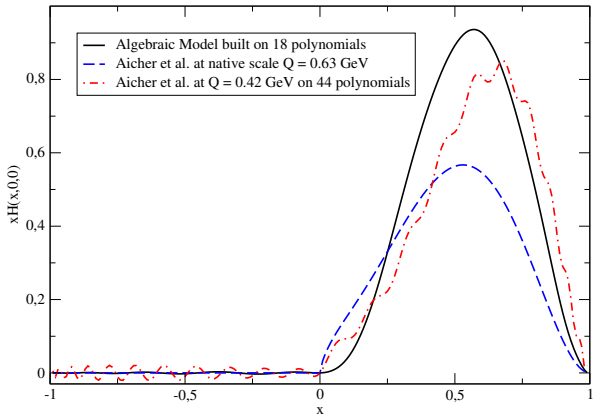

Figure 3.10: Evolution of the parameterisation done in Ref. [215] at scale $Q = 0.42$ GeV. The algebraic model is plotted for $\nu = 1$.

3.3.2 Tensorial structure of Mellin Moments and identification with Double Distributions

The computation of the Mellin moments (equation (3.85)) can be also seen in terms of twist-two local operator projected on the lightcone, *i.e.* :

$$\mathcal{M}_m(\xi,t) = n_\mu n_{\mu_1} n_{\mu_2} ... n_{\mu_m} \left\langle P + \frac{\Delta}{2} \right| O^{\{\mu\mu_1\mu_2...\mu_m\}} \left| P - \frac{\Delta}{2} \right\rangle \tag{3.92}$$

where the $\{\}$ denotes a fully symmetrised and traceless operator. Following this approach, also adopted in Ref. [204], equation (3.85) can be written as:

$$\begin{aligned}
\langle x^m \rangle^q_{\text{direct}} &= \frac{M^2}{2\pi^2 f_\pi^2} \int_0^1 \mathrm{d}x\,\mathrm{d}y\,\mathrm{d}u\,\mathrm{d}v\,\mathrm{d}w \int_{-1}^{+1} \mathrm{d}z\,\mathrm{d}z'\,\delta(x+y+u+v+w-1) x^{\nu-1} y^{\nu-1} \rho(z)\rho(z') \frac{M^{4\nu}}{2} \\
&\left[\frac{\Gamma(2\nu+1)}{\Gamma(\nu)^2} \left(\left(f\Delta^{\{\mu} + gP^{\{\mu} \left(\left(\frac{\Delta}{2} \right)^2 - P^2 \right) - 2P^{\{\mu} \left(\frac{\Delta}{2} \right)^2 \right) \frac{1}{(M')^{2\nu+1}} \right. \right. \\
&+ \frac{\Gamma(2\nu)}{\Gamma(\nu)^2} \frac{1}{2} \left(P^{\{\mu} + \frac{\Delta}{2}^{\{\mu} \right) \delta(v) \frac{1}{(M')^{2\nu}} + \frac{\Gamma(2\nu)}{\Gamma(\nu)^2} \frac{1}{2} \left(P^{\{\mu} - \frac{\Delta}{2}^{\{\mu} \right) \delta(w) \frac{1}{(M')^{2\nu}} \\
&\left. \left. + \frac{\Gamma(2\nu)}{\Gamma(\nu)^2} \left(f\Delta^{\{\mu} + gP^{\{\mu} \right) \delta(u) \frac{1}{(M')^{2\nu}} \right] (f\Delta + gP)^{\mu_1\}} \dots (f\Delta + gP)^{\mu_m\}} n_\mu ... n_{\mu_m}. \right.
\end{aligned} \tag{3.93}$$

This allows one to recognise $\left\langle P + \frac{\Delta}{2} \right| O^{\{\mu\mu_1\mu_2...\mu_m\}} \left| P - \frac{\Delta}{2} \right\rangle$, which can be expanded as:

$$\begin{aligned}
\left\langle P + \frac{\Delta}{2} \right| O^{\{\mu\mu_1\mu_2...\mu_m\}} \left| P - \frac{\Delta}{2} \right\rangle &= P^{\{\mu} \sum_{j=0}^{m} \binom{m}{j} F_{m,j}(t) P^{\mu_1} ... P^{\mu_j} \left(-\frac{\Delta}{2} \right)^{\mu_{j+1}} ... \left(-\frac{\Delta}{2} \right)^{\mu_m\}} \\
&- \frac{\Delta}{2}^{\{\mu} \sum_{j=0}^{m} \binom{m}{j} G_{m,j}(t) P^{\mu_1} ... P^{\mu_j} \left(-\frac{\Delta}{2} \right)^{\mu_{j+1}} ... \left(-\frac{\Delta}{2} \right)^{\mu_m\}}
\end{aligned} \tag{3.94}$$

where $F_{m,j}(t)$ and $G_{m,j}(t)$ are the Mellin moments of the DDs $F(\beta,\alpha,t)$ and $G(\beta,\alpha,t)$ defined in equations (2.13) and (2.14). Equation (3.94) is in fact a generalisation of equation (2.11). Since a function is uniquely defined by the ensemble of all its Mellin moments (see section 1.3.2), it is possible to identify the DDs $F(\beta,\alpha)$ and $G(\beta,\alpha)$ in equation (3.93), providing that the arguments β and α can be defined as functions of the integration parameters, and more precisely that they live inside the rhombus defining the DD support shown on figure 2.2. The natural candidates are:

$$\left\{ \begin{array}{rcl} \beta &=& g \\ \alpha &=& -f \end{array} \right. , \tag{3.95}$$

defined in equations (3.78) and (3.79). This is indeed the case as illustrated on figure 3.11 which illustrates the values of f and g when generating randomly the Feynman parameters and the vertex parameters z and z'. The proof can be shown using barycentric coordinates

$(x_i)_{1\leq i\leq 4}$ in $[0,1]$ such that [216]:

$$\begin{aligned} x &= x_4, && (3.96)\\ y &= x_3(1-x_4), && (3.97)\\ u &= x_2(1-x_3)(1-x_4), && (3.98)\\ v &= x_1(1-x_2)(1-x_3)(1-x_4), && (3.99)\\ w &= (1-x_1)(1-x_2)(1-x_3)(1-x_4). && (3.100) \end{aligned}$$

Using those barycentric coordinates, it is possible to write:

$$\begin{aligned} \beta+\alpha &= 1-\big(x4(1+z)+(1-x_4)[2x_1(1-x_2)(1-x_3)]\big), && (3.101)\\ \beta-\alpha &= -1+2\left(x_4+(1-x_4)\left[x_3\frac{1-z'}{2}+(1-x_3)\big(x_2+(1-x_2)x_1\big)\right]\right). && (3.102) \end{aligned}$$

Looking closely at equation (3.101), one can identify the centre of mass of a system $(1+z)$ and $2x_1(1-x_2)(1-x_3)$ with respective weights x_4 and $(1-x_4)$. Thus, $x4(1+z)+(1-x_4)[2x_1(1-x_2)(1-x_3)$ belongs to the segment $[0,2]$, and $-1\leq\beta+\alpha\leq 1$. The same kind of interpretation occurs for equation (3.102), leading to $-1\leq\beta-\alpha\leq 1$. Finally, one gets $|\alpha|+|\beta|\leq 1$, which describe the DD support shown on figure 2.2. Dealing with a valence quark distribution, β is positive when computing the left-hand side diagram of figure 3.6 and negative when computing the right-hand side diagram. This is fully consistent with a quark and anti-quark interpretation.

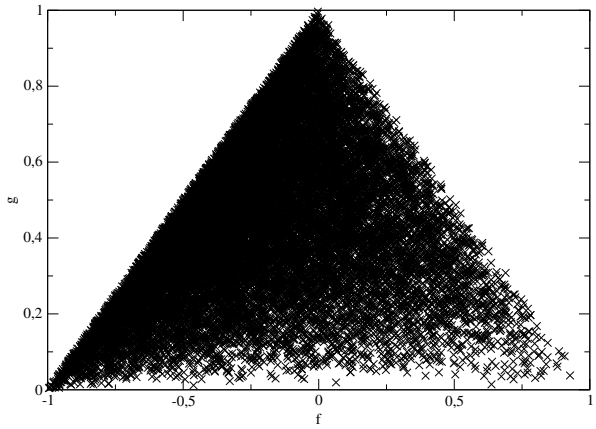

Figure 3.11: Values of f and g when generating the Feynman parameters in a Monte-Carlo approach using 2.10^5 points.

No doubt subsisting about the DD definition domain, it is possible to compute the DDs F^q and G^q using the following change of variables [216]:

$$\int_0^1 \mathrm{d}x\,\mathrm{d}y\,\mathrm{d}u\,\mathrm{d}v\,\mathrm{d}w\int_{-1}^{+1}\mathrm{d}z\,\mathrm{d}z'\,\delta(x+y+u+v+w-1)\phi(x,y,u,v,w,z,z')=\int_\Omega \mathrm{d}\beta\,\mathrm{d}\alpha\Phi(\beta,\alpha), \tag{3.103}$$

with:

$$\begin{aligned}\Phi(\beta,\alpha) &= \frac{1}{16}\int_{\beta+\alpha}^{+1}\mathrm{d}B\int_{\beta-\alpha}^{+1}\mathrm{d}B'\int_{-1}^{\beta+\alpha}\mathrm{d}A\int_{-1}^{\beta-\alpha}\mathrm{d}A'\,\theta(A+A'\geq 0)\frac{1}{(B-A)(B'-A')}\\ &\quad\phi\left(\frac{-A+B}{2},\frac{B'-A'}{2},\frac{A+A'}{2},\frac{1-B}{2},\frac{1-B'}{2},\right.\\ &\quad\left.\frac{-(A+B)+2(\beta+\alpha)}{A-B},\frac{-(A'+B')+2(\beta-\alpha)}{A'-B'}\right).\end{aligned}\tag{3.104}$$

For instance, in the case $\nu=1$, one gets:

$$\begin{aligned}F^u(\beta,\alpha,t) &= \frac{48}{5}\left\{-\frac{18M^4t(\beta-1)(\alpha-\beta+1)(\alpha+\beta-1)\left(\left(\alpha^2-(\beta-1)^2\right)\tanh^{-1}\left(\frac{2\beta}{-\alpha^2+\beta^2+1}\right)+2\beta\right)}{\left(4M^2+t\left((\beta-1)^2-\alpha^2\right)\right)^3}\right.\\ &+\frac{9M^4(\alpha-\beta+1)\left(-4\beta\left(-\alpha^2+\beta^2+1\right)+2\tanh^{-1}\left(\frac{2\beta}{-\alpha^2+\beta^2+1}\right)\right)}{4(\alpha-\beta-1)\left(4M^2+t\left((\beta-1)^2-\alpha^2\right)\right)^2}\\ &+\frac{9M^4(\alpha-\beta+1)\left(\left(\alpha^4-2\alpha^2\left(\beta^2+1\right)+\beta^2\left(\beta^2-2\right)\right)\log\left(\frac{(\alpha-\beta-1)(\alpha+\beta+1)}{\alpha^2-(\beta-1)^2}\right)\right)}{4(\alpha-\beta-1)\left(4M^2+t\left((\beta-1)^2-\alpha^2\right)\right)^2}\\ &+\frac{9M^4(\alpha+\beta-1)\left(-4\beta\left(-\alpha^2+\beta^2+1\right)+2\tanh^{-1}\left(\frac{2\beta}{-\alpha^2+\beta^2+1}\right)\right)}{4(\alpha+\beta+1)\left(4M^2+t\left((\beta-1)^2-\alpha^2\right)\right)^2}\\ &+\frac{9M^4(\alpha+\beta-1)\left(\left(\alpha^4-2\alpha^2\left(\beta^2+1\right)+\beta^4-2\beta^2\right)\log\left(\frac{(\alpha-\beta-1)(\alpha+\beta+1)}{\alpha^2-(\beta-1)^2}\right)\right)}{4(\alpha+\beta+1)\left(4M^2+t\left((\beta-1)^2-\alpha^2\right)\right)^2}\\ &\left.+\frac{9M^4\beta(\alpha-\beta+1)^2(\alpha+\beta-1)^2\left(\frac{2\left(\alpha^2\beta-\beta^3+\beta\right)}{\alpha^4-2\alpha^2(\beta^2+1)+(\beta^2-1)^2}-\tanh^{-1}(\alpha-\beta)+\tanh^{-1}(\alpha+\beta)\right)}{\left(4M^2+t\left((\beta-1)^2-\alpha^2\right)\right)^2}\right\},\end{aligned}\tag{3.105}$$

and

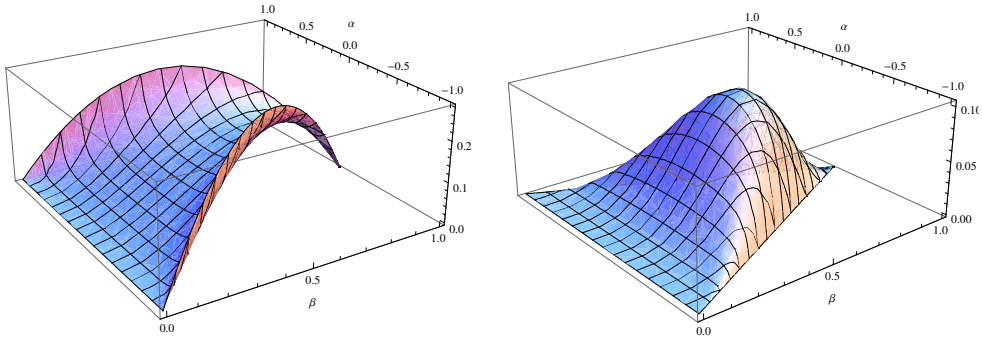

Figure 3.12: DDs F for $\nu=1$ (left-hand side) and $\nu=2$ (right-hand side).

$$
\begin{aligned}
G^u(\beta,\alpha,t) \;=\; & \frac{48}{5}\Bigg\{ -\frac{18M^4 t\alpha(\alpha-\beta+1)(\alpha+\beta-1)\left(\left(\alpha^2-(\beta-1)^2\right)\tanh^{-1}\left(\frac{2\beta}{-\alpha^2+\beta^2+1}\right)+2\beta\right)}{\left(4M^2+t\left((\beta-1)^2-\alpha^2\right)\right)^3} \\
& -\frac{9M^4(\alpha-\beta+1)\left(-4\beta\left(-\alpha^2+\beta^2+1\right)+2\tanh^{-1}\left(\frac{2\beta}{-\alpha^2+\beta^2+1}\right)\right)}{4(\alpha-\beta-1)\left(4M^2+t\left((\beta-1)^2-\alpha^2\right)\right)^2} \\
& -\frac{9M^4(\alpha-\beta+1)\left(\left(\alpha^4-2\alpha^2\left(\beta^2+1\right)+\beta^2\left(\beta^2-2\right)\right)\log\left(\frac{(\alpha-\beta-1)(\alpha+\beta+1)}{\alpha^2-(\beta-1)^2}\right)\right)}{4(\alpha-\beta-1)\left(4M^2+t\left((\beta-1)^2-\alpha^2\right)\right)^2} \\
& +\frac{9M^4(\alpha+\beta-1)\left(-4\beta\left(-\alpha^2+\beta^2+1\right)+2\tanh^{-1}\left(\frac{2\beta}{-\alpha^2+\beta^2+1}\right)\right)}{4(\alpha+\beta+1)\left(4M^2+t\left((\beta-1)^2-\alpha^2\right)\right)^2} \\
& +\frac{9M^4(\alpha+\beta-1)\left(\left(\alpha^4-2\alpha^2\left(\beta^2+1\right)+\beta^4-2\beta^2\right)\log\left(\frac{(\alpha-\beta-1)(\alpha+\beta+1)}{\alpha^2-(\beta-1)^2}\right)\right)}{4(\alpha+\beta+1)\left(4M^2+t\left((\beta-1)^2-\alpha^2\right)\right)^2} \\
& +\frac{9M^4\alpha(\alpha-\beta+1)^2(\alpha+\beta-1)^2\left(\frac{2\left(\alpha^2\beta-\beta^3+\beta\right)}{\alpha^4-2\alpha^2(\beta^2+1)+(\beta^2-1)^2}-\tanh^{-1}(\alpha-\beta)+\tanh^{-1}(\alpha+\beta)\right)}{\left(4M^2+t\left((\beta-1)^2-\alpha^2\right)\right)^2}\Bigg\}.
\end{aligned}
\tag{3.106}
$$

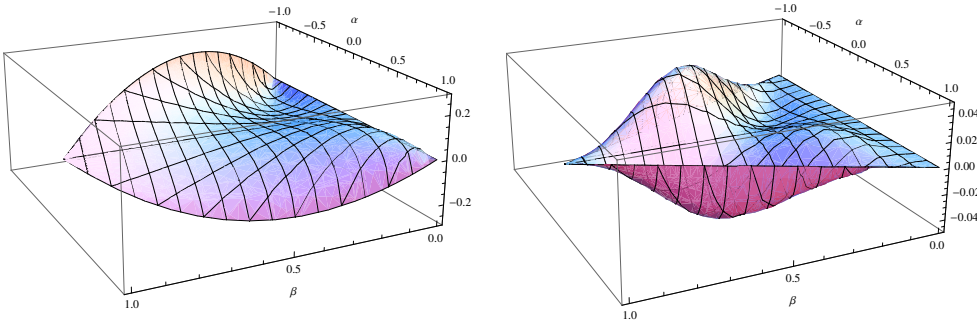

Figure 3.13: DDs G for $\nu = 1$ (left-hand side) and $\nu = 2$ (right-hand side).

3.3.3 Full reconstruction of the GPD

As seen previously in section 2.2.1, the GPD H is the Radon transform of the DDs F and G. Therefore, injecting equations (3.105) and (3.106) in equation (2.5), one can analytically

compute the GPD H in the DGLAP region:

$$
\begin{aligned}
H^u_{x\geq\xi}(x,\xi,0) \;=\; & \frac{48}{5}\Bigg\{\frac{3\left(-2(x-1)^4\left(2x^2-5\xi^2+3\right)\log(1-x)\right)}{20\left(\xi^2-1\right)^3} \\
& \frac{3\left(+4\xi\left(15x^2(x+3)+(19x+29)\xi^4+5(x(x(x+11)+21)+3)\xi^2\right)\tanh^{-1}\left(\frac{(x-1)\xi}{x-\xi^2}\right)\right)}{20\left(\xi^2-1\right)^3} \\
& +\frac{3\left(x^3(x(2(x-4)x+15)-30)-15(2x(x+5)+5)\xi^4\right)\log\left(x^2-\xi^2\right)}{20\left(\xi^2-1\right)^3} \\
& +\frac{3\left(-5x(x(x(x+2)+36)+18)\xi^2-15\xi^6\right)\log\left(x^2-\xi^2\right)}{20\left(\xi^2-1\right)^3} \\
& +\frac{3\left(2(x-1)\left((23x+58)\xi^4+(x(x(x+67)+112)+6)\xi^2+x(x((5-2x)x+15)+3)\right)\right)}{20\left(\xi^2-1\right)^3} \\
& +\frac{3\left(\left(15(2x(x+5)+5)\xi^4+10x(3x(x+5)+11)\xi^2\right)\log\left(1-\xi^2\right)\right)}{20\left(\xi^2-1\right)^3} \\
& +\frac{3\left(2x(5x(x+2)-6)+15\xi^6-5\xi^2+3\right)\log\left(1-\xi^2\right)}{20\left(\xi^2-1\right)^3}\Bigg\}, \qquad (3.107)
\end{aligned}
$$

and in the ERBL region:

$$
\begin{aligned}
H^u_{|x|\leq\xi}(x,\xi,0) \;=\; & \frac{48}{5}\Bigg\{\frac{6\xi(x-1)^4\left(-\left(2x^2-5\xi^2+3\right)\right)\log(1-x)}{40\xi\left(\xi^2-1\right)^3} \\
& +\frac{6\xi\left(-4\xi\left(15x^2(x+3)+(19x+29)\xi^4+5(x(x(x+11)+21)+3)\xi^2\right)\log(2\xi)\right)}{40\xi\left(\xi^2-1\right)^3} \\
& +\frac{6\xi(\xi+1)^3\left((38x+13)\xi^2+6x(5x+6)\xi+2x(5x(x+2)-6)+15\xi^3-9\xi+3\right)\log(\xi+1)}{40\xi\left(\xi^2-1\right)^3} \\
& +\frac{6\xi(x-\xi)^3\left((7x-58)\xi^2+6(x-4)x\xi+x(2(x-4)x+15)+15\xi^3+75\xi-30\right)\log(\xi-x)}{40\xi\left(\xi^2-1\right)^3} \\
& +\frac{3(\xi-1)(x+\xi)\left(4x^4\xi-2x^3\xi(\xi+7)+x^2(\xi((119-25\xi)\xi-5)+15)\right)}{40\xi\left(\xi^2-1\right)^3} \\
& +\frac{3(\xi-1)(x+\xi)\left(x\xi(\xi(\xi(71\xi+5)+219)+9)+2\xi(\xi(2\xi(34\xi+5)+9)+3)\right)}{40\xi\left(\xi^2-1\right)^3}\Bigg\}, \qquad (3.108)
\end{aligned}
$$

at vanishing t. The results present apparent singularities. But taking the limits properly, when $\xi \to 0$ or 1, no divergencies can be seen. For instance, in the forward limit, *i.e.* $\xi \to 0$, equation (3.107) gives for the PDF:

$$
q_\pi^{\mathrm{Tr}}(x) = \frac{72}{25}\Big((30-15x+8x^2-2x^3)x^3\log x+(3+2x^2)(1-x)^4\log(1-x)+(3+15x+5x^2-2x^3)x(1-x)\Big). \qquad (3.109)
$$

where Tr stands for triangle diagram. The result is finite for $x \to 0$ or 1.

Double Distribution properties

The Double Distribution approach has several advantages. First of all, concerning symmetries, the parity in α of the DD F (even in α) and G (odd in α) can be analytically checked on

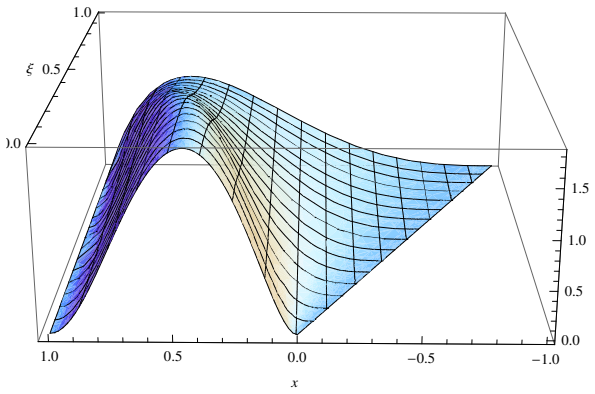

Figure 3.14: GPD H at vanishing t.

equations (3.105) and (3.106) and is manifest on figures 3.12 and 3.13. It ensures the time reversal invariance and therefore the parity in ξ of the GPD. The polynomiality property, which can already be seen in equation (3.85), is fulfilled. The support properties are also satisfied automatically providing that the DDs have themselves the good support properties. As illustrated on figure 3.11, this is indeed the case for the DDs, and thus also for the GPD as shown on figure 3.14.

Last but not least, when $x \to 1$, it is possible to check analytically that the algebraic model gives back the perturbative result, *i.e.* that:

$$H(x,0,0) = q(x) \simeq \frac{108}{5}(1-x)^2 \text{ when } x \to 1^-. \tag{3.110}$$

This is illustrated on figure 3.15.

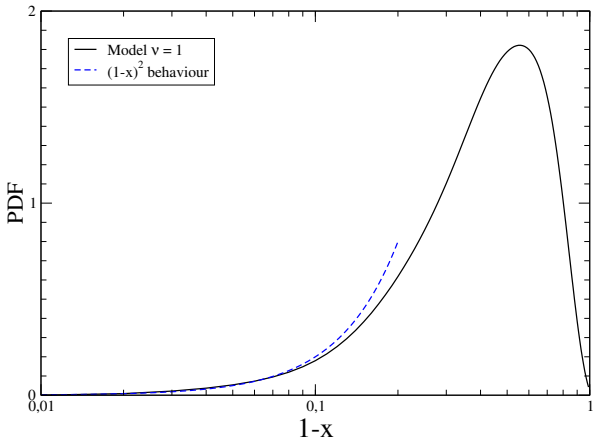

Figure 3.15: Behaviour of the algebraic model for $\nu = 1$ at large x compared to the perturbative prediction.

3.3.4 Limitations

If the algebraic model defined by the equations (3.37) and (3.39) and using the so-called triangle diagram approximation fulfils many properties of GPDs and is in agreement with the available experimental data, it presents nonetheless several limitations.

Forward case

In the forward case, the algebraic model should give a PDF symmetric with respect to the exchange $x \to 1-x$. Indeed, the isospin symmetry completed by the charge conjugation ensures that the PDFs of the two valence quarks of the pion are the same. In addition, the momentum conservation in this two-body system implies that the probability density to find a quark with a momentum fraction x has to be the same that the one to find the other quark with a momentum fraction $1-x$. This is highlighted on figure 3.16.

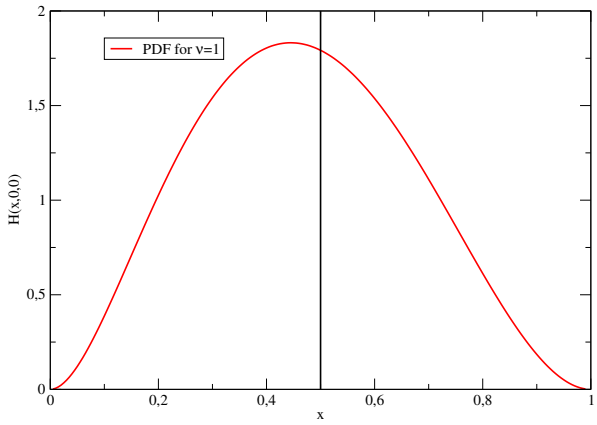

Figure 3.16: PDF for $\nu = 1$. In order to make the asymmetry more visible the line $x = 0.5$ is also plotted.

Positivity

As highlighted in section 1.3.3, in the DGLAP region, the GPD has an upper bound given by a Cauchy-Schwarz inequality. In our two-body system, this condition, when $x \to \xi$ gives:

$$|H(x,\xi,t)| \leq \sqrt{H\left(\frac{x-\xi}{1-\xi},0,0\right) H\left(\frac{x+\xi}{1+\xi},0,0\right)} \to 0 \text{ when } x \to \xi. \tag{3.111}$$

Consequently, the GPD must vanish on the diagonal $x = \xi$, which is not the case as shown on figure 3.14.

Soft pion theorem

The pion GPD can be related to the pion DA through the so-called soft pion theorem [158]. When $\xi = 1$, the following relation stands for the isoscalar and isovector pion GPDs:

$$H^{I=0}(x,1,0) = 0 \quad \text{and} \quad H^{I=1}(x,1,0) = \varphi_\pi\left(\frac{1+x}{2}\right), \tag{3.112}$$

where φ_π is the pion DA defined in equation (2.40). As shown on figure 3.17, this property is not fulfilled within the algebraic model. Explanations will be given in the next chapter.

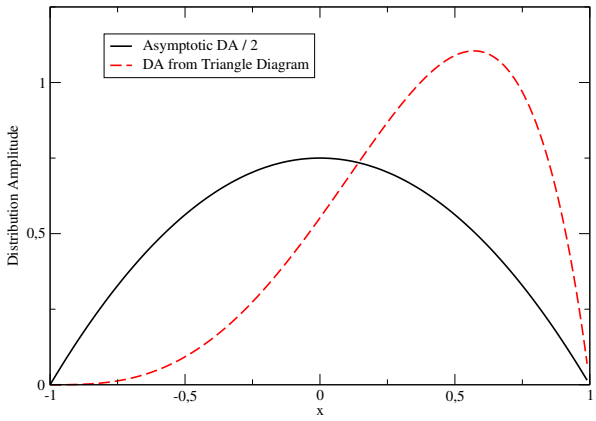

Figure 3.17: Comparison of quark GPD (dashed red) given by the algebraic model for $\nu = 1$ at $\xi = 1$ and $t = 0$ with the asymptotic pion DA (solid black).

Large-t issue

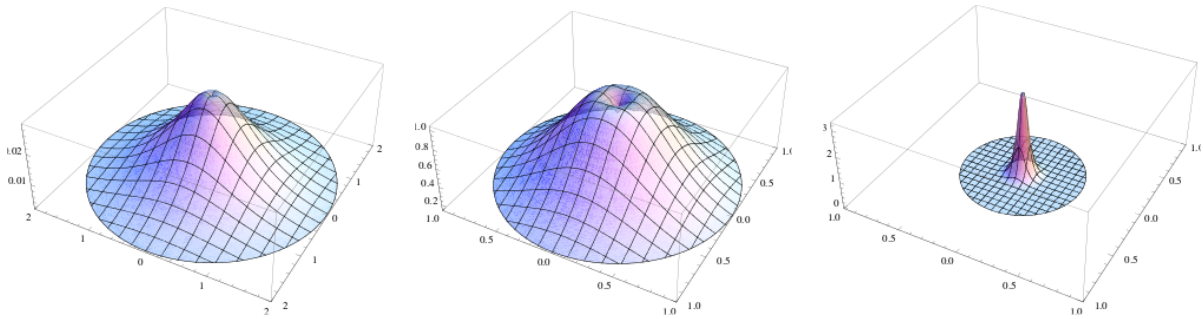

Figure 3.18: Density plots in the transverse plane with rexpect to the impact parameter $\mathbf{b}_\perp$ for different values of x. From left to right: $x = 0.05$, $x = 0.5$ and $x = 0.95$.

Following equation (1.70), it is a possible to compute the three dimensional probability density to find a quark at a given position $\mathbf{b}_\perp$ in the transverse plane and carrying a momentum fraction x along the lightcone. The general trend of figure 3.18 is quite intuitive. At $x \sim 1$ the considered quark defines the center of mass of the transverse plane, and thus the probability density in the transverse plane is very narrow. On the contrary, when x becomes small, the density is much wider. Yet, it appears that the probability density reaches a maximum which is not at $\mathbf{b}_\perp = 0$, as one can expect due to the behaviour of the Bessel function with respect to $|\mathbf{b}_\perp|$. Plus the position of this maximum depends on x, as shown on figure 3.19, suggesting that some of the correlations between x and t are not well described within this model. Indeed, a decrease in the density probability can be related to a change of sign at large t in $H^q(x, 0, t)$.

Discussion on the correlations between x and t are left for chapter 4 .

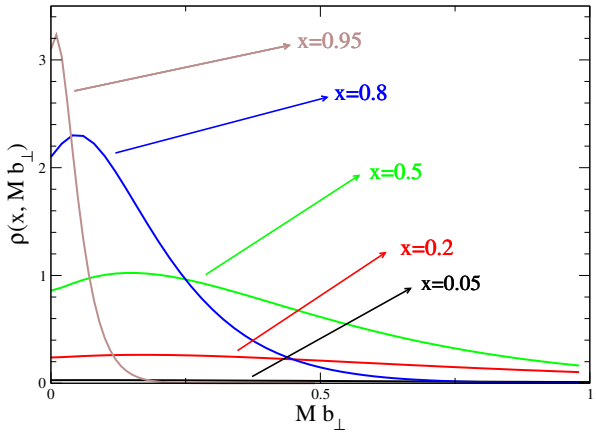

Figure 3.19: Probability density in the transverse plane for different values of x for $b_\perp = |\mathbf{b}_\perp|$. The position of the maximum to the large $b_\perp$ at smaller x.

Chapter 4

Unravelling gluon ladders

«Jamais un désir n'est à la lettre exaucé,
du fait précisément de l'abîme qui sépare le réel de l'imaginaire.»
Jean-Paul Sartre in *L'imaginaire.*

4.1 Soft pion theorem

Within the approach of Ref. [158], both PCAC and crossing symmetry play a key role in the proof of the soft pion theorem. Within the framework of Dyson-Schwinger equations, the preservation of the AVWTI is expected to be a *sine qua non* condition to get back the soft pion theorem.

4.1.1 Consequences of Axial Vector Ward Takahashi Identity

The axial-vector vertex $\Gamma^5_\mu(k,P)$ and the axial vertex $\Gamma_5(k,P)$ can be written in terms of the pion Bethe-Salpeter amplitude $\Gamma^j_\pi(k,P)$ [189]:

$$\begin{aligned}\Gamma^{5j}_\mu(k,P) &= \frac{\tau^j}{2}\gamma_5\left[\gamma_\mu F_{AV}(k,P)+\gamma\cdot k k_\mu G_{AV}(k,P)-\sigma_{\mu\nu}k^\nu H_{AV}(k,P)\right]\\ &\quad+\tilde{\Gamma}^{5j}_\mu(k,P)+\frac{f_\pi P_\mu}{P^2+m_\pi^2}\Gamma^j_\pi(k,P),\end{aligned}\tag{4.1}$$

and

$$\begin{aligned}i\Gamma^{5j}(k,P) &= \frac{\tau^j}{2}\gamma_5\left[iE_A(k,P)+\gamma\cdot P F_A(k,P)+\gamma\cdot k k\cdot P G_{AV}(k,P)\right.\\ &\quad\left.+\sigma_{\mu\nu}k^\nu P^\mu H_A(k,P)\right]+\frac{\rho_\pi}{P^2+m_\pi^2}\Gamma^j_\pi(k,P),\end{aligned}\tag{4.2}$$

where ρ_π is a constant and j is the isospin index. The E,F,G and H functions have neither Dirac nor Lorentz structures and present no singularities at $P^2=-m_\pi^2$. $\tilde{\Gamma}^{5j}_\mu$ takes into account the part of the axial-vector which cannot be included in any of the functions introduced above and which is not singular at $P^2=-m_\pi^2$. In both equations (4.1) and (4.2) the different functions are regular at $P^2=-m_\pi^2$ *i.e.* the poles at $P^2=m_\pi^2$ have been explicitely written. Consequently, the pion Bethe-Salpeter amplitude is directly related to the axial-vector and

axial vertices in the chiral limit $m_\pi^2 = 0$ through:

$$\lim_{P\to 0} P^\mu \Gamma_\mu^{5j}(k,P) = f_\pi \Gamma_\pi^j(k,0), \tag{4.3}$$

$$\lim_{P^2\to 0} iP^2 \Gamma_5^j(k,P) = \rho_\pi \Gamma_\pi^j(k,P)\big|_{P^2=0}. \tag{4.4}$$

Those equations can be seen as applications of the Lehmann-Symanzik-Zimmermann reduction formula [217]. Injecting equation (4.4) within the Axial-Vector WTI defined in equation (3.19) one gets:

$$f_\pi \Gamma_\pi^j(k,0) = i\gamma_5 \frac{\tau^j}{2} S^{-1}(k) + iS^{-1}(k)\gamma_5 \frac{\tau^j}{2}, \tag{4.5}$$

in the chiral limit. Using the parameterisations of $\Gamma_\pi^j(k,0)$ in equation (3.15) and of $S^{-1}(k)$ in equation (3.6), it is possible to simplify equation (4.5) in a Goldberger-Treimann-like relation [189, 218]:

$$f_\pi E_\pi(k,0) = B_q(k^2) = M_q(k^2) A_q(k^2). \tag{4.6}$$

The AVWTI relates the running quark mass with one of the structure function of the pion Bethe-Salpeter amplitude. It should be noticed here that, doing so, the running quark mass may have significant effect on pion-related observables, or on the pion structure.

Within the algebraic model defined in equations (3.37)-(3.40) and used to derive the pion GPD (3.107) and (3.108), one has:

$$f_\pi E_\pi(k,0) = M \frac{M^2}{k^2+M^2} \neq B(k^2) = M. \tag{4.7}$$

The breaking of relation (4.6) and beyond it of the AVWTI certainly plays a role in the violation of the soft pion theorem described in section 3.3.4, as the proof of this theorem relies on PCAC arguments [158].

4.1.2 Recovering the soft pion theorem

Elaborating on the previous argument, it must be possible to recover the soft pion theorem as soon as all the "relevant" properties are fulfilled. In other words, GPDs computed using vertices and propagators consistent with WTI and AVWTI must fulfil the soft pion theorem. This is indeed the case in the chiral limit and in the RL framework as it is shown below.

First of all, in the chiral limit, the kinematics associated with the soft pion theorem, *i.e.* $\xi = 1$ and $t = 0$ yields:

$$\begin{aligned} \xi = 1 &\Rightarrow \Delta^+ = -2P^+, \\ m_\pi^2 = 0 &\Rightarrow \Delta^- = 0, \\ t = 0 &\Rightarrow \Delta_\perp = 0, \end{aligned} \tag{4.8}$$

which means that the momentum of the outgoing pion vanishes: $p_2 = P + \frac{\Delta}{2} \to 0$. Yet, according to equation (4.3), a vanishing pion momentum allows to rewrite the Bethe-Salpeter amplitude as the axial-vector vertex contracted with p_2. On the other hand, since $p_1 = P - \frac{\Delta}{2} = 2P$ when $\xi \to 1$ and $t \to 0$, one thus has $p_1^2 \approx t$. Within this kinematics, equation (4.4) relates the pion Bethe-Salpeter amplitude with the pseudoscalar vertex $\Gamma_5(k,p_1)$. Consequently one

can rewrite the triangle diagram expression for the Mellin moment of the GPD (3.69) in the soft pion limit as:

$$\begin{aligned}\lim_{t\to 0}\lim_{\xi\to 1}\mathcal{M}_m(\xi,t) &= \lim_{t\to 0}\lim_{p_2\to 0}\mathrm{Tr}_{\mathrm{CFD}}\left[\int\frac{\mathrm{d}^4k}{(2\pi)^4}\frac{(k\cdot n)^m\tau_-}{2(P\cdot n)^{m+1}}\,i\frac{p_2^\mu}{f_\pi}\bar{\Gamma}^5_\mu\left((k-P),p_2\right)\right.\\ &\quad S(k-P)\;i\;n\cdot\Gamma(k-P,k+P)\;S(k+P)\\ &\quad\left.\tau_+ i\frac{it}{\rho_\pi}\Gamma_5\left((k+P),p_1\right)S(k-P)\right],\end{aligned}\tag{4.9}$$

transforming the Bethe-Salpeter amplitudes, which fulfil the homogeneous Bethe-Salpeter equation (3.16), into axial-vector and pseudo-scalar vertices which fulfil inhomogenous Bethe-Salpeter equations. This is illustrated on figure 4.1 and has strong consequences in terms of gluon ladders as it will be shown below.

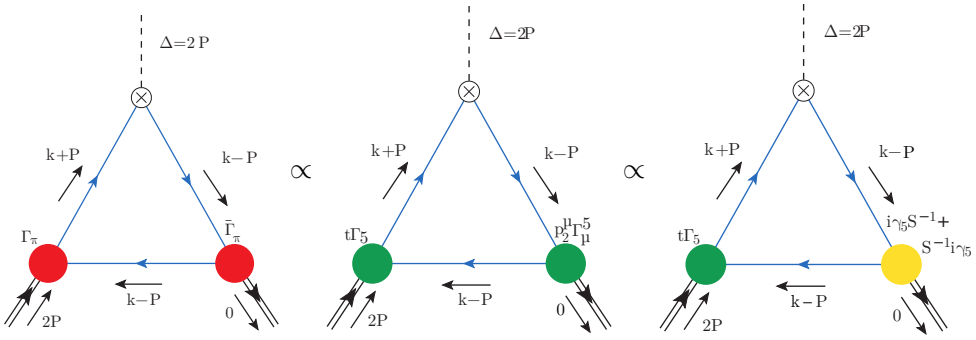

Figure 4.1: Diagrammatic representation of the different steps of the soft pion theorem proof. Left-hand side: triangle diagram in the soft pion limit, red vertices standing for pion Bethe-Salpeter amplitudes. Center: results after transforming pion Bethe-Salpeter amplitudes into axial vector and pseudo-scalar vertices. Those vertices fulfil inhomogeneous Bethe-Salpeter equations and thus are shown in green, consistently with figure 3.5. Right-hand side: injection of the AVWTI in the Axial-Vector vertex expression highlighted in yellow.

The second step consists in injecting the AVWTI (3.19) in equation (4.9) and to take the limit $p_2 \to 0$. This will impact the Axial-Vector vertex as:

$$p_2^\mu\bar{\Gamma}^5_\mu\left((k-P),p_2\right) = i\gamma_5 S^{-1}(k-P) + S^{-1}(k-P)i\gamma_5,\tag{4.10}$$

and thus will simplify equation (4.9):

$$\begin{aligned}\lim_{t\to 0}\lim_{\xi\to 1}\mathcal{M}_m(\xi,t) &= \lim_{t\to 0}\mathrm{Tr}_{\mathrm{CFD}}\left[\int\frac{\mathrm{d}^4k}{(2\pi)^4}\frac{(k\cdot n)^m\tau_-}{2(P\cdot n)^{m+1}}\,\frac{i}{f_\pi}\right.\\ &\quad\left(i\gamma_5\;i\;n\cdot\Gamma(k-P,k+P)\;S(k+P)\;\tau_+ i\frac{it}{\rho_\pi}\Gamma_5\left((k+P),p_1\right)S(k-P)\right.\\ &\quad\left.\left.+i\gamma_5 S(k-P)\;i\;n\cdot\Gamma(k-P,k+P)\;S(k+P)\tau_+ i\frac{it}{\rho_\pi}\Gamma_5\left((k+P),p_1\right)\right)\right].\end{aligned}\tag{4.11}$$

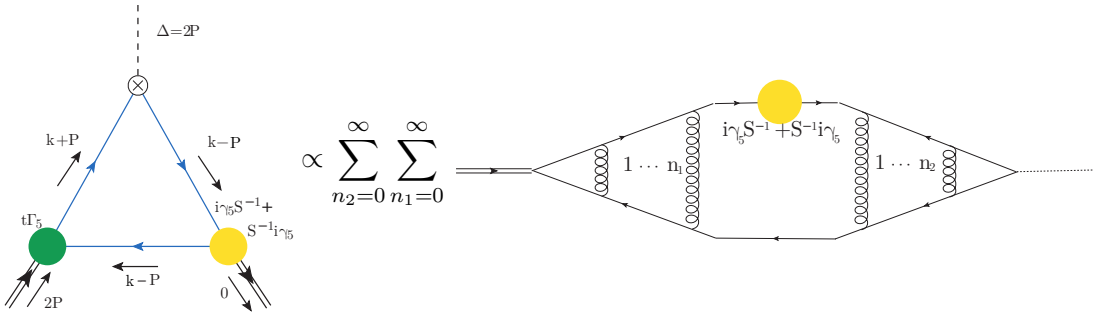

Figure 4.2: Decomposition of the triangle structure in terms of gluon ladders.

Consequently, one now has to deal with two diagrams each containing two vertices. However, at this step none of them looks like a DA diagram yet. In order to recover it, it is necessary to transform those remaining vertices.

This can be done when looking carefully at the structure of the considered vertices. Indeed, the vertices fulfilling an inhomogenous Bethe-Salpeter equation in the RL truncation scheme can be seen as an infinite sum on the number n of exchanged gluons labelled from 1 to n:

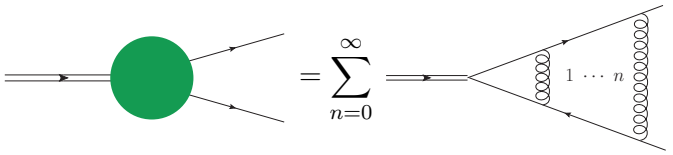

(4.12)

such that when $n = 0$, no gluon is exchanged between the two quark. In the gluon ladders approximation, which have been detailed in chapter 3, this structure appears both for the pseudoscalar vertex Γ_5 and for the electromagnetic vertex Γ^μ. Consequently, the two $i\gamma_5$ Dirac matrices coming from the AVWTI are trapped between gluons ladders as shown on figure 4.2. The sum described on figure 4.2 can be reordered by introducing n, the total number of exchanged gluons, and j such as the AVWTI (yellow disk on figure 4.2) is inserted between the j^{th} and the $(j+1)^{\text{th}}$ gluons. Then, splitting the contributions of the AVWTI, one gets:

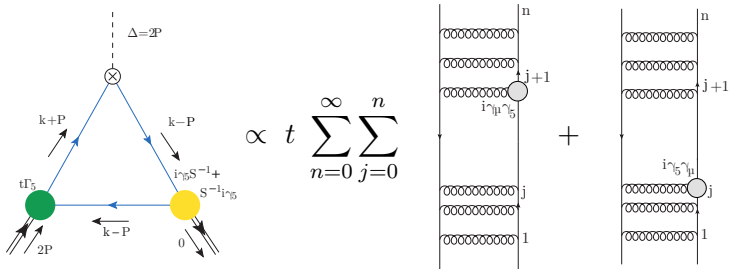

(4.13)

Considering the first of the two ladders, the anti-commutation relation between γ_5 and γ_μ generates a minus when transferring the $i\gamma_5$ from the bottom of the $(j+1)^{\text{th}}$ gluon vertex to the top of it. This minus sign is crucial as it cancels all the terms of the sum on j except $j = n$ for the first ladder and $j = 0$ for the second. In both cases, all the gluons are in the same side of the $i\gamma_5$ leading to the two contributions shown on figure 4.3. Due to the previous

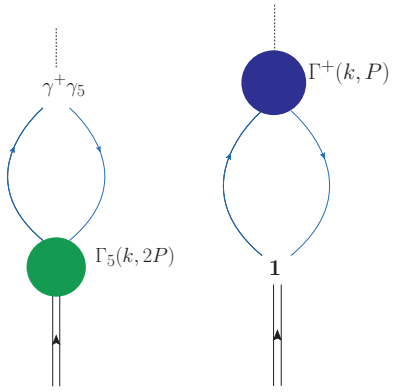

Figure 4.3: The two contributions obtained in equation (4.14).

arguments, equation (4.11) reads:

$$\begin{aligned}\lim_{t\to 0}\lim_{\xi\to 1}\mathcal{M}_m(\xi,t) &= \lim_{t\to 0}\mathrm{Tr}_{\mathrm{CFD}}\left[\int\frac{\mathrm{d}^4k}{(2\pi)^4}\frac{(k\cdot n)^m\tau_-}{2(P\cdot n)^{m+1}}\frac{i}{f_\pi}\right.\\ &\left(i\gamma_5\ i\ n\cdot\gamma\ S(k+P)\ \tau_+ i\frac{it}{\rho_\pi}\Gamma_5\left((k+P),p_1\right)S(k-P)\right.\\ &\left.\left.+S(k-P)\ i\ n\cdot\Gamma(k-P,k+P)\ S(k+P)\tau_+ i\frac{it}{\rho_\pi}i(\gamma_5)^2\right)\right].\end{aligned} \tag{4.14}$$

The next step is to take the limit $t\to 0$ within equation (4.14). The result for the term proportional to Γ_5 is known from equation (4.4). The second term generates no bound states when $t\to 0$ and thus is regular at vanishing t. Therefore, the term proportional to $n\cdot\Gamma$ does not contribute to the soft pion theorem and one is left with:

$$\mathcal{M}_m(1,0)=\mathrm{Tr}_{\mathrm{CFD}}\left[\frac{1}{f_\pi}\int\frac{\mathrm{d}^4k}{(2\pi)^4}\frac{(k\cdot n)^m\tau_-}{2(P\cdot n)^{m+1}}\gamma_5\ n\cdot\gamma\ S(k+P)\ \tau_+\Gamma_\pi\left((k+P),p_1\right)S(k-P)\right]. \tag{4.15}$$

Using the relation $p_1=2P$ and translating k such that $k'=k+P$ one gets:

$$\begin{aligned}\mathcal{M}_m(1,0) &= \mathrm{Tr}_{\mathrm{CFD}}\left[\frac{1}{f_\pi}\int\frac{\mathrm{d}^4k'}{(2\pi)^4}\frac{(k'\cdot n-P\cdot n)^m\tau_-}{2(P\cdot n)^{m+1}}\gamma_5\ n\cdot\gamma\ \tau_+\ \chi_\pi(k',p_1)\right]\\ &= \mathrm{Tr}_{\mathrm{CFD}}\left[\frac{1}{f_\pi\ p_1\cdot n}\int\frac{\mathrm{d}^4k'}{(2\pi)^4}\left(2\frac{k'\cdot n}{p_1\cdot n}-1\right)^m\gamma_5\ n\cdot\gamma\ \tau_+\ \chi_\pi(k',p_1)\right]\\ &= \mathrm{Tr}_{\mathrm{CFD}}\left[\int\mathrm{d}u(2u-1)^m\frac{1}{f_\pi}\int\frac{\mathrm{d}^4k'}{(2\pi)^4}\ \delta(u\ p_1\cdot n-k\cdot n)\gamma_5\ n\cdot\gamma\ \tau_+\ \chi_\pi(k',p_1)\right]\\ &= \int\mathrm{d}u(2u-1)^m\varphi_\pi(u),\end{aligned} \tag{4.16}$$

φ_π being the pion DA defined in terms of the Bethe-Salpeter wave function in equation (3.42). As a continuous function is uniquely defined through its Mellin moments, one concludes that:

$$H^q_\pi(x,1,0)=\frac{1}{2}\varphi^q_\pi\left(\frac{1+x}{2}\right), \tag{4.17}$$

in agreement with the literature [69][1]. Considering the isospin symmetry, the soft pion theorem can be reformulated as in equation (3.112). This approach has been first outlined in Ref. [105].

This analysis shows that the triangle diagram approximation is sufficient to get back the soft pion theorem, providing that:

- progators and vertices are computed within the RL approximation (the previous arguments may be generalised to any well-defined and symmetry-preserving truncation scheme but we stick here to the RL truncation scheme),
- the vertices and propagators fulfil the AVWTI.

Consequently, it is expected that when using the numerical solutions of the Dyson-Schwinger and Bethe-Salpeter equations in order to model GPDs, the soft pion theorem is recovered.

4.2 Forward case

The approach developed in chapter 3 is based on the assumption that the Mellin moments of the pion GPD could be described using the so-called impulse approximation, *i.e.* the relevant associated Feynman diagrams giving the main contribution are the "triangles ones" (figure 3.6). The small breaking of the $x \leftrightarrow 1-x$ symmetry shown on figure 3.16 can be explained by additional terms contributing to the Mellin moments of the pion PDF.

4.2.1 Additional contributions to the triangle diagram

Within the triangle diagram approximation, the insertion of the local twist-two operators was done directly on a quark propagator, between the two pion Bethe-Salpeter vertices (figure 3.6). Yet, it is possible to imagine that the twist-two operators could act directly inside the vertices, either for the incoming pion or the outgoing one, leading to additional contributions depicted on figure 4.4.

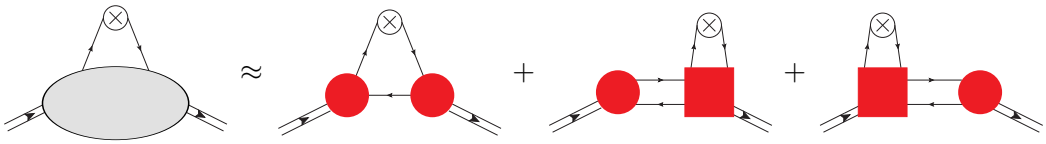

Figure 4.4: Additional contributions to the triangle diagrams. The circle vertices correspond to the Bethe-Salpeter amplitudes, whereas the squared vertices denote a new non-perturbative object related to the Bethe-Salpeter amplitude but on which the twist-two operators also act.

In order to get insights of how those additional vertices are related to the Bethe-Salpeter amplitude, and thus to be able to compute their contributions to the pion PDF, it is valuable to carefully look at their internal structures in terms of quarks and gluons. Within the RL approximation, the Bethe-Salpeter amplitude can be seen as an infinite number of gluon exchanges between the two quarks. Consequently, it is possible to include the local twist-two

[1] Depending on the conventions used, an additional factor $1/2$ may appear in the literature, like for instance in Ref. [158].

operator between any of the gluon ladders (figure 4.5). On can also imagine that, due to the possible splitting of a gluon into a quark and antiquark pair, contributions coming from the gluon ladders themselves should also be taken into account (figure 4.5). This is true when looking at the sea-quark GPDs, but in the case of the valence quark GPDs, contributions coming from quark and antiquark pairs cancel out, living only the possibility for the local twist-two operators to act on quarks between ladders. Consequently, one can see the "squared" vertex as a sum over all possibilities to include the local twist-two operators between two gluon ladders, *i.e.* :

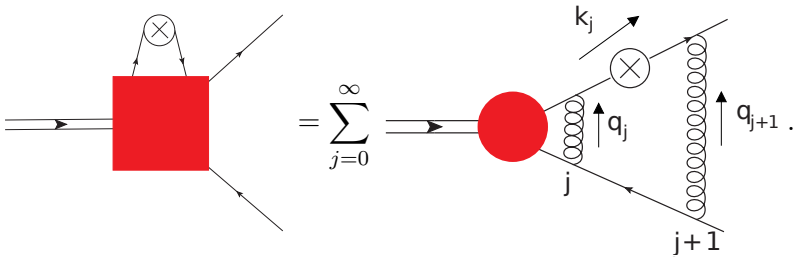

(4.18)

The corresponding operator is the same as in the case of the triangle diagram, thus, one has to deal with:

$$n_\mu n_{\mu_1} \cdots n_{\mu_m} O^{\{\mu,\mu_1 \cdots \mu_m\}} \to (k \cdot n)^m \; i \; \Gamma(k - \frac{\Delta}{2}, k + \frac{\Delta}{2}) \cdot n, \tag{4.19}$$

where Γ^μ is the electromagnetic vertex, which has to fulfil the WTI defined in equation (3.68).

In the case of the forward limit, *i.e.* of vanishing Δ, the WTI relates the electromagnetic vertex Γ^μ with the quark propagator as:

$$i\Gamma^\mu(k_j, k_j) = \frac{\partial S^{-1}}{\partial k_j^\mu}(k_j), \tag{4.20}$$

where the subscript j indicates the momentum running between the j^{th} and $(j+1)^{\text{th}}$ ladders. Denoting by q_j the momentum of the gluon in the j^{th} ladder, momentum conservation imposes $k_{j+1} = k_j + q_{j+1}$. Being given the momentum of the outgoing quarks and of the incoming pion, the accessible phase space is given by the $\{q_j\}$. Perturbative QCD teaches us that a singularity would appear for any of the $q_j \to 0$ (the so-called "soft" divergence). In the Dyson-Schwinger approach, there is no such singularities (see *e.g.* equation (3.28)). Nevertheless, one can expect that the dominant contribution to the "square" vertex takes place when:

$$\forall j, \quad q_j \approx 0. \tag{4.21}$$

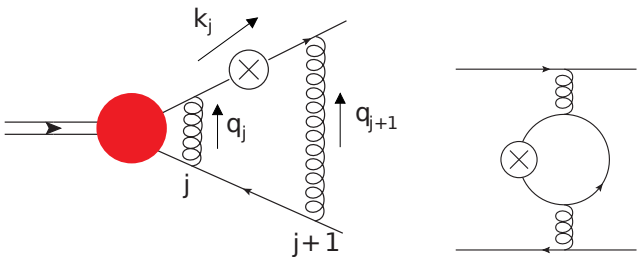

Figure 4.5: Possible inclusions of the twist-two operator inside the Bethe-Salpeter amplitude. Left-hand side: valence contribution. Right-hand side: sea contribution.

This immediately gives:

$$\forall j, \quad k_j = k_{j+1} = k, \tag{4.22}$$

and therefore, equation (4.20) becomes independent of the considered ladder. Then, using the fact that:

$$\frac{\partial}{\partial k^\mu}\left[S(k)S^{-1}(k)\right] = 0, \tag{4.23}$$

which directly leads to:

$$\frac{\partial S}{\partial k^\mu}(k) = -S(k)\frac{\partial S^{-1}}{\partial k^\mu}(k)S(k), \tag{4.24}$$

the infinite sum over all the possible insertions can be seen as an infinite sum on the derivatives of the propagators with respect to k. With the gluons having vanishing momenta, this can be reduced to the derivative of the Bethe-Salpeter amplitude itself:

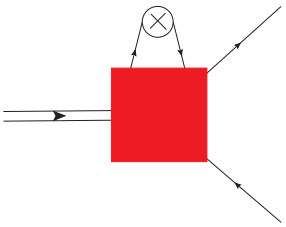

$$= -\frac{1}{2}(k\cdot n)^m n^\mu \frac{\partial \Gamma_\pi^q}{\partial k^\mu}(k,P)\,, \tag{4.25}$$

where the 1/2 factor is introduced to avoid double counting. Indeed, the derivation also acts on the anti-quark line, leading to twice the desired correction. This additional contibution has been originally introduced in Ref. [219].

4.2.2 Double Distribution Computations

Using the algebraic model developed in section 3.1.5, and more specifically equation (3.39), it is possible to get an Ansatz for the additional contribution:

$$\frac{\partial \Gamma_\pi^q}{\partial k^\mu}\left(k, P-\frac{\Delta}{2}\right) = -2\nu\int \mathrm{d}z \frac{M^{2\nu}\rho(z)\left(k^\mu - (\frac{1-z}{2}-\eta)(P-\frac{\Delta}{2})^\mu\right)}{\left[\left(k-(\frac{1-z}{2}-\eta)(P-\frac{\Delta}{2})\right)^2 + M^2\right]^{\nu+1}}. \tag{4.26}$$

With such an Ansatz in the forward limit, both the derivatives of Γ_π and $\bar{\Gamma}_\pi$ give the same result, allowing to compute a single additional term instead of two. The additional contribution $\mathcal{M}_m^{\mathrm{ad}}(0,0)$ to the Mellin moments $\mathcal{M}_m(\xi,t)$ can be computed as:

$$\mathcal{M}_m^{\mathrm{ad}}(0,0) = \mathrm{Tr}_{\mathrm{CFD}}\left[-\int \frac{\mathrm{d}^4k}{(2\pi)^4}\frac{(k\cdot n)^m}{2(P\cdot n)^{m+1}}\tau_- i\bar{\Gamma}_\pi(k+,P)\,S(k)\tau_+ i n^\mu \frac{\partial \Gamma_\pi}{\partial k^\mu}(k,P)\,S(k-P)\right]. \tag{4.27}$$

The computing techniques developed in chapter 3 are still available here. Using the Feynman parameters to rewrite the denominators and multiplying the result by:

$$1 = \int \mathrm{d}v\,\delta(v), \tag{4.28}$$

in order to insert one additional parameter, one gets:

$$\begin{aligned}\mathcal{M}_m^{\mathrm{ad}}(0,0) \quad = \quad & -\frac{1}{8\pi^2}\int \mathrm{d}z\mathrm{d}z'\mathrm{d}x_i\; x^\nu y^{\nu-1}\delta(1-x-y-u-w-v)\delta(v)\rho(z)\rho(z') \\ & (-2)(\delta(w)+\delta(u))\left(g-(\frac{1-z}{2})\right)P^{\{\mu}gP^{\mu_1}...gP^{\mu_n\}}\end{aligned} \tag{4.29}$$

with $\mathrm{d}x_i$ indicates that one has to integrate over the Feynman parameters x, y, u, v and w. g is the function defined previously in equation (3.79) in terms of Feynman parameters. Applying the change of variables defined in equations (3.103) and (3.104), it is possible to get back a DD. Of course, since this has been done in the forward limit, *i.e.* $t = 0$ and $\xi = 0$, the computation is sensitive only to the DD $F^{\mathrm{ad}}(\beta, \alpha, 0)$. Integrating with respect to the introduced variables, symmetrising with respect to α to take into account the two additional diagrams of figure 4.4 one gets:

$$
\begin{aligned}
F^{\mathrm{ad}}(\beta,\alpha,0) \;=\; & \frac{54}{40}\Bigg[(\alpha-\beta+1)(\alpha+\beta-1)\left(\frac{\left(\alpha^2(\beta+3)-\beta^2(\beta+1)+\beta+1\right)\log\left(\frac{(\alpha-\beta+1)(\alpha+\beta-1)}{\alpha^2-(\beta+1)^2}\right)}{\left(\alpha^2-(\beta+1)^2\right)^2}\right. \\
& -\frac{4\beta\left(\alpha^4(\beta-5)+\alpha^2(6-2(\beta-4)\beta(\beta+2))+\beta^5+\beta^4-\beta-1\right)}{\left(\alpha^2-(\beta+1)^2\right)^2} \\
& +\frac{2\left(\alpha^6(-(\beta-5))+\alpha^4(3\beta((\beta-3)\beta-5)-11)\right)}{\left(\alpha^2-(\beta+1)^2\right)^2} \\
& +\frac{2\left(+\alpha^2\left(\beta\left(\beta\left(3\beta\left(-\beta^2+\beta+6\right)+22\right)+18\right)+10\right)\tanh^{-1}\left(\frac{2\beta}{-\alpha^2+\beta^2+1}\right)\right)}{\left(\alpha^2-(\beta+1)^2\right)^2} \\
& \left.+\frac{2(\beta-1)\beta^2(\beta+1)^2\left(\beta^2-2\right)\tanh^{-1}\left(\frac{2\beta}{-\alpha^2+\beta^2+1}\right)}{\left(\alpha^2-(\beta+1)^2\right)^2}\right)+16\alpha\beta\tanh^{-1}\left(\frac{2\alpha\beta}{\alpha^2+\beta^2-1}\right) \\
& -2\left(+(\beta-1)\left(2\beta\left(\alpha^2-\beta^2+3\right)+\left(\alpha^4-2\alpha^2\left(\beta^2+3\right)+\beta^4+2\beta^2\right)\tanh^{-1}\left(\frac{2\beta}{-\alpha^2+\beta^2+1}\right)\right)\right) \\
& -2\left(+(8\alpha+3\beta-3)\tanh^{-1}\left(\frac{\beta}{\alpha-1}\right)+(8\alpha-3\beta+3)\tanh^{-1}\left(\frac{\beta}{\alpha+1}\right)\right)\Bigg]. \qquad (4.30)
\end{aligned}
$$

The shape of this DD is illustrated on figure 4.6. From this additional component, it is possible to compute a new term of the PDF denoted $q_\pi^{\mathrm{ad}}(x)$:

$$
\begin{aligned}
q_\pi^{\mathrm{ad}}(x) \;&=\; \int_{-1+x}^{1-x}\mathrm{d}\alpha F^{\mathrm{ad}}(x,\alpha,0) \\
&=\; \frac{72}{25}\Bigg(-\left(2x^3+4x+9\right)(x-1)^3\log(1-x)+x^3(2x((x-3)x+5)-15)\log(x) \\
&\quad -x(x-1)(2x-1)((x-1)x-9)\Bigg). \qquad (4.31)
\end{aligned}
$$

As shown on figure 4.6, this term compensates exactly the asymmetry found in the case of the triangle diagram with $q_\pi^{\mathrm{Tr}}(x)$ defined in equation (3.109). One gets:

$$
\begin{aligned}
q_\pi^{\mathrm{tot}}(x) \;&=\; q_\pi^{\mathrm{Tr}}(x)+q_\pi^{\mathrm{ad}}(x) \\
&=\; \frac{72}{25}\Bigg(x^3(x(2x-5)+15)\log(x)-\left(2x^2+x+12\right)(x-1)^3\log(1-x) \\
&\quad -2x(x-1)((x-1)x+6)\Bigg). \qquad (4.32)
\end{aligned}
$$

Consequently, q_π^{tot} is fully consistent with the symmetries considered in the present model,

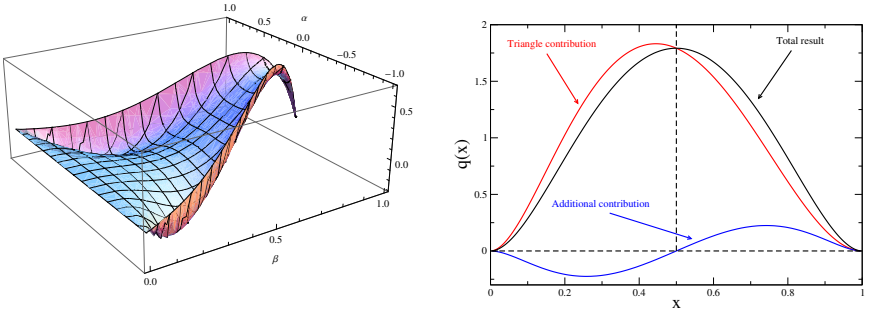

Figure 4.6: Additional contributions. Left-hand side: the DD $F^{\mathrm{ad}}(\beta, \alpha, 0)$ plotted on the (β, α) half-rhombus. Right-hand side: all contributions to the PDF depending on the momentum fraction x.

and thus solves one of the issues raised in chapter 3. Yet, this is the case only for the forward limit, since the additional term has been computed here only for $\xi = 0$ and $t = 0$. The generalisation of this term to the off-forward case is *a priori* required in order to get a fully consistent GPD in a two-body modeling.

4.2.3 Limitations in the off-forward case

The generalisation of equation (4.32) to the off-forward case remains a hard task. Indeed, as momentum is transferred in the t-channel, the WTI formulation used in equation (4.20) does not hold anymore and instead one has to use equation (3.68). Consequently, it is expected that an Ansatz such as the one in equation (4.25) cannot well describe the GPD far from the forward limit.

Still, several conditions can be stated in order to build an Ansatz. First of all, in the forward case one should of course get back the symmetric PDF q_π^{tot} defined in equation (4.32) and thus an Ansatz for the additional vertex which collapses to the derivative of the Bethe-Salpeter amplitude in the forward limit, consistently with equation (4.25). In addition, as it was proved in section 4.1, the triangle diagram is sufficient to ensure the soft pion theorem, providing that the Bethe-Salpeter amplitudes, the propagators and the local twist-two operators are consistently computed in the RL truncation scheme and fulfil the WTI and AVWTI. Within those conditions, any additional contribution has to vanish when $\xi \to 1$ and $t \to 0$. And of course, it also has to satisfy the GPD polynomiality property and the parity in ξ.

If the previous properties were mandatory, others are desirable. Indeed, as it has been shown before in section 3.3.4, the model based on the triangle diagram does not verify the positivity condition given in equation (1.56). It would be an important progress if an additional contribution to the triangle diagram could correct this, which could actually come from both a limitation of the triangle diagram itself, like the breaking of the $x \leftrightarrow 1 - x$ symmetry in the forward case, or a consequence of the algebraic model itself of the same type than for the soft pion theorem. Moreover, as it has been emphasised in section 3.3.4, the large-t behaviour of the model based on the triangle diagram is questionable. Thus, the large-t condition of any additional off-forward contribution needs to be well inspired.

It is possible for instance to make an educated guess in order to extend the vertex of the additional contribution of equation (4.25). Doing so leads to the computation of an additional

term to the GPD Mellin moments as:

$$\begin{aligned}\mathcal{M}_m^{\mathrm{ad}}(\xi,t) &= \frac{1}{2}\int\frac{\mathrm{d}^4k}{(2\pi)^4}n\cdot\frac{\partial\bar{\Gamma}_\pi}{\partial\bar{k}}(k+\frac{\Delta}{2},P+\frac{\Delta}{2})S(k-P)\Gamma_\pi(k-\frac{\Delta}{2},P-\frac{\Delta}{2})S(k-\frac{\Delta}{2})\\ &+\frac{1}{2}\int\frac{\mathrm{d}^4k}{(2\pi)^4}\bar{\Gamma}_\pi(k+\frac{\Delta}{2},P+\frac{\Delta}{2})S(k-P)n\cdot\frac{\partial\Gamma_\pi}{\partial k}(k-\frac{\Delta}{2},P-\frac{\Delta}{2})S(k+\frac{\Delta}{2}).\end{aligned} \tag{4.33}$$

But this rough continuation hardly fulfils any of the previous requirements. If polynomiality and parity in ξ are satisfied due to the DD formalism, computations show that things get worse at large-ξ and large-t. No significant changes can be seen on positivity. This shows the limitation of the current approach, arguing for a new formalism.

4.3 Sketching the pion 3D structure

If the description of the full domain of definition of the GPD requires a novel approach, it is still possible to get information on a restricted domain. The following section is devoted to the study of our model in the kinematic limit $\xi \to 0$ but non-vanishing t. Indeed, if the educated guess of equation (4.33) cannot give directly an extension of the additional terms, it still sheds light on the possible correlations between x and t.

4.3.1 Correlations between x and t

Summing the DDs F obtained in equations (3.105) and (4.30) it is possible to define the total DD generating the symmetric PDF $q_\pi^{\mathrm{tot}}(x)$ of equation (4.32):

$$F^{\mathrm{tot}}(\beta,\alpha,t) = F^{\mathrm{Tr}}(\beta,\alpha,t) + F^{\mathrm{ad}}(\beta,\alpha,t). \tag{4.34}$$

The DD F^{tot} can be written as:

$$F^{\mathrm{tot}}(\beta,\alpha,t) = F^{\mathrm{sym}}(\beta,\alpha)\left(\phi(\beta,\alpha,t)\right)^2 + \frac{t}{4M^2}V(\beta,\alpha)\left(\phi(\beta,\alpha,t)\right)^3, \tag{4.35}$$

where:

$$F^{\mathrm{sym}}(\beta,\alpha) = F^{\mathrm{tot}}(\beta,\alpha,0), \tag{4.36}$$

$V(\beta,\alpha)$ is a contribution arising from the triangle diagram only, and:

$$\phi(\beta,\alpha,t) = \frac{1}{1+\frac{t}{4M^2}(1+\alpha-\beta)(1-\alpha-\beta)}. \tag{4.37}$$

The t-dependent denominator here comes directly from the Feynman parameterisation introduced in the computing method developed in chapter 3. More precisely, it is controlled by the denominator dependence on Δ^2 and $P^2 = m_\pi^2 - \frac{\Delta^2}{4}$ coming from the propagators (3.37) and of the Bethe-Salpeter amplitude (3.39).

The $x \leftrightarrow 1-x$ symmetry, which was a key point in the forward case, does not hold anymore as soon as t is non-vanishing. Consequently, it is expected that correlations between x and

t appear, breaking more and more the previous symmetry as t grows. This can be seen in equation (4.35). $\phi(\beta, \alpha)$ generates an asymmetry at vanishing x, since it behaves like[2]:

$$\lim_{x\to 0} \phi(x, \alpha, t) = \frac{1}{1 + \frac{t}{4M^2}(1+\alpha)(1-\alpha)}, \tag{4.38}$$

whereas when x goes to 1:

$$\lim_{x\to 1} \phi(x, \alpha, t) = 1, \tag{4.39}$$

as $|\alpha| \leq 1 - x$. As $V(x \approx 1, \alpha \approx 0)$ goes to 0, one can note that in the case of large x, the t dependence is vanishing and the behaviour of $H(x \approx 1, 0, t)$ is similar to the PDF one. This is fully consistent with results coming from perturbation theory [220].

4.3.2 Pion 3D structure

Following Ref. [105] it is possible from the previous analysis to build a 3D representation of the pion by modeling the correlations between x and t from insights of section 4.3.1. For instance, equation (4.35) illustrates that negative contributions at large-t come only from the $V(\beta, \alpha)$ contribution.

Before building any consistent Ansatz following Ref. [105] for the pion GPD at $\xi = 0$, one should note that the GPD H^q_π can be seen as:

$$H^q_\pi(x, 0, t) = H^q_\pi(x, 0, 0)\mathcal{N}(t)C_\pi(x, t)F_\pi(t), \tag{4.40}$$

where $F_\pi(t)$ is the pion form factor, $C(x, t)$ which encodes the correlations between x and t, and $\mathcal{N}(t)$ is a normalisation factor:

$$1 = \mathcal{N}(t) \int \mathrm{d}x \; H^q_\pi(x, 0, 0)C_\pi(x, t). \tag{4.41}$$

If the study done in section 3.3.4 shows that the $x - t$ correlations are not perfectly described (especialy at large t), the form factor computed within the triangle diagram approximation remains in good agreement with the available experimental data as shown on figure 3.7. Yet it is also improved, using the dressing factor introduced in Ref. [186]. The $n \cdot \gamma$ is then dressed with an additional factor $R(t)$, encoding the fact that the vertex is not point-like, such that:

$$R(t) = \frac{1}{1 + \kappa(t)}, \tag{4.42}$$

with:

$$\kappa(t) = \frac{1}{3\pi^2}\frac{t}{M^2} \int \mathrm{d}y \; y(1-y)\Gamma\left(0, y(1-y)\frac{t}{M^2}\frac{M^2}{\Lambda^2_{\mathrm{UV}}}\right). \tag{4.43}$$

$\Gamma(a, x)$ denotes here the incomplete gamma function defined as:

$$\Gamma(a, x) = \int_x^\infty \mathrm{d}\tau \; \tau^{a-1}e^{-\tau}. \tag{4.44}$$

Λ_{UV} is an ultraviolet cut-off which is numerically chosen large enough not to affect the value of κ. This additional dressing can be taken into account as a multiplicative function in our

[2]Due to the Dirac $\delta(x - \beta)$ in the relation between GPDs and DDs when $\xi \to 0$ (see equation (2.5)), the notation x is used in the following instead of the DD variable β.

previous computations, since it generates nor $x-t$ neither $\xi-t$ correlations. Its general effect on the agreement of the model with the form factor consists in shifting the mass-scale M toward higher energies, *i.e.* $M = 0.4$ GeV instead of 0.35 GeV.

Coming back to equation (4.40), the PDF $H_\pi^q(x,0,0) = q_\pi^{\text{tot}}(x)$ (equation (4.32)) is directly provided by the previous computations. As $\mathcal{N}(t)$ is fixed by equation (4.41), the only missing piece is $C_\pi(x,t)$. In order to model it, insights must be gained from the previous analysis in term of DDs. As explained before, the term $V(\beta,\alpha)$ defined in equation (4.35) generates difficulties at large t. Apart from the correlations generated by $V(\beta,\alpha)$, the variables x and t talk to each other only through the function $\phi(\beta,\alpha,t)$. For the sake of simplicity, $C_\pi(x,t)$ is chosen as:

$$C_\pi(x,t) = \phi(x,0,t)^2 = \frac{1}{\left(1+\frac{t}{4M}(1-x)^2\right)^2}. \tag{4.45}$$

It is then possible to compute the GPD for any value of x and t as illustrated on figure 4.7 and evolve it using the DGLAP equations. Indeed, the DGLAP kernel remains valid for the GPD at any value of t providing that ξ remains vanishing. Defining x_p such that at a given t the distribution is maximal at $x = x_p$, figure 4.7 shows that x_p increases with t. At a given value of x close to 1 denoted x_1, a peak is observed at x_1 for a given value of t, say t_1, *i.e.* $x_1 = x_p(t_1)$. If this general trend is conserved by evolution equations, it appears that getting a peak at the same value x_1 requires a value of t denoted t_2 larger than t_1 if the new factorisation scale μ_{F_2} is bigger than the previous one. This is consistent with the following intuitive picture. When increasing the factorisation scale, evolution equations somehow reveal the components of the dressed quarks in terms of quarks and gluons. All those revealed quarks and gluons carry a smaller fraction of the hadron momentum than the previous dressed quarks, and thus the peak in x is shifted toward 0.

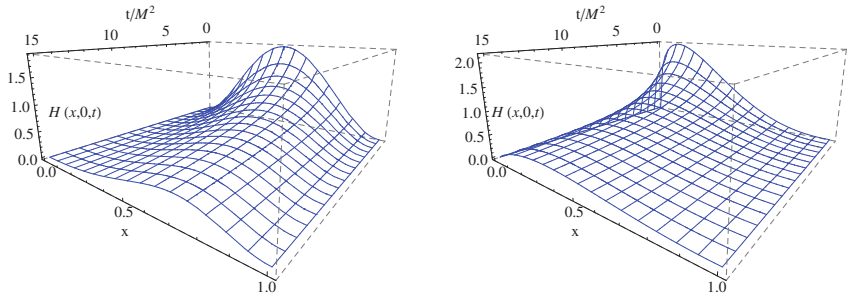

Figure 4.7: $H(x,0,t)$ using the correlation model of equation (4.45). Left-hand side: Original scale $\mu_F = 0.51$ GeV. Right-hand side: Evolved GPD at scale $\mu_F = 2$ GeV.

Using equation (1.70) it is now possible to compute a 3D picture of the pion. As shown on figure 4.8, the distribution becomes narrower in $|\mathbf{b}_\perp|$ as x goes to 1. This is quite natural since when the parton carries almost all the longitudinal momentum, it defines the barycenter of the transverse plan, and thus cannot be located far from $|\mathbf{b}_\perp| = 0$. When x leaves the neighbourhood of 1, this constraint is released and consequently, the distribution becomes broader. This also explains the broadening of the distribution when evolving it at higher scales, since evolution shifts the distribution toward the smaller x as shown on figure 4.8.

This broadening can be illustrated when computing the second moment of the distribution in $\mathbf{b}_\perp$:

$$\left\langle \mathbf{b}_\perp(x)^2 \right\rangle = \int \mathrm{d}^2\mathbf{b}_\perp \; q(x,\mathbf{b}_\perp)\mathbf{b}_\perp^2, \tag{4.46}$$

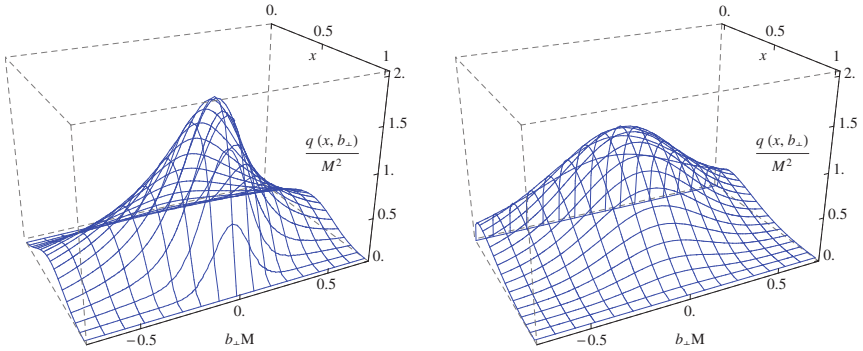

Figure 4.8: $q(x, \mathbf{b}_\perp)$ using the correlation model of equation (4.45). Left-hand side: Original scale $\mu_F = 0.51$ GeV. Right-hand side: Final scale at $\mu_F = 2$ GeV.

as shown on figure 4.9.

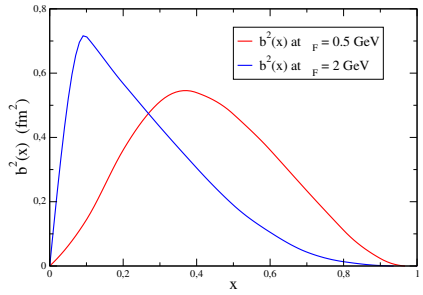

Figure 4.9: Distribution of the pion's mean-square transverse extend $\left\langle |\mathbf{b}_\perp(x)|^2 \right\rangle$ from equation (4.46) as a function of the longitudinal momentum fraction x.

If the approach developed in this section allows to bypass the difficulties encountered with the limitations of the triangle diagram and the algebraic model in the limit $\xi \to 0$, it precludes any simple improvement of the model at non-vanishing ξ. In order to do so, new techniques have to be developed.

Chapter 5

The overlap representation

«Und diess Geheimniss redete das Leben selber zu mir.
Siehe, sprach es, ich bin das, was sich immer selber überwinden muss.»
Friedrich Nietzsche in *Also Sprach Zarathustra*

5.1 GPDs as an overlap of wave functions

The previous models of GPDs have been derived either from DD phenomenological parameterisations (chapter 2) or from a covariant triangle diagram leading also to computations of DDs (chapter 3). Yet, as shown in chapter 4, the triangle diagram approximation generates issues which are hard to overcome. It is especially difficult to get a fully consistent model for the twist-two operators and the additional term generalising the results of Ref. [219] described in section 4.2. In order to avoid this difficulty, another approach is described in this chapter: the overlap of Lightcone Wave Functions (LCWF).

5.1.1 Lightcone computations

This section is an adaptation of Ref. [72] in the case of the pion. The conventions and notations used in this section are defined in appendix E and are fully consistent with Ref. [72].

Hadronic Fock space

A given hadronic state $|H;P,\lambda\rangle$ characterised by the considered hadron H, its momentum P and its polarisation λ can be decomposed in a Fock basis as:

$$|H;P,\lambda\rangle = \sum_{N,\beta} \int [\mathrm{d}x]_N [\mathrm{d}^2\mathbf{k}_\perp]_N \Psi^\lambda_{N,\beta}(\Omega)\, |N,\beta,k_1\cdots k_N\rangle \tag{5.1}$$

where $\Psi^\lambda_{N,\beta}$ is the lightcone wave function of the associated parton state, *i.e.* caracterised by N partons, and having the corresponding quantum numbers β (flavour, colour and helicity of the partons). Ω denotes the momenta of every parton, *i.e.* :

$$\Omega = (x_1, \mathbf{k}_{\perp 1}, \cdots, x_N, \mathbf{k}_{\perp N}). \tag{5.2}$$

Choosing an example relevant for the following, the 2-body pion LCWF is given by:

$$\begin{aligned}\Psi_{+-}(x,\mathbf{k}_\perp - x\mathbf{P}_\perp) &= -\frac{1}{2\sqrt{3}}\int \mathrm{d}z^- \mathrm{d}\mathbf{z}_\perp e^{i(2x-1)P^+z^-/2} e^{-i(2\mathbf{k}_\perp - \mathbf{P}_\perp)\mathbf{z}_\perp} \\ &\quad \langle \pi, P| \bar{\psi}^q(-\frac{z}{2})\gamma^+\gamma^5\psi(\frac{z}{2})\,|0\rangle\Big|_{z^+=0}, \end{aligned} \tag{5.3}$$

choosing the normalisation of Ref. [73]. The "+" and "-" indices stand for the polarisation of the partons. The measures introduced in equation (5.1) are given by:

$$[\mathrm{d}x]_N = \prod_{i=1}^N \mathrm{d}x_i\ \delta\left(1-\sum_{i=1}^N x_i\right), \tag{5.4}$$

$$[\mathrm{d}^2\mathbf{k}_\perp]_N = \frac{1}{(16\pi^3)^{N-1}}\prod_{i=1}^N \mathrm{d}^2\mathbf{k}_{\perp i}\ \delta^2\left(\sum_{i=1}^N \mathbf{k}_{\perp i} - \mathbf{P}_\perp\right). \tag{5.5}$$

Finally, the normalisation of the partonic states given in appendix E leads to:

$$\begin{aligned}&\Psi^\lambda_{N,\beta'}(\Omega')\Psi^\lambda_{N,\beta}(\Omega)\left\langle N',\beta,k'_1\cdots k'_N\right| N,\beta,k_1\cdots k_N\rangle \\ =\ & |\Psi^\lambda_{N,\beta}(\Omega)|^2\delta_{NN'}\delta_{\beta\beta'}\prod_{i=1}^N 16\pi^3 k_i^+\delta(k_i^+ - k_i'^+)\delta^2(\mathbf{k}_{\perp i} - \mathbf{k'}_{\perp i}),\end{aligned} \tag{5.6}$$

which yields the following normalisation of the hadron states on the lightcone:

$$\left\langle H;P',\lambda'\right| H;P,\lambda\rangle = 16\pi^3 P^+\delta(P'^+ - P^+)\delta^2(\mathbf{P'}_\perp - \mathbf{P}_\perp)\delta_{\lambda'\lambda}, \tag{5.7}$$

due to the canonical normalisation of the wave function:

$$\sum_{N,\beta}\int [\mathrm{d}x]_N[\mathrm{d}^2\mathbf{k}_\perp]_N|\Psi^\lambda_{N,\beta}(\Omega)|^2 = 1. \tag{5.8}$$

Overlap representation of GPDs

The definition of GPDs given in equations (1.26) for a nucleon and (1.30) for the pion involve an equal lightcone time operator, and are thus suitable for interpretation in terms of lightcone Fock space and LCWFs. The representation of GPDs as overlap of LCWFs has been introduced and derived in Ref. [72].

Before starting one should note that the bilocal quark field operator defining the GPDs can be written in terms of good lightcone components (see *e.g.* Ref. [221]):

$$\bar{\psi}^q\left(-\frac{z}{2}\right)\gamma^+\psi\left(\frac{z}{2}\right) = \sqrt{2}\phi^\dagger_q\left(-\frac{z}{2}\right)\phi_q\left(\frac{z}{2}\right), \tag{5.9}$$

which leads to the following description of the pion GPD when expanding the pion incoming and outgoing states on a Fock basis:

$$\begin{aligned}H(x,\xi,t) &= \sqrt{2}\sum_{N,N'}\sum_{\beta,\beta'}\int [\mathrm{d}\hat{x}']_{N'}[\mathrm{d}^2\hat{\mathbf{k}}'_\perp]_{N'}[\mathrm{d}\tilde{x}]_N[\mathrm{d}^2\tilde{\mathbf{k}}_\perp]_N \Psi^*_{N',\beta'}(\hat{\Omega}')\Psi_{N,\beta}(\tilde{\Omega}) \\ &\quad \times\int\frac{\mathrm{d}z^-}{2\pi}e^{iP^+z^-}\left\langle N',\beta,k'_1\cdots k'_N\right|\phi^{q\dagger}\left(-\frac{z}{2}\right)\phi^q\left(\frac{z}{2}\right)|N,\beta,k_1\cdots k_N\rangle,\end{aligned} \tag{5.10}$$

where the hat variables are given in the outgoing pion wave function frame, and the tilde ones in the incoming pion wave function frame. The other are considered in the GPD symmetric frame, *i.e.* the frame such that $p_1 = P - \frac{\Delta}{2}$ and $p_2 = P + \frac{\Delta}{2}$. The Fourier transform of the non-local operator $\bar{\psi}^q\left(-\frac{z}{2}\right)\gamma^+\psi\left(\frac{z}{2}\right)$ gives:

$$\begin{aligned}
&\frac{1}{2\pi}\int \mathrm{d}z^- e^{ixP^+z^-}\bar{\psi}^q\left(-\frac{z}{2}\right)\gamma^+\psi\left(\frac{z}{2}\right)\\
=\;& 2\sqrt{2}\int\frac{\mathrm{d}k'}{k'^+}\frac{\mathrm{d}\mathbf{k}'_\perp}{16\pi^3}\theta(k'^+)\int\frac{\mathrm{d}k}{k_1^+}\frac{\mathrm{d}^2\mathbf{k}_\perp}{16\pi^3}\theta(k^+)\sum_{s,s'}\\
&\Big[\delta(2xP^+ - k'^+ - \tilde{k}^+)b_q^\dagger(\omega')b_q(\omega)u_+^\dagger(\omega')u_+(\omega)\\
&+\delta(2xP^+ + k'^+ + \tilde{k}^+)d_q^\dagger(\omega')d_q(\omega)v_+^\dagger(\omega')v_+(\omega)\\
&+\delta(2xP^+ + k'^+ - \tilde{k}^+)d_q(\omega')b_q(\omega)v_+^\dagger(\omega')u_+(\omega)\\
&+\delta(2xP^+ - k'^+ + \tilde{k}^+)b_q^\dagger(\omega')d_q^\dagger(\omega)u_+^\dagger(\omega')v_+(\omega)\Big],
\end{aligned}\tag{5.11}$$

when writing the lightcone fields in terms of Fourier transform of lightcone creation and annihilation operators (see appendix E for expression of fields in terms of creation operators). This formula highlights the parton interpretation mentioned in chapter 1. Momentum conservation in the t-channel leads to:

$$k^+ - k' = p_1^+ - p_2^+ = 2\xi P. \tag{5.12}$$

Focusing on the DGLAP region in terms of quarks, only the first line of the operator in equation (5.11) is non-vanishing. In this case, the non-vanishing contributions of the Fock state composing the considered hadron are of the form:

$$\begin{aligned}
&\left\langle N', \beta, k'_1\cdots k'_N\right|\phi^{q\dagger}\left(-\frac{z}{2}\right)\phi^q\left(\frac{z}{2}\right)\left|N, \beta, \tilde{k}_1\cdots\tilde{k}_N\right\rangle\\
=\;&\sum_{j=1}^{N}\frac{\left\langle s'_j,\omega'_j\right|\phi^{q\dagger}\left(-\frac{z}{2}\right)\phi^q\left(\frac{z}{2}\right)\left|s_j,\omega_j\right\rangle}{\sqrt{\hat{x}'_1\cdots\hat{x}'_N}\sqrt{\tilde{x}_1\cdots\tilde{x}_N}}\prod_{i\neq j}^{N}\left\langle s'_i,\omega'_i\right|\left.s_i,\omega_i\right\rangle,
\end{aligned}\tag{5.13}$$

with

$$\tilde{x}_i = \frac{\tilde{k}_i^+}{p_1^+} \quad , \quad \hat{x}'_i = \frac{\hat{k}'_i}{p_2^+}. \tag{5.14}$$

In order to describe both the initial and final states with the same variables, the average variables $\bar{k}_i$ are introduced as:

$$\bar{k}_i = \frac{1}{2}(k_i + k'_i) \quad , \quad \bar{x}_i = \frac{\bar{k}_i^+}{P^+}, \tag{5.15}$$

and satisfy the following constraints due to momentum conservation:

$$\sum_{i=1}^{N}\bar{x}_i = 1 \quad , \quad \sum_{i=1}^{N}\bar{\mathbf{k}}_{\perp i} = P_\perp = 0. \tag{5.16}$$

Momentum conservation also imposes the following conditions on the active parton (labelled "j"):

$$x_j = \bar{x}_j + \xi \quad , \quad x'_j = \bar{x} - \xi \quad , \tag{5.17}$$

and

$$\mathbf{k}_{\perp j} = \bar{\mathbf{k}}_{\perp j} - \frac{\Delta_\perp}{2} \quad , \quad \mathbf{k}'_{\perp j} = \bar{\mathbf{k}}'_{\perp j} + \frac{\Delta_\perp}{2} \quad , \tag{5.18}$$

whereas for the spectator partons (labelled "i") one gets:

$$k'_i = \bar{k}_i = k_i. \tag{5.19}$$

It is then possible to boost the "hat" and "tilde" variables into the GPD symmetric frame, and thus write them in terms of "bar" variables. For the incoming pion it gives:

$$\begin{aligned} \tilde{x}_i &= \frac{\bar{x}_i}{1+\xi}, & \tilde{\mathbf{k}}_{\perp i} &= \bar{\mathbf{k}}_{\perp i} + \frac{\bar{x}_i}{1+\xi}\frac{\Delta_\perp}{2}, & \text{for } i \neq j \\ \tilde{x}_j &= \frac{\bar{x}_j + \xi}{1+\xi}, & \tilde{\mathbf{k}}_{\perp j} &= \bar{\mathbf{k}}_{\perp j} - \frac{1-\bar{x}_i}{1+\xi}\frac{\Delta_\perp}{2}, & \end{aligned} \tag{5.20}$$

and for the outgoing one:

$$\begin{aligned} \hat{x}'_i &= \frac{\bar{x}_i}{1-\xi}, & \hat{\mathbf{k}}'_{\perp i} &= \bar{\mathbf{k}}_{\perp i} - \frac{\bar{x}_i}{1-\xi}\frac{\Delta_\perp}{2}, & \text{for } i \neq j \\ \hat{x}'_j &= \frac{\bar{x}_j - \xi}{1-\xi}, & \hat{\mathbf{k}}'_{\perp j} &= \bar{\mathbf{k}}_{\perp j} + \frac{1-\bar{x}_i}{1-\xi}\frac{\Delta_\perp}{2}. & \end{aligned} \tag{5.21}$$

Expressing the normalisation condition of a single particle state given in equation (E.12), with those variables, one gets:

$$\left\langle s'_i, \omega'_i \right| s_i, \omega_i \rangle = 16\pi^3 \hat{x}'_i \delta\left(\hat{x}_i - \tilde{x}_i \frac{1+\xi}{1-\xi}\right) \delta^2\left(\hat{\mathbf{k}}_{\perp i} - \tilde{\mathbf{k}}_{\perp i} + \frac{\tilde{x}_i}{1-\xi}\Delta_\perp\right) \delta_{ss'}\delta_{\mu\mu'}. \tag{5.22}$$

Coming back to equations (5.11) and (5.13), the Fourier transform of the remaining matrix element in the DGLAP region leads to:

$$\int \frac{\mathrm{d}z^-}{2\pi} \left\langle s'_j, \omega'_j \right| \phi_q^\dagger\left(-\frac{z}{2}\right) \phi_q\left(\frac{z}{2}\right) \left| s_j, \omega_j \right\rangle = \frac{1}{P^+}\delta(x - \bar{x}_j) u_+^\dagger(\omega'_j) u_+(\omega_j) \delta_{s_j s'_j} \delta_{s_j q}. \tag{5.23}$$

Evaluating the spinor product to its asymptotic limit ($P^+ \to \infty$):

$$u_+^\dagger(\omega'_j) u_+(\omega_j) = \frac{1}{\sqrt{2}} \bar{u}(\omega'_j)\gamma^+ u(\omega_j) = \sqrt{2(1-\xi^2)\hat{x}'_j \tilde{x}_j} P^+ \delta_{\mu_j \mu'_j}, \tag{5.24}$$

and inserting equation (5.13) in (5.10), it is possible to simplify the result using equations (5.22), (5.23) and (5.24). Then, integrating over the "hat" variables and applying the following change of variables:

$$[\mathrm{d}\tilde{x}]_N = \frac{1}{1+\xi}[\mathrm{d}\bar{x}]_N, \qquad [\mathrm{d}^2\tilde{\mathbf{k}}_\perp]_N = [\mathrm{d}^2\bar{\mathbf{k}}_\perp]_N, \tag{5.25}$$

the pion GPD finally reads:

$$\begin{aligned} H_\pi^q(x,\xi,t)|_{\xi \leq x \leq 1} \quad = \quad & \sqrt{1-\xi}^{2-N} \sqrt{1+\xi}^{2-N} \sum_{\beta=\beta'} \sum_j \delta_{s_j q} \\ & \int [\mathrm{d}\bar{x}]_N [\mathrm{d}^2\bar{\mathbf{k}}_\perp]_N \delta(x - \bar{x}_j) \Psi^*_{N,\beta'}(\hat{\Omega}') \Psi_{N,\beta}(\tilde{\Omega}). \end{aligned} \tag{5.26}$$

Further details can be found in the original paper [72].

Computation in the ERBL region follows the same path. However, the main difference relies on the parton numbers N and N' . The DGLAP region selects the trace on the number of involved partons, whereas in the ERBL region $N = N' + 2$ for physically accessible kinematics.

5.1.2 Modeling the pion Lightcone Wave Function

Coming back to equation (5.26), the two valence quark contributions to the pion GPD can be computed on the lightcone:

$$H_\pi^q(x,\xi,t)|_{\xi\leq x\leq 1}^{2-\text{body}} = \sum_{\beta=\beta'}\sum_j \delta_{s_j q}\int [\mathrm{d}\bar{x}]_2[\mathrm{d}^2\bar{\mathbf{k}}_\perp]_2\delta(x-\bar{x}_j)\Psi^*_{2,\beta'}(\hat{\Omega}')\Psi_{2,\beta}(\tilde{\Omega}). \tag{5.27}$$

Consequently, computing the GPD in the DGLAP region through LCWFs allows to avoid the triangle diagram approximation and thus the issue of generalising section 4.2 to non-vanishing ξ and t. But to do so, it is necessary to compute first LCWFs.

In a Bethe-Salpeter framework, the LCWF Ψ can be computed by integrating over k^- the pion Bethe-Salpeter wave function $\chi_\pi(k,P)$ projected on $\gamma^+\gamma_5$:

$$\Psi(k^+,\mathbf{k}_\perp,P) = -\frac{1}{2\sqrt{3}}\int\frac{dk^-}{2\pi}\mathrm{Tr}\left[\gamma^+\gamma_5\chi_\pi(k,P)\right], \tag{5.28}$$

with $\chi_\pi(k,P)$ defined in equation (3.9). In the following, other possible projections of the Bethe-Salpeter wave function are not taken into account. Indeed, this exploratory work is dedicated to the study of the possibility to compute the GPD using lightcone overlap in both the DGLAP and ERBL regions using the inversion of the Radon transform. A complete computation is left for future works. So, coming back to the algebraic model defined in equations (3.37) to (3.41), it is *a priori* possible to compute the associated LCWF through equation (5.28). Yet, proceeding so is ignoring that the algebraic model has been defined in Euclidean space, where the lightcone variable k^+ and k^- are complex conjugates. However, their product $k^+k^- = -(k^3)^2-(k^4)^2$ is well defined in the euclidean space. The idea is thus to integrate both on k^+ and k^- to be able to perform a change of variable leading to integration on the real variable k^3 and k^4. Doing so is nothing else than computing the Mellin moments of the LCWF Ψ from the Bethe-Salpeter wave function. Consequently, the 4-vector k is split as $q+\mathbf{k}_\perp$, with $q=(q^+,q^-,0)$, and the Mellin moments reads:

$$\begin{aligned}\int_0^1 \mathrm{d}x\ x^m\Psi(x,\mathbf{k}_\perp,P) &= \frac{-1}{2\sqrt{3}}\int_0^1\mathrm{d}x\ x^m\int\frac{\mathrm{d}q^-\mathrm{d}q^+}{(2\pi)^2}\mathrm{Tr}\left[\gamma^+\gamma_5\chi_\pi(q+\mathbf{k}_\perp,P)\right]\delta(xP\cdot n-q\cdot n)\\ &= -\frac{1}{2\sqrt{3}}\int\frac{\mathrm{d}^2q(q\cdot n)^m}{(2\pi)^2(P\cdot n)^{(m+1)}}\mathrm{Tr}\left[\gamma^+\gamma_5\chi_\pi(q+\mathbf{k}_\perp,P)\right],\end{aligned} \tag{5.29}$$

with $\mathrm{d}^2q=\mathrm{d}q^+\mathrm{d}q^-$. Equation (5.29) is really close to equation (3.42). Computing the trace of the numerator leads to the following factor:

$$-4MP\cdot n. \tag{5.30}$$

As previously, it is possible to use the approach of Feynman parameters in order to write the integral as:

$$\begin{aligned}\int_0^1 \mathrm{d}x\ x^m\Psi(x,\mathbf{k}_\perp,P) &= -\frac{1}{2\sqrt{3}}\int\frac{\mathrm{d}^2q(q\cdot n)^m\Gamma(\nu)}{(2\pi)^2(P\cdot n)^m\Gamma(\nu+2)}\mathrm{d}u\mathrm{d}v\mathrm{d}y\\ &\quad\frac{(-4)M^{2\nu+1}\rho_\nu(z)y^{\nu-1}\delta(1-u-v-y)}{\left[(q-\kappa(z,y,v)P)^2+(\mathbf{k}_\perp-\kappa(z,y,v)\mathbf{P}_\perp)^2+M^2\right]^{\nu+2}}\end{aligned} \tag{5.31}$$

with $\kappa(z,y,v)=\frac{1-z}{2}y+v$. One can then integrate over d^2q, by changing $q'=q-\kappa(z,y,v)P$, keeping in mind that $n^2=0$ which kills (after the change of variables) the contributions $(q'\cdot n)^j$ for j different from 0. Summarising the computations, one gets:

$$\begin{aligned}\int_0^1 \mathrm{d}x\ x^m\Psi(x,\mathbf{k}_\perp,P) &= \frac{1}{2\pi\sqrt{3}}\int \mathrm{d}u\mathrm{d}v\mathrm{d}y\frac{\Gamma(\nu)\Gamma(\nu+1)}{\Gamma(\nu+2)^2}\\ &\quad\frac{M^{2\nu+1}\rho_\nu(z)y^{\nu-1}\delta(1-u-v-y)}{[(\mathbf{k}_\perp-\kappa(z,y,v)\mathbf{P}_\perp)^2+M^2]^{\nu+1}}\kappa(z,y,v)^m,\end{aligned}\tag{5.32}$$

from which it is possible to deduce:

$$\Psi(x,\mathbf{k}_\perp,P)=\frac{1}{2\pi\sqrt{3}}\int \mathrm{d}u\mathrm{d}v\mathrm{d}y\frac{\Gamma(\nu)\Gamma(\nu+1)}{\Gamma(\nu+2)^2}\frac{M^{2\nu+1}\rho_\nu(z)y^{\nu-1}\delta(1-u-v-y)}{[(\mathbf{k}_\perp-\kappa(z,y,v)\mathbf{P}_\perp)^2+M^2]^{\nu+1}}\delta(x-\kappa(z,y,v)).\tag{5.33}$$

Applying the following change of variables:

$$\left\{\begin{array}{rcl}\zeta &=& \frac{1+z}{2}\\ u' &=& 1-u\\ \beta &=& (1-\zeta)u'+\zeta v\end{array}\right.,\tag{5.34}$$

which leads to $\kappa(z,y,v)=\beta$, one can rewrite the wave function as (omitting $'$ in u'):

$$\Psi(x,\mathbf{k}_\perp,P)=\frac{1}{2\pi\sqrt{3}}\int_0^1\mathrm{d}\beta\int_0^\beta\mathrm{d}v\int_\beta^1\mathrm{d}u\frac{\Gamma(\nu)\Gamma(\nu+1)}{\Gamma(\nu+2)^2}\frac{M^{2\nu+1}\tilde{\rho}_\nu(\beta,u,v)(u-v)^{\nu-1}}{[(\mathbf{k}_\perp-\beta\mathbf{P}_\perp)^2+M^2]^{\nu+1}(u-v)}\delta(x-\beta),\tag{5.35}$$

with:

$$\tilde{\rho}_\nu(\beta,u,v)=4^\nu R_\nu\left(1-\frac{u-\beta}{u-v}\right)^\nu\left(\frac{u-\beta}{u-v}\right)^\nu,\tag{5.36}$$

R_ν being the normalisation constant introduced in the algebraic model in equation (3.40). Integrating out u and v, one gets:

$$\Psi(x,\mathbf{k}_\perp,P)=\frac{1}{2\pi\sqrt{3}}\frac{\Gamma(\nu)^2\Gamma(\nu+1)}{\Gamma(\nu+2)^3}\frac{M^{2\nu+1}4^\nu R_\nu}{[(\mathbf{k}_\perp-x\mathbf{P}_\perp)^2+M^2]^{\nu+1}}x^\nu(1-x)^\nu.\tag{5.37}$$

5.1.3 Distributions on the lightcone

Pion DA

The pion DA is related to the LCWF through integration over the transverse momentum:

$$f_\pi\phi_\pi(x)=-4\sqrt{3}\int\frac{\mathrm{d}^2\mathbf{k}_\perp}{16\pi^3}\int\mathrm{d}k^+\delta(xP^+-k^+)\Psi(k^+,\mathbf{k}_\perp,P),\tag{5.38}$$

f_π being the pion decay constant. Injecting equation (5.37) and integrating over $\mathbf{k}_\perp$, one gets:

$$f_\pi\phi_\pi(x)=-\frac{4^\nu}{(2\pi)^4}\frac{M\Gamma(\nu)^3}{\Gamma(\nu+2)^3}R_\nu x^\nu(1-x)^\nu.\tag{5.39}$$

Normalising the DA yields:

$$\phi_\pi(x)=\kappa_\nu x^\nu(1-x)^\nu,\tag{5.40}$$

where κ_ν is a normalisation constant. Consequently we recover the results of Ref. [196].

Pion PDF

It is also possible to compute the PDF, which is a special case of equation (5.27) for $\xi = 0$ and $t = 0$. This greatly simplifies the expression of Ω and Ω' thanks to equations (5.20) and (5.21):

$$\Omega = (\bar{x}_1, \bar{\mathbf{k}}_{\perp 1}, \bar{x}_2, \bar{\mathbf{k}}_{\perp 2}) = \Omega'. \tag{5.41}$$

Equation (5.27) thus becomes:

$$q_\pi(x)|^{2-\text{body}} = \sum_\beta \sum_j \delta_{s_j q} \int [\mathrm{d}\bar{x}]_2 [\mathrm{d}^2\bar{\mathbf{k}}_\perp]_2 \delta(x - \bar{x}_j) |\Psi_{2,\beta}(\Omega)|^2. \tag{5.42}$$

As the x and $\mathbf{k}_\perp$ dependencies can be decoupled thanks to a change of variables when integrating over $\mathbf{k}_\perp$, the x-dependence of the PDF is not affected by the convolution of the two wave functions. Therefore, without any additional computations, it is possible to conclude that:

$$q_\pi(x) = \kappa'_\nu x^{2\nu}(1-x)^{2\nu}. \tag{5.43}$$

In the case of $\nu = 1$, the normalisation constant required to ensure the normalisation of the form factor if $\kappa'_1 = 30$. Then it is possible to compare this PDF with the one computed in the covariant approach (4.32). The comparison is shown on figure 5.1 and the agreement between the two approaches is stricking.

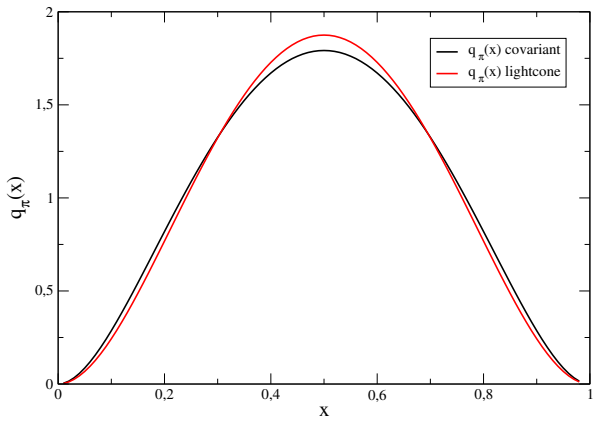

Figure 5.1: Comparison of the PDF computed in the covariant approach and in the lightcone formalism.

Pion GPD

The result obtained in the case of the PDF can be expanded to the entire DGLAP region through equation (5.27). Consistently with chapter 3 and more specifically with equations (3.107) and (3.108), computations are done for vanishing t, *i.e.* $\Delta_\perp = 0$. Using the LCWF computed in equation (5.37), equation (5.27) yields:

$$H^q_\pi(x,\xi,0)|_{\text{DGLAP}} = C^q \int \mathrm{d}^2\mathbf{k}_\perp \Psi^* \left(\frac{x-\xi}{1-\xi}, \mathbf{k}_\perp, P + \frac{\Delta}{2} \right) \Psi \left(\frac{x+\xi}{1+\xi}, \mathbf{k}_\perp, P - \frac{\Delta}{2} \right), \tag{5.44}$$

where C^q is a constant. Using the notation x_1 and x_2 introduced in equation (1.53) and integrating equation (5.44) over $\mathbf{k}_\perp$, one gets:

$$H_\pi^q(x,\xi,0)|_{\text{DGLAP}} = \kappa'_\nu \; x_1^\nu (1-x_1)^\nu x_2^\nu (1-x_2)^\nu \tag{5.45}$$

$$= \kappa'_\nu \frac{(1-x)^{2\nu}\left(x^2-\xi^2\right)^\nu}{\left(1-\xi^2\right)^{2\nu}} \tag{5.46}$$

It is easy to check that in the forward limit, equation (5.45) is fully consistent with our previous PDF result shown in equation (5.43). Then κ'_ν is fixed through the PDF normalisation, for instance, in the case $\nu = 1$, $\kappa'_1 = 30$. the normalised result is shown on figure 5.2.

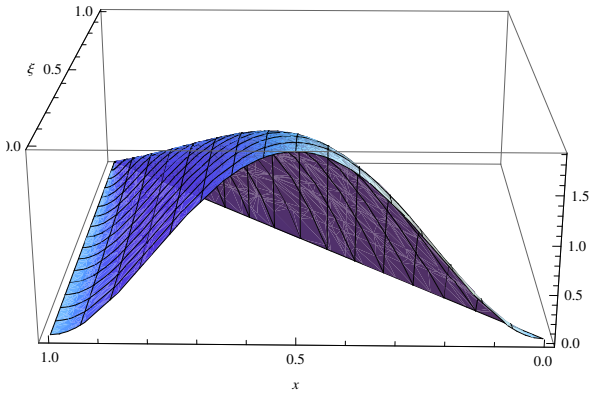

Figure 5.2: Pion GPD H_π^q as a function of x and ξ obtained through overlap of LCWFs in the DGLAP region.

The result obtained in equation (5.45) deserves some comments. First of all, comparing the overlap GPD in the DGLAP region of figure 5.2 with the results of the triangle diagram model shown on figure 3.14, it appears that the two DGLAP regions are very different, though they have been computed within the same algebraic model for the Bethe-Salpeter amplitude. But indeed, in computations using overlap of LCWFs, the GPD vanishes on the line $x = \xi$, whereas in the triangle diagram approximation, it is far from 0, leading to a major consequence. The GPD computed in the overlap framework fulfils the positivity property detailed in section 1.3.3 and defined in equation (1.56). At vanishing t, the formulae obtained for the GPD (5.45) and the PDF (5.43) lead to a relation stronger than the positivity condition, since:

$$H_\pi^q(x,\xi,0)|_{\text{DGLAP}} = \sqrt{q_\pi(x_1) q_\pi(x_2)}. \tag{5.47}$$

This relation between the GPD and the PDF is presumably a feature of the algebraic model defined in equations (3.37)-(3.41).

The fact that the two-body GPD model vanishes on the line $x = \xi$ is actually not a surprise and has been highlighted previously for instance in Ref. [222] and Ref. [223]. Moreover, the authors of Ref. [223] also considered an additional three-body Fock state $q\bar{q}g$. Using the same computing techniques than in the two-body case, the additional gluon generates a non-vanishing GPD on the line $x = \xi$, indicating that in this kinematic area, the GPD is dramatically sensitive to the truncation in the Fock states. This is of deep phenomenological

interest, as the imaginary part of the CFF $\mathcal{H}$ is directly proportional to $H(\xi,\xi,t)$ at leading order.

The computation of the ERBL region cannot be directly done in a two-body approach on the lightcone. Indeed, the first contribution to the ERBL region comes from the overlap of the two-body and four-body LCWFs.

5.2 Radon Inverse transformation

5.2.1 Problem statement

If the two-body approximation does not allow to compute an ERBL contribution, there is an alternative way to get one. Indeed, in Ref. [83] and Ref. [84] the authors argue that if the LCWF model fulfils the Lorentz symmetry, then it is possible to write the GPD in the DGLAP region in terms of DDs. Once the DDs have been exhibited, it becomes easy to get back the ERBL part of the GPD through equation (2.5). And indeed in their case, using a LCWF such that:

$$\Psi(x,\mathbf{k}_\perp) \propto \frac{M^{2p}}{\sqrt{1-x}} x^{-p} \left(M^2 - \frac{\mathbf{k}_\perp^2 + m^2}{x} - \frac{\mathbf{k}_\perp + \lambda^2}{1-x} \right)^{-p-1}, \tag{5.48}$$

where M, λ and m are respectively the hadron, the spectator and the quark masses, they manage to identify a DD through a simple change of variables and thus to extend their model in the ERBL region. The associated DD $e(\beta,\alpha,t)$ for the GPD $E(x,\xi,t)$ is then given by:

$$e(\beta,\alpha,t) = N \frac{\left(\frac{m}{M}+\beta\right)\left((1-\beta)^2-\alpha^2\right)^p}{\left[(1-\beta)\frac{m^2}{M^2} + \beta\frac{\lambda^2}{M^2} - \beta(1-\beta) - \left((1-\beta)^2-\alpha^2\right)\frac{t}{4M^2}\right]^{2p+1}}, \tag{5.49}$$

with N an overall normalisation constant.

As the LCWF model of equation (5.37) is computed from the pion Bethe-Salpeter amplitude, it satisfies Lorentz symmetry. Therefore, it should exist a DD such that, in the DGLAP region, one get back the GPD of equation (5.45). However, in the present case, we have found no obvious change of variable in the overlap representation leading to DDs. Therefore we turn to a more general way to proceed: the inverse Radon transform.

5.2.2 Derivation of the inverse transform

DDs have been introduced in chapter 2 as Radon amplitudes of GPDs. Then applying the inverse Radon transform on GPDs should in principle allow one to recover the DDs. As the Radon transform is not a common tool in hadron physics, details are given below.

Before dealing with the Radon transform of the DDs, one can focus on the bidimensional Fourier transform $\hat{f}$ of a DD f:

$$\hat{f}(b,a) = \int_{-\infty}^{+\infty} \mathrm{d}\beta \mathrm{d}\alpha \, f(\beta,\alpha) e^{i(b\beta+a\alpha)}, \tag{5.50}$$

for two real numbers a and b. Inserting the identity operator expressed as an integral over a Dirac function:

$$\hat{f}(b,a) = \int_{-\infty}^{+\infty} \mathrm{d}\beta \mathrm{d}\alpha \, f(\beta,\alpha) e^{i(b\beta+a\alpha)} \int_{-\infty}^{+\infty} \mathrm{d}s \, \delta\big(s - (b\beta+a\alpha)\big), \tag{5.51}$$

and switching to polar coordinates in Fourier space: $b = r\cos\phi$ and $a = r\sin\phi$ with $r > 0$ and $\phi \in [-\pi, \pi]$, it is possible to derive the following expression of the bidimensional Fourier transform:

$$\begin{aligned}\hat{f}(r\cos\phi, r\sin\phi) &= \int_{-\infty}^{+\infty} \mathrm{d}\beta\mathrm{d}\alpha\, f(\beta,\alpha) e^{ir(\beta\cos\phi+\alpha\sin\phi)} \int_{-\infty}^{+\infty} \mathrm{d}s\, \delta\big(s - r(\beta\cos\phi+\alpha\sin\phi)\big) \\ &= \int_{-\infty}^{+\infty} \mathrm{d}\beta\mathrm{d}\alpha\, f(\beta,\alpha) e^{ir(\beta\cos\phi+\alpha\sin\phi)} \int_{-\infty}^{+\infty} \frac{\mathrm{d}s}{r}\, \delta\left(\frac{s}{r} - (\beta\cos\phi+\alpha\sin\phi)\right).\end{aligned} \tag{5.52}$$

Changing the variable s to s/r, one gets:

$$\begin{aligned}\hat{f}(r\cos\phi, r\sin\phi) &= \int_{-\infty}^{+\infty} \mathrm{d}\beta\mathrm{d}\alpha\, f(\beta,\alpha) e^{ir(\beta\cos\phi+\alpha\sin\phi)} \int_{-\infty}^{+\infty} \mathrm{d}s\, \delta\big(s - (\beta\cos\phi+\alpha\sin\phi)\big) \\ &= \int_{-\infty}^{+\infty} \mathrm{d}s \int_{-\infty}^{+\infty} \mathrm{d}\beta\mathrm{d}\alpha\, \delta\big(s - (\beta\cos\phi+\alpha\sin\phi)\big) f(\beta,\alpha) e^{irs} \\ &= \int_{-\infty}^{+\infty} \mathrm{d}s\, e^{irs} \mathcal{R}f(s,\phi),\end{aligned} \tag{5.53}$$

where $\mathcal{R}f$ denotes the Radon transform of f. This last result is known as the Fourier Slice theorem, which is a specific case of a more general theorem known as the General projection slice Theorem (see *e.g.* Ref. [224]). Therefore the DD can be computed as:

$$f(\beta,\alpha) = \frac{1}{(2\pi)^2} \int_{-\infty}^{+\infty} \mathrm{d}b\mathrm{d}a\, \hat{f}(b,a) e^{-i(b\beta+a\alpha)}, \tag{5.54}$$

which in terms of polar coordinates and Radon transform yields:

$$f(\beta,\alpha) = \frac{1}{(2\pi)^2} \int_{0}^{+\infty} \mathrm{d}r r \int_{-\pi}^{\pi} \mathrm{d}\phi\, e^{-ir(\beta\cos\phi+\alpha\sin\phi)} \int_{-\infty}^{+\infty} \mathrm{d}s e^{irs} \mathcal{R}f(s,\phi). \tag{5.55}$$

Equation (5.55) requires to integrate over $\phi \in [-\pi, \pi]$. Yet as stated in chapter 2, $\xi = \tan(\phi)$ and as GPDs are defined for $-1 \leq \xi \leq 1$, the information available is restricted to $\phi \in [-\frac{\pi}{4}, \frac{\pi}{4}] \cup [\frac{3\pi}{4}, \frac{5\pi}{4}]$. Outside this area in ξ one has to deal with GDA. Therefore, in the present case, it is not possible to use the full Radon Transform but rather the so-called limited angle Radon transform. It consists in projecting the Fourier transform of equation (5.54) on a cone delimited by the angle ϕ_1 and ϕ_2:

$$f_{\phi_1\phi 2}(\beta,\alpha) = \frac{1}{(2\pi)^2} \int_{-\infty}^{+\infty} \mathrm{d}b\mathrm{d}a\, \mathcal{I}_{[\phi_1,\phi_2]\cup[\phi_1+\pi,\phi_2+\pi]} \hat{f}(b,a) e^{-i(b\beta+a\alpha)}. \tag{5.56}$$

Writing equation (5.56) in terms of the Radon transform, one gets:

$$f_{\phi_1\phi_2}(\beta,\alpha) = \frac{1}{(2\pi)^2} \int_{0}^{\infty} \mathrm{d}r\, r \int_{0}^{2\pi} \mathrm{d}\phi\, \mathcal{I}_{[\phi_1,\phi_2]\cup[\phi_1+\pi,\phi_2+\pi]} e^{-ir(\beta\cos(\phi)+\alpha\sin(\phi))} \int_{-\infty}^{\infty} \mathrm{d}s e^{irs} \mathcal{R}f(s,\phi) \tag{5.57}$$

Using the following property of the Radon transform:

$$\mathcal{R}f(-s,\phi) = \mathcal{R}f(s,\phi \pm \pi), \tag{5.58}$$

equation (5.57) can be written for $\phi \in [-\frac{\pi}{2}, \frac{\pi}{2}]$ and $r \in \mathbb{R}$:

$$\begin{aligned} f_{\phi_1\phi_2}(\beta,\alpha) &= \frac{1}{(2\pi)^2}\int_0^\infty \mathrm{d}r\ r\int_{\phi_1}^{\phi_2}\mathrm{d}\phi\ e^{-ir(\beta\cos(\phi)+\alpha\sin(\phi))}\int_{-\infty}^{\infty}\mathrm{d}s e^{irs}\mathcal{R}f(s,\phi) \\ &\quad + \frac{1}{(2\pi)^2}\int_0^\infty \mathrm{d}r\ r\int_{\phi_1+\pi}^{\phi_2+\pi}\mathrm{d}\phi\ e^{-ir(\beta\cos(\phi)+\alpha\sin(\phi))}\int_{-\infty}^{\infty}\mathrm{d}s e^{irs}\mathcal{R}f(s,\phi) \qquad (5.59) \\ &= \frac{1}{(2\pi)^2}\int_0^\infty \mathrm{d}r\ r\int_{\phi_1}^{\phi_2}\mathrm{d}\phi\ e^{-ir(\beta\cos(\phi)+\alpha\sin(\phi))}\int_{-\infty}^{\infty}\mathrm{d}s e^{irs}\mathcal{R}f(s,\phi) \\ &\quad + \frac{1}{(2\pi)^2}\int_{-\infty}^0 \mathrm{d}r\ (-r)\int_{\phi_1}^{\phi_2}\mathrm{d}\phi\ e^{-ir(\beta\cos(\phi)+\alpha\sin(\phi))}\int_{-\infty}^{\infty}\mathrm{d}s e^{irs}\mathcal{R}f(-s,\phi+\pi) \\ &= \frac{1}{(2\pi)^2}\int_{-\infty}^\infty \mathrm{d}r\ \int_{\phi_1}^{\phi_2}\mathrm{d}\phi\ e^{-ir(\beta\cos(\phi)+\alpha\sin(\phi))}\int_{-\infty}^{\infty}\mathrm{d}s\ \mathrm{sgn}(r) r e^{irs}\mathcal{R}f(s,\phi), \end{aligned} \qquad (5.60)$$

through several changes of variables. The sign function $\mathrm{sgn}(r)$ defined as:

$$\left\{\begin{array}{lcl} \mathrm{sgn}(r) &=& 1 \text{ for } r>0 \\ \mathrm{sgn}(r) &=& 0 \text{ for } r=0 \\ \mathrm{sgn}(r) &=& -1 \text{ for } r<0 \end{array}\right. , \qquad (5.61)$$

is also introduced. It admits the following integral representation:

$$\mathrm{sgn}(x) = -2i\ \int_{-\infty}^{\infty}\frac{\mathrm{d}\tau}{2\pi}\ \mathrm{PV}\left[\frac{1}{\tau}\right] e^{ix\tau}, \qquad (5.62)$$

where PV stands for the principal value distribution:

$$\int_{-\infty}^{\infty}\mathrm{d}x\ \mathrm{PV}\left[\frac{1}{x}\right] u(x) = \int_0^\infty \mathrm{d}x \frac{u(x)-u(-x)}{x}. \qquad (5.63)$$

Therefore, one can rewrite $f_{\phi_1\phi_2}(\beta,\alpha)$ as:

$$\begin{aligned} f_{\phi_1\phi_2}(\beta,\alpha) &= \frac{-2i}{(2\pi)^3}\int_{-\infty}^\infty \mathrm{d}r\ \int_{\phi_1}^{\phi_2}\mathrm{d}\phi\ \int_{-\infty}^{\infty}\mathrm{d}s \\ &\quad \int_{-\infty}^{\infty}\mathrm{d}\tau\ \mathrm{PV}\left[\frac{1}{\tau}\right]\left(e^{i\tau r}\right) r e^{irs} e^{-ir(\beta\cos(\phi)+\alpha\sin(\phi))}\mathcal{R}f(s,\phi) \\ &= \frac{-2i}{(2\pi)^3}\int_{-\infty}^\infty \mathrm{d}r\ \int_{\phi_1}^{\phi_2}\mathrm{d}\phi\ \int_{-\infty}^{\infty}\mathrm{d}s\ \int_{-\infty}^{\infty}\mathrm{d}\tau \\ &\quad \frac{1}{\tau} r\left(e^{ir(s-\beta\cos(\phi)-\alpha\sin(\phi)+\tau)} - e^{ir(s-\beta\cos(\phi)-\alpha\sin(\phi)-\tau)}\right)\mathcal{R}f(s,\phi). \end{aligned} \qquad (5.64)$$

Choosing $s' = s - \beta\cos(\phi) - \alpha\sin(\phi) \pm \tau$, one gets:

$$\begin{aligned} f_{\phi_1\phi_2}(\beta,\alpha) &= \frac{-2i}{(2\pi)^3}\int_{-\infty}^\infty \mathrm{d}r\ \int_{\phi_1}^{\phi_2}\mathrm{d}\phi\ \int_{-\infty}^{\infty}\mathrm{d}s \\ &\quad \int_{-\infty}^{\infty}\mathrm{d}\tau\ (-i)\left(\frac{\partial}{\partial s'}e^{irs'}\right)\mathrm{PV}\left[\frac{1}{\tau}\right]\left(\mathcal{R}f(s'+\beta\cos(\phi)+\alpha\sin(\phi)-\tau,\phi)\right). \end{aligned} \qquad (5.65)$$

Integrating by parts yields:

$$f_{\phi_1\phi_2}(\beta,\alpha) = \frac{2}{(2\pi)^3}\int_{-\infty}^{\infty}\mathrm{d}r\int_{\phi_1}^{\phi_2}\mathrm{d}\phi\int_{-\infty}^{\infty}\mathrm{d}s \int_{-\infty}^{\infty}\mathrm{d}\tau\, e^{irs'}\mathrm{PV}\left[\frac{1}{\tau}\right]\left(\frac{\partial}{\partial s'}\mathcal{R}f(s+\beta\cos(\phi)+\alpha\sin(\phi)-\tau,\phi)\right). \quad (5.66)$$

Finally, integrating over r generates a factor $\delta(s')$ which kills the integral over s', and one gets:

$$f_{\phi_1\phi_2}(\beta,\alpha) = \frac{2}{(2\pi)^2}\int_{\phi_1}^{\phi_2}\mathrm{d}\phi\int_{-\infty}^{\infty}\mathrm{d}\tau\ \mathrm{PV}\left[\frac{1}{\tau}\right]\left(\frac{\partial}{\partial s'}\mathcal{R}f(s'+\beta\cos(\phi)+\alpha\sin(\phi)-\tau,\phi)\right)\Big|_{s'=0}. \quad (5.67)$$

5.2.3 A simple example

Radon transform

The final expression (5.67) remains difficult to use in practice despite the algebraic formula. Therefore an example is given here in the case of the full inverse transform (*i.e.* $\phi_1 = -\frac{\pi}{2}$ and $\phi_2 = \frac{\pi}{2}$) for a constant DD on the rhombus Ω (see figure 2.2):

$$f(\beta,\alpha) = I_\Omega, \quad (5.68)$$

where:

$$\begin{cases} I_\Omega = 1 & \text{for } |\alpha|+|\beta| \leq 1 \\ I_\Omega = 0 & \text{for } |\alpha|+|\beta| \geq 1 \end{cases}. \quad (5.69)$$

Computing the Radon transform of such a DD leads to:

$$\mathcal{F} = \int_\Omega \mathrm{d}\beta\mathrm{d}\alpha\delta(s-\beta\cos\phi-\alpha\sin\phi) \quad (5.70)$$

in terms of canonical Radon transform. When dealing with GPD natural variables, equation (5.70) yields:

$$H(x,\xi) = \sqrt{1+\xi^2}\int_\Omega \mathrm{d}\beta\mathrm{d}\alpha\delta(x-\beta-\alpha\xi), \quad (5.71)$$

where the variable t is omitted in this section as it does not play any role. Integrating (5.71) over α leads to:

$$H(x,\xi) = \frac{\sqrt{1+\xi^2}}{|\xi|}\int_{-1}^{1}\mathrm{d}\beta\ \theta\left(\frac{x-\beta}{\xi}-(-1+|\beta|)\right)\theta\left(1-|\beta|-\frac{x-\beta}{\xi}\right). \quad (5.72)$$

The next step is then to identify the integration boundaries in β which depend on x and ξ. Focusing on the case $\beta \geq 0$, from which it is possible to deduce the case $\beta \leq 0$, one has the following inequalities:

$$-1+\beta \leq \frac{x-\beta}{\xi} \leq 1-\beta, \quad (5.73)$$

which can be split into different cases:

$$\xi \geq 0 \Rightarrow \begin{cases} \beta(1+\xi) \leq x+\xi \\ \beta(1-\xi) \geq x-\xi \end{cases}, \quad (5.74)$$

$$\xi \leq 0 \Rightarrow \left\{ \begin{array}{lcl} \beta(1+\xi) & \geq & x+\xi \\ \beta(1-\xi) & \leq & x-\xi \end{array} \right. , \tag{5.75}$$

and written in terms of $|\xi|$ as:

$$\left\{ \begin{array}{lcl} \beta(1+|\xi|) & \leq & x+|\xi| \\ \beta(1-|\xi|) & \geq & x-|\xi| \end{array} \right. . \tag{5.76}$$

Equations (5.76) clearly emphasises a change of behaviour between the GPD kinematic area ($|\xi| \leq 1$) and the GDA one ($|\xi| \geq 1$). Then splitting the Radon transform H into a GPD contribution $H^{\beta \geq 0}_{\text{GPD}}$ and a GDA one $H^{\beta \geq 0}_{\text{GDA}}$, one gets:

$$H^{\beta \geq 0}_{\text{GDA}}(x,\xi) = \frac{\sqrt{1+\xi^2}}{|\xi|} \theta\left(|\xi|-1\right) \int_0^{\text{Max}\left[\text{Min}\left(\frac{x+|\xi|}{1+|\xi|}, \frac{x-|\xi|}{1-|\xi|}, 1\right), 0\right]} \mathrm{d}\beta, \tag{5.77}$$

$$H^{\beta \geq 0}_{\text{GPD}}(x,\xi) = \frac{\sqrt{1+\xi^2}}{|\xi|} \theta\left(1-|\xi|\right) \int_{\text{Min}\left[\text{Min}\left(\frac{x+|\xi|}{1+|\xi|}, 1\right), \text{Max}\left(0, \frac{x-|\xi|}{1-|\xi|}\right)\right]}^{\text{Max}\left[\text{Min}\left(\frac{x+|\xi|}{1+|\xi|}, 1\right), \text{Max}\left(0, \frac{x-|\xi|}{1-|\xi|}\right)\right]} \mathrm{d}\beta. \tag{5.78}$$

Studying the behaviour of the functions:

$$\tilde{x}_1 = \frac{x-|\xi|}{1-|\xi|}, \tag{5.79}$$

$$\tilde{x}_2 = \frac{x+|\xi|}{1+|\xi|}, \tag{5.80}$$

it is possible to simplify equations (5.77) and (5.78) as:

$$H^{\beta \geq 0}_{\text{GDA}}(x,\xi) = \frac{\sqrt{1+\xi^2}}{|\xi|} \theta\left(|\xi|-1\right) \theta\left(|\xi|-|x|\right) \left[\theta\left(1-x\right) \tilde{x}_2 + \theta\left(x-1\right) \tilde{x}_1\right], \tag{5.81}$$

$$H^{\beta \geq 0}_{\text{GPD}}(x,\xi) = \frac{\sqrt{1+\xi^2}}{|\xi|} \theta\left(1-|\xi|\right) \theta\left(1-x\right) \left[\theta\left(x-|\xi|\right) \left(\tilde{x}_2 - \tilde{x}_1\right) + \theta\left(|\xi|-|x|\right) \tilde{x}_2\right]. \tag{5.82}$$

Coming back to equation (5.72), and noting that:

$$\begin{aligned} H(x,\xi) &= \frac{\sqrt{1+\xi^2}}{|\xi|} \left[\int_0^1 \mathrm{d}\beta \; \theta\left(\frac{x-\beta}{\xi} - (-1+|\beta|)\right) \theta\left(1-|\beta| - \frac{x-\beta}{\xi}\right) \right. \\ &\quad \left. + \int_{-1}^0 \mathrm{d}\beta \; \theta\left(\frac{x-\beta}{\xi} - (-1+|\beta|)\right) \theta\left(1-|\beta| - \frac{x-\beta}{\xi}\right) \right] \\ &= \frac{\sqrt{1+\xi^2}}{|\xi|} \left[\int_0^1 \mathrm{d}\beta \; \theta\left(\frac{x-\beta}{\xi} - (-1+|\beta|)\right) \theta\left(1-|\beta| - \frac{x-\beta}{\xi}\right) \right. \\ &\quad \left. + \int_0^1 \mathrm{d}\beta \; \theta\left(\frac{-x-\beta}{-\xi} - (-1+|\beta|)\right) \theta\left(1-|\beta| - \frac{-x-\beta}{-\xi}\right) \right], \end{aligned} \tag{5.83}$$

one can consequently deduce the full GPD $H(x,\xi)$ from $H^{\beta \geq 0}(x,\xi)$ by symmetrising it with respect to x. So introducing the variable $\hat{x}_2$ and $\hat{x}_1$ defined as:

$$\hat{x}_1 = -\frac{x+|\xi|}{1-|\xi|}, \tag{5.84}$$

$$\hat{x}_2 = -\frac{x-|\xi|}{1+|\xi|}, \tag{5.85}$$

The GDA and GPD contributions read:

$$\begin{aligned} H_{\mathrm{GDA}}(x,\xi) &= \frac{\sqrt{1+\xi^2}}{|\xi|}\theta\left(|\xi|-1\right)\theta\left(|\xi|-|x|\right)\Big[\theta\left(1-|x|\right)\left(\tilde{x}_2+\hat{x}_2\right) \\ &\quad +\theta\left(x-1\right)\left(\tilde{x}_1+\hat{x}_2\right)+\theta\left(-1-x\right)\left(\tilde{x}_2+\hat{x}_1\right)\Big], \qquad (5.86) \\ H_{\mathrm{GPD}}(x,\xi) &= \frac{\sqrt{1+\xi^2}}{|\xi|}\theta\left(1-|\xi|\right)\Big[\theta\left(1-x\right)\theta\left(x-|\xi|\right)\left(\tilde{x}_2-\tilde{x}_1\right) \\ &\quad +\theta\left(|\xi|-|x|\right)\left(\tilde{x}_2+\hat{x}_2\right)+\theta\left(1+x\right)\theta\left(-|\xi|-x\right)\left(\hat{x}_2-\hat{x}_1\right)\Big]. \qquad (5.87) \end{aligned}$$

The GPD and the GDA corresponding to those formulae are illustrated on figure 5.3.

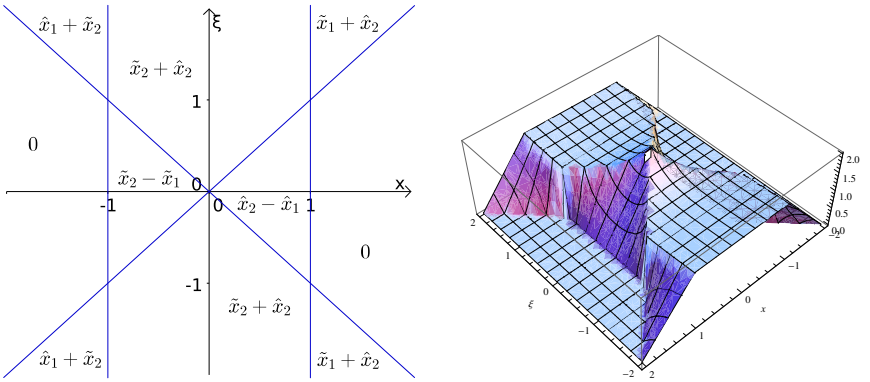

Figure 5.3: GPD and GDA computed with a constant DD through the canonical Radon transform. Left-Hand side: algebraic structure in the (x,ξ) plane, the overall factor $\frac{\sqrt{1+\xi^2}}{|\xi|}$ is not explicitely written on this figure. Right-hand side: 3D plot of the GPD and GDA contribution in the (x,ξ) plane.

Inverse Radon transform

Inverting the GPD and GDA of equations (5.87) and (5.86) through the inversion formula (5.67) must be done carefully due to all the possible contributions. First of all, it is necessary to compute the derivative of H with respect to the canonical variable s of the Radon transform. This generates of course different functions to integrate depending on the values of x and ξ. The derivatives of the Heaviside θ functions appearing in equations (5.86) and (5.87) do not contribute due to the continuity of $H(x,\xi)$. And therefore, one is left with the following contributions:

- In the GDA region $1<x<|\xi|$ the derivative of H leads to:

$$\left.\frac{\partial H}{\partial s}\right|_{1<x<|\xi|} = \frac{1}{|\sin\phi|}\left(\frac{1}{\cos\phi-|\sin\phi|}-\frac{1}{\cos\phi+|\sin\phi|}\right), \qquad (5.88)$$

  which is independent of τ. Thus, the integration on variable τ only affects Heaviside θ

functions, leading to the following contributions C_1:

$$\begin{aligned} C_1 &= \int \mathrm{d}\tau \ \mathrm{PV}\left[\frac{1}{\tau}\right] \theta\left(|\sin\phi| - |\beta\cos\phi + \alpha\sin\phi + \tau|\right) \theta\left(\beta\cos\phi + \alpha\sin\phi + \tau - \cos\phi\right) \\ &= \int_{R-|\sin\phi|}^{R-\cos\phi} \frac{\mathrm{d}\tau}{\tau} \theta\left(R - \cos\phi\right) \theta\left(R - |\sin\phi|\right) + \int_{|\sin\phi|-R}^{R-\cos\phi} \frac{\mathrm{d}\tau}{\tau} \theta\left(R - \cos\phi\right) \theta\left(-R + |\sin\phi|\right) \\ &\quad - \int_{\cos\phi-R}^{|\sin\phi|-R} \frac{\mathrm{d}\tau}{\tau} \theta\left(-R + \cos\phi\right) \theta\left(-R + |\sin\phi|\right) \\ &= \int_{|R-|\sin\phi||}^{|R-\cos\phi|} \frac{\mathrm{d}\tau}{\tau}, \end{aligned} \tag{5.89}$$

where $R = \beta\cos\phi + \alpha\sin\phi$.

- In the GDA region $-1 > x > -|\xi|$, computations are very similar as:

$$\left.\frac{\partial H}{\partial s}\right|_{-1>x>-|\xi|} = \frac{1}{|\sin\phi|}\left(\frac{1}{\cos\phi + |\sin\phi|} - \frac{1}{\cos\phi - |\sin\phi|}\right). \tag{5.90}$$

  The integral over τ can be then simplified as:

$$C_2 = \int_{|\cos\phi+R|}^{||\sin\phi|+R|} \frac{\mathrm{d}\tau}{\tau}. \tag{5.91}$$

- The central GDA ($|x| \leq 1$) and GPD ($|x| \leq |\xi|$) regions present a functional form which is independent of x and thus of s. Consequently, the derivative in this kinematic region is 0 and it does not bring any contribution to the inverse transform.

- The contribution of the GPD region $x \geq |\xi|$ can be computed through:

$$\left.\frac{\partial H}{\partial s}\right|_{1>x>|\xi|} = \frac{1}{|\sin\phi|}\left(\frac{1}{\cos\phi + |\sin\phi|} - \frac{1}{\cos\phi - |\sin\phi|}\right). \tag{5.92}$$

  The contribution to the integration over τ leads to:

$$C_3 = \int_{|\cos\phi-R|}^{||\sin\phi|-R|} \frac{\mathrm{d}\tau}{\tau}. \tag{5.93}$$

- Finally, the last contribution is the one of the GPD for $x \leq -|\xi|$. The derivation yields:

$$\left.\frac{\partial H}{\partial s}\right|_{-1<x<-|\xi|} = \frac{1}{|\sin\phi|}\left(\frac{1}{\cos\phi - |\sin\phi|} - \frac{1}{\cos\phi + |\sin\phi|}\right), \tag{5.94}$$

  and

$$C_4 = \int_{||\sin\phi|+R|}^{|\cos\phi+R|} \frac{\mathrm{d}\tau}{\tau}. \tag{5.95}$$

This leads to the following expression for the DD $f(\beta,\alpha)$:

$$\begin{aligned} f(\beta,\alpha) &= \frac{2}{(2\pi)^2}\int_{-\frac{\pi}{2}}^{\frac{\pi}{2}}\frac{\mathrm{d}\phi}{|\sin\phi|}\left(\frac{1}{\cos\phi-|\sin\phi|}-\frac{1}{\cos\phi+|\sin\phi|}\right) \\ &\quad \Big[\theta(|\sin\phi|-\cos\phi)\,(C_1-C_2)+\theta(\cos\phi-|\sin\phi|)\,(C_4-C_3)\Big]. \end{aligned} \tag{5.96}$$

Noticing that $C_1=-C_3$ and $C_2=-C_4$, it is possible to simplify equation (5.96):

$$\begin{aligned} f(\beta,\alpha) &= \frac{2}{(2\pi)^2}\int_{-\frac{\pi}{2}}^{\frac{\pi}{2}}\frac{\mathrm{d}\phi}{|\sin\phi|}\left(\frac{1}{\cos\phi-|\sin\phi|}-\frac{1}{\cos\phi+|\sin\phi|}\right) \\ &\quad \left[\ln\left(\frac{|\cos\phi+R|}{||\sin\phi|+R|}\right)+\ln\left(\frac{|\cos\phi-R|}{||\sin\phi|-R|}\right)\right] \\ &= \frac{2}{(2\pi)^2}\int_{-\frac{\pi}{2}}^{\frac{\pi}{2}}\frac{\mathrm{d}\phi}{|\sin\phi|}\left(\frac{1}{\cos\phi-|\sin\phi|}-\frac{1}{\cos\phi+|\sin\phi|}\right)\ln\left(\frac{|\cos^2\phi-R^2|}{|\sin^2\phi-R^2|}\right). \end{aligned} \tag{5.97}$$

Equation (5.97) presents apparent singularities at $\phi=\pm\frac{\pi}{4}$ due to a term $\cos\phi-|\sin\phi|$ in the denominator. This singularity is compensated by the logarithm as:

$$\ln\left(\frac{|\cos^2\phi-R^2|}{|\sin^2\phi-R^2|}\right)\leq\ln\left(\frac{|\cos^2\phi-\sin^2\phi|}{|\sin^2\phi-R^2|}+1\right) \tag{5.98}$$

Expanding the right-hand side of equation (5.98) compensates the apparent singularity at $\phi=\pm\frac{\pi}{4}$. Getting an analytic expression for $f(\beta,\alpha)$ from equation (5.97) remains a difficult task. Yet numerical integration can be performed and results are shown on figure 5.4. The inversion formula provides the constant DD on the Rhombus, up to numerical noise. The problem of numerical noise in computation of DDs from GPDs and GDAs has already been stressed in Ref. [135].

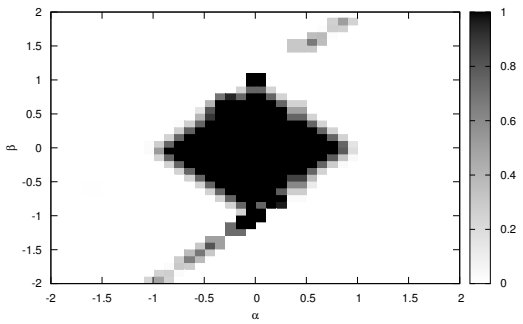

Figure 5.4: Numerical computations of the inverse Radon transform. The shape of the rhombus appears distinctly even if numerical precision generates noise on the edges and outside.

5.2.4 Perspective on the lightcone

The use of the inverse Radon transform may allow to get back the ERBL contribution of the GPD and even a GDA model. It would then be possible to fulfil both polynomiality (ensured by the inverse Radon transform) and positivity (a consequence of the overlap representation) properties. Yet, in practice, the inverse Radon transform is difficult to solve algebraically, even when dealing with the Radon transform on the entire (x, ξ) plane as shown by equation (5.97). So knowing only the DGLAP region of the GPD, the inversion becomes a real challenge. However, the constraints coming from the Lorentz symmetry may restrict sufficiently the DD to allow numerical computations. Systematic effects due to the truncation in the (x, ξ) plane need to be studied. Moreover, the D-term itself is a *pure* ERBL contribution, and consequently may not *a priori* be determined by a reconstruction through the DGLAP region only. Still, using the 1CDD scheme of the DD, it is possible to get an unambiguous ERBL region, providing that $H(x, \xi, t)/x$ is not too singular.

Consequently, the lightcone approach provides an alternative way to compute GPDs which needs to be further explored to get fully consistent GPD models. Nevertheless, as emphasised previously, many progresses are required to fully exploit the lightcone formalism, which makes the topic both challenging and exciting.

Conclusion

The study of hadron remains today one of the most exciting physics fields. The present work explores only a small part of it, focused on Generalised Parton Distributions. Still, GPDs concentrate difficulties as their theoretical framework provides key constraints, and only a small part of the kinematic domain has been experimentally explored. Yet, several phenomenological parameterisations and models have been developed since the 1990s, each one presenting both advantages and drawbacks. Such approaches played a decisive role in validating the overall GPD framework. They have also stressed the need for next-to-leading order computations of the hard scattering kernels, and recently the strong impact of target-mass corrections at Jefferson Laboratory kinematics. Nevertheless, they cannot describe hadron structure as a full dynamical effect of QCD.

An improvement of one of these phenomenological parameterisations has been achieved here, using the so-called Double Distributions framework. The idea was to exploit the Double Distributions intrinsic ambiguity coming from their relation with GPDs and to consider it as an additional degree of freedom. This way, it was possible to improve the flexibility of the parameterisation for spinless targets, and to add an intrisic D-term. Results were not as good on spin-1/2 targets, as most of the modification is included in the GPD $E(x, \xi, t)$ rather than $H(x, \xi, t)$, the available data being hardly sensitive to the former. Therefore, transversaly polarised target data are required before drawing any definitive conclusion on this parameterisation.

Any dynamical description of the structure of hadrons is beyond the reach of phenomenological approaches, but can be achieved through *ab-initio* computations. The Dyson-Schwinger formalism, among others, provides a framework to dynamically convert fundamental degrees of freedom into effective ones. Therefore they are used in this work to model the pion valence GPD in terms of an effective quark and anti-quark pair. The computations have been performed algebraically and the results are in good agreement with available data. Still, a few theoretical constraints are not fulfilled in this approach such as the soft-pion theorem. Nevertheless, this remains a feature of the algebraic starting point rather than an issue of the approach itself, and disappears as soon as one uses a Dyson-Schwinger truncation scheme which satisfies the relevant symmetry properties, more specifically the Axial-Vector Ward-Takahashi Identities. Moreover, it appears that the so-called impulse approximation, used to perform computations, actually breaks the $x \leftrightarrow 1 - x$ symmetry which appears in a two-body problem, providing that the considered objects have the same dynamics. This issue has been solved in the forward case. If generalisation to off-forward kinematics has not been reached rigorously, the forward case nonetheless provides useful insights which have led to an Ansatz for the pion GPD at $\xi = 0$, and therefore to a 3D description of the pion in terms of effective degrees of freedom.

Despite the improvement brought to the pion GPD model based on Dyson-Schwinger

equations, it has not been possible to fulfil the positivity condition within a covariant model (triangle diagram and beyond). This suggests the necessity of a radical change, and thus the present work started to explore the possibilities of modeling GPDs as overlaps of Lightcone Wave Functions. This approach allows to stick on the Dyson-Schwinger formalism through the computation of Lightcone Wave Functions themselves, but also ensures positivity. However, in a two-body truncation of the Fock space, only the DGLAP region can be directly computed. The relevant ERBL region must then be recovered through the Lorentz symmetry, and more specifically in order to satisfy the polynomiality property. This may be achieved through the inverse Radon transform. Yet this part remains at an exploratory stage.

Performing the inverse Radon transform on the lightcone to get an ERBL region for the pion is certainly the next step of the work detailed here. Still, on a longer time scale, other points deserve study. Among them, taking into account additional Fock states is of high phenomenological relevance, as they modify the diagonal $x = \xi$. The GPD H evaluated at $x = \xi$ is directly proportional, at leading order, to the DVCS beam-helicity-dependent cross-section. Another interesting point is the treatment of the Wilson line, which is thought to have a small impact on GPDs computed in the Landau gauge, but which would probably have a significant impact when dealing with Transverse Momentum Distributions or Generalised Transverse Momentum Distributions. If one was able to develop a pioneering approach of the Wilson lines within the Dyson-Schwinger formalism, it may allow to define a general framework to compute all non-perturbative objects mentioned above.

Turning from the pion case to the proton case is of course of great phenomenological relevance, as most of the available experimental data have been taken on the proton. The easiest way to move from pion to proton would be to consider the latter as a two-body system composed of a quark and a diquark. Doing so would greatly simplify the computations from a full three-quark system, even if it remains unclear how this truncation in the Fock space would impact the comparison with experimental data. Yet, as Jefferson Laboratory halls are about to start running exclusive experiments at 12 GeV with a high statistical precision, the need for a dynamical description of the proton structure has never been so strong.

Appendix A

Conventions and Notations

Four-vectors and metric

Four-vector are denoted with normal character *e.g.* $p = (p^0, p^1, p^2, p^3)$, whereas three- and two-vector are written in bold font: $\mathbf{p} = (p^1, p^2, p^3)$. The metric used in this thesis in Minkowskian space is:

$$\eta_{\mu\nu} = \eta^{\mu\nu} = \begin{pmatrix} 1 & 0 & 0 & 0 \\ 0 & -1 & 0 & 0 \\ 0 & 0 & -1 & 0 \\ 0 & 0 & 0 & -1 \end{pmatrix}, \tag{A.1}$$

such that:

$$p^2 = (p^0)^2 - \mathbf{p}^2 = M^2. \tag{A.2}$$

Lightcone variables

The lightcone variables for a four-vector v are defined as:

$$v^+ = \frac{1}{\sqrt{2}}(v^0 + v^3) \quad , \quad v^- = \frac{1}{\sqrt{2}}(v^0 - v^3) \quad \text{and} \quad \mathbf{v}_\perp = (v^1, v^2). \tag{A.3}$$

Dirac space

The Dirac matrices obey the four-dimensional Clifford Algebra:

$$\{\gamma^\mu, \gamma^\nu\} = 2\eta^{\mu\nu}. \tag{A.4}$$

In all this work, the Weyl representation of the γ^μ is used:

$$\gamma^\mu = \begin{pmatrix} 0 & \bar{\sigma}^\mu \\ \sigma^\mu & 0 \end{pmatrix}, \tag{A.5}$$

with:

$$\sigma^\mu = (1, \boldsymbol{\sigma}) \quad , \quad \bar{\sigma}^\mu = (1, -\boldsymbol{\sigma}), \tag{A.6}$$

and the σ^i are the Pauli matrices. The $\sigma^{\mu\nu}$ tensor is defined as:

$$\sigma^{\mu\nu} = \frac{i}{2}\left[\gamma^\mu, \gamma^\nu\right]. \tag{A.7}$$

Particle state

The state of a particle H of momentum p is denoted $|p\rangle = |H, p, \{\alpha\}\rangle$, where $\{\alpha\}$ corresponds to the additional relevant quantum numbers. It is normalised as

$$\langle p' | p \rangle = 2E_p(2\pi)^3\delta^{(3)}(\mathbf{p'} - \mathbf{p})\delta_{\{\alpha'\}\{\alpha\}}. \tag{A.8}$$

Fourier transform

The Fourier transform convention used in this work is the following one:

$$\hat{f}(p) = \int \mathrm{d}^4x f(x) e^{ip\cdot x}, \tag{A.9}$$

and

$$f(x) = \int \frac{\mathrm{d}^4p}{(2\pi)^4} \hat{f}(p) e^{-ip\cdot x}, \tag{A.10}$$

for the inverse Fourier transform.

Acronyms

1CDD:	One-Component Double Distribution
2CDD:	Two-Component Double Distribution
AVWTI:	Axial-Vector Ward-Takahashi Identity
BSE:	Bethe-Salpeter Equation
CFF:	Compton Form Factors
DA:	Distribution Amplitude
DCSB:	Dynamical Chiral Symmetry Breaking
DD:	Double Distribution
DIS:	Deep Inelastic Scattering
DSE:	Dyson-Schwinger Equation
DVCS:	Deep-Virtual Compton Scattering
DVMP:	Deep-Virtual Meson Production
EIC:	Electron-Ion Collider
FF:	Form Factor
GDA:	Generalised Distribution Amplitude
GPD:	Generalised Parton Distribution
LO:	Leading Order
NLO:	Next-to-Leading Order
OPE:	Operator Product Expansion
PDF:	Parton Distribution Function
QCD:	Quantum Chromodynamics
RL:	Rainbow Ladder
TCS:	Time-like Compton Scattering
WTI:	Ward-Takahashi Identity

Appendix B

Euclidean time vs. Minkowskian time

Wick Rotation

Euclidean time in quantum field theory is generally encountered in pertubative computations, especially when dealing with the so-called dimensional regularisation. Euclidean momentum variables (k^1, k^2, k^3, k^4) are introduced through the following change of variables:

$$k^4 = ik^0 \quad , \quad \mathbf{k}^E = \mathbf{k}^M, \tag{B.1}$$

where the subscripts E and M respectively denote Euclidean and Minkowskian spaces. This correspond in fact to the deformation of a contour integral in the complex plane k^0 which is known as the Wick rotation [200]. Yet, his procedure requires that no poles appears in the first and third quadrants of the complex plane. This is the case in perturbation theory when discarding the possibility that singularities could be dynamically generated within those quadrants.

Computing non pertubative objects in the Dyson-Schwinger equations framework, a tempting procedure would be to start with Dyson-Schwinger equations obtained from the Minkowskian theory, then applying the Wick rotation to get back an Euclidean metric. But when dealing with non-pertubative approaches, the assumption concerning dynamically generated singularities may not hold anymore as shown in Ref. [225]. Studying QED, its authors pointed out that the electron propagator has two complex conjugate branch points within their truncation scheme. It is therefore not possible to apply the Wick rotation straightforwardly in this case. The question of dynamical generation of singularities in the complex plane has since been deeply studied for the quark propagator in QCD, like for instance in Ref. [226–229]. In all these works, the direct transcription of equation (B.1) has been found invalid, due to dynamical generation of singularities. Even if it remains unclear if those singularities are genuine ones or due to the truncation scheme, all the previously cited work suggest to use a different approach.

Euclidean theory

As argued for instance in Ref. [166], instead of the Wick rotation, it is usually possible to define a Euclidean quantum field theory which is the counterpart of the Minkowskian one

providing that:

$$\int \mathrm{d}^4x^M = -i\int \mathrm{d}^4x^E, \tag{B.2}$$

$$\gamma^M\cdot\partial^M = i\gamma^E\cdot\partial^E \tag{B.3}$$

$$p^M\cdot\gamma^M = -ip^E\cdot\gamma^E \tag{B.4}$$

$$p^M\cdot q^M = -p^E\cdot q^E, \tag{B.5}$$

with $\eta^E_{\mu\nu}=\delta_{\mu\nu}$ and $x^4=ix^0$. The Euclidean Clifford algebra is given by:

$$\left\{\gamma^E_\mu,\gamma^E_\nu\right\}=2\delta_{\mu\nu}, \tag{B.6}$$

leading to:

$$\gamma^E_4=\gamma^0_M,\quad \gamma^E_j=-i\gamma^j_M \quad \text{for } j=1,2,3,\quad \gamma^E_5=-\gamma^E_1\gamma^E_2\gamma^E_3\gamma^E_4=\gamma^5_M. \tag{B.7}$$

Within this formalism, one can introduce the Euclidean partition function Z^E, and thus define an Euclidean field theory based on a Lagrangian approach. Euclidean QED is for instance given by:

$$Z^E_{\mathrm{QED}}\left[\bar\eta^E,\eta^E,J^E_\mu\right]=\int \mathrm{d}\mu^E(\psi^E,\bar\psi^E,A^E_\mu)e^{-S\left(\psi^E,\bar\psi^E,A^E_\mu\right)}\exp\left(\int \mathrm{d}^4x^E\ \bar\eta^E\psi^E+\bar\psi^E\eta^E+A^E_\mu J^{\mu\,E}\right), \tag{B.8}$$

with S being the Euclidean QED action:

$$S\left(\psi^E,\bar\psi^E,A^E_\mu\right)=\int \mathrm{d}^4x^E\ \bar\psi^E\left(\gamma^E\cdot\partial^E+m+ie\gamma^E\cdot A^E\right)\psi^E+\frac{1}{4}F^E_{\mu\nu}F^{\mu\nu\,E}. \tag{B.9}$$

At this point, the Schwinger functions $\int_n$, defined as moments of the Euclidean measure, can be computed as:

$$\mathcal{S}_{i,j,k}(x_1,\cdots,x_i,y_1,\cdots,y_j,z_1,\cdots,z_k)=\frac{\partial^{i+j+k}Z^E_{\mathrm{QED}}}{(\partial\bar\eta^E)^i(\partial\eta^E)^j(\partial J^{\mu\,E})^k}\left[0,0,0\right]. \tag{B.10}$$

Providing that the Euclidean measure follows the so-called Osterwalder-Schrader axioms [230, 231] (see also [169]), it is possible to relate them with their Minkowskian counterparts called Wightman functions $\mathcal{W}_n(x_1,\cdots,x_n)$ through analytic continuation:

$$\mathcal{W}_n(x_1,\cdots,x_n)=\lim_{x_i^4\to 0}\mathcal{S}_n\left((\mathbf{x}_1,x_1^4+ix_1^0),\cdots(\mathbf{x}_n,x_n^4+ix_n^0)\right). \tag{B.11}$$

These Wightman functions correspond to those of a Minkowskian field theory deduced from analytic continuation of the time parameter, *i.e.* :

$$\phi_E(\mathbf{x},t)=\phi_M(it,\mathbf{x}), \tag{B.12}$$

where ϕ stand for any field of the considered theory. The Osterwalder-Schrader axioms of the Euclidean measure ensure that the Minkowskian theory is well defined, *i.e.* fulfils the Wightman and the Haag-Kastler axioms. It is then possible to get back Minkowskian field operators through Wighthman functions thanks to the Wightman reconstruction theorem [167]. Moreover, one can get back Green functions by time-ordering Wightman functions. Details can be found for instance in Ref. [167–169].

To summarise the approach, an Euclidean theory is defined in which the Euclidean Dyson-Schwinger equations can be derived. Then solving them leads to Schwinger functions. Wightman and Green functions are then deduced from analytic continuation of the computed Schwinger ones.

Appendix C

Relation between Γ and $\bar{\Gamma}$

In this appendix, the proof of the relation (3.14) is given in details. Looking at $\bar{\chi}_{ij;q_1q_2}(p,P)$ defined in equation (3.12) and applying charge conjugation, one gets:

$$\begin{aligned}
\bar{\chi}_{ij;q_1q_2}(p,P) &= \delta(K-k_1-k_2)\int \frac{\mathrm{d}^4x}{(2\pi)^4} e^{+ip\cdot x}\,\langle\pi,P|\,T\{\psi_i^{q_1}(x_1)\bar{\psi}_j^{q_2}(x_2)\}\,|0\rangle & \text{(C.1)}\\
&= \delta(K-k_1-k_2)\int \frac{\mathrm{d}^4x}{(2\pi)^4} e^{+ip\cdot x}\\
&\quad \langle\pi,P|\,\theta(x_1^0-x_2^0)\psi_i^{q_1}(x_1)\bar{\psi}_j^{q_2}(x_1)-\theta(x_2^0-x_1^0)\bar{\psi}_j^{q_2}(x_2)\psi_i^{q_1}(x_1)\,|0\rangle & \text{(C.2)}\\
&= \delta(K-k_1-k_2)\int \frac{\mathrm{d}^4x}{(2\pi)^4} e^{+ip\cdot x}\\
&\quad \langle\bar{\pi},P|\,\theta(x_1^0-x_2^0)C_{i,l}(\bar{\psi}_l^{q_1}(x_1))^t(\psi_n^{q_2}(x_2))^tC_{j,n}-...\;|0\rangle & \text{(C.3)}\\
&= \delta(K-k_1-k_2)\int \frac{\mathrm{d}^4x}{(2\pi)^4} e^{+ip\cdot x}\\
&\quad C_{i,l}\,\left[\langle 0|-\theta(x_1^0-x_2^0)\psi_n^{q_2}(x_2)\bar{\psi}_l^{q_1}(x_1))+...\;|\pi,P\rangle\right]^t\,C_{n,j} & \text{(C.4)}\\
&= \delta(K-k_1-k_2)\int \frac{\mathrm{d}^4x}{(2\pi)^4} e^{+ip\cdot x}C_{i,l}[\langle 0|\,\theta(x_1^0-x_2^0)\bar{\psi}_l^{q_1}(x_1)\psi_n^{q_2}(x_2)-...\;|\pi,P\rangle]^tC_{n,j}\\
&= \delta(K-k_1-k_2)C_{i,l}\underbrace{\int \frac{\mathrm{d}^4x}{(2\pi)^4} e^{+ip\cdot x}\left[\langle 0|\,T\{\bar{\psi}_l^{q_1}(x_1)\psi_n^{q_2}(x_2)\}\,|\pi,P\rangle\right]^t}_{\chi^t_{ij;q_1q_2}(-p,-P)}\,C_{n,j}\;, & \text{(C.5)}
\end{aligned}$$

where $C=-i\gamma^0\gamma^2$ and the flow for the three momenta involved in $\bar{\chi}_\pi$ (p_1, p_2 and P) is the opposite to the one we draw in the right diagram of Fig. 3.3, which corresponds to $\bar{\Gamma}_\pi$. Then, we can write:

$$\begin{aligned}
\bar{\chi}_{ij;q_1q_2}(p,P) &= S_{il}(-p+\eta_2P)\bar{\Gamma}_{ln;q_1q_2}(p,P)S_{nj}(p+\eta_1P)\\
C_{il}\chi^t_{ln;q_1q_2}(-p,-P)C_{nj} &= C_{il}S^t_{lk}(p-\eta_2P)\Gamma^t_{kn;q_1q_2}(-p;-P)S^t_{nm}(-p-\eta_1P)C_{mj}\;, & \text{(C.6)}
\end{aligned}$$

and will be left with

$$\begin{aligned}
\bar{\Gamma}_{ij;q_1q_2}(p,P) &= S^{-1}_{il}(-p+\eta_2P)C_{lk}S^t_{km}(p-\eta_2P)\Gamma^t_{mn;q_1q_2}(-p;-P)\\
&\quad S^t_{no}(-p-\eta_1P))C_{or}S^{-1}_{rj}(p+\eta_1P)\\
&= C_{il}\Gamma^t_{ln;q_1q_2}(-p;-P)C_{nj}\;, & \text{(C.7)}
\end{aligned}$$

where we used

$$C_{il}S^t_{lm}(k) = S_{il}(-k)C_{lm} \ , \tag{C.8}$$

that can be easily obtained after noticing the following:

$$\left\{ \begin{array}{rcl} \left(\gamma^0\right)^t & = & \gamma^0 \\ \left(\gamma^2\right)^t & = & \gamma^2 \end{array} \right. \quad \text{and} \quad \left\{ \begin{array}{rcl} \left(\gamma^1\right)^t & = & -\gamma^1 \\ \left(\gamma^3\right)^t & = & -\gamma^3 \end{array} \right. \ . \tag{C.9}$$

Appendix D

Effect of Time Reversal on GPDs

Wigner's theorem [232] implies that symmetries can be represented as unitary or anti-unitary transformations on the Hilbert space of states. Contrary to the most common symmetries in physics, time-reversal operator $\mathcal{T}$ acts as an anti-linear and anti-unitary operator, *i.e.* $\mathcal{T}f = f^*\mathcal{T}$ and

$$\langle\Omega_1|\,\mathcal{T}^\dagger\mathcal{T}\,|\Omega_2\rangle = \langle\Omega_1|\,\Omega_2\rangle^* = \langle\Omega_2|\,\Omega_1\rangle\,. \tag{D.1}$$

Thus, considering the operator $O_\Gamma(-z,z)$ defined by:

$$O_\Gamma(-z,z) = \bar\Psi\left(-\frac{z}{2}\right)\Gamma\Psi\left(\frac{z}{2}\right), \tag{D.2}$$

where $\Psi(z)$ is defined in equation (1.23) and Γ is a given Dirac structure, it is possible to insert three anti-unitary operations as:

$$\langle\Omega_2|\,O_\Gamma(-z,z)\,|\Omega_1\rangle = \langle\Omega_2|\,\mathcal{T}^\dagger\mathcal{T}\bar\Psi\left(-\frac{z}{2}\right)\mathcal{T}^\dagger\Gamma^*\mathcal{T}\Psi\left(\frac{z}{2}\right)\mathcal{T}^\dagger\mathcal{T}\,|\Omega_1\rangle^*\,. \tag{D.3}$$

In order to proceed in the evaluation of the matrix element of equation (D.3), one has to go back from the lightcone coordinate to the usual time coordinates, as the operation of time reversal is more transparent within this set of coordinate. Indeed on quarks fields, the time reversal operators act as:

$$\mathcal{T}\psi(z^0,\mathbf{z})\mathcal{T}^\dagger = \eta_T(-i\gamma_5 C)\psi(-z^0,\mathbf{z}) \quad , \quad \mathcal{T}\bar\psi(z^0,\mathbf{z})\mathcal{T}^\dagger = \eta_T^*\bar\psi(-z^0,\mathbf{z})(i\gamma_5 C^\dagger) \tag{D.4}$$

with $|\eta_T|^2 = 1$ and C being the charge conjugation matrix. Consequently, dealing with the matrix elements defining the GPDs, *i.e.* $\Gamma = \gamma^+$, and in the lightcone gauge in order to avoid to deal with a Wilson line, one gets:

$$\begin{aligned}
\langle\Omega_2|\,O_{\gamma^+}(-z,z)\,|\Omega_1\rangle &= \langle\Omega_2|\,\mathcal{T}^\dagger\bar\psi\left(\frac{z^0}{2},-\frac{\mathbf{z}}{2}\right)(iC^\dagger\gamma_5)(\gamma^+)^*(-i\gamma_5 C)\psi\left(\frac{-z^0}{2},\frac{\mathbf{z}}{2}\right)\mathcal{T}\,|\Omega_1\rangle^* \\
&= \langle\Omega_1|\,\mathcal{T}^\dagger\bar\psi\left(\frac{-z^0}{2},\frac{\mathbf{z}}{2}\right)\gamma^0(iC^\dagger\gamma_5)(\gamma^+)^T(-i\gamma_5 C)\gamma^0\psi\left(\frac{z^0}{2},\frac{-\mathbf{z}}{2}\right)\mathcal{T}\,|\Omega_2\rangle \\
&= \langle\Omega_1|\,\mathcal{T}^\dagger\bar\psi\left(\frac{-z^0}{2},\frac{\mathbf{z}}{2}\right)\gamma^0(\gamma^+)\gamma^0\psi\left(\frac{z^0}{2},\frac{-\mathbf{z}}{2}\right)\mathcal{T}\,|\Omega_2\rangle\,.
\end{aligned} \tag{D.5}$$

Introducing the parity operator $\mathcal{P}$ which acts on quark fields as:

$$\mathcal{P}\psi(z^0,\mathbf{z})\mathcal{P}^\dagger = \eta_P\gamma^0\psi(z^0,-\mathbf{z}) \quad , \quad \mathcal{P}\bar\psi(z^0,\mathbf{z})\mathcal{P}^\dagger = \eta_P^*\bar\psi(z^0,-\mathbf{z})\gamma^0, \tag{D.6}$$

with$|\eta_P|^2 = 1$, and inserting it in equation (D.5):

$$\langle \Omega_2 | \, O(-z^-, z^-) \, | \Omega_1 \rangle = \langle \Omega_1 | \, \mathcal{T}^\dagger \mathcal{P}^\dagger \bar{\psi} \left(\frac{-z^-}{2} \right) \gamma^+ \psi \left(\frac{z^-}{2} \right) \mathcal{P}\mathcal{T} \, | \Omega_2 \rangle \, . \tag{D.7}$$

The combined effect of parity and time reversal on a state is known:

$$\mathcal{P}\mathcal{T} \, | p, s \rangle = e^{i\phi(s)} \, | p, -s \rangle \, , \tag{D.8}$$

where $\phi(s) = \phi_0 + \pi(s - s_z)$, ϕ_0 being the intrinsic parity of the considered state. In the case of scalar target (see *e.g.* the pion GPD defined in equation (1.30)), $s = 0$ and thus equation D.8 generates a constant phase term which vanishes when dealing with the matrix element of equation (D.7). Therefore, the PT symmetry switches the incoming and outgoing states which leads directly to the expected result:

$$H(x, \xi, t) = H(x, -\xi, t). \tag{D.9}$$

In the case of a spin-1/2 hadron, the additional phase $\phi(s)$ is compensated when changing $\bar{u}_{-s}$ and u_{-s} into $\bar{u}_s$ and u_s, leading to equation (D.9) and its equivalent for the GPD E. Additional details concerning the others GPDs can be found in Ref. [69].

Appendix E

Light front formalism

GPDs depend on a twist-two operator taken at $z^+ = 0$, *i.e.* the two quark fields are taken at the same lightcone time. This make them suitable for lightcone quantisation, which consists in quantising fields at the same lightcone time rather than "usual" time (see *e.g.* Ref. [233]). At the same lightcone time, the field can be split into the so-called good (denoted by a "+" index) and bad (denoted by a "−"index) such that:

$$\psi^q = \phi^q_+ + \phi^q_-, \tag{E.1}$$

with

$$\phi^q_\pm = \Lambda_\pm \psi \quad , \quad \Lambda_\pm = \frac{1}{2}\gamma^\mp\gamma^\pm. \tag{E.2}$$

The "bad" component can be fully determined from QCD equations of motions and thus is not considered in the following. Consequently, the good component of the Dirac field on the lightcone is denoted ϕ^q, omitting the "+" index. In terms of creation and annihilation operators, it is denoted as:

$$\begin{aligned}\phi^q(z^-, z_\perp) = \int \frac{\mathrm{d}k^+}{k^+}\frac{\mathrm{d}^2\mathbf{k}_\perp}{16\pi^2}\theta(k^+)\sum_\mu \Big[& b_q(\omega)u_+(\omega)e^{-ik^+z^- + i\mathbf{k}_\perp\cdot\mathbf{z}_\perp} \\ & + d^\dagger_q(\omega)v_+(\omega)e^{ik^+z^- - i\mathbf{k}_\perp\cdot\mathbf{z}_\perp}\Big],\end{aligned} \tag{E.3}$$

where b_q is the annihilation operator of the good quark component field and $d^\dagger_q$ is the creation operator of the good anti-quark field. θ is the Heaviside function and:

$$\omega = (k^+, \mathbf{k}_\perp, \mu, c), \tag{E.4}$$

with μ denoting the quark helicity and c the colour. u_+ and v_+ are the projections of the usual Dirac spinors:

$$u_+(\omega) = \Lambda_+ u(\omega) \quad , \quad v_+(\omega) = \Lambda_+\omega. \tag{E.5}$$

Working in the lightcone gauge, *i.e.* $A^+ = 0$, the transverse components of the gluon fields $A_\nu(z^-, z_\perp)$ (for $\nu \in \{1, 2\}$) are given by:

$$\begin{aligned}A_\nu(z^-, z_\perp) = \int \frac{\mathrm{d}k^+}{k^+}\frac{\mathrm{d}^2\mathbf{k}_\perp}{16\pi^2}\theta(k^+)\sum_\mu \Big[& a(\omega)\epsilon_\nu(\omega)e^{-ik^+z^- + i\mathbf{k}_\perp\cdot\mathbf{z}_\perp} \\ & + a^\dagger(\omega)\epsilon^*_\nu(\omega)e^{ik^+z^- - i\mathbf{k}_\perp\cdot\mathbf{z}_\perp}\Big],\end{aligned} \tag{E.6}$$

where ϵ_ν is the polarisation vector. The Dirac operators fulfil the following anti-commutation relations:

$$\left\{b_{q'}(\omega'), b_q^\dagger(\omega)\right\} = \left\{d_{q'}(\omega'), d_q^\dagger(\omega)\right\} = 16\pi^3 k^+ \delta\left(k'^+ - k^+\right) \delta\left(\mathbf{k}'_\perp - \mathbf{k}_\perp\right) \delta_{\mu'\mu}\delta_{c'c}\delta_{q'q}, \quad \text{(E.7)}$$

whereas the gluon creation and annihilation operators fulfil:

$$\left[a(\omega'), a^\dagger(\omega)\right] = 16\pi^3 k^+ \delta\left(k'^+ - k^+\right) \delta\left(\mathbf{k}'_\perp - \mathbf{k}_\perp\right) \delta_{\mu'\mu}\delta_{c'c}\delta_{q'q}. \quad \text{(E.8)}$$

Single quark, anti-quark and gluon momentum eigenstates are generated from the vacuum[1] through:

$$|q,\omega\rangle = b_q^\dagger(\omega)\,|0\rangle\,, \quad \text{(E.9)}$$

$$|\bar{q},\omega\rangle = d_q^\dagger(\omega)\,|0\rangle\,, \quad \text{(E.10)}$$

$$|g,\omega\rangle = a^\dagger(\omega)\,|0\rangle\,. \quad \text{(E.11)}$$

The commutations relations leads to the following normalisation of the 1-particle states of type s ($s \in \{q, \bar{q}, g\}$):

$$\left\langle s',\omega'\right| s,\omega\rangle = 16\pi^3 k^+ \delta\left(k'^+ - k^+\right) \delta\left(\mathbf{k}'_\perp - \mathbf{k}_\perp\right) \delta_{\mu'\mu}\delta_{c'c}\delta_{s's}. \quad \text{(E.12)}$$

Consequently, a N-particles state Fock state is given by:

$$|N,\beta,k_1\cdots k_N\rangle = \frac{1}{\sqrt{f_{N,\beta}}} \prod_i \frac{b_{q_i}^\dagger(\omega_i)}{\sqrt{x_i}} \prod_j \frac{d_{q_j}^\dagger(\omega_j)}{\sqrt{x_j}} \prod_l \frac{a^\dagger(\omega_l)}{\sqrt{x_l}}\,|0\rangle\,, \quad \text{(E.13)}$$

with $f_{N,\beta}$ a normalisation constant such that:

$$\langle N',\beta',k'_1\cdots k'_N\,|N,\beta,k_1\cdots k_N\rangle = \delta_{NN'}\delta_{\beta\beta'} \prod_{i=1}^{N} 16\pi^3 k_i^+ \delta\left(k_i'^+ - k_i^+\right) \delta\left(\mathbf{k}'_{\perp i} - \mathbf{k}_{\perp i}\right). \quad \text{(E.14)}$$

Those definitions and normalisation conditions are heavily used in chapter 5 in order to derive equation (5.26).

[1] A usual pertubative vacuum is considered here.

Bibliography

[1] Georges Aad et al. Observation of a new particle in the search for the Standard Model Higgs boson with the ATLAS detector at the LHC. *Phys.Lett.*, B716:1–29, 2012, 1207.7214.

[2] Serguei Chatrchyan et al. Observation of a new boson at a mass of 125 GeV with the CMS experiment at the LHC. *Phys.Lett.*, B716:30–61, 2012, 1207.7235.

[3] F. Englert and R. Brout. Broken Symmetry and the Mass of Gauge Vector Mesons. *Phys.Rev.Lett.*, 13:321–323, 1964.

[4] Peter W. Higgs. Broken Symmetries and the Masses of Gauge Bosons. *Phys.Rev.Lett.*, 13:508–509, 1964.

[5] H. David Politzer. Reliable Perturbative Results for Strong Interactions? *Phys.Rev.Lett.*, 30:1346–1349, 1973.

[6] D.J. Gross and Frank Wilczek. Asymptotically Free Gauge Theories. 1. *Phys.Rev.*, D8:3633–3652, 1973.

[7] David J. Gross and Frank Wilczek. Ultraviolet Behavior of Nonabelian Gauge Theories. *Phys.Rev.Lett.*, 30:1343–1346, 1973.

[8] E. Rutherford. Collision of α particles with light atoms iv. an anomalous effect in nitrogen. *Phil. Mag.*, 37:581, 1919.

[9] R. Frisch and O. Stern. Über die magnetische ablenkung von wasserstoffmolekülen und das magnetische moment des protons. i / magnetic deviation of hydrogen molecules and the magnetic moment of the proton. *Z. Phys. 85*, 85:4, 1933.

[10] I. Estermann and O. Stern. Über die magnetische ablenkung von wasserstoffmolekülen und das magnetische moment des protons. ii / magnetic deviation of hydrogen molecules and the magnetic moment of the proton. *Zs. f. Phys*, 85:17, 1933.

[11] R.W. Mcallister and R. Hofstadter. Elastic Scattering of 188-MeV Electrons From the Proton and the α Particle. *Phys.Rev.*, 102:851–856, 1956.

[12] Robert Hofstadter. Electron scattering and nuclear structure. *Rev.Mod.Phys.*, 28:214–254, 1956.

[13] Murray Gell-Mann. A Schematic Model of Baryons and Mesons. *Phys.Lett.*, 8:214–215, 1964.

[14] G. Zweig. An $su(3)$ model for strong interaction symmetry and its breaking. Report No.8182/TH.401, CERN, 1964.

[15] G. Zweig. An $su(3)$ model for strong interaction symmetry and its breaking ii. Report No.8419/TH.412, CERN, 1964.

[16] Elliott D. Bloom, D.H. Coward, H.C. DeStaebler, J. Drees, Guthrie Miller, et al. High-Energy Inelastic e p Scattering at 6-Degrees and 10-Degrees. *Phys.Rev.Lett.*, 23:930–934, 1969.

[17] Martin Breidenbach, Jerome I. Friedman, Henry W. Kendall, Elliott D. Bloom, D.H. Coward, et al. Observed Behavior of Highly Inelastic electron-Proton Scattering. *Phys.Rev.Lett.*, 23:935–939, 1969.

[18] J.D. Bjorken. Asymptotic Sum Rules at Infinite Momentum. *Phys.Rev.*, 179:1547–1553, 1969.

[19] J.D. Bjorken and Emmanuel A. Paschos. Inelastic Electron Proton and gamma Proton Scattering, and the Structure of the Nucleon. *Phys.Rev.*, 185:1975–1982, 1969.

[20] Richard P. Feynman. Very high-energy collisions of hadrons. *Phys.Rev.Lett.*, 23:1415–1417, 1969.

[21] Jr. Callan, Curtis G. and David J. Gross. High-energy electroproduction and the constitution of the electric current. *Phys.Rev.Lett.*, 22:156–159, 1969.

[22] O.W. Greenberg. Spin and Unitary Spin Independence in a Paraquark Model of Baryons and Mesons. *Phys.Rev.Lett.*, 13:598–602, 1964.

[23] M.Y. Han and Yoichiro Nambu. Three Triplet Model with Double SU(3) Symmetry. *Phys.Rev.*, 139:B1006–B1010, 1965.

[24] B.V. Struminsky N.N. Bogoliubov and A.N. Tavkhelid ze. On composite models in the theory of elementary particle. *Preprint JINR D-1968*, 1965.

[25] Yoneji Miyamoto. Relativistic three field model (12 dimensional pseudunitary group) and weak current. *Progress of Theoretical Physics*, 33(6):1131–1132, 1965, http://ptp.oxfordjournals.org/content/33/6/1131.full.pdf+html.

[26] Chen-Ning Yang and Robert L. Mills. Conservation of Isotopic Spin and Isotopic Gauge Invariance. *Phys.Rev.*, 96:191–195, 1954.

[27] H. Fritzsch, Murray Gell-Mann, and H. Leutwyler. Advantages of the Color Octet Gluon Picture. *Phys.Lett.*, B47:365–368, 1973.

[28] Yuri L. Dokshitzer. Calculation of the Structure Functions for Deep Inelastic Scattering and e+ e- Annihilation by Perturbation Theory in Quantum Chromodynamics. *Sov.Phys.JETP*, 46:641–653, 1977.

[29] V.N. Gribov and L.N. Lipatov. Deep inelastic e p scattering in perturbation theory. *Sov.J.Nucl.Phys.*, 15:438–450, 1972.

[30] Guido Altarelli and G. Parisi. Asymptotic Freedom in Parton Language. *Nucl.Phys.*, B126:298, 1977.

[31] K.A. Olive et al. Review of Particle Physics. *Chin.Phys.*, C38:090001, 2014.

[32] D. Amati, R. Petronzio, and G. Veneziano. Relating Hard QCD Processes Through Universality of Mass Singularities. *Nucl.Phys.*, B140:54, 1978.

[33] D. Amati, R. Petronzio, and G. Veneziano. Relating Hard QCD Processes Through Universality of Mass Singularities. 2. *Nucl.Phys.*, B146:29–49, 1978.

[34] R. Keith Ellis, Howard Georgi, Marie Machacek, H. David Politzer, and Graham G. Ross. Perturbation Theory and the Parton Model in QCD. *Nucl.Phys.*, B152:285, 1979.

[35] Stephen B. Libby and George F. Sterman. Mass Divergences in Two Particle Inelastic Scattering. *Phys.Rev.*, D18:4737, 1978.

[36] John Collins. *Foundations of Pertubative QCD.* Cambridge Monographs On particle physics, nuclear physics and cosmology, 2011.

[37] George Sterman. *An Introduction to Quantum Field Theory.* Cambridge University Press, 1993.

[38] S. Wallon. *Hard exclusive processes in perturbative QCD: from medium to asymptotical energies.* PhD thesis, Université Paris XI, 2009.

[39] L.D. Landau. On analytic properties of vertex parts in quantum field theory. *Nucl.Phys.*, 13:181–192, 1959.

[40] S. Coleman and R.E. Norton. Singularities in the physical region. *Nuovo Cim.*, 38:438–442, 1965.

[41] George F. Sterman. Mass Divergences in Annihilation Processes. 1. Origin and Nature of Divergences in Cut Vacuum Polarization Diagrams. *Phys.Rev.*, D17:2773, 1978.

[42] A.V. Efremov and A.V. Radyushkin. HARD PROCESSES, PARTON MODEL AND QCD. *Riv.Nuovo Cim.*, 3N2:1–87, 1980.

[43] Jun Gao, Marco Guzzi, Joey Huston, Hung-Liang Lai, Zhao Li, et al. CT10 next-to-next-to-leading order global analysis of QCD. *Phys.Rev.*, D89(3):033009, 2014, 1302.6246.

[44] Eugene P. Wigner. On the quantum correction for thermodynamic equilibrium. *Phys.Rev.*, 40:749–760, 1932.

[45] J.E. Moyal. Quantum mechanics as a statistical theory. *Proc.Cambridge Phil.Soc.*, 45:99–124, 1949.

[46] M. Hillery, R.F. O'Connell, M.O. Scully, and Eugene P. Wigner. Distribution functions in physics: Fundamentals. *Phys.Rept.*, 106:121–167, 1984.

[47] H. Weyl. Quantum mechanics and group theory. *Z.Phys.*, 46:1, 1927.

[48] Xiang-dong Ji. Viewing the proton through 'color' filters. *Phys.Rev.Lett.*, 91:062001, 2003, hep-ph/0304037.

[49] Andrei V. Belitsky, Xiang-dong Ji, and Feng Yuan. Quark imaging in the proton via quantum phase space distributions. *Phys.Rev.*, D69:074014, 2004, hep-ph/0307383.

[50] Matthias Burkardt. Impact parameter dependent parton distributions and off forward parton distributions for zeta —> 0. *Phys.Rev.*, D62:071503, 2000, hep-ph/0005108.

[51] C. Lorce and B. Pasquini. Quark Wigner Distributions and Orbital Angular Momentum. *Phys.Rev.*, D84:014015, 2011, 1106.0139.

[52] Stephan Meissner, Andreas Metz, Marc Schlegel, and Klaus Goeke. Generalized parton correlation functions for a spin-0 hadron. *JHEP*, 0808:038, 2008, 0805.3165.

[53] Stephan Meissner, Andreas Metz, and Marc Schlegel. Generalized parton correlation functions for a spin-1/2 hadron. *JHEP*, 0908:056, 2009, 0906.5323.

[54] Cedric Lorce, Barbara Pasquini, Xiaonu Xiong, and Feng Yuan. The quark orbital angular momentum from Wigner distributions and light-cone wave functions. *Phys.Rev.*, D85:114006, 2012, 1111.4827.

[55] Cedric Lorce, Barbara Pasquini, and Marc Vanderhaeghen. Unified framework for generalized and transverse-momentum dependent parton distributions within a 3Q light-cone picture of the nucleon. *JHEP*, 1105:041, 2011, 1102.4704.

[56] C. Lorcé and B. Pasquini. Structure analysis of the generalized correlator of quark and gluon for a spin-1/2 target. *JHEP*, 1309:138, 2013, 1307.4497.

[57] K. Kanazawa, C. Lorcé, A. Metz, B. Pasquini, and M. Schlegel. Twist-2 generalized transverse-momentum dependent parton distributions and the spin/orbital structure of the nucleon. *Phys.Rev.*, D90(1):014028, 2014, 1403.5226.

[58] C. Lorcé, B. Pasquini, and P. Schweitzer. Unpolarized transverse momentum dependent parton distribution functions beyond leading twist in quark models. *JHEP*, 1501:103, 2015, 1411.2550.

[59] John C. Collins, Leonid Frankfurt, and Mark Strikman. Factorization for hard exclusive electroproduction of mesons in QCD. *Phys.Rev.*, D56:2982–3006, 1997, hep-ph/9611433.

[60] Xiang-Dong Ji and Jonathan Osborne. One loop corrections and all order factorization in deeply virtual Compton scattering. *Phys.Rev.*, D58:094018, 1998, hep-ph/9801260.

[61] John C. Collins and Andreas Freund. Proof of factorization for deeply virtual Compton scattering in QCD. *Phys.Rev.*, D59:074009, 1999, hep-ph/9801262.

[62] Dieter Mueller, D. Robaschik, B. Geyer, F.M. Dittes, and J. Hořejši. Wave functions, evolution equations and evolution kernels from light ray operators of QCD. *Fortsch.Phys.*, 42:101–141, 1994, hep-ph/9812448.

[63] A.V. Efremov and A.V. Radyushkin. Factorization and Asymptotical Behavior of Pion Form-Factor in QCD. *Phys.Lett.*, B94:245–250, 1980.

[64] A.V. Radyushkin. ALPHA REPRESENTATION AND SPECTRAL PROPERTIES OF MULTIPARTON FUNCTIONS. *Theor.Math.Phys.*, 61:1144, 1985.

[65] A.V. Radyushkin. Scaling limit of deeply virtual Compton scattering. *Phys.Lett.*, B380:417–425, 1996, hep-ph/9604317.

[66] A.V. Radyushkin. Nonforward parton distributions. *Phys.Rev.*, D56:5524–5557, 1997, hep-ph/9704207.

[67] Markus Diehl and Thierry Gousset. Time ordering in off diagonal parton distributions. *Phys.Lett.*, B428:359–370, 1998, hep-ph/9801233.

[68] P.V. Landshoff and J.C. Polkinghorne. Models for hadronic and leptonic processes at high-energy. *Phys.Rept.*, 5:1–55, 1972.

[69] A.V. Belitsky and A.V. Radyushkin. Unraveling hadron structure with generalized parton distributions. *Phys.Rept.*, 418:1–387, 2005, hep-ph/0504030.

[70] Xiang-Dong Ji. Off forward parton distributions. *J.Phys.*, G24:1181–1205, 1998, hep-ph/9807358.

[71] Krzysztof J. Golec-Biernat and Alan D. Martin. Off diagonal parton distributions and their evolution. *Phys.Rev.*, D59:014029, 1999, hep-ph/9807497.

[72] M. Diehl, T. Feldmann, R. Jakob, and P. Kroll. The Overlap representation of skewed quark and gluon distributions. *Nucl.Phys.*, B596:33–65, 2001, hep-ph/0009255.

[73] M. Diehl. Generalized parton distributions. *Phys.Rept.*, 388:41–277, 2003, hep-ph/0307382.

[74] Kenneth G. Wilson. Nonlagrangian models of current algebra. *Phys.Rev.*, 179:1499–1512, 1969.

[75] S.A. Anikin and O.I. Zavyalov. Short Distance and Light Cone Expansions for Products of Currents. *Annals Phys.*, 116:135–166, 1978.

[76] B. Pire, Jacques Soffer, and O. Teryaev. Positivity constraints for off - forward parton distributions. *Eur.Phys.J.*, C8:103–106, 1999, hep-ph/9804284.

[77] P.V. Pobylitsa. Inequalities for generalized parton distributions H and E. *Phys.Rev.*, D65:077504, 2002, hep-ph/0112322.

[78] P.V. Pobylitsa. Disentangling positivity constraints for generalized parton distributions. *Phys.Rev.*, D65:114015, 2002, hep-ph/0201030.

[79] M. Diehl. Generalized parton distributions in impact parameter space. *Eur.Phys.J.*, C25:223–232, 2002, hep-ph/0205208.

[80] B.C. Tiburzi and G.A. Miller. Generalized parton distributions for q anti-q pions. *Phys.Rev.*, D67:013010, 2003, hep-ph/0209178.

[81] A. Mukherjee, I.V. Musatov, H.C. Pauli, and A.V. Radyushkin. Power law wave functions and generalized parton distributions for pion. *Phys.Rev.*, D67:073014, 2003, hep-ph/0205315.

[82] P.V. Pobylitsa. Solution of polynomiality and positivity constraints on generalized parton distributions. *Phys.Rev.*, D67:034009, 2003, hep-ph/0210150.

[83] D.S. Hwang and Dieter Mueller. Implication of the overlap representation for modelling generalized parton distributions. *Phys.Lett.*, B660:350–359, 2008, 0710.1567.

[84] Dieter Müller and Dae Sung Hwang. The concept of phenomenological light-front wave functions – Regge improved diquark model predictions. 2014, 1407.1655.

[85] B. Geyer, D. Robaschik, Michael Bordag, and J. Horejsi. NONLOCAL LIGHT CONE EXPANSIONS AND EVOLUTION EQUATIONS. *Z.Phys.*, C26:591–600, 1985.

[86] T. Braunschweig, B. Geyer, J. Horejsi, and D. Robaschik. Hadron Operators on the Light Cone. *Z.Phys.*, C33:275, 1986.

[87] F.M. Dittes, Dieter Mueller, D. Robaschik, B. Geyer, and J. Horejsi. The Altarelli-Parisi Kernel as Asymptotic Limit of an Extended Brodsky-Lepage Kernel. *Phys.Lett.*, B209:325–329, 1988.

[88] Xiang-Dong Ji. Deeply virtual Compton scattering. *Phys.Rev.*, D55:7114–7125, 1997, hep-ph/9609381.

[89] I.I. Balitsky and A.V. Radyushkin. Light ray evolution equations and leading twist parton helicity dependent nonforward distributions. *Phys.Lett.*, B413:114–121, 1997, hep-ph/9706410.

[90] A.V. Radyushkin. Double distributions and evolution equations. *Phys.Rev.*, D59:014030, 1999, hep-ph/9805342.

[91] Johannes Blumlein, Bodo Geyer, and Dieter Robaschik. On the evolution kernels of twist-2 light ray operators for unpolarized and polarized deep inelastic scattering. *Phys.Lett.*, B406:161–170, 1997, hep-ph/9705264.

[92] Johannes Blumlein, Bodo Geyer, and Dieter Robaschik. The Virtual Compton amplitude in the generalized Bjorken region: twist-2 contributions. *Nucl.Phys.*, B560:283–344, 1999, hep-ph/9903520.

[93] Andrei V. Belitsky and Dieter Mueller. Next-to-leading order evolution of twist-2 conformal operators: The Abelian case. *Nucl.Phys.*, B527:207–234, 1998, hep-ph/9802411.

[94] Andrei V. Belitsky and Dieter Mueller. Broken conformal invariance and spectrum of anomalous dimensions in QCD. *Nucl.Phys.*, B537:397–442, 1999, hep-ph/9804379.

[95] Andrei V. Belitsky, Dieter Mueller, and A. Freund. Reconstruction of nonforward evolution kernels. *Phys.Lett.*, B461:270–279, 1999, hep-ph/9904477.

[96] Andrei V. Belitsky and Dieter Mueller. Exclusive evolution kernels in two loop order: Parity even sector. *Phys.Lett.*, B464:249–256, 1999, hep-ph/9906409.

[97] Andrei V. Belitsky, A. Freund, and Dieter Mueller. Evolution kernels of skewed parton distributions: Method and two loop results. *Nucl.Phys.*, B574:347–406, 2000, hep-ph/9912379.

[98] A.V. Efremov and A.V. Radyushkin. Asymptotical Behavior of Pion Electromagnetic Form-Factor in QCD. *Theor.Math.Phys.*, 42:97–110, 1980.

[99] V.L. Chernyak, A.R. Zhitnitsky, and V.G. Serbo. Asymptotic hadronic form-factors in quantum chromodynamics. *JETP Lett.*, 26:594–597, 1977.

[100] Glennys R. Farrar and Darrell R. Jackson. The Pion Form-Factor. *Phys.Rev.Lett.*, 43:246, 1979.

[101] G. Peter Lepage and Stanley J. Brodsky. Exclusive Processes in Quantum Chromodynamics: Evolution Equations for Hadronic Wave Functions and the Form-Factors of Mesons. *Phys.Lett.*, B87:359–365, 1979.

[102] G. Peter Lepage and Stanley J. Brodsky. Exclusive Processes in Perturbative Quantum Chromodynamics. *Phys.Rev.*, D22:2157, 1980.

[103] A.V. Vinnikov. Code for prompt numerical computation of the leading order GPD evolution. 2006, hep-ph/0604248.

[104] V.M. Braun, G.P. Korchemsky, and Dieter Mueller. The Uses of conformal symmetry in QCD. *Prog.Part.Nucl.Phys.*, 51:311–398, 2003, hep-ph/0306057.

[105] C. Mezrag, L. Chang, H. Moutarde, C.D. Roberts, J. Rodríguez-Quintero, et al. Sketching the pion's valence-quark generalised parton distribution. *Phys.Lett.*, B741:190–196, 2014, 1411.6634.

[106] M. Guidal. A Fitter code for Deep Virtual Compton Scattering and Generalized Parton Distributions. *Eur.Phys.J.*, A37:319–332, 2008, 0807.2355.

[107] H. Moutarde. Extraction of the Compton Form Factor H from DVCS measurements at Jefferson Lab. *Phys.Rev.*, D79:094021, 2009, 0904.1648.

[108] Kresimir Kumerički and Dieter Mueller. Deeply virtual Compton scattering at small x_B and the access to the GPD H. *Nucl.Phys.*, B841:1–58, 2010, 0904.0458.

[109] Kresimir Kumerički, Dieter Müller, and Morgan Murray. Revealing CFFs and GPDs from experimental measurements. *Nuovo Cim.*, C036(05):159–165, 2013, 1302.7308.

[110] Kresimir Kumericki, Dieter Mueller, and Andreas Schafer. Neural network generated parametrizations of deeply virtual Compton form factors. *JHEP*, 1107:073, 2011, 1106.2808.

[111] Xiang-Dong Ji and Jonathan Osborne. One loop QCD corrections to deeply virtual Compton scattering: The Parton helicity independent case. *Phys.Rev.*, D57:1337–1340, 1998, hep-ph/9707254.

[112] L. Mankiewicz, G. Piller, E. Stein, M. Vanttinen, and T. Weigl. NLO corrections to deeply virtual Compton scattering. *Phys.Lett.*, B425:186–192, 1998, hep-ph/9712251.

[113] Andrei V. Belitsky, Dieter Mueller, L. Niedermeier, and A. Schafer. Deeply virtual Compton scattering in next-to-leading order. *Phys.Lett.*, B474:163–169, 2000, hep-ph/9908337.

[114] Andreas Freund and Martin McDermott. A Detailed next-to-leading order QCD analysis of deeply virtual Compton scattering observables. *Eur.Phys.J.*, C23:651–674, 2002, hep-ph/0111472.

[115] A. Freund and M.F. McDermott. A Next-to-leading order analysis of deeply virtual Compton scattering. *Phys.Rev.*, D65:091901, 2002, hep-ph/0106124.

[116] Andreas Freund and Martin F. McDermott. A Next-to-leading order QCD analysis of deeply virtual Compton scattering amplitudes. *Phys.Rev.*, D65:074008, 2002, hep-ph/0106319.

[117] B. Pire, L. Szymanowski, and J. Wagner. NLO corrections to timelike, spacelike and double deeply virtual Compton scattering. *Phys.Rev.*, D83:034009, 2011, 1101.0555.

[118] H. Moutarde, B. Pire, F. Sabatie, L. Szymanowski, and J. Wagner. On timelike and spacelike deeply virtual Compton scattering at next to leading order. *Phys.Rev.*, D87:054029, 2013, 1301.3819.

[119] T. Altinoluk, B. Pire, L. Szymanowski, and S. Wallon. Resumming soft and collinear contributions in deeply virtual Compton scattering. *JHEP*, 1210:049, 2012, 1207.4609.

[120] Otto Nachtmann. Positivity constraints for anomalous dimensions. *Nucl.Phys.*, B63:237–247, 1973.

[121] Howard Georgi and H. David Politzer. Freedom at Moderate Energies: Masses in Color Dynamics. *Phys.Rev.*, D14:1829, 1976.

[122] V.M. Braun, A.N. Manashov, and B. Pirnay. Finite-t and target mass corrections to DVCS on a scalar target. *Phys.Rev.*, D86:014003, 2012, 1205.3332.

[123] V.M. Braun, A.N. Manashov, and B. Pirnay. Finite-t and target mass corrections to deeply virtual Compton scattering. *Phys.Rev.Lett.*, 109:242001, 2012, 1209.2559.

[124] M. Defurne, M. Amaryan, K.A. Aniol, M. Beaumel, H. Benaoum, et al. The E00-110 experiment in Jefferson Lab's Hall A: Deeply Virtual Compton Scattering off the Proton at 6 GeV. 2015, 1504.05453.

[125] Peter Kroll, Herve Moutarde, and Franck Sabatie. From hard exclusive meson electroproduction to deeply virtual Compton scattering. *Eur.Phys.J.*, C73:2278, 2013, 1210.6975.

[126] Morgan J. Murray. Physics Updates from HERMES. *AIP Conf.Proc.*, 1523:46–50, 2012, 1301.1482.

[127] Michel Guidal, Hervé Moutarde, and Marc Vanderhaeghen. Generalized Parton Distributions in the valence region from Deeply Virtual Compton Scattering. *Rept.Prog.Phys.*, 76:066202, 2013, 1303.6600.

[128] A. Accardi, J.L. Albacete, M. Anselmino, N. Armesto, E.C. Aschenauer, et al. Electron Ion Collider: The Next QCD Frontier - Understanding the glue that binds us all. 2012, 1212.1701.

[129] C. Muñoz Camacho et al. Scaling tests of the cross-section for deeply virtual compton scattering. *Phys.Rev.Lett.*, 97:262002, 2006, nucl-ex/0607029.

[130] H.S. Jo et al. Cross sections for the exclusive photon electroproduction on the proton and Generalized Parton Distributions. 2015, 1504.02009.

[131] F.X. Girod et al. Measurement of Deeply virtual Compton scattering beam-spin asymmetries. *Phys.Rev.Lett.*, 100:162002, 2008, 0711.4805.

[132] A.V. Radyushkin. Asymmetric gluon distributions and hard diffractive electroproduction. *Phys.Lett.*, B385:333–342, 1996, hep-ph/9605431.

[133] K. Goeke, Maxim V. Polyakov, and M. Vanderhaeghen. Hard exclusive reactions and the structure of hadrons. *Prog.Part.Nucl.Phys.*, 47:401–515, 2001, hep-ph/0106012.

[134] Maxim V. Polyakov and C. Weiss. Skewed and double distributions in pion and nucleon. *Phys.Rev.*, D60:114017, 1999, hep-ph/9902451.

[135] O.V. Teryaev. Crossing and radon tomography for generalized parton distributions. *Phys.Lett.*, B510:125–132, 2001, hep-ph/0102303.

[136] J. Radon. Über die bestimmung von funktionen durch ihre integralwerte längs gewisser mannigfaltigkeiten. *Berichte Sächsische Akademie der Wisssenschaften ,Leipzig, Math-Phys. Kl.*, 69:262, 1917.

[137] S.R. Deans. *The Radon transform and some of its applications.* A Wiley-Interscience publication. Wiley, 1983.

[138] B.C. Tiburzi. Double distributions: Loose ends. *Phys.Rev.*, D70:057504, 2004, hep-ph/0405211.

[139] Andrei V. Belitsky, Dieter Mueller, A. Kirchner, and A. Schafer. Twist three analysis of photon electroproduction off pion. *Phys.Rev.*, D64:116002, 2001, hep-ph/0011314.

[140] M. Diehl, T. Gousset, B. Pire, and O. Teryaev. Probing partonic structure in gamma* gamma —> pi pi near threshold. *Phys.Rev.Lett.*, 81:1782–1785, 1998, hep-ph/9805380.

[141] M. Diehl, T. Gousset, and B. Pire. Exclusive production of pion pairs in gamma* gamma collisions at large Q**2. *Phys.Rev.*, D62:073014, 2000, hep-ph/0003233.

[142] M. Vanderhaeghen, Pierre A.M. Guichon, and M. Guidal. Hard electroproduction of photons and mesons on the nucleon. *Phys.Rev.Lett.*, 80:5064–5067, 1998.

[143] Pierre A.M. Guichon and M. Vanderhaeghen. Virtual Compton scattering off the nucleon. *Prog.Part.Nucl.Phys.*, 41:125–190, 1998, hep-ph/9806305.

[144] M. Vanderhaeghen, Pierre A.M. Guichon, and M. Guidal. Deeply virtual electroproduction of photons and mesons on the nucleon: Leading order amplitudes and power corrections. *Phys.Rev.*, D60:094017, 1999, hep-ph/9905372.

[145] M. Guidal, M.V. Polyakov, A.V. Radyushkin, and M. Vanderhaeghen. Nucleon form-factors from generalized parton distributions. *Phys.Rev.*, D72:054013, 2005, hep-ph/0410251.

[146] S.V. Goloskokov and P. Kroll. Vector meson electroproduction at small Bjorken-x and generalized parton distributions. *Eur.Phys.J.*, C42:281–301, 2005, hep-ph/0501242.

[147] S.V. Goloskokov and P. Kroll. The Role of the quark and gluon GPDs in hard vector-meson electroproduction. *Eur.Phys.J.*, C53:367–384, 2008, 0708.3569.

[148] S.V. Goloskokov and P. Kroll. An Attempt to understand exclusive pi+ electroproduction. *Eur.Phys.J.*, C65:137–151, 2010, 0906.0460.

[149] I.V. Musatov and A.V. Radyushkin. Evolution and models for skewed parton distributions. *Phys.Rev.*, D61:074027, 2000, hep-ph/9905376.

[150] S.V. Goloskokov and P. Kroll. The Longitudinal cross-section of vector meson electroproduction. *Eur.Phys.J.*, C50:829–842, 2007, hep-ph/0611290.

[151] J. Pumplin, D.R. Stump, J. Huston, H.L. Lai, Pavel M. Nadolsky, et al. New generation of parton distributions with uncertainties from global QCD analysis. *JHEP*, 0207:012, 2002, hep-ph/0201195.

[152] A.V. Radyushkin. Generalized Parton Distributions and Their Singularities. *Phys.Rev.*, D83:076006, 2011, 1101.2165.

[153] C. Mezrag, H. Moutarde, and F. Sabatié. Test of two new parameterizations of the Generalized Parton Distribution H. *Phys.Rev.*, D88:014001, 2013, 1304.7645.

[154] Anatoly V. Radyushkin. Singularities of generalized parton distributions. *Int.J.Mod.Phys.Conf.Ser.*, 20:251–265, 2012.

[155] M.V. Polyakov and A.G. Shuvaev. On'dual' parametrizations of generalized parton distributions. 2002, hep-ph/0207153.

[156] A.V. Radyushkin. Modeling Nucleon Generalized Parton Distributions. *Phys.Rev.*, D87(9):096017, 2013, 1304.2682.

[157] Dieter Mueller and A. Schafer. Complex conformal spin partial wave expansion of generalized parton distributions and distribution amplitudes. *Nucl.Phys.*, B739:1–59, 2006, hep-ph/0509204.

[158] Maxim V. Polyakov. Hard exclusive electroproduction of two pions and their resonances. *Nucl.Phys.*, B555:231, 1999, hep-ph/9809483.

[159] Maxim V. Polyakov and Kirill M. Semenov-Tian-Shansky. Dual parametrization of GPDs versus double distribution Ansatz. *Eur.Phys.J.*, A40:181–198, 2009, 0811.2901.

[160] Dieter Müller, Maxim V. Polyakov, and Kirill M. Semenov-Tian-Shansky. Dual parametrization of generalized parton distributions in two equivalent representations. *JHEP*, 1503:052, 2015, 1412.4165.

[161] F.J. Dyson. The S matrix in quantum electrodynamics. *Phys.Rev.*, 75:1736–1755, 1949.

[162] Julian S. Schwinger. On the Green's functions of quantized fields. 1. *Proc.Nat.Acad.Sci.*, 37:452–455, 1951.

[163] Julian S. Schwinger. On the Green's functions of quantized fields. 2. *Proc.Nat.Acad.Sci.*, 37:455–459, 1951.

[164] Claude Itzykson and Jean-Bernard Zuber. *Quantum field theory*. International series in pure and applied physics. McGraw-Hill, New York, NY, 1980. Also a reprint ed.: Mineola, Dover, 2005.

[165] James D Bjorken and Sidney David Drell. *Relativistic quantum fields*. International series in pure and applied physics. McGraw-Hill, New York, NY, 1965. Companion volume to : Relativistic quantum mechanics. New York : McGraw-Hill, 1964 -.

[166] Craig D. Roberts and Anthony G. Williams. Dyson-Schwinger equations and their application to hadronic physics. *Prog.Part.Nucl.Phys.*, 33:477–575, 1994, hep-ph/9403224.

[167] R.F. Streater and A.S. Wightman. *PCT, spin and statistics, and all that*. W.A. Benjamin Inc, 1980.

[168] E. Seiler. *Gauge Theories as a problem of Constructive Quantum Field Theory and Statistical Mechanics*. Springer-Verlag, 1982.

[169] J. Glimm and Arthur M. Jaffe. *QUANTUM PHYSICS. A FUNCTIONAL INTEGRAL POINT OF VIEW*. Springer-Verlag, 1987.

[170] A. Holl, A. Krassnigg, P. Maris, C.D. Roberts, and S.V. Wright. Electromagnetic properties of ground and excited state pseudoscalar mesons. *Phys.Rev.*, C71:065204, 2005, nucl-th/0503043.

[171] Jacques C.R. Bloch. Numerical investigation of fermion mass generation in QED. 1995, hep-ph/0208074.

[172] M.S. Bhagwat, M.A. Pichowsky, C.D. Roberts, and P.C. Tandy. Analysis of a quenched lattice QCD dressed quark propagator. *Phys.Rev.*, C68:015203, 2003, nucl-th/0304003.

[173] M.S. Bhagwat and P.C. Tandy. Analysis of full-QCD and quenched-QCD lattice propagators. *AIP Conf.Proc.*, 842:225–227, 2006, nucl-th/0601020.

[174] Patrick O. Bowman, Urs M. Heller, Derek B. Leinweber, Maria B. Parappilly, Anthony G. Williams, et al. Unquenched quark propagator in Landau gauge. *Phys.Rev.*, D71:054507, 2005, hep-lat/0501019.

[175] Adnan Bashir, Lei Chang, Ian C. Cloet, Bruno El-Bennich, Yu-Xin Liu, et al. Collective perspective on advances in Dyson-Schwinger Equation QCD. *Commun.Theor.Phys.*, 58:79–134, 2012, 1201.3366.

[176] E.E. Salpeter and H.A. Bethe. A Relativistic equation for bound state problems. *Phys.Rev.*, 84:1232–1242, 1951.

[177] Murray Gell-Mann and Francis Low. Bound states in quantum field theory. *Phys.Rev.*, 84:350–354, 1951.

[178] Julian S. Schwinger. The Theory of quantized fields. 2. *Phys.Rev.*, 91:713–728, 1953.

[179] C.H. Llewellyn-Smith. A relativistic formulation for the quark model for mesons. *Annals Phys.*, 53:521–558, 1969.

[180] D. Lurié, A. J. Macfarlane, and Y. Takahashi. Normalization of bethe-salpeter wave functions. *Phys. Rev.*, 140:B1091–B1099, Nov 1965.

[181] Pieter Maris and Peter C. Tandy. Bethe-Salpeter study of vector meson masses and decay constants. *Phys.Rev.*, C60:055214, 1999, nucl-th/9905056.

[182] H.J. Munczek. Dynamical chiral symmetry breaking, Goldstone's theorem and the consistency of the Schwinger-Dyson and Bethe-Salpeter Equations. *Phys.Rev.*, D52:4736–4740, 1995, hep-th/9411239.

[183] A. Bender, Craig D. Roberts, and L. Von Smekal. Goldstone theorem and diquark confinement beyond rainbow ladder approximation. *Phys.Lett.*, B380:7–12, 1996, nucl-th/9602012.

[184] Lei Chang and Craig D. Roberts. Sketching the Bethe-Salpeter kernel. *Phys.Rev.Lett.*, 103:081601, 2009, 0903.5461.

[185] Lei Chang and Craig D. Roberts. Tracing masses of ground-state light-quark mesons. *Phys.Rev.*, C85:052201, 2012, 1104.4821.

[186] H.L.L. Roberts, A. Bashir, L.X. Gutierrez-Guerrero, C.D. Roberts, and D.J. Wilson. pi- and rho-mesons, and their diquark partners, from a contact interaction. *Phys.Rev.*, C83:065206, 2011, 1102.4376.

[187] Murray Gell-Mann and M Levy. The axial vector current in beta decay. *Nuovo Cim.*, 16:705, 1960.

[188] S.L. Adler and R.F. Dashen. *Current Algebras*. W.A. Benjamin Inc, 1968.

[189] Pieter Maris, Craig D. Roberts, and Peter C. Tandy. Pion mass and decay constant. *Phys.Lett.*, B420:267–273, 1998, nucl-th/9707003.

[190] John M. Cornwall, R. Jackiw, and E. Tomboulis. Effective Action for Composite Operators. *Phys.Rev.*, D10:2428–2445, 1974.

[191] Axel Bender, William Detmold, C.D. Roberts, and Anthony William Thomas. Bethe-Salpeter equation and a nonperturbative quark gluon vertex. *Phys.Rev.*, C65:065203, 2002, nucl-th/0202082.

[192] Pieter Maris and Craig D. Roberts. Pi- and K meson Bethe-Salpeter amplitudes. *Phys.Rev.*, C56:3369–3383, 1997, nucl-th/9708029.

[193] Lei Chang, Craig D. Roberts, and Sebastian M. Schmidt. Dressed-quarks and the nucleon's axial charge. *Phys.Rev.*, C87:015203, 2013, 1207.5300.

[194] Si-xue Qin, Lei Chang, Yu-xin Liu, Craig D. Roberts, and David J. Wilson. Interaction model for the gap equation. *Phys.Rev.*, C84:042202, 2011, 1108.0603.

[195] James S. Ball and Ting-Wai Chiu. Analytic Properties of the Vertex Function in Gauge Theories. 1. *Phys.Rev.*, D22:2542, 1980.

[196] Lei Chang, I.C. Cloet, J.J. Cobos-Martinez, C.D. Roberts, S.M. Schmidt, et al. Imaging dynamical chiral symmetry breaking: pion wave function on the light front. *Phys.Rev.Lett.*, 110:132001, 2013, 1301.0324.

[197] M. Bhagwat, M.A. Pichowsky, and Peter C. Tandy. Confinement phenomenology in the Bethe-Salpeter equation. *Phys.Rev.*, D67:054019, 2003, hep-ph/0212276.

[198] Noboru Nakanishi. Partial-Wave Bethe-Salpeter Equation. *Phys.Rev.*, 130:1230–1235, 1963.

[199] V.A. Karmanov and J. Carbonell. Solving Bethe-Salpeter equation in Minkowski space. *Eur.Phys.J.*, A27:1–9, 2006, hep-th/0505261.

[200] G.C. Wick. Properties of Bethe-Salpeter Wave Functions. *Phys.Rev.*, 96:1124–1134, 1954.

[201] I.V. Anikin, A.E. Dorokhov, A.E. Maximov, L. Tomio, and V. Vento. Off diagonal quark distribution functions of the pion within an effective single instanton approximation. 1999, hep-ph/9905332.

[202] Wojciech Broniowski and Enrique Ruiz Arriola. Impact parameter dependence of the generalized parton distribution of the pion in chiral quark models. *Phys.Lett.*, B574:57–64, 2003, hep-ph/0307198.

[203] Wojciech Broniowski, Enrique Ruiz Arriola, and Krzysztof Golec-Biernat. Generalized parton distributions of the pion in chiral quark models and their QCD evolution. *Phys.Rev.*, D77:034023, 2008, 0712.1012.

[204] B.C. Tiburzi and G.A. Miller. Generalized parton distributions and double distributions for q anti-q pions. *Phys.Rev.*, D67:113004, 2003, hep-ph/0212238.

[205] L. Theussl, S. Noguera, and V. Vento. Generalized parton distributions of the pion in a Bethe-Salpeter approach. *Eur.Phys.J.*, A20:483–498, 2004, nucl-th/0211036.

[206] F. Bissey, J.R. Cudell, J. Cugnon, J.P. Lansberg, and P. Stassart. A Model for the off forward structure functions of the pion. *Phys.Lett.*, B587:189–200, 2004, hep-ph/0310184.

[207] A. Van Dyck, T. Van Cauteren, and Jan Ryckebusch. Support of generalized parton distributions in Bethe-Salpeter models of hadrons. *Phys.Lett.*, B662:413–416, 2008, 0710.2271.

[208] T. Frederico, E. Pace, B. Pasquini, and G. Salme. Pion Generalized Parton Distributions with covariant and Light-front constituent quark models. *Phys.Rev.*, D80:054021, 2009, 0907.5566.

[209] Alexander E. Dorokhov, Wojciech Broniowski, and Enrique Ruiz Arriola. Generalized Quark Transversity Distribution of the Pion in Chiral Quark Models. *Phys.Rev.*, D84:074015, 2011, 1107.5631.

[210] S. Mandelstam. Dynamical variables in the Bethe-Salpeter formalism. *Proc.Roy.Soc.Lond.*, A233:248, 1955.

[211] K. Nishijima and A. H. Singh. Normalization of bethe-salpeter amplitudes. *Phys. Rev.*, 162:1740–1746, Oct 1967.

[212] Daniela Amrath, Markus Diehl, and Jean-Philippe Lansberg. Deeply virtual Compton scattering on a virtual pion target. *Eur.Phys.J.*, C58:179–192, 2008, 0807.4474.

[213] S.R. Amendolia et al. A Measurement of the Space - Like Pion Electromagnetic Form-Factor. *Nucl.Phys.*, B277:168, 1986.

[214] G.M. Huber et al. Charged pion form-factor between Q**2 = 0.60-GeV**2 and 2.45-GeV**2. II. Determination of, and results for, the pion form-factor. *Phys.Rev.*, C78:045203, 2008, 0809.3052.

[215] Matthias Aicher, Andreas Schafer, and Werner Vogelsang. Soft-gluon resummation and the valence parton distribution function of the pion. *Phys.Rev.Lett.*, 105:252003, 2010, 1009.2481.

[216] C. Mezrag, H. Moutarde, J. Rodríguez-Quintero, and F. Sabatié. Towards a Pion Generalized Parton Distribution Model from Dyson-Schwinger Equations. 2014, 1406.7425.

[217] H. Lehmann, K. Symanzik, and W. Zimmermann. On the formulation of quantized field theories. *Nuovo Cim.*, 1:205–225, 1955.

[218] M.L. Goldberger and S.B. Treiman. Form-factors in Beta decay and muon capture. *Phys.Rev.*, 111:354–361, 1958.

[219] Lei Chang, Cédric Mezrag, Hervé Moutarde, Craig D. Roberts, Jose Rodriguez-Quintero, et al. Basic features of the pion valence-quark distribution function. *Phys.Lett.*, B737:23–29, 2014, 1406.5450.

[220] Feng Yuan. Generalized parton distributions at x —> 1. *Phys.Rev.*, D69:051501, 2004, hep-ph/0311288.

[221] Robert L. Jaffe. Spin, twist and hadron structure in deep inelastic processes. *Lect.Notes Phys.*, 496:178, 1997, hep-ph/9602236.

[222] Ho-Meoyng Choi, Chueng-Ryong Ji, and L.S. Kisslinger. Continuity of skewed parton distributions for the pion virtual Compton scattering. *Phys.Rev.*, D66:053011, 2002, hep-ph/0204321.

[223] Chueng-Ryong Ji, Yuriy Mishchenko, and Anatoly Radyushkin. Higher Fock state contributions to the generalized parton distribution of pion. *Phys.Rev.*, D73:114013, 2006, hep-ph/0603198.

[224] F. Natterer and F. Wübbeling. *Mathematical Method in image Reconstruction.* Monographs on Mathematical Modeling and Computation, Society for Industrial and Applied Mathematics, New York, 2001.

[225] D. Atkinson and D.W.E. Blatt. Determination of the Singularities of the Electron Propagator. *Nucl.Phys.*, B151:342, 1979.

[226] S.J. Stainsby and R.T. Cahill. IS SPACE-TIME EUCLIDEAN 'INSIDE' HADRONS? *Phys.Lett.*, A146:467–470, 1990.

[227] P. Maris and H.A. Holties. Determination of the singularities of the Dyson-Schwinger equation for the quark propagator. *Int.J.Mod.Phys.*, A7:5369–5386, 1992.

[228] Conrad J. Burden, Craig D. Roberts, and Anthony G. Williams. Singularity structure of a model quark propagator. *Phys.Lett.*, B285:347–353, 1992.

[229] S.J. Stainsby and R.T. Cahill. The Analytic structure of quark propagators. *Int.J.Mod.Phys.*, A7:7541–7559, 1992.

[230] Konrad Osterwalder and Robert Schrader. AXIOMS FOR EUCLIDEAN GREEN'S FUNCTIONS. *Commun.Math.Phys.*, 31:83–112, 1973.

[231] Konrad Osterwalder and Robert Schrader. Axioms for Euclidean Green's Functions. 2. *Commun.Math.Phys.*, 42:281, 1975.

[232] E. P. Wigner. *Gruppentheorie und ihre Anwendung auf die Quanten mechanik der Atomspektren (in German).* Friedrich Vieweg und Sohn, 1931.

[233] T. Heinzl. Light cone quantization: Foundations and applications. *Lect.Notes Phys.*, 572:55–142, 2001, hep-th/0008096.